EFFECT OF TUNNELLING ADJACENT TO PILE FOUNDATIONS

LOGANATHAN NAGENDRAN

RARE BOOKS LIB.

The University of Sydney

Copyright in relation to this thesis*

Under the Copyright Act 1968 (several provision of which are referred to below), this thesis must be used only under the normal conditions of scholarly fair dealing for the purposes of research, criticism or review. In particular no results or conclusions should be extracted from it, nor should it be copied or closely paraphrased in whole or in part without the written consent of the author. Proper written acknowledgement should be made for any assistance obtained from this thesis.

Under Section 35(2) of the Copyright Act 1968 'the author of a literary, dramatic, musical or artistic work is the owner of any copyright subsisting in the work'. By virtue of Section 32(1) copyright 'subsists in an original literary, dramatic, musical or artistic work that is unpublished' and of which the author was an Australian citizen, an Australian protected person or a person resident in Australia.

The Act, by Section 36(1) provides: 'Subject to this Act, the copyright in a literary, dramatic, musical or artistic work is infringed by a person who, not being the owner of the copyright and without the licence of the owner of the copyright, does in Australia, or authorises the doing in Australia of, any act comprised in the copyright'.

Section 31(1)(a)(i) provides that copyright includes the exclusive right to 'reproduce the work in a material form'. Thus, copyright is infringed by a person who, not being the owner of the copyright, reproduces or authorises the reproduction of a work, or of more than a reasonable part of the work, in a material form, unless the reproduction is a 'fair dealing' with the work 'for the purpose of research or study' as further defined in Sections 40 and 41 of the Act.

Section 51(2) provides that "Where a manuscript, or a copy, of a thesis or other similar literary work that has not been published is kept in a library of a university or other similar institution or in an archives, the copyright in the thesis or other work is not infringed by the making of a copy of the thesis or other work by or on behalf of the officer in charge of the library or archives if the copy is supplied to a person who satisfies an authorized officer of the library or archives that he requires the copy for the purpose of research or study'.

*'Thesis' includes 'treatise', dissertation' and other similar productions.

This thesis has been accepted for the award of the degree in the Faculty of Engineering

EFFECT OF TUNNELLING ADJACENT TO PILE FOUNDATIONS

by

Loganathan NAGENDRAN
BSc (Eng.) Hons., MPhil, MEng.

This dissertation is submitted for the degree of
Doctor of Philosophy
of
The University of Sydney

Department of Civil Engineering

December 1999

ABSTRACT

This thesis describes a study of the tunnelling-induced ground deformations and their effects on adjacent pile foundations. Current design practice to predict tunnelling-induced ground movements is generally based on empirical methods that are subjected to some important limitations. For a ground deformation predicted due to tunnelling to be accurate, the prediction methods should account for the effect of a number of parameters, such as tunnel construction method and tunnel driving details, tunnel depth and diameter, initial stress state, and stress-strain behaviour of the soil around tunnel. In this study, the traditional definition of the ground loss parameter is redefined as "equivalent ground loss parameter" with respect to gap "g" parameters and incorporated in to analytical soulutions to predict the ground movements around tunnel in clays. In addition, design charts are established to estimate the ground loss values due to tunnel excavation based on tunnel depth and diameter, subsurface soil parameters, and geometry of tunnel boring machine. The applicability of these proposed analytical solutions and the design charts to estimate the ground loss values are then checked with some case records, which encompass a range of ground conditions from very stiff to soft clays. In general, predicted and observed values are in good agreement.

Numerical analyses and a parametric study were performed to examine the effects of tunnelling-induced ground movements on adjacent pile foundations. The analytical solutions proposed have been incorporated into the numerical computation code used in this study. Through the parametric study, it is shown that the influence of tunnelling on pile response depends on a number of factors, including tunnel geometry, ground loss ratio, soil strength, pile diameter, and ratio of pile length to tunnel cover depth. Simple design charts are established for estimating tunnelling-induced pile responses and may be used in practice to assess the behaviour of existing piles adjacent to tunnelling operations. A published case history has been studied in which the measured lateral pile deflections are compared with those estimated from the design charts and fair agreement is found.

One of the main thrusts of this research program is to obtain experimental data, with a total of three centrifuge model tests undertaken to obtain accurate and detailed data in order to check the applicability of the proposed analytical solutions which predict the tunnelling-induced ground deformations and the proposed design charts that estimate the tunnelling-induced pile behaviour. The tunnel excavation procedure has been modelled by "equivalent ground loss values" and the specified ground loss values have been

achieved by reducing the diameter of the model tunnel. Model piles (a single pile and a 2 x 2 pile group) have been driven into the pre-consolidated Kaolin clay sample by a miniature pile driving actuator. The performance of the pile group and the single pile are compared at the same time in the same package. Tunnel depths have been varied in each test in order to assess the influence of tunnel depth on movements, axial pile forces, pile settlements, and lateral pile deformations. The models were instrumented substantially to measure tunnelling-induced vertical and lateral ground movements and the tunnelling-induced behaviour of the piles. A model scale of 1/100 was used with a nominal centrifuge acceleration of 100g. The centrifuge test results have been found to be internally consistent, and compare well with the ground movements predicted using proposed analytical solutions and pile behaviours estimated from the proposed design charts.

Recommendations regarding the estimation of tunnelling-induced pile behaviour and limitations of existing methods are outlined. Finally, areas requiring further research, or where additional work may be beneficial, are highlighted.

PREFACE

The work described in this thesis was carried out by the candidate during the period from July 1997 to November 1999. The candidate was supervised by Professor H. G. Poulos, Professor of Civil Engineering, during the entire period of his candidature.

The By-Laws of the University of Sydney require a candidate for the degree of Doctor of Philosophy to indicate which sections of the thesis are original. To this end, the acknowledgement of information obtained from other sources and references is made in the text and the Author claims originality for the following:

- The development of closed-form solutions to assess tunnelling-induced ground deformations by modifying the Verrujit and Booker (1996) solutions;
- The theoretical predictions using closed-form solutions, and comparisons with a total of eleven (11) case histories, described in Chapter 3;
- Establishing a design chart to assess the tunnelling-induced ground loss as described in Chapter 3;
- Numerical analyses and comparisons of tunnelling-induced pile behaviour using the boundary element program, GEPAN, finite difference program, FLAC 3D, and the finite element program, PECPLAS 3D, described in Chapter 4;
- The planning and performance of laboratory centrifuge tests described in Chapter 5, especially the development of model tunnel and ground loss concept;
- The interpretation and presentation of experimental results described in Chapter 6;
- Theoretical predictions using the boundary element program, GEPAN, and the finite difference program, FLAC 3D, and the comparisons with experimental results, presented in Chapter 6;
- Establishing design charts to assess the tunnelling-induced pile behaviour by performing a parametric study, and comparisons with centrifuge test results and a published case history.

The following research papers were published and prepared by the Author and Professor Poulos during the period of the author's candidature, and are presented in support of this candidature.

1. Loganathan N and Poulos H G (1998), "Analytical Predictions of Tunnelling Induced Ground Movements", ASCE, Journal of Geotechnical and Geoenvironmental Engineering, Sept., 1998, Vol. 124, No. 9.

2. Loganathan N, Poulos H G and Stewart D P (2000), "Centrifuge Model Testing of Tunnelling Induced Ground and Pile Deformations", *Geotechnique 50*, UK (In Press).

3. Loganathan N, Poulos H G and Xu K J (2000), "Ground and Pile-Group responses due to Tunnelling", Soils and Foundation, Japanese Geotechnical Journal (Accepted for Publication).

4. Loganathan N and Poulos H G (1999), "Tunnelling-Induced Ground Deformations and their Effect on Adjacent Foundations", The Race for Space - 10th Australian Tunnelling Conference, Melbourne, Australia, March 1999.

5. Loganathan N, Poulos H G and Bustos-Ramirez A (2000), "Estimation of Ground Loss During Tunnel Excavations", prepared for GeoEng2000, Melbourn, Australia, November 2000.

I certify that the contents of this thesis are original and have not been previously presented in whole or part, to any other university or institution for a higher degree.

N. Loganathan

ACKNOWLEDGEMENTS

I would like to express my indebtedness and deepest gratitude to my supervisor Professor Harry G. Poulos for his valuable guidance, encouragement and help given throughout the course of this study and for the opportunity to work in the Department of Civil Engineering at the University of Sydney.

I wish to thank Australian Research Council (ARC) for providing a Research Scholarship to undertake this study.

I am grateful to academic and technical staff at the University of Western Australia (UWA) for their support during my stay at UWA to carry out the centrifuge tests. Special thanks are due to Dr. D. P. Stewart and Professor M. F. Randolph for their timely help and for making the testing programme possible.

I wish to acknowledge the following for their assistance and help; Mr. Alfredo Bustos-Ramirez, Design Manager, Transfield Bouygues Joint Venture, for providing field data and details of Airport Link Tunnelling Project, Sydney, Australia, Dr. Hussein Mroueh of University des Science et Technologies de Lille, France, for providing PECPLAS 3D numerical results for the comparison study, and Dr. P van den Berg, Head, Strategic Research Department of Delft Geotechnics, The Netherlands, for providing technical documents of their previous centrifuge tests.

I would be failing in my duty if I do not thank my colleagues and academic and non-academic staff of Department of Civil Engineering, University of Sydney for their assistance.

Finally, I wish to record my many thanks to my family and would like to dedicate this thesis work to the memory of my late father.

TABLE OF CONTENTS

NOTATION

Roman

A, B - constants

BM - bending moment

c - cohesion of soil

c_u - undrained shear strength

c_v - coefficient of consolidation

D - tunnel diameter

d - pile diameter

e_{cs} - void ratio at p'=1 kPa on critical state line

E_p - Young's Modulus of pile

E_s - Young's Modulus of soil

E_u - undrained Modulus of soil

E_pI_p - pile bending stiffness

f_{cu} - soil strength correction factor

f_{PG} - physical gap correction factor

G - elastic shear modulus

g - gap parameter

G_p - physical gap

G_s - soil particle density

H - tunnel depth

i - surface settlement trough width

k - soil-cutter resistance

k_0 - earth-pressure coefficient at rest

k_s - shear spring constant

k_n normal spring constant

L - length of shield

L_p - length of pile

LI - liquidity index

LL - liquid limit

m - a constant

M - critical state friction constant

$M_{max.}$ - maximum bending moment

M_y - yield bending moment

N - centrifuge scale factor

N - SPT value

NP - stability parameter

OCR - over consolidation ratio

PL - plastic limit

$+P_{max.}$ - +ve maximum axial down drag force

$-P_{max.}$ - +ve maximum axial down drag force

P_u - ultimate load carrying capacity of pile

P'_v - vertical effective stress

P'_w - pore-water pressure at tunnel springline

P_i - tunnel support pressure

PG -physical gap parameter

R - tunnel radius

r - spacing ratio (critical state parameter)

s - pile spacing

$S_{max.}$ - maximum settlement

S_p - pile head settlement

S_f - greenfield settlement

T^* - thickness of the annulus gap

t - thickness of tail piece

$U_{z=0}$ - tunnelling-induced surface settlement

U_z - tunnelling-induced subsurface settlement

U_x - tunnelling-induced lateral deformation

U^*_{3D} - 3-D elasto-plastic deformation

x - lateral distance from tunnel centreline

z - depth

Greek

β - soil movement wedge angle with horizontal

γ - unit weight of soil

ω - workmanship factor

δ - ground loss due to the long-term ovalisation of the tunnel

δ - pile head rotation

δ_x - tunnel face soil intrusion

Δ - thickness of the tail piece

ε - uniform radial ground loss

ε_F - ground loss ratio ($R^2\varepsilon_0$)

ε_{BF} - base ground loss ratio

ε_0 - equivalent ground loss

$\varepsilon_{x,z}$ - modified equivalent ground loss

ε_{NP} - base ground loss component attributed to stability factor

ε_{cu} - base ground loss component attributed to soil strength

φ - angle of shearing resistance

ρ - lateral deflection of pile

ν - Poisson's ratio

λ - slope of consolidation line

κ - slope of swelling line

ζ - clearance of erection lining

CHAPTER ONE

INTRODUCTION

1.1 Background

1.2 Objective

1.3 Organisation of the Dissertation

1.1 BACKGROUND

Rapid growth in urban development has resulted in increased demand for the construction of transportation systems, water supply, and sewage disposal systems. Tunnels are an essential component of these schemes and constitute one of the major portions of project expenditure. Recent advances in tunnelling technology reduce construction time with consequent decreases in cost. However, even with modern equipment, experience has shown that subsidence inevitably occurs in areas above and adjacent to tunnels passing through soft soil deposits. These deformations may significantly affect nearby structures and need to be considered during design. Unfortunately, theoretical advances have not kept pace with the recent advances in tunnelling technology and at present there is no universally accepted theoretically sound method of predicting ground subsidence before construction.

At present, the prediction of tunnelling-induced ground deformations is largely based on empirical relationships. However, these empirical formulae are subjected to some important limitations; first, in their applicability to different ground conditions and construction techniques, and second, in the limited information they provide about the horizontal movements and subsurface settlements. Therefore, there is an apparent need for a theoretically-based design procedure that will provide a consistent means of predicting tunnelling-induced ground deformations.

In an urban enviornment, many high rise buildings are supported by piled foundations and, generally, tunnelling will cause ground movements, which in turn have the potential to impose axial and lateral forces on the piled foundations. Relatively little research work associated with this kind of problem can be found in the literature and a limited amount of field data has been published concerning tunnelling-induced pile behaviour. A number of researchers have used numerical methods to assess the tunnelling-induced ground deformations and their effect on adjacent piles. However, there has been relatively little discussion of the general theoretical and practical factors that should be considered if these advanced numerical techniques are to play a routine role in practical design application.

In recent years, laboratory centrifuge tests have become a popular tool to assess the tunnelling-induced ground deformations and their effects on adjacent pile foundations. The use of centrifuge testing techniques in studying the development of collapse

mechanisms is widely appreciated and major advances in understanding tunnel behaviour have been made using data from centrifuge models.

This research project was inspired by a need for a theoretically-based but easy-to-use procedure to estimate the tunnelling-induced ground deformations and their effect on adjacent pile foundations, and also to obtain additional experimental data to clarify the theoretically-based procedure.

1.2 OBJECTIVE

The overall aim of this research project was to examine the tunnelling-induced ground deformations and their effects on adjacent pile foundations.

The major objectives of this project were:

- development of a theoretically-based procedure to predict the tunnelling-induced ground deformations;
- numerical analyses, using available numerical tools, to assess the tunnelling-induced ground deformations and pile behaviour:
- the establishment of design charts to estimate tunnelling-induced ground loss values and adjacent pile behaviour:
- development and proof testing of experimental apparatus, techniques and preparation procedures for centrifuge tests;
- testing of a series of centrifuge models for different tunnel depths and review of centrifuge data;
- comparisons of centrifuge data and available field data with the theoretically based formulae and design charts established in this study; and
- to provide recommendations for further research for possible improvement of the theoretically-based design methods.

1.3 ORGANISATION OF THE DISSERTATION

A review of the literature relevant to this research topic is presented in Chapter 2. This review covers various methods available to assess tunnelling-induced ground deformations, tunnelling-induced behaviour of adjacent shallow and deep foundations, and various laboratory testing methods.

The methodology adopted in the derivation of closed-form formulae to assess the tunnelling-induced ground deformations and design charts to estimate the tunnelling-induced ground loss values are presented in Chapter 3. The applicability of these closed-form solutions and ground loss design charts are examined by comparisons with available published field and laboratory data.

Chapter 4 presents a detailed numerical study on tunnelling-induced pile behaviour and the results of a parametric study. The predictions using closed-form solutions are also compared with the results obtained from the numerical study.

The centrifuge experimental programme, apparatus and testing techniques are fully described in Chapter 5. The experimental results are presented in Chapter 6, where the data are discussed and also compared with numerical predictions.

Chapter 7 presents design charts developed in order to assess tunnelling-induced pile behaviour. Comparisons are also presented between predicted behaviour and that obtained from both the centrifuge test results and existing field data. The major conclusions and recommendations arising from the work are summarised in Chapter 8. Areas requiring further research, or where additional work may be beneficial, are also highlighted.

The theoretical background of the GAP parameters and a typical worksheet to estimate the GAP parameter are presented in Appendix A.

CHAPTER TWO

LITERATURE REVIEW

2.1 INTRODUCTION

In urban areas, it is essential to protect pre-existing structures and underground conduits from damage during shield tunnelling. An accurate estimation of tunnelling-induced ground movements is one of the main requirements in the design and construction of urban tunnels. Engineers responsible for the design and construction of tunnels must have some technique for estimating the ground movements as precisely as possible so that they can assess whether neighbouring buildings will be subject to excessive movements.

The purpose of this chapter includes three aspects and they are:

1. to examine the existing empirical, analytical and numerical methods for predicting the tunnelling-induced ground movements and identify a method which predicts the tunnelling-induced ground movements reasonably accurately considering factors such as computation time, availability of soil parameters, computer capabilities, and cost involved with the assessment,
2. to study the existing methods for assessing the tunnelling-induced shallow and deep foundation behaviour. The outcome of this study will be used as a guideline to the tunnelling-induced pile behaviour assessment to be adopted in this study, and
3. to assess various pile and tunnel modelling techniques and data acquisition methods used in reported centrifuge model tests and laboratory "1g" tests, and extract useful information to adopt in the centrifuge tests to be performed in this study.

2.2 TUNNELLING-INDUCED GROUND MOVEMENTS

2.2.1 Introduction

Several approaches have been developed for prediction of the ground deformations associated with tunnelling, and these fall into three different categories, namely, empirical methods, analytical methods and numerical methods. Each method has merits and de-merits and limitations. The selection of the appropriate method depends on the complexity of the problem and resources available for the analysis.

2.2.2 Empirical Methods

In engineering practice, the ground deformations are often described by empirical formulae, based upon field observations, most commonly a normal (Gaussian)

distribution curve (Peck, 1969, Attewell and Woodman,1982). The Gaussian normal probability curve for the transverse settlement profile, proposed by Peck (1969), has no theoretical basis, the only reasons for its use being its shape, which is similar to the usually observed profiles, and the fact that the curve is simply defined by a few parameters, so that it can be easily fitted to each particular case.

The shape of the ground surface settlement trough is shown in Figure 2.1.

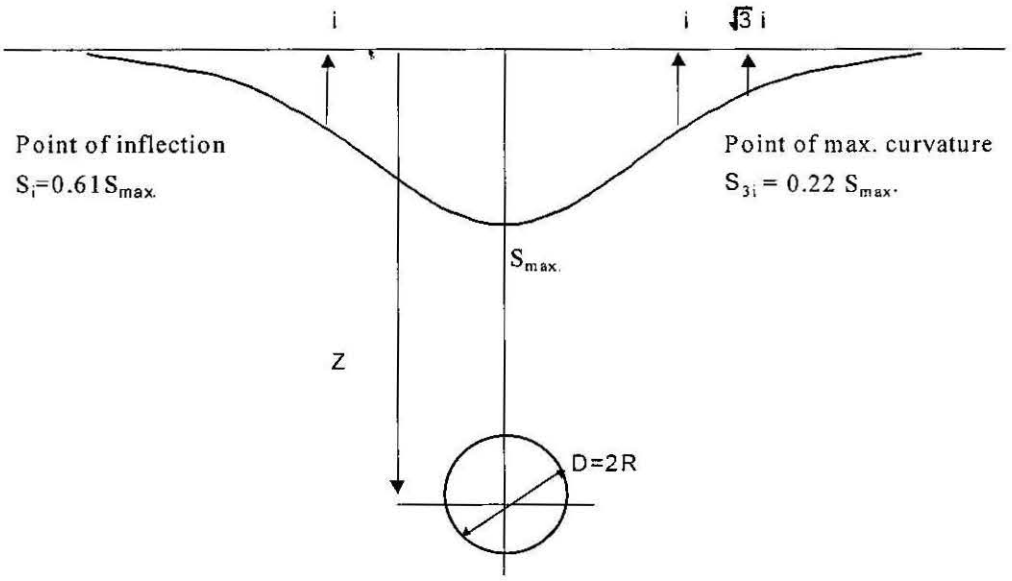

Settlement Trough Volume, $V_T = 2.5\ i\ S_{max}$ (approx.)

Tunnel opening volume, $V_o = 2\pi R^2$

Ground Loss, $V_L = \frac{V_T}{V_o} x100\ \%$

$$S_{max.} = \frac{0.313 V_L D^2}{i}$$

Figure 2.1: Surface Settlement Trough

The settlement trough is normally approximated by an error function as shown in equation (2.1).

$$S = S_{max.} \exp\left(\frac{-x^2}{2i^2}\right) \qquad (2.1)$$

where, S = surface settlement at a transverse distance x from the tunnel centerline, S_{max} = maximum settlement at x=0, and i = location of maximum settlement gradient or point of inflexion. A significant amount of research involving field observations and model tests was devoted to the estimation of S_{max} and the i values for different ground conditions. The estimation of i values by various researchers are given below;

- Peck (1969) – Based on field observations:

  $\frac{i}{R} = \left(\frac{Z}{2R}\right)^n$ where: n = 0.8 to 1.0 and Z = tunnel depth

- Atkinson and Potts (1979) – Based on field observations and model tests:

  $i = 0.25(Z + R)$ for loose sand, and

  $i = 0.25(1.5Z + 0.5R)$ for dense sand and over consolidated clay

- O'Reilly and New (1982)- Based on field observations of UK tunnels:

  $i = 0.43Z + 1.1$ for cohesive soil

  $i = 0.28Z - 0.1$ for granular soil

- Mair et al (1993)- Based on field observations worldwide and centrifuge test

  $i = 0.5Z$

The other correlations are based on the parameters defined in equation (2.2).

$$\frac{i}{R} = \alpha\left(\frac{Z}{2R}\right)^n \tag{2.2}$$

- Attewell (1977), $\alpha = 1.0$ and $n = 1.0$
- Clough and Schmidt (1981), $\alpha = 1.0$ and $n = 0.8$
- Sagaseta (1987), $\alpha = 1.15$ and $n = 1.0$

The maximum settlement, S_{max} is defined as given in equation (2.3).

$$S_{max} = \frac{V_s}{2.5i} \tag{2.3}$$

where V_s = volume of the settlement trough. S_{max} has been correlated to tunnel geometry by the following researchers;

- Attewell and Farmer (1974):

For $\frac{Z}{R} \geq 8$, $\frac{S_{max}}{2R} = 0.2 - 0.35\,\%$, and

For $\frac{Z}{R} \leq 4$, $\frac{S_{max}}{2R} \geq 1\,\%$

- Wong and Kaiser (1987):

$$\frac{S_{max}}{S_c} = \exp\left\{\frac{1}{2}\left[\frac{1 + \left(\frac{H}{a}\right).\cot(\beta)}{\frac{i}{a}}\right]^2\right\}$$

where β is an angle defining the trough width relative to the tunnel depth, and S_c is the settlement at the crown of the tunnel.

Alternatively, S_{max} has been correlated to volume loss (V_L) parameter by O'Reilly and New (1982) (Ref. Figure 2.1) and they used the following empirical values to choose the ground loss parameter for various tunnelling conditions.

V_L = 0.5 - 3.0 %,	Stiff fissured clay;	Shield or none tunnel
= 2.0 - 2.5 %,	Glacial deposits;	Shield tunnel in free air
= 30.0 - 40.0 %	Silty clay deposits;	Shield tunnel in free air
= 2.0 - 20.0 %	Silty clay deposits	Shield tunnel in compressed air

Sub-surface settlements

A considerable amount of data is available from field measurements of surface settlement profile above tunnels in clays. In contrast to surface settlement measurements, few field measurements of subsurface profiles are available. It is often assumed that the shapes of subsurface settlement profiles developed during tunnel construction are characterized by

the Gaussian distribution, in the same manner as are those for surface settlement profiles (Mair et al, 1993).

The following empirical relationships were derived by various researchers in order to establish the subsurface settlement profiles;

- Mair et al (1993):

$$i_z = k(Z_0 - Z)$$

where, $k = \dfrac{0.175 + 0.325\left(1 - \dfrac{Z}{Z_0}\right)}{1 - \dfrac{Z}{Z_0}}$, Z_0 = depth to tunnel axis and Z = depth from the surface.

Therefore, $\dfrac{S_{Z,\max}}{R} = \dfrac{1.25V_L}{0.175 + 0.325\left(1 - \dfrac{Z}{Z_0}\right)} \cdot \dfrac{R}{Z_0}$

The settlement trough at a depth z, S_z,can be written as shown in equation (2.4).

$$S_z = S_{z,\max} \exp\left(\frac{-x^2}{2i_z}\right) \tag{2.4}$$

- Atkinson and Potts (1979)- For shallow tunnels based on model tests:

$$\frac{S_c}{S_{z,\max}} = 1.0 - \alpha\left(\frac{Z - R}{2R}\right)$$

where,

$\alpha = 0.57$: dense sand

$\alpha = 0.40$: loose sand

$\alpha = 0.13$: over consolidated clay

- Vermeer et al (1991):

$$S_z = \left(\frac{Z_0}{Z_0 - Z}\right) S_{z,\max} \exp\left(\frac{-x^2}{2i^2}\right)$$

These solutions are not accurate when Z approaches Z_0. The settlement become infinite, which is obviously not true for actual field conditions.

Lateral Deformations

Lateral displacements are traditionally related to settlements via one of two assumptions;

1. The horizontal displacement at a point is proportional to the slope of the settlement trough, and
2. The horizontal displacement at a point corresponds to the ground movements that are directed towards the centre of the excavation.

Very few attempts were made in the past to predict the lateral deformations using empirical methods. Available methods are not accurate in predicting the lateral deformation of the subsurface, but the following researchers established very approximate empirical correlations to predict the lateral deformation;

- Ortigao et al (1996):

$$\delta_T^{\max} = 0.12\, S_{\max}$$

where δ_T^{max} is the maximum lateral deformation and S_{max} is the maximum settlement.

- Norgrove (1979):

$$\delta_{hs} = -\frac{ny}{Z_0}.\delta_{vs}$$

$$\delta_{hs\,\max} = -0.606 \cdot \frac{V_s n}{\sqrt{2\pi}} \cdot \frac{1}{Z_0}$$

where y is the depth at which the lateral deformation is required and Z_0 is the tunnel depth (from ground surface to tunnel centerline).

- Steensen-Bach et al (1991) – based on model tests, and applicable only for very shallow tunnels:

$$\frac{S_x}{t} = -0.6\left(\frac{Z_0}{2R}\right)^{-1.1} \exp\left[-0.52\left(\frac{x}{R}\right)^2\left(\frac{Z_0}{2R}\right)^{-1.1}\right].\frac{x}{R}$$

where t = vertical extension of tail void.

Limitations

The empirical methods are subjected to many limitations, including;

1. They can not be applied to different tunnel geometries,
2. The variability of ground conditions, such as soil type, ground water conditions , in-situ stress conditions can not be considered in a systematic manner, and
3. Different construction techniques are not considered in the estimation of ground loss values.

2.2.3 Analytical Methods

For ground deformation prediction to be of practical use it should account for the effect of a number of parameters, such as the construction method and tunnel driving details, tunnel depth and diameter, ground water condition, initial stress state and stress-strain-strength behaviour of the soil around tunnel.

Current "rules" to estimate ground settlement upon tunnelling operations have been generally derived from empirical correlations between some of those variables and settlement observed in actual tunnels (see Section 2.2.2 above). Hence they account for only a few of the significant factors, and extrapolation to other cases is questionable mainly because similitude conditions are generally not fulfilled.

Only a few attempts appear to have been made to develop numerical methods (closed form solutions) which incorporate all factors which contribute to ground deformations. Sagaseta (1987) presented closed form solutions for obtaining the strain field in an initially isotropic and homogeneous incompressible soil due to near-surface ground loss due to tunnelling. He considered the problem as strain-controlled and obtained strains by using only the incompressibility condition.

Verruijt and Booker (1996) presented an analytical solution for a tunnel in a homogeneous elastic half space, using an approximate method suggested by Sagaseta (1987) for the case of ground loss. The solution given by Verruijt and Booker (1996) is a generalisation of Sagaseta's solution in that it gives the solution for the case of ground loss not only for the incompressible case, but for arbitrary values of Poisson's ratio, and that it includes the effect of ovalisation.

The closed form solution presented by Verruijt and Booker (1996) for the estimation of the settlement U_z and the lateral deformation U_x is shown in equations (2.5) and (2.6).

$$U_x = -\varepsilon R^2\left(\frac{x}{r_1^2}+\frac{x}{r_2^2}\right)+\delta R^2\left(\frac{z_1(x^2-kz_1^2)}{r_1^4}+\frac{x(x^2-kz_2^2)}{r_2^4}\right)$$
$$-\frac{2\varepsilon R^2 x}{m}\left(\frac{1}{r_2^2}-\frac{2mzz_2}{r_2^4}\right)-\frac{4\delta R^2 xh}{m+1}\left(\frac{z_2}{r_2^4}+\frac{mz(x^2-3z_2^2)}{r_2^6}\right) \quad (2.5)$$

$$U_z = -\varepsilon R^2\left(\frac{z_1}{r_1^2}+\frac{z_2}{r_2^2}\right)+\delta R^2\left(\frac{z_1(kx^2-z_2^2)}{r_1^4}+\frac{z_2(kx^2-z_2^2)}{r_2^4}\right)$$
$$+\frac{2\varepsilon R^2}{m}\left(\frac{(m+1)z_2}{r_2^2}+\frac{mz(x^2-z_2^2)}{r_2^4}\right)-2\delta R^2 h\left(\frac{x^2-z_2^2}{r_2^4}+\frac{m}{m+1}\frac{2zz_2(3x^2-z_2^2)}{r_2^6}\right) \quad (2.6)$$

where ε and δ are parameters indicating the relative displacement of the tunnel surface, for the uniform radial displacement case and the ovalisation case respectively. In these solutions $z_1 = z - h$, $z_2 = z + h$, and $r_1^2 = x^2+z_1^2$, $r_2^2=x^2+z_2^2$, R and h are tunnel radius and depth, $m = 1/(1-2\nu)$, $k = \nu/(1-\nu)$.

Figure 2.2 shows predictions of surface settlement trough using various empirical methods and Verruijt and Booker method for a Heathrow Express Trial Tunnel configuration (Deane and Bassett, 1995). Parameters used are shown in Section 3.5.2.

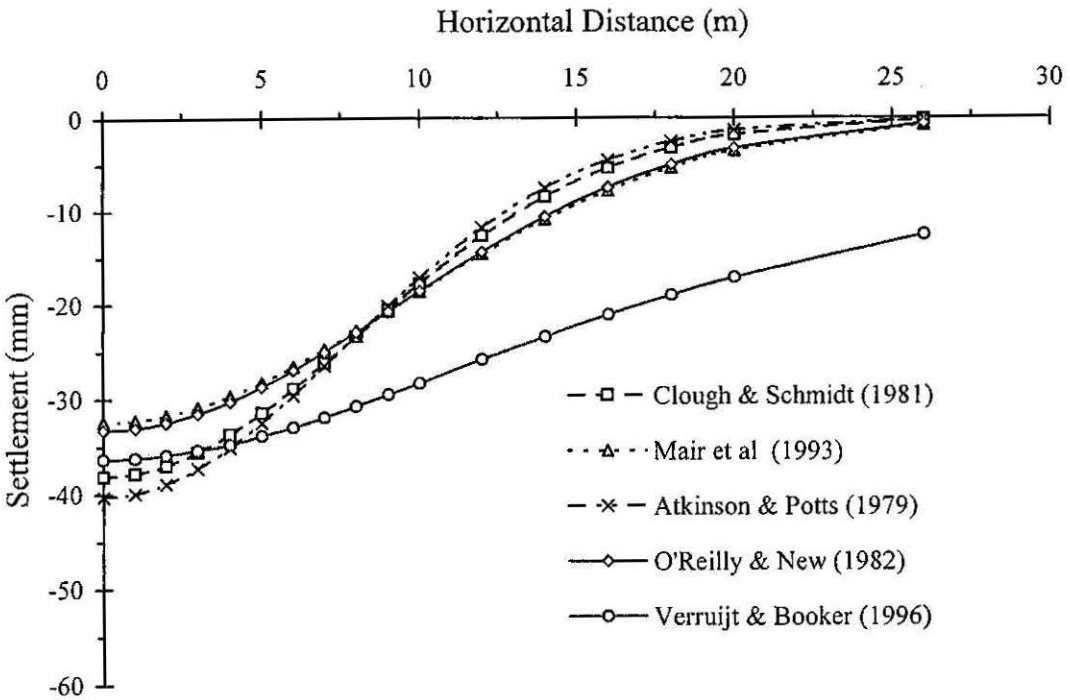

Figure 2.2: Observed and Predicted Surface Settlement Troughs

Figure 2.2 shows that the maximum settlement predicted by these methods varies from 33 to 41 mm for the ground loss value of 1.4%. The settlement trough obtained from Verruijt and Booker method is much wider compared to the empirical methods (Figure 2.2). The reasons for this difference may be attributed to the following reasons:

- Actual soil behaviour is non-linear, and exhibits plastic as well as elastic behaviour,
- Verruijt's method assumes uniform radial ground movement, and
- Consolidation components have not been considered in the analysis.

2.2.4 Numerical Methods

At least some of the limitations of empirical and analytical methods may be overcome by numerical methods, which have indeed been used widely for tunneling analyses. Numerical methods can overcome these limitations reasonably, if appropriate constitutive models with correct input data are used. Due to limitations both of software and hardware, three dimensional (3D) situations are often analysed as though they were two dimensional (2D). A number of 2D finite element simplifications have been developed to model 3D tunnel problems, e.g. the axi-symmetric case (Rowe and Lee, 1992), cross sectional plane strain analysis (Mair et al., 1981, Rowe and Lee, 1989; Leca and Clough, 1992; Atzl and Mayr,1994) and longitudinal plane strain analyses (Guo et al., 1994).

Rowe and Kack (1983) found that their finite element technique could generally give good estimates of soil settlements as compared with those measured, although unfavourable comparisons were also found in some cases. Successful predictions of lateral soil movements by the finite element method were also reported by Lee et al. (1994). However, Gunn (1993) reported that a finite element analysis, even with a refined constitutive soil model, gave poor predictions for surface settlements. He found that the surface settlement trough given by the finite element method was too wide and shallow as compared with measured values. The reason was quickly identified as being the elastic part of any constitutive model used to represent the stress-strain behaviour of soil. Gunn (1993) showed the improvement in predicted surface settlement gained with non-linear elastic, rather than linear elastic, behaviour pre-failure. Figure 2.3 shows the surface settlement troughs estimated by Gunn (1993) for various constitutive relationships.

Lee and Rowe (1989) carried out linear elastic perfectly plastic finite element analyses of tunnelling, specifically to show the influence of cross-anisotropic parameters pre-failure. They concluded that particular attention should be given to the ratio of independent shear modulus to vertical modulus. Gunn (1993) in referring to Lee and Rowe (1989) stated that, in his experience, the predictions of ground deformations above tunnels in heavily overconsolidated London Clay were not improved by the use of appropriate anisotropic elastic moduli.

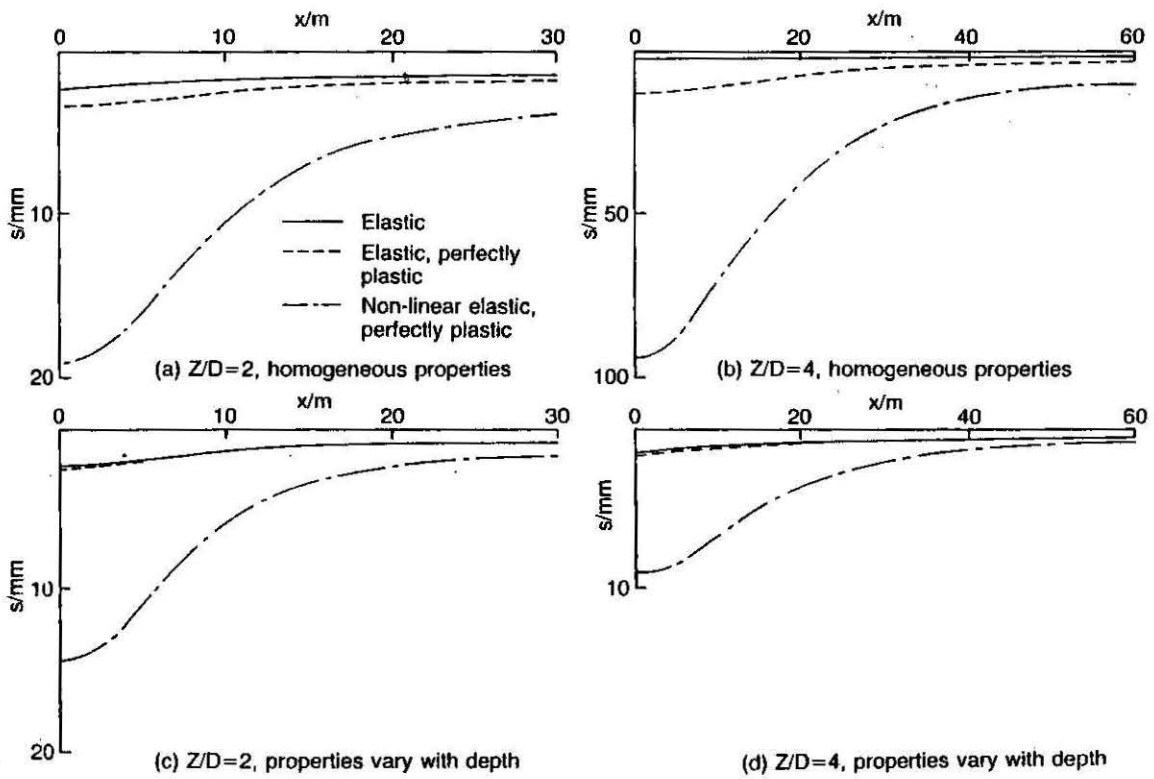

Figure 2.3: Comparison of Surface Settlement Troughs (Gunn, 1993)

Simpson et al (1996) concluded from analyses of excavation in London Clay that the predicted surface settlement trough is substantially influenced by the anisotropic shear modulus, but little influenced by non-linearity.

Addenbrooke et al (1997) carried out finite element analyses adopting five different constitutive models for pre-failure soil behaviour to predict the tunnelling-induced deformation of Jubilee Line Extension Project Tunnels (London, UK). The models adopted were; (1) isotropic linear elastic perfectly plastic, (2) anisotropic linear elastic perfectly plastic, (3) isotropic non-linear elastic perfectly plastic with shear stiffness

dependent on deviatoric strain and mean effective stress, (4) anisotropic non-linear elastic perfectly plastic with shear stiffness dependent on deviatoric strain and mean effective stress, and (5) isotropic non-linear elastic perfectly plastic with shear and bulk stiffness dependent on deviatoric strain level, mean effective stress, and loading reversal. The study showed the importance of modelling non-linear elasticity, and the effect of introducing a soft independent shear modulus. Figure 2.4 shows the comparison of surface settlement troughs predicted and measured.

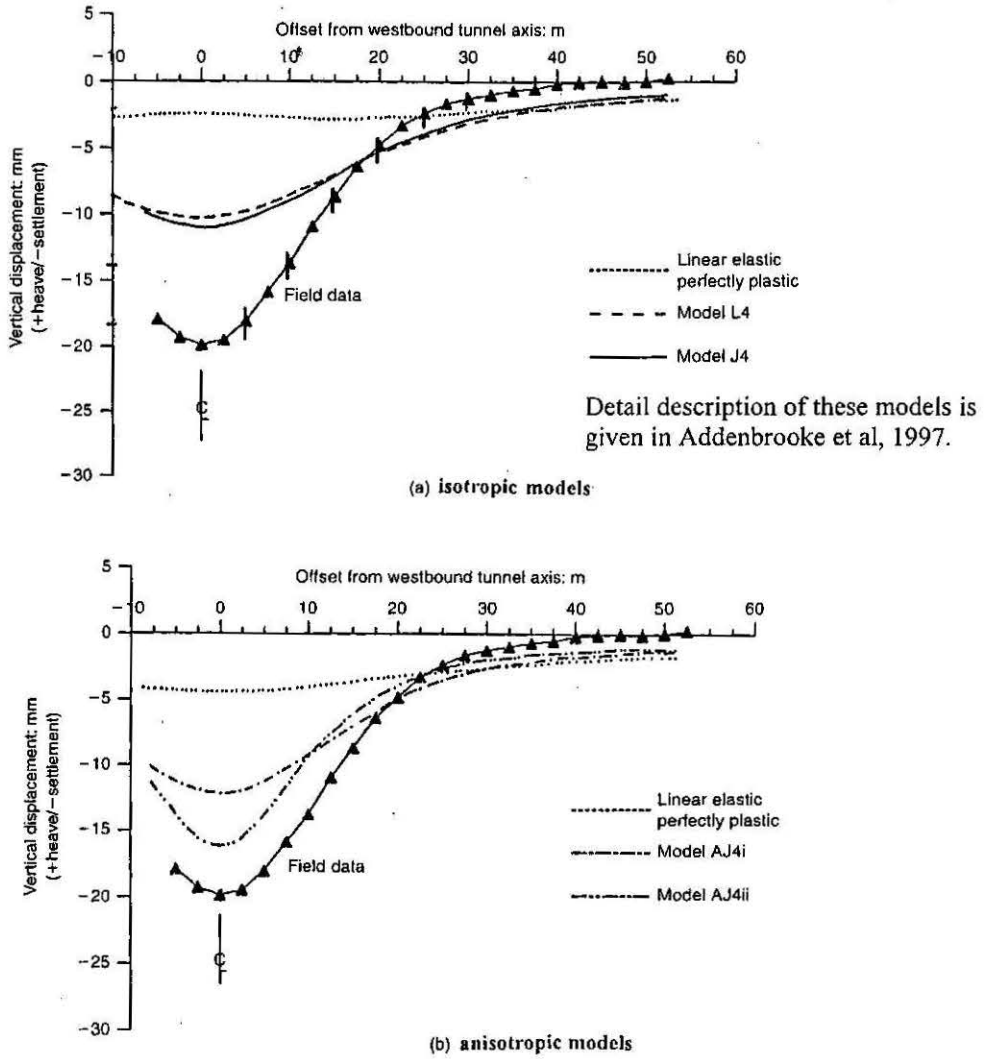

Figure 2.4: Comparison of Surface Settlement Troughs (Addenbrooke et al, 1997)

The findings by various researchers discussed above appear contradictory in terms of selection of appropriate soil models in order to predict the tunnelling-induced ground deformation.

Lee et al (1992) analysed the Thunder Bay tunnel in 3D using the gap parameter method. A gap may be physically meaningful for overbreak produced by tunnel boring machine which occur prior to shotcreting. Akagi (1994) analysed the progressive advance of a shield tunnel in soft ground in 3D. He concluded that the ground displacements and pore pressure predictions depend greatly on changes in the inclination of the shield machine.

2.3 TUNNELLING-INDUCED BEHAVIOUR OF SHALLOW FOUNDATIONS

The construction of tunnels inevitably causes ground movements. In the urban environment such movements present a risk of damage to buildings and structures. The assessment of the degree of risk of such damage is important from the point of view of engineering design.

The accuracy of any estimation of tunnelling-induced damage to buildings founded on shallow footings is related to the accuracy of evaluating the following steps;

- tunnelling-induced surface settlement,
- foundation settlement as a function of surface settlement, and
- building damage as a function of differential foundation settlement

Heath and West (1996) carried out an analysis to establish a method to predict sub-surface settlement in London Clay and subsequent building damage potential. Error in settlement prediction resulted in even greater error in the predicted building strain and angular distortion which are directly related to building damage. They recommended that further improvement is required in regard to the assessment of ground loss prediction and the consequent building response.

Burland (1997) presented a simplified methodology to assess the damage potential of buildings founded on shallow foundations. He stated that building damage can also result from horizontal tensile strain, and therefore predictions of horizontal movements are required. Figure 2.5 shows the relation between the settlement trough, the horizontal displacements and the horizontal strains occurring at ground level.

Potts and Addenbrooke (1996) presented a design chart to assess the building damage considering the interactive nature of the tunnelling-induced green-field ground settlements and the effect of the existing structure on predicted green-field settlements.

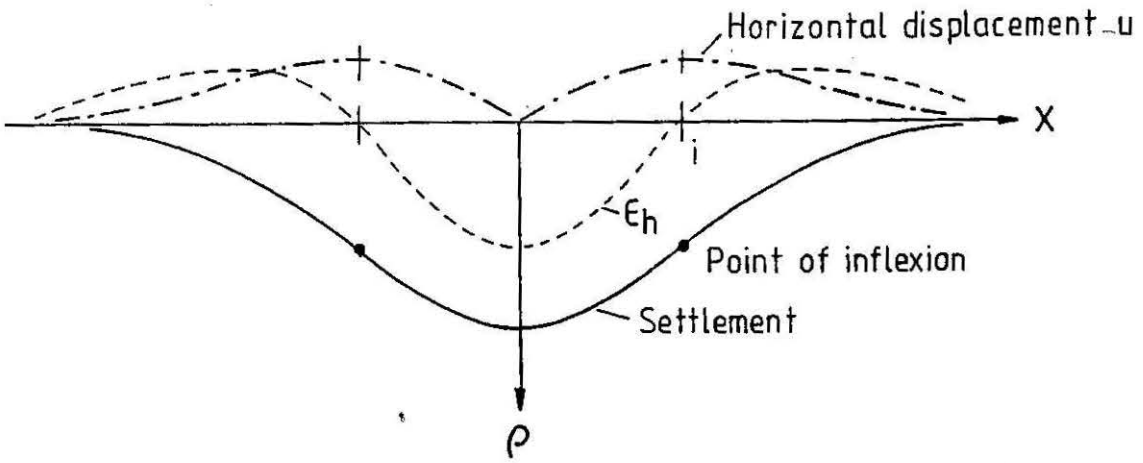

Figure 2.5: Transverse Settlement trough, Horizontal Displacement and Horizontal Strain Occuring at Ground Level

2.4 TUNNELLING-INDUCED BEHAVIOUR OF PILE FOUNDATIONS

In an urban environment, many high rise buildings are supported by piled foundations and, generally, tunneling will cause ground movements, which in turn will impose axial and lateral forces on the piled foundations. Relatively little research work associated with this kind of problem can be found in the literature. Facing some tunnel construction near existing piled foundations, Morton and King (1979) were inspired to carry out laboratory testing to investigate the effects of tunneling on the bearing capacity and settlement of piled foundations. Figure 2.6 shows the limiting pile failure zones derived from the model tests.

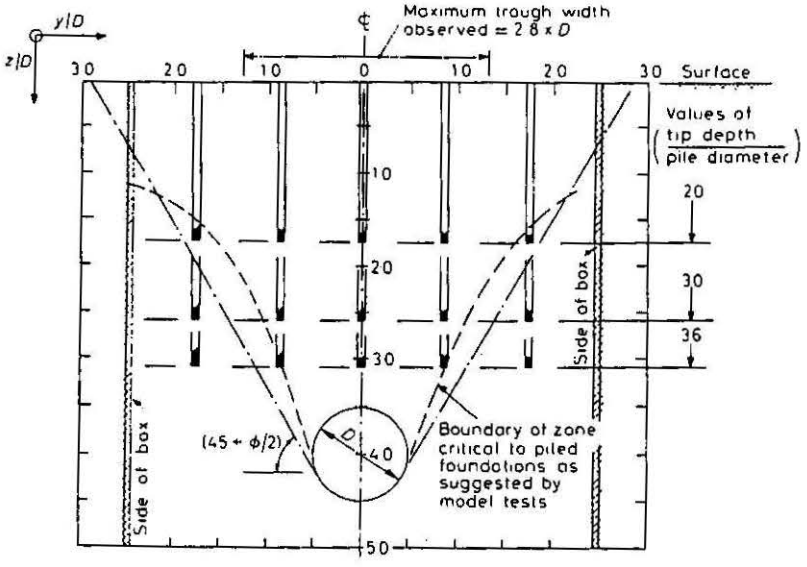

Figure 2.6: Limiting Pile Failure Zones Derived From Model Tests

It may be observed that the limiting pile failure zone almost coincides with the a line drawn from the tunnel spring line at an angle (45+φ/2) to the horizontal, where φ is the angle of shearing resistance of the soil. In addition, they found that piles may be greatly affected by tunneling and therefore concluded that the effects of tunneling on existing adjacent or superincumbent piled foundations in weak soils may be a major and governing concern in the design and execution of underground works.

Lee et al. (1994) (see also Mair, 1993) reported a case where a tunnel was to be driven between newly-constructed piled foundations supporting a seven storey building with a two-storey basement. Although the total long-term ground settlement was assessed, its likely influence on the piled foundation was not identified, or at least not reported. Instead, the pile shafts were sleeved to reduce the effects of negative skin friction. However, the lateral pile deflection was estimated using a finite element analysis and the computed maximum value was used to design the piles.

Attewell et al. (1986) reported a case where bituminous slip coatings were applied to piles, which were anticipated to experience negative skin friction to be caused by a future tunnel construction.

An accurate assessment of tunnelling-induced settlements and lateral soil movements is important in the assessment of the damage of a building founded on piles. At present there are no empirical relationships available to predict the tunnelling-induced ground movements. This further emphasises the limitations of the empirical methods.

2.5 LABORATORY MODEL TESTING

2.5.1 Introduction

Although the behavioural patterns of piled foundations are reasonably well defined for various soils, scant data exist on their performance in relation to adjacent tunnelling work. Laboratory model tests are generally performed to gain an insight into the mechanisms involved and to provide a framework for the interpretation of field data. Based on the study requirements, laboratory model tests are generally carried out in '1g' conditions, while centrifuge tests are used for increased 'g' conditions.

2.5.2 Static '1g' Testing

There are few such laboratory tests which were performed in order to assess the tunnelling induced pile and ground deformations. As mentioned above, Morton and King

(1979) carried out static '1g' laboratory model tests to assess the performance of piles in medium dense to compact granular soils when the founding stratum was undermined by excavation of a tunnel. Conclusions arrived from these laboratory tests are: (i) the effect of tunnelling on existing adjacent piled foundation in weak soils will be a major, and may well be a governing, consideration in the design and execution of underground works, (ii) the settlement of friction piles is controlled mostly by the ground deformation that is induced at or close to the pile-tip location by the tunnelling operation, (iii) the prime factor in inducing failure of the piles is dilatancy of the soil within a zone above the tunnel, (iv) the critical pile failure zone defined in the model tests is relatively narrow except for short piles that rely upon the soils at shallow depth for significant support of working loads, and (v) the width of the critical pile failure zone and the surface settlement trough width are not limited to any theoretically derived zone of ground failure.

Moffatt (1977) performed similar laboratory tests to assess the effect of shield tunnelling beneath pile foundations. Szoke (1977) also carried out similar tests to assess the pile and pile group capacity and soil collapse mechanisms in granular soils. De Moor (1987) performed static model testing to study the behaviour of deep tunnels in clay. These experiments were designed to investigate the changes in pore pressure on excavation of a deep tunnel face. The influence of time and initial pore pressure on the magnitude of deformation of the tunnel face has been demonstrated by these tests. As time increases, the negative excess pore pressures dissipate rapidly and tend towards near- zero values in the region of the tunnel face.

A series of laboratory model tests were carried out by Cairncross (1973) and Orr (1976) at Cambridge University to examine the behaviour of shallow tunnels in sand and in overconsolidated clay. These model tests illustrated in particular how deformations occurring at the tunnel "migrate" through the soil and appear at the surface as subsidence.

Adachi et al (1979) in their model tests considered, for simplicity, a square-section tunnel and analysed both undrained and drained behaviour. They found a yielded zone encompassed the tunnel opening in the undrained condition and it was associated with a reduction in pore pressure near the tunnel which became negative at the tunnel surface.

From these model tests conclusions were drawn regarding the key influence of soil dilation and the existence of a definable zone of potential pile failure, the limits of which are critically dependent on the tunnelling method and on the amount of ground loss.

2.5.3 Centrifuge Testing

The stress-strain behaviour of soil is nonlinear and soil strength depends on the actual effective stress level. Due to the effective weight of the soil, the effective stresses increase with depth. In order to obtain reliable model test results, not only should the mean effective stress in the model be representative of the prototype under investigation, but also the distribution of the stresses should be representative (Hergarden et al, 1996). Centrifuge testing is a powerful tool for investigating such geotechnical problems. Small-scale soil models can be subjected to prototype effective stress distributions. From such testing, a realistic representation of ground movements induced by tunnel excavation can be obtained. Atkinson et al (1977) described the basic principles involved with centrifuge model testing.

Mair (1979) and Taylor (1998) carried out centrifuge tests to investigate certain aspects of soil behaviour due to tunnelling. The 50mm diameter tunnel was constructed by a latex rubber membrane and compressed air was fed to the tunnel to balance the increasing overburden pressure as the speed of the centrifuge increased. The tunnelling process was modelled by gradually reducing the support pressure within the model tunnel over a short period. Transverse settlement troughs were determined from low-voltage displacement transducers (LVDT), for range of ground losses. A typical model used by Taylor (1998) is shown in Figure 2.7.

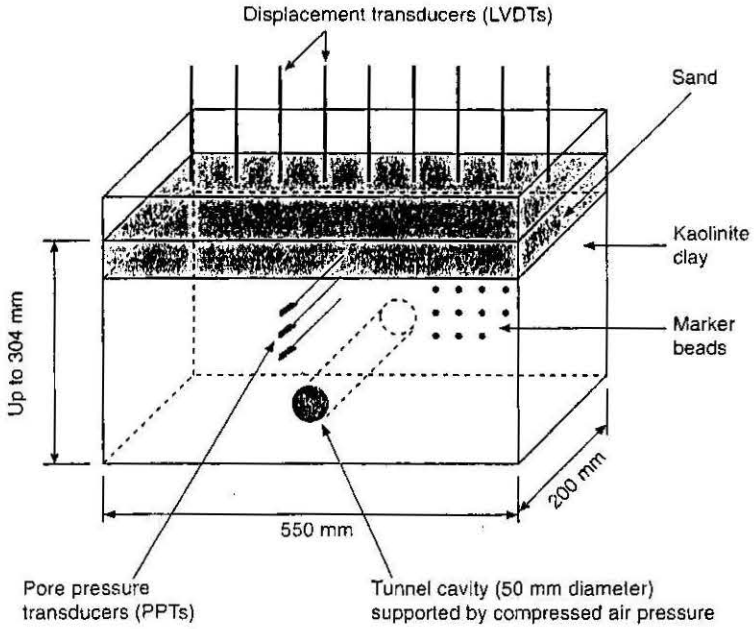

Figure 2.7: Schematic of Centrifuge Model (Taylor, 1998)

Marker beads were placed on a face of the soil sample and the overall displacement pattern was obtained by digital image analysis of images recorder from the CCTV camera mounted on the centrifuge arm. The technique adopted in this study allows details of prefailure movements to be obtained which will be of enormous benefit in the application of centrifuge modelling to geotechnical engineering design.

Bezuijen and Schrier (1994) carried out centrifuge tests to assess the tunnelling-induced ground movements and their effects on adjacent pile foundations. The model tunnel consisted of four synthetic tunnel elements, placed on an aluminium core. By moving the core relative to the tunnel elements, the outer diameter could be varied. The cross-section of their centrifuge model is shown in Figure 2.8. It shows the soil model, the piles and the model tunnel.

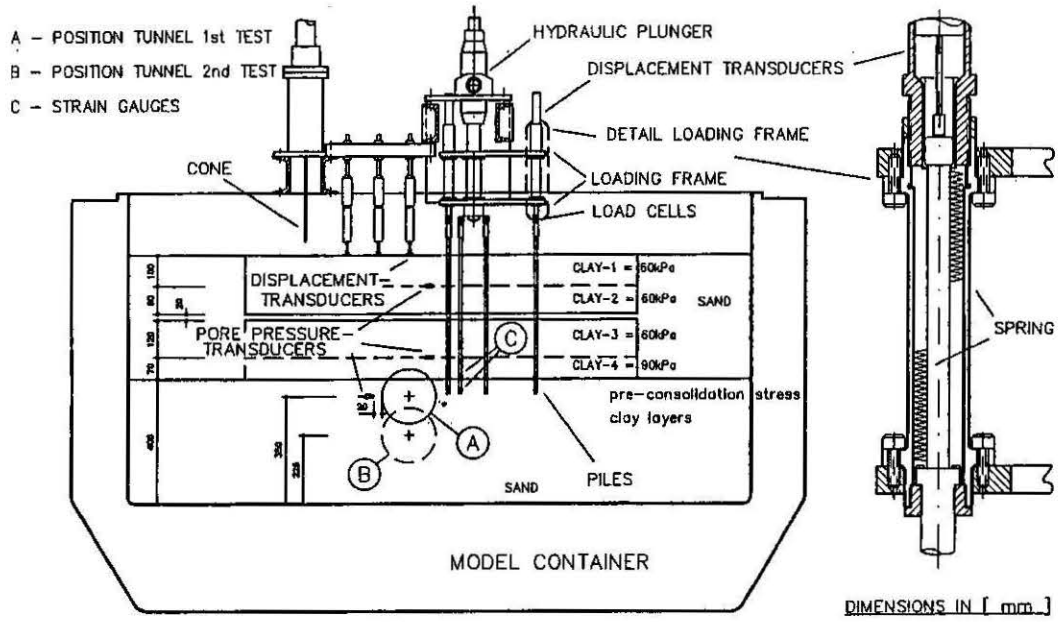

Figure 2.8: Cross-section Through the Centrifuge Model (Bezuijen and Schrier, 1994)

In these tests, two piles were located at both 0.04 and at 0.08m from the tunnel, one at 0.16m and one at 0.32m, resulting in a total of 6 piles. The positions of the piles were determined in a way to minimise group effect. Forces on the piles have been monitored by a load cell on top of the piles and strain-gauges at 0.05m and 0.01m from the pile tip. The load cell on top of the pile measured the total load. Lateral displacements were not measured in these tests.

These tests showed large settlements of the piles close to the tunnel and also a significant reduction in the pile resistance. In addition, the surface settlement trough width was smaller in the tests where the tunnel was completely surrounded with sand.

2.6 SUMMARY

The available empirical methods for estimating tunnelling-induced ground movements are subjected to some important limitations; first, in their applicability to different ground conditions and construction techniques, and second, in the limited information they provide about the horizontal movements and subsurface settlements. An accurate assessment of subsurface ground movements is important in order to assess the tunnelling-induced behaviour of adjacent piles. Therefore, a proper analytical method is desirable to better estimate the tunnelling-induced ground movements.

Various researchers have found that surface settlement troughs predicted by numerical methods are generally wider that those obtained from empirical methods and from field measurements. More realistic estimates of tunnelling-induced pile behaviour are possible if 3D numerical analyses with appropriate constitutive relations are adopted. However, such analyses are time-consuming compared to closed-form analytical methods.

Ground loss during tunnel excavation is an important factor which determines the displacement pattern around the tunnel. In practice, empirical methods derived from past experience are often used to estimate the ground loss. It is however important to have a rational method to estimate the ground loss values, considering such factors as soil conditions and tunnel boring methods.

Conventional "1g" laboratory static tests are not adequate to model the representative stress field during tunnel excavation. Centrifuge tests are a useful tool to model and assess the tunnelling-induced ground movements and their effects on adjacent pile foundations. The tunnel model used in a centrifuge test should represent the actual tunnel properties in prototype.

To date, research work on the effects of tunneling on piled foundations appears to be inadequate, and the main purposes of the present study are to develop a more reliable means of predicting pile responses to ground movements and to gain a better understanding of the behaviour of piles influenced by tunneling operations.

CHAPTER THREE

TUNNELLING-INDUCED GROUND MOVEMENTS - ANALYTICAL METHOD

3.1 INTRODUCTION

An accurate estimation of tunnelling-induced ground movements is one of the main problems in the design and construction of urban tunnels. Engineers responsible for the design and construction of tunnels must have some technique for estimating the ground movements as accurately as possible so that they can assess whether neighbouring buildings will be subject to excessive movements. Several approaches have been used for prediction of the ground deformations associated with tunnelling. There are three different categories of approaches, namely, empirical methods, numerical methods and finite element methods, that are commonly used in practice to estimate the ground deformations due to tunnelling. The selection of the appropriate method depends on the complexity of the problem. The details of these existing methods were described in Chapter 2.

The purposes of this chapter include the following:

- To establish a design chart to estimate the ground loss values from first principles using the configuration of the tunnel boring machine, tunnelling technique, and subsurface soil properties,
- To derive closed-form analytical solutions to predict the tunnelling-induced ground movements,
- To examine the applicability of the ground loss design chart and the analytical solutions via a study of some published case histories, and
- To compare analytical solutions with the results predicted from 3D numerical analyses.

3.2 GROUND LOSS

In general the ground loss during tunnel excavation is defined as a percentage of the ratio of the surface settlement trough volume and the tunnel volume per unit length. At present, the ground loss is obtained from empirical observations that do not always consider tunnelling methods and tunnel configuration. In reality, the ground loss values may vary, depending on the tunnelling methods, tunnel configuration, soil types, etc. The fact that such a variation in empirical observations exists suggests the need for a more logical approach to the estimation of the ground losses and thus the ground movement predictions due to tunnelling. In this study, the traditional method of estimating ground

loss is redefined as "Equivalent Ground Loss (EGL)" value based on the "gap parameter" (Rowe and Kack, 1983).

3.2.1 Determination of Equivalent Ground Loss

The estimated ground deformation pattern is greatly influenced by the ground loss parameter. The ground loss occurs in two stages: (i) loss in the undrained state, immediately after the passing of the tunnel head, and (ii) loss due to time-dependent consolidation and creep of the ground. The duration of gap (tail void) formation is short and may be regarded as occurring under the undrained condition. Thus, the release of stress causes the development of negative pore pressure in the soil around the tunnel and the negative pore pressure subsequently dissipates, resulting in an expansion of the soil. Therefore, the equivalent ground loss estimated using the gap parameter is only applicable to undrained conditions. The advantages in using the gap parameter in order to define the equivalent undrained ground loss parameter are; (i) the various construction methods and tunnelling equipment configurations can be considered, and (ii) elasto-plastic behavior of the soil can be incorporated.

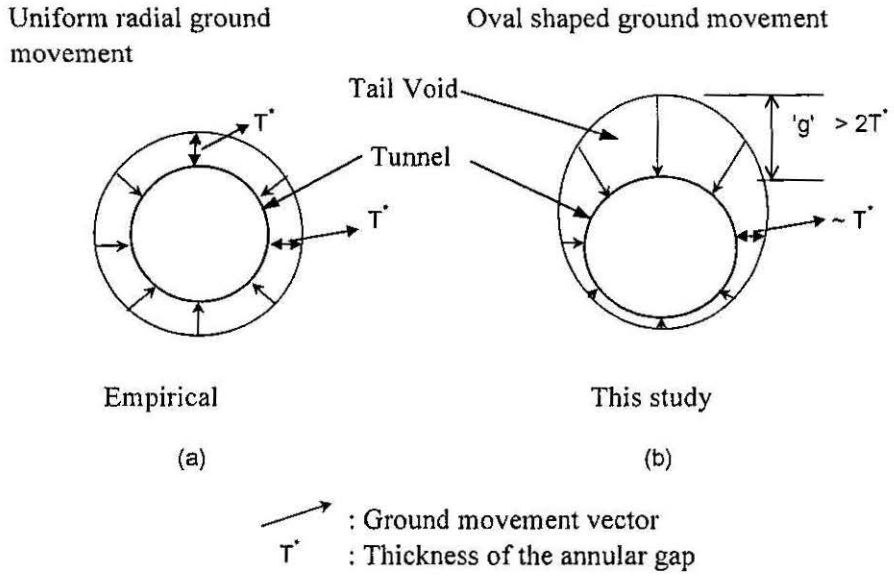

Figure 3.1: Circular and Oval-Shaped Ground Deformation Patterns around Tunnel Section

Excavation of the tunnel provides an opening into which the soil can deform. The movement of the soil into the opening can be related to the concept of "loss of ground,"

which is defined as the volume of material (whether through the face or radial encroachment over and around or behind the shield) that has been excavated in excess of the theoretical design volume of excavation. In empirical methods, the ground loss is assumed to be the result of uniform ground movement around the tunnel opening as shown in Fig. 3.1(a). In practice, as pointed out by Rowe and Kack (1983), the radial ground movement into the tunnel excavation is not uniform since the equivalent two dimensional (2D) gap (tail void) around the tunnel is noncircular (e.g., typically oval-shaped) as shown in Fig. 3.1(b). The possible reasons for the formation of an oval-shaped gap around the tunnel are: (1) tunnel operators advance the shield at a lightly upward pitch relative to the actual design grade to avoid the diving tendency of the shield; (2) the tunnel lining settles on the ground when the tail piece is removed; and (3) 3D elastoplastic movement of the soil occurs at the tunnel face.

In this study, the ground loss estimated assuming uniform radial ground movement (average ground loss) is denoted as ε_0. In practice, the soil movement around the tunnel is non-uniform (due to the oval-shaped gap), and the ground loss parameter representing an oval-shaped gap is defined as, $\varepsilon_{x,z}$. Therefore the equivalent average undrained ground loss (ε_0) is defined with respect to the gap parameter as shown in equation (3.1):

$$\varepsilon_0 = \frac{\pi(R+\frac{g}{2})^2 - \pi R^2}{\pi R^2} \cdot 100\% = \frac{4gR+g^2}{4R^2} \cdot 100\% \qquad (3.1)$$

where R = the radius of the tunnel, and g = the gap estimated as shown in Appendix A.

Before the formation of the gap, all the initial stresses in the soil are in equilibrium. The stresses around the tunnel are released in a non-uniform manner due to the oval-shaped gap geometry. The movements of the surrounding soil into the gap due to the stress release determine the ground deformation pattern. In the present study, the ground loss parameter obtained in equation (3.1) is further modified in order to incorporate the non-uniform radial movement of the soil around the tunnel, which basically influences the deformation pattern of the surrounding soil. The equivalent ground loss parameter ($\varepsilon_{x,z=0}$) which causes the surface settlement may be derived by adopting an exponential function for the average equivalent ground loss parameter (ε_0), that models the non-uniform movement of the soil around the tunnel, as shown in equation (3.2):

$$\varepsilon_{x,z=0} = \varepsilon_0 . B \ \exp\left(-Ax^2\right) \qquad (3.2)$$

where A, B are constants and ε_0 is the average equivalent ground loss as obtained from equation (3.1). Constants A and B are derived based on the boundary conditions described below.

When the portion of the soil above the tunnel crown touches the tunnel lining, the soil at the side of the tunnel displaces towards the bottom of the tunnel. Therefore, the upward movement of the soil below the tunnel is limited. Centrifuge model tests carried out by Stallebrass et al (1996) revealed similar results. In this study, it is assumed that about 75% of the vertical ground movement occurs within the upper annulus of the gap around the tunnel. Figure 3.2 shows the vertical ground movement influence zone where most of the soil displacements occur.

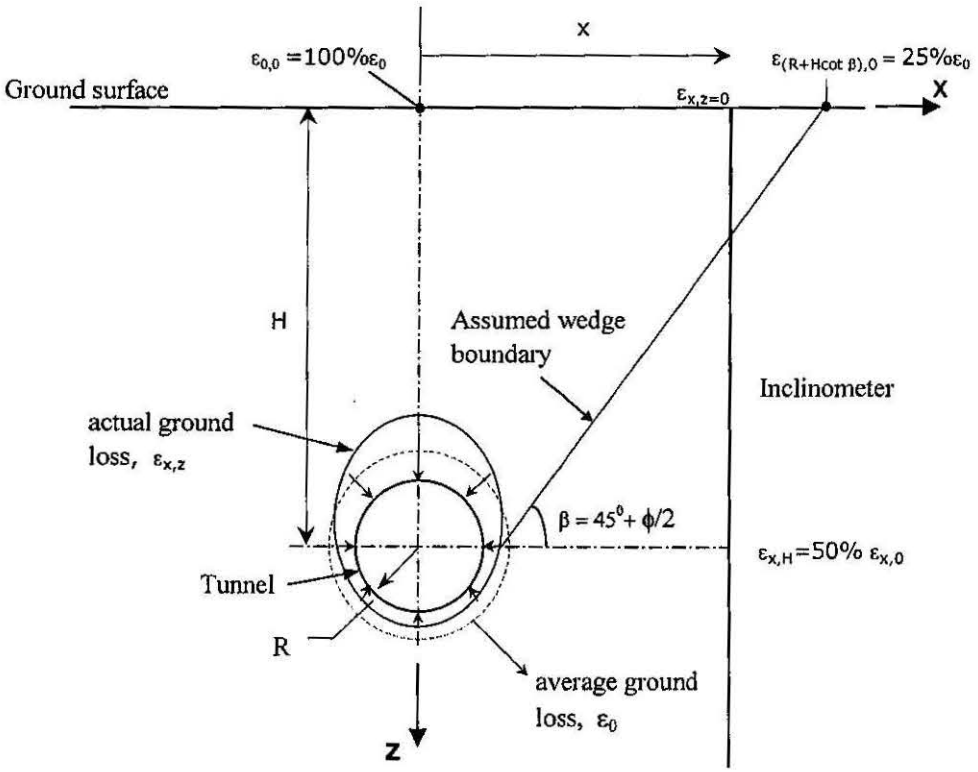

Figure 3.2: Ground Deformation Patterns and Ground Loss Boundary Conditions

The relationship between settlement trough width (which is an indirect measure of the ground movement influence zone) and the tunnel depth can be expressed as a vertical angle, β, drawn from the spring line of the tunnel to the width of the settlement trough at the surface. In sandy soil, the limit angle, β, is defined as $(45+\phi/2)$, where ϕ=angle of shearing resistance of the sand. For soft to stiff clay β may be assumed to be 45^0 based on the observations made by Cording and Hansmire (1975), i.e. it is assumed that the ground

movement occurs predominantly within the 45^0 wedge in between the ground surface and the tunnel. Therefore, it may be assumed that the surface settlement above the tunnel axis is the resultant of the complete cumulative equivalent average ground loss (100% ε_0) around the tunnel and the surface settlement at the horizontal distance (H+Rcotβ) is the resultant of partial cumulative equivalent average ground loss (25% ε_0). These boundary conditions are shown in Figure 3.2.

By applying these boundary conditions (refer Fig. 3.2) to equation (3.2), the equivalent ground loss component which models the non-uniform vertical movement is derived as shown in equation (3.3).

$$\varepsilon_{x,z=0} = \varepsilon_0 \exp\left[-\frac{1.38x^2}{(R+H\cot\beta)^2}\right] \tag{3.3}$$

The horizontal ground movement into the tail void or gap is a maximum at the spring line of the tunnel and is zero at the crown and the invert of the tunnel. Therefore, the lateral ground movement is symmetrical about the tunnel axis. The lateral movement component is incorporated in to the ground loss as shown in equation (3.4):

$$\varepsilon_{x,z} = \varepsilon_{x,z=0}.C \exp\left(-Dz^2\right) \tag{3.4}$$

where C and D are constants, derived on the basis of the boundary conditions described below.

It is assumed that the magnitude of the horizontal movement at the tunnel springline is approximately half of the vertical movement (g) at the tunnel crown (which causes 75% of the ground movement into the upper annulus of the oval shaped gap around the tunnel). Therefore, the equivalent ground loss component due to the horizontal movement at horizontal distance x and the depth H ($\varepsilon_{x,H}$) is approximately 50% of the equivalent ground loss causing surface settlement ($\varepsilon_{x,z=0}$) at horizontal distance x.

By applying these boundary conditions (refer Fig. 3.2) and substituting equation (3.3) in to equation (3.4), the modified equivalent ground loss parameter, incorporating the non-linear ground movement around the tunnel soil interface, may be defined as:

$$\varepsilon_{x,z} = \varepsilon_0 \exp\left\{-\left[\frac{1.38x^2}{(R+H\cot\beta)^2}+\frac{0.69z^2}{H^2}\right]\right\} \tag{3.5}$$

where H = the depth of the tunnel from the ground surface, and R = radius of the tunnel

In addition, $\varepsilon_{x,z}$ can also be interpreted as the equivalent ground loss component at the tunnel soil interface due to the ground movements at point (x, z).

3.2.2 Ground Loss Design Chart

The estimated ground deformation pattern is greatly influenced by the Ground Loss parameter. The ground loss occurs in 2 stages.

1. Undrained
2. Consolidation and creep.

Rowe and Lee (1992) proposed a procedure to estimate the ground loss parameter for the undrained condition. The components of loss of ground induced by tunnelling in cohesive soils are represented quantitatively by the so called gap parameters.
The undrained ground loss occurs in 3 stages.

1. Ahead of the face
2. Over the shield
3. Upon the erection of the lining.

The gap is the sum of the 3D elasto-plastic deformation at the tunnel face, over-excavation of soil around the periphery of the tunnel shield due to poor workmanship, and the physical gap that is related to the machine, shield, and lining geometry. The physical gap is determinable once the machine support system is chosen.

This gap parameter, g, can be used to estimate the case-specific ground loss parameter. Details are shown in Appendix A.

The undrained gap is estimated as shown in equation (3.6).

$$g = G_p + U^*_{3D} + \omega \tag{3.6}$$

U^*_{3D} is the equivalent 3D elasto-plastic deformation at the tunnel face. The volume of soil that intrudes into the tunnel face owing to pressure release at the face will eventually be excavated. There is a volume of lost ground equal to the amount of over excavated material at the face called the face loss, V_f.

G_p is the physical gap of the tunnel system given by $G_p = 2\Delta+\delta$ where Δ is the thickness of Tailpiece and δ is the clearance for erection of lining.

ω takes into account the quality of workmanship. This component includes the radial ground loss due to over cutting bead.

Estimation of ground loss based on the gap parameter, g, is shown in equation (3.1).

Based on the analytical results presented by Rowe and Lee (1992), and by combining equations (3.1) and (3.6), an attempt was made to produce charts to estimate the ground loss values. A parametric study was carried out to assess the influence of various soil and tunnel configuration parameters. Basic factors considered are: tunnel depth/tunnel diameter ratio, soil strength, earth pressure coefficient, soil unit weight, Poisson's ratio, internal air pressure applied during tunnelling, length of the shield, thickness of tail piece, clearance for erection of lining, maximum allowable excess pitch, bead thickness, and the grouting history.

The following dimensionless parameters were considered in the parametric study:

1. Stability Parameter, NP

$$NP = \frac{H\ \gamma - p_0}{c_u} \tag{3.7}$$

where H = depth of tunnel from the surface, γ = bulk unit weight if the soil, p_0 = total stress removed at the tunnel face, and c_u = undrained strength of the soil.

$$p_0 = (k_0' p_v' + p_w) - p_i \tag{3.8}$$

where k_0' = effective coefficient of earth pressure at rest, p_v' = vertical effective stress at the tunnel spring line, p_w = pore pressure at springline prior to excavation, and p_i = tunnel face supporting pressure.

2. Average undrained soil strength, c_u and undrained soil Young's Modulus, E_u; here it is assumed that $E_u = 400\ c_u$.

3. Physical gap parameter, PG

$$PG = t + \Delta + L\theta + t_b \tag{3.9}$$

where t = thickness of tail piece, Δ = clearance for the erection of lining, L = length of shield, θ = maximum allowable excess pitch, and t_b = thickness of cutter bead.

Since the stability parameter plays a major role (Mair et al, 1981) in the magnitude of the ground loss, the ground loss values are calculated for various NP values. The other parameters are then varied and the influence of each factor are estimated. The ground loss may be expressed as in equation (3.10):

$$\varepsilon_0 = \varepsilon_{NP} f_{cu} f_{PG} \tag{3.10}$$

where ε_{NP} = base ground loss component attribute to the stability factor, f_{cu} = undrained soil strength correction factor, and f_{PG} = physical gap parameter correction factor.

The ground loss component attributed to the stability number may be obtained from Figure 3.3.

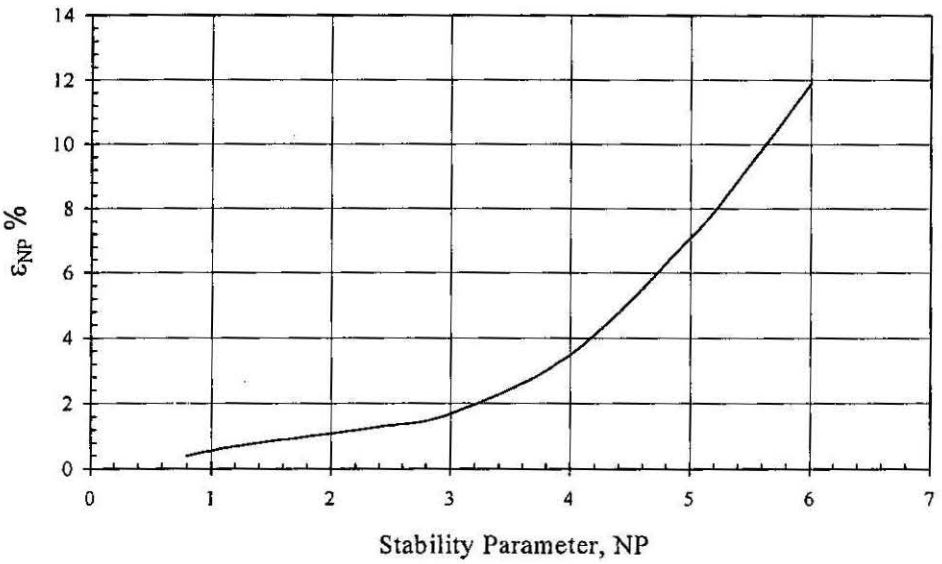

Figure 3.3: Ground loss component ε_{NP} % vs. Stability Parameter, NP

It is observed that the Poisson's ratio ν does not have any significant influence in the estimation of the ground loss. The Young's modulus of the ground is estimated using the relationship $400c_u$. The ground loss components corresponding to various ground stiffness (in terms of soil strength) are calculated and the correction factor for soil strength f_{cu} is calculated as shown in equation (3.11):

$$f_{cu} = \frac{\varepsilon_{cu}}{\varepsilon_{NP}} \tag{3.11}$$

The ground loss correction factor variation with c_u is shown in Figure 3.4.

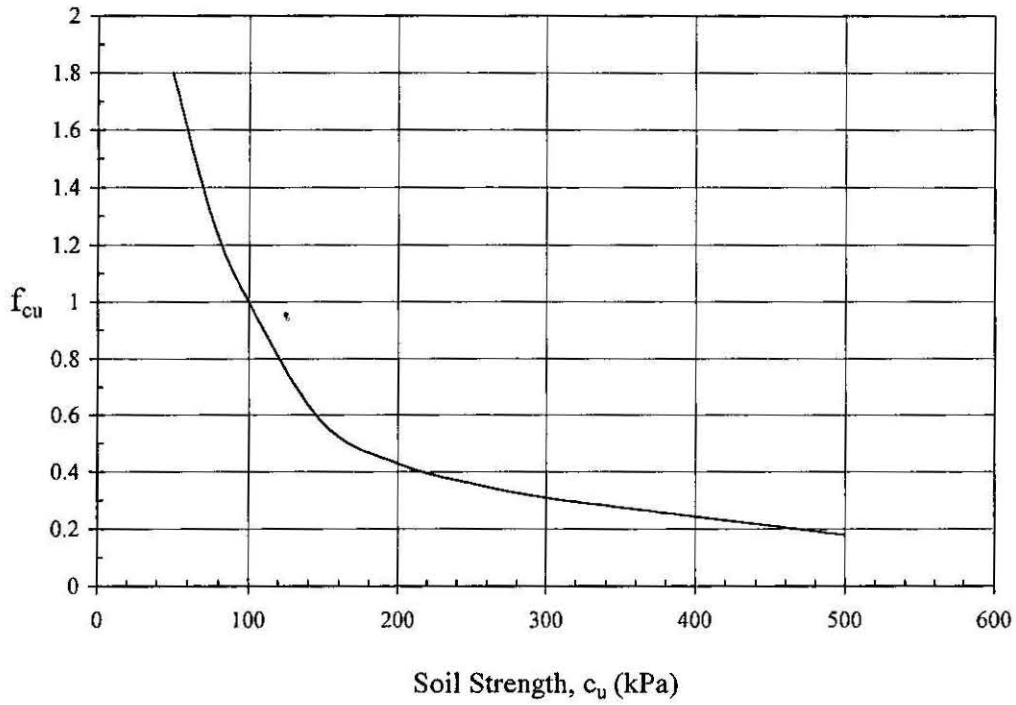

Figure 3.4: Ground Loss Correction Factor vs. Soil Strength, c_u

Similarly, the ground loss correction factors for the physical gap parameter, f_{PG}, is shown in Figure 3.5.

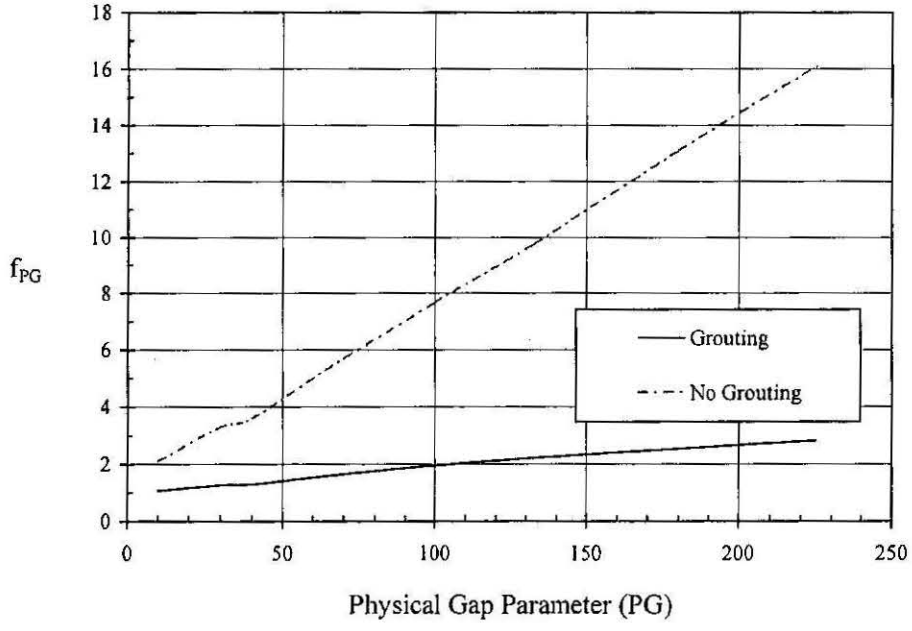

Figure 3.5: Ground Loss Correction Factor vs. Physical Gap Parameter

3.3 SURFACE AND SUBSURFACE SETTLEMENTS

A closed form solution has been presented by Verruijt and Booker (1996) for the estimation of the ground settlement due to a uniform radial ground loss, as shown in equation (3.12):

$$U_z = -\varepsilon R^2\left(\frac{z_1}{r_1^2}+\frac{z_2}{r_2^2}\right)+\delta R^2\left(\frac{z_1(kx^2-z_2^2)}{r_1^4}+\frac{z_2(kx^2-z_2^2)}{r_2^4}\right)$$
$$+\frac{2\varepsilon R^2}{m}\left(\frac{(m+1)z_2}{r_2^2}+\frac{mz(x^2-z_2^2)}{r_2^4}\right)-2\delta R^2 h\left(\frac{x^2-z_2^2}{r_2^4}+\frac{m}{m+1}\frac{2zz_2(3x^2-z_2^2)}{r_2^6}\right) \quad (3.12)$$

where, ε = uniform radial ground loss as shown in Figure 3.1a, δ = long term ground deformation due to the ovalization of the tunnel lining, $z_1 = z - H$, $z_2 = z + H$, $r_1^2 = x^2 + z_1^2$, $r_2^2 = x^2 + z_2^2$, R and H are tunnel radius and depth, $m = 1/(1-2\nu)$, $k = \nu/(1-\nu)$, and ν = soil Poisson's ratio.

It has been found that equation (3.12) under-predicts maximum settlements and gives a much wider settlement trough when compared with empirical methods and field measurements. The reasons for this observation are; (i) actual soil behavior is non-linear, and exhibits some elements of plastic behavior, and (ii) empirical ground loss values, which imply a uniform radial ground movement at the tunnel soil interface, may not be realistic.

Equation (3.12) has been modified in order to accommodate the newly defined ground loss parameter that incorporates the non-linear ground movement around the tunnel soil interface. Since this study is concerned only with short-term undrained conditions, the ground deformations due to ovalization may be neglected (δ=0). By combining equations (3.5) and (3.12), the modified formula for the prediction of surface settlement can be expressed as:

$$U_{z=0} = \varepsilon_0 R^2 . \frac{4H(1-\nu)}{H^2+x^2} . \exp\left\{-\frac{1.38x^2}{(H\cot\beta+R)^2}\right\} \quad (3.13)$$

A comparison of the settlements predicted by equation (3.12) and the modified equation (3.13) is shown in Figure 3.6 for the Heathrow Express Trial Tunnel configuration and for soil parameters reported by Deane and Bassett (1995) (refer to Table 3.2). The modified equation (3.13) gives a narrower surface settlement trough than the original Verruijt and Booker equation.

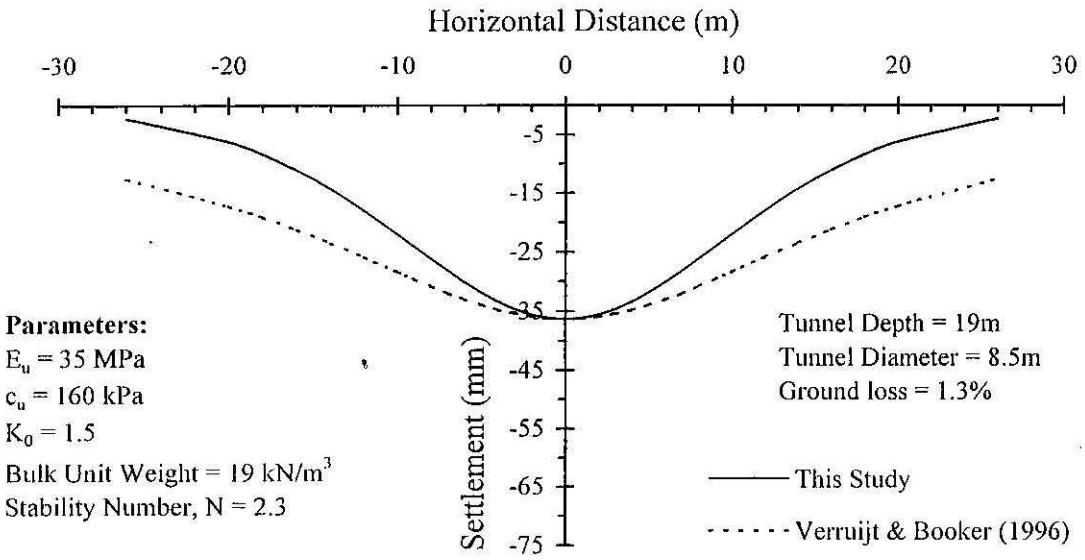

Figure 3.6: Comparison of Surface Settlements Predicted by Proposed Formula and Verruijt & Booker Formula.

In empirical methods, the trough width (i) is considered as an important parameter in the determination of the surface settlement trough. The relationship between normalized i/R and H/2R parameters for the proposed analytical solution is obtained as described below:

Equation (3.13) can be written in the following form;

$$U_{z=0} = A\frac{H}{x^2 + H^2}Exp(-Bx^2) \tag{3.13a}$$

where, $A = 2\varepsilon_0 R^2 \frac{m+1}{m}$ and $B = \frac{1.38}{(H\cot\beta + R)^2}$

The maximum slope, $\frac{du}{dx}$, of the settlement trough will be at x = i (trough width).

Therefore, $\frac{d^2u}{d\,x^2} = 0$ at x = i

The resulting equation after double differentiation is:

$$2B^2i^6 + (4B^2H^2 - B)i^4 + (3 - 2BH^2 + 2B^2H^4)i^2 - (BH^4 + H^2) = 0 \tag{3.14}$$

The settlement trough width parameter, i, for various R and H values can be obtained by solving the equation (3.14). The following correlation was derived to estimate the settlement trough width parameters.

$$\frac{i}{R} = \frac{1.15}{(\tan\beta)^{0.35}}\left(\frac{H}{2R}\right)^{\frac{0.9}{(\tan\beta)^{0.23}}} \tag{3.15}$$

The settlement trough width parameter obtained from equation 3.15 is compared with various empirical methods in Table 3.1.

Table 3.1: Comparison of Trough Width

Tunnel Depth/Diameter (H/D)	Settlement Trough Width, i				
	This Study	Mair et al (1983)	Sagaseta (1987)	O'Reilly & New (1982)	Clough & Schmidt (1981)
18/6 (=3)	9.3	9.0	10.3	8.8	7.2
16/4 (=4)	8.0	8.0	9.2	8.0	6.1
25/5 (=5)	9.8	10.0	11.5	9.7	7.2
18/3 (=6)	8.7	9.0	10.3	8.8	6.3

The predictions made using equation (3.15) are in good agreement with the values predicted by Mair et al (1983) and O'Reilly and New (1982).

The following equation obtained from equations (3.5) and (3.12), gives the modified sub-surface settlement profiles:

$$U_z = \varepsilon_0 R^2\left(-\frac{z-H}{x^2+(z-H)^2}+(3-4\nu)\frac{z+H}{x^2+(z+H)^2}-\frac{2z[x^2-(z+H)^2]}{[x^2+(z+H)^2]^2}\right) \cdot\exp\left\{-\left[\frac{1.38x^2}{(H\cot\beta+R)^2}+\frac{0.69z^2}{H^2}\right]\right\} \tag{3.16}$$

Figure 3.7 shows a comparison of the maximum sub-surface settlements predicted using equation (3.16) and equation (3.12) for a typical tunnel configuration. The modified equation (3.16) gives a smaller displacement at depth than the original Verruijt and Booker equation.

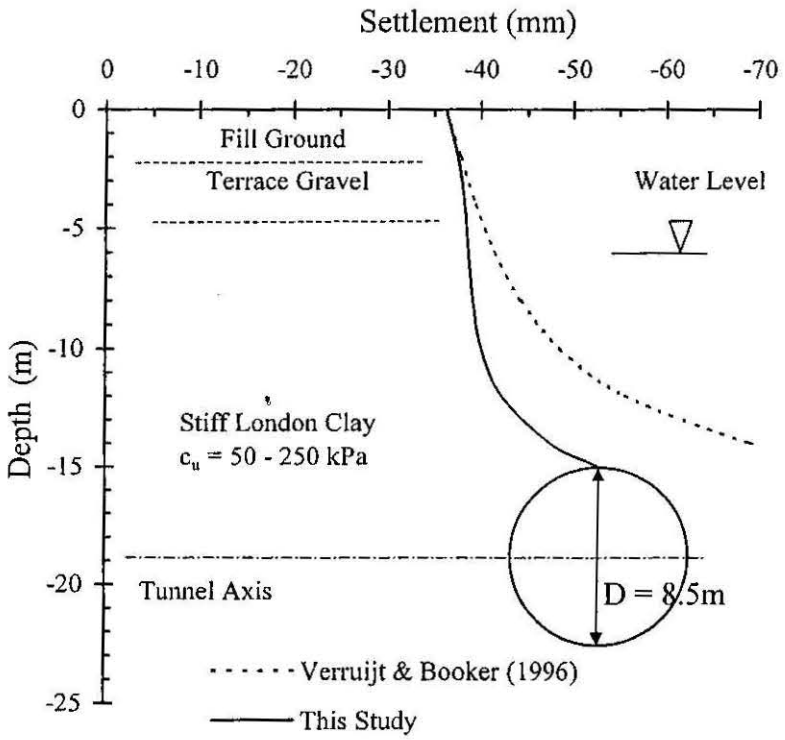

Figure 3.7: Comparison of Sub-surface Settlements Predicted by Proposed Formula and Verruijt & Booker Formula

3.4 LATERAL DEFORMATION

The closed form solution to predict horizontal movements, proposed by Verruijt and Booker (1996), is shown in equation (3.17):

$$U_x = -\varepsilon R^2\left(\frac{x}{r_1^2}+\frac{x}{r_2^2}\right)+\delta R^2\left(\frac{z_1(x^2-kz_1^2)}{r_1^4}+\frac{x(x^2-kz_2^2)}{r_2^4}\right) - \frac{2\varepsilon R^2 x}{m}\left(\frac{1}{r_2^2}-\frac{2mzz_2}{r_2^4}\right)-\frac{4\delta R^2 xh}{m+1}\left(\frac{z_2}{r_2^4}+\frac{mz(x^2-3z_2^2)}{r_2^6}\right) \tag{3.17}$$

Assuming δ=0 for the undrained condition, and substituting equation (3.5) in equation (3.17), the modified formula for the prediction of the horizontal ground movements around a tunnel may be given as:

$$U_x = -\varepsilon_0 R^2 x\left[\frac{1}{x^2+(H-z)^2}+\frac{3-4\nu}{x^2+(H+z)^2}-\frac{4z(z+H)}{(x^2+(H+z)^2)^2}\right] \cdot\exp\left\{-\left[\frac{1.38x^2}{(H\cot\beta+R)^2}+\frac{0.69z^2}{H^2}\right]\right\} \tag{3.18}$$

where z = the depth measured from the ground surface, and x = the lateral distance, from the tunnel axis, of the point where the horizontal movement is required. Figure 3.8 shows the comparison of the lateral movements predicted using equations (3.18) and (3.17) for a typical tunnel configuration. The present approach gives a similar horizontal movement distribution to the original equation, but the actual magnitudes of the movement are smaller, by factor of about 2, at the level of the tunnel axis.

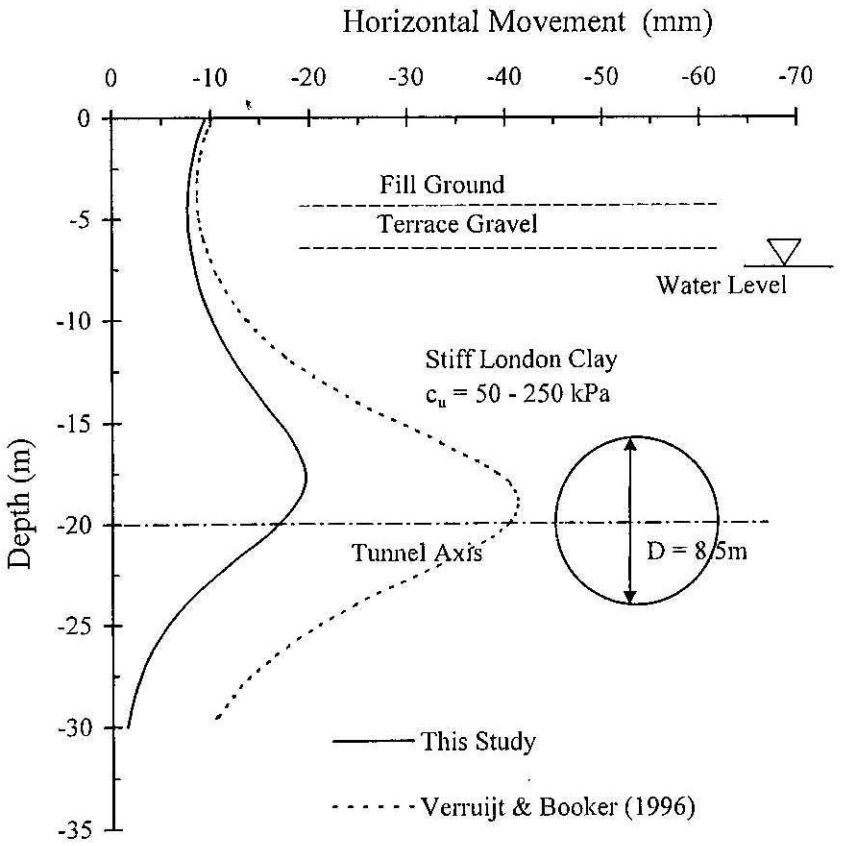

Figure 3.8.- Comparison of Lateral Deformation Predicted by Proposed Formula and Verruijt & Booker Formula
Lateral distance, x = 6m

3.5 CASE STUDIES

3.5.1 Introduction

A total of nine case histories encompassing soft to stiff clay and sandy soils have been selected in this study to assess the applicability of the proposed analytical solutions to real situations. All but one of the case histories considered in this study have been previously published by various authors. The ground loss values were reassessed using gap parameters, as described in Appendix A, for the first five cases where the tunnels

were constructed in soft to stiff clay. Table 3.2 shows the tunnel details, subsurface soil profiles, and gap parameters estimated using the theoretical method proposed by Rowe and Lee (1992)(Appendix A) for the first five cases (tunnels in clayey soil).

A total of two case histories (Cases 6 & 7), previously published by other authors and involving tunnelling in sandy soil, have been selected in this study to assess the applicability of proposed formula for sandy soils. In both cases soil strengths are reported in terms of SPT 'N' values. In this study, the angle of shearing resistance ϕ has been obtained by using the relationship reported by Kishida (1964), as shown in equation (3.19).

$$\phi^0 = \sqrt{20N} + 15^0 \tag{3.19}$$

Table 3.3 shows the tunnel details and subsurface soil profiles for both cases.

Case 8 shows the applicability of the proposed formulae to the centrifuge test results published by Taylor et al (1998).

3.5.2 CASE 1: Heathrow Express Trail Tunnel, UK

Heathrow Express is a high-speed rail link from central London to Heathrow Airport. The 8 km of 5.6m diameter running tunnels were designed using traditional open face tunnelling shields with rings of expanded precast concrete segments providing the permanent lining. The construction of the trial tunnel was started on site in February 1992 and was completed in early June. Deane and Bassett (1995) have presented a summary of the tunnel details and the field measurements.

The equivalent ground loss estimated using the proposed method in this study is about 1.36% which is almost same as the empirical ground loss value reported (1.2-1.3%) by Deane and Bassett (1995). The predicted undrained surface settlement profile and the observed surface settlement are plotted in Figure 3.9.

The predicted surface settlements are in good agreement with the observed settlement. Figure 3.10 shows the predicted maximum sub-surface settlement and measured field profiles with depth. The trends (curvatures) of both predicted and measured profiles are very similar although the maximum sub-surface settlements are slightly under-predicted by the proposed analytical method.

Table 3.2.- Tunnel, Soil Details and Estimated Gap and Ground Loss Values

No.	Case	Soil Type	H/D	GAP, g (mm)	Ground Loss, (%)		References
					This Study (Equivalent)	Reported (Empirical)	
1	Heathrow Express Trail Tunnel, UK	0-2m Fill ground, 2-4m Terrace gravel, > 4m Stiff London Clay (C_u=50-250kPa)	19/ 8.5	58	1.4	1.3	Deane and Bassett (1995)
2	Thunder Bay Tunnel, Canada	0-8m Silty sand with occasional clay seams, 8-13m soft to firm clay (C_u=30-60kPa), 13-25m firm to stiff clay (C_u >60kPa)	10.7/2.47	164	13.7	5.5	Palmer and Belshaw (1980), Rowe and Lee (1992)
3	Green Park Tunnel, UK	0-2m sand and gravel, >2m stiff fissured clay (C_u=50-250kPa)	29.4/4.14	34	1.6	1.3	Attewell and Farmer (1974), Rowe and Lee (1992)
4	Barcelona Subway Network Extension Tunnel, Barcelona	Red and Brown clay with some gravel (C_u=30-150kPa)	10.0/8.0	31	0.8	1.2	Ledesma and Romero (1997)
5	Bangkok Sewer Tunnel, Thailand	0-12m very soft to soft clay (C_u ~15-25kPa), 12-25m stiff clay (C_u ~50kPa), 25-35m fine sand, >35m very stiff silty clay	18.5/2.66	81	6.2	6.0	Phienwej (1997), Ramasamy (1992)

Table 3.3: Tunnel Details and Soil Profiles for Cases of Tunnels in Sands

Case No.	Name and Location	Tunnel depth / Diameter	Soil Profile
6	Taipei Transit System Tunnel, Taipei	18.5/6	0 - 4m: Fill and silty CLAY 4 - 17m: Silty SAND, SPT "N" = 5 - 15 17 - 21m: Silty CLAY, SPT "N" = 5 - 11 > 21m: Silty SAND, SPT "N > 15
7	Grouholz Tunnel, switzerland	12.3/11.6	0 - 12m: Dense fine to medium SAND, SPT "N" = 25 - 35 > 12m: Dense SILT, SPT "N" > 50

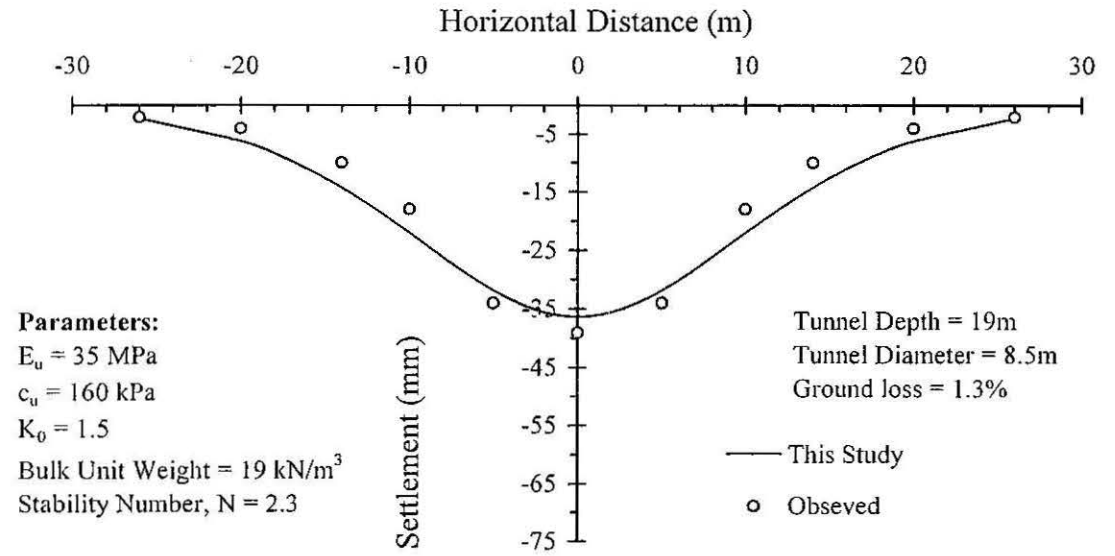

Figure 3.9: Observed and Predicted Surface Settlement- Case1: Heathrow Express Trial Tunnel (Field Data Based on Deane and Bassett, 1995)

Figures 3.11(a) and 3.11(b) compare the predicted and observed horizontal ground movements at inclinometer locations 6m and 9m away from the tunnel axis. The observed and predicted horizontal movements at an inclinometer location about 6m away from the tunnel center axis (Figure 3.11(a)) are in good agreement, but the proposed

analytical method under-predicts the horizontal movements below the tunnel axis at the inclinometer location about 9m away from the tunnel axis (Figure 3.11(b)).

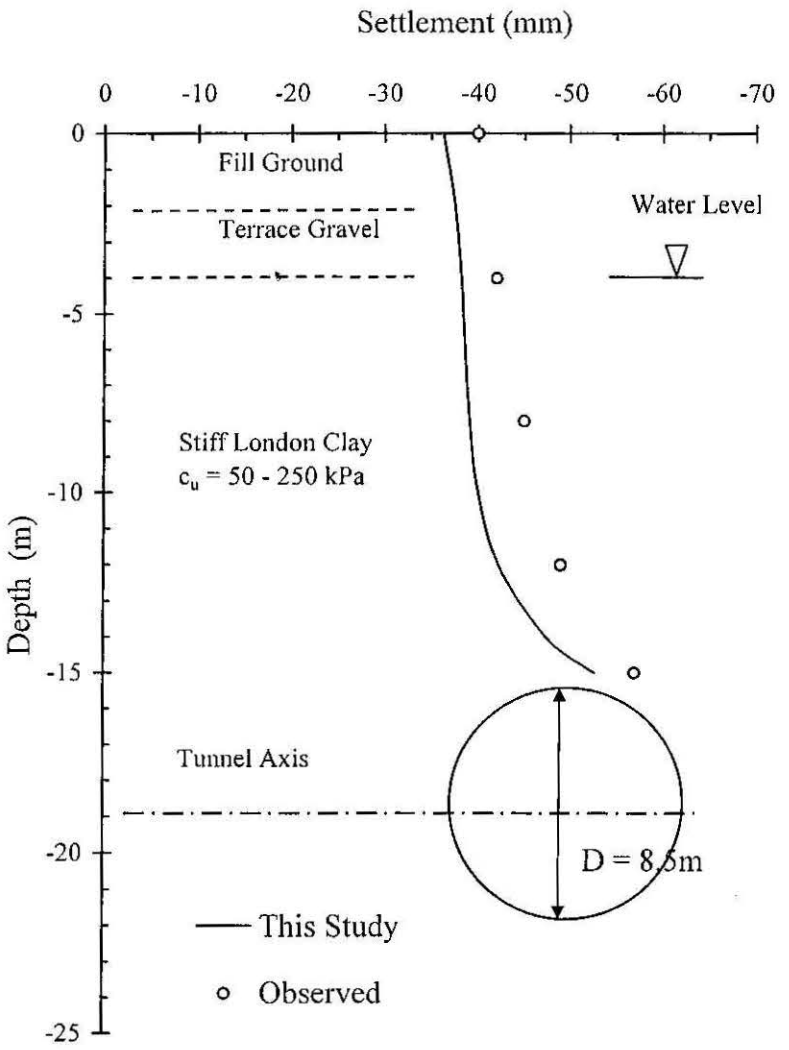

Figure 3.10: Observed and Predicted Sub-surface Settlements above the Centreline - The Heathrow Express Trial Tunnel (Field data based on Deane and Bassett, 1995)

3.5.3 CASE 2: Thunder Bay Tunnel, Canada

A 3.3km long and a 2.16m diameter section of the sanitary trunk sewer tunnel in the city of Thunder Bay, Ontario was constructed in 1976. The tunnel was constructed through soft clay soil using a tunnel boring machine together with a segmented precast concrete tunnel lining. The details of tunnel construction, soil conditions and the tunnel dimensions were published elsewhere by Palmer and Belshaw (1978).

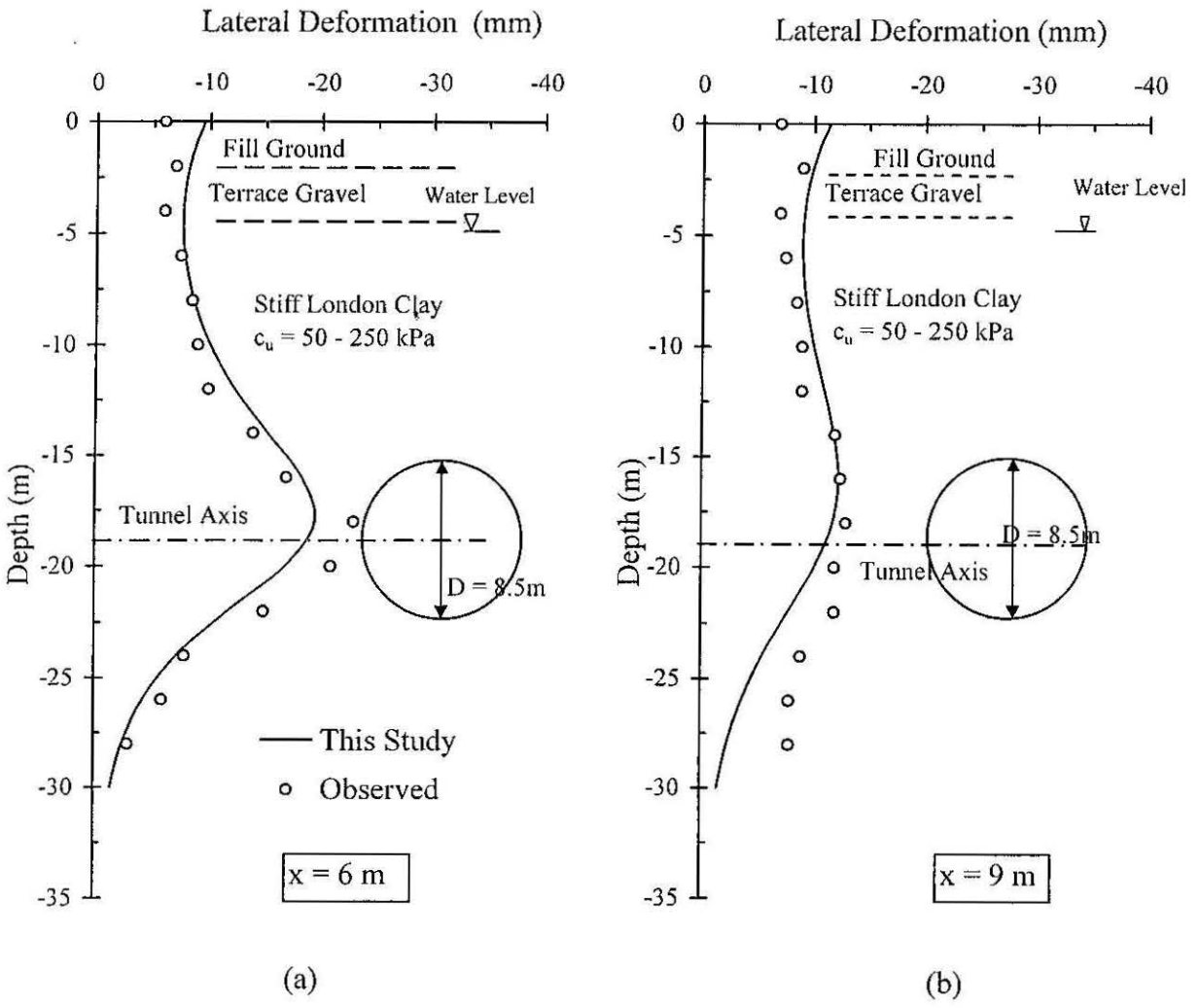

Figure 3.11: Obsrved and Predicted Horizontal Displacements- Case 1: Heathrow Express Trial Tunnel (Field Data Based on Deane and Bassett (1995))

The equivalent ground loss estimated using the modified method is about 14%, which is significantly higher than the reported ground loss of 5.5%. The 3-D elasto-plastic face loss, which is significant in soft clay tunnelling, may have contributed to the higher ground loss estimation. The predicted settlement trough is wider than the field measurements, as shown in Figure 3.12. The excess movement of yielded soft clay into the upper annulus of the gap around the tunnel may have caused the unusually large maximum settlement observed at the surface.

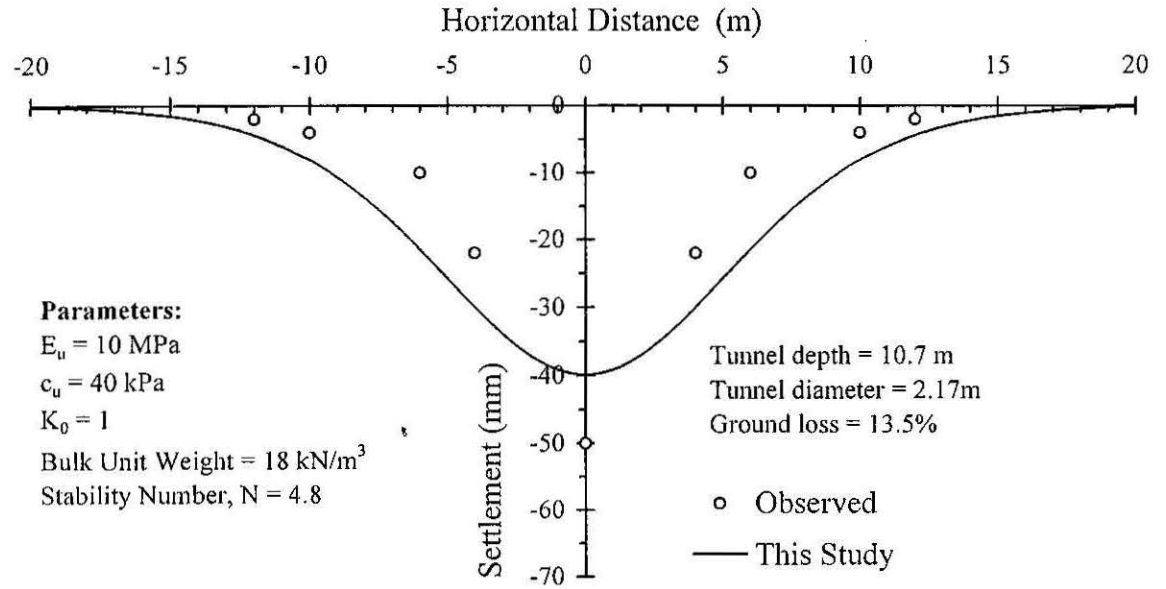

Figure 3.12: Observed and Predicted Surface Settlement - Case 2: Thunder Bay Tunnel (Field data based on Lee and Rowe, 1992)

Figure 3.13 shows that the proposed analytical solution under-predicts maximum subsurface settlements slightly, but the trends of both predicted and observed profiles are very similar.

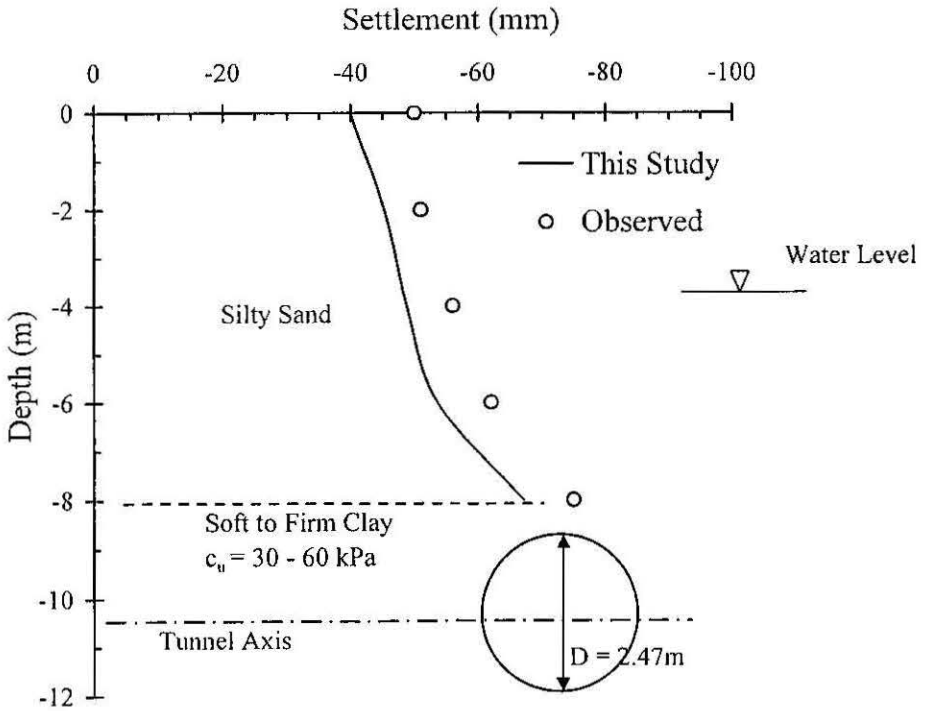

Figure 3.13:- Observed and Predicted Sub-surface Settlements above the Centreline - Thunder Bay Tunnel (Field data based on Lee and Rowe, 1992)

The horizontal movements predicted and observed at an inclinometer location about 2.2m away from the tunnel axis are shown in Figure 3.14 The predicted horizontal movements below the tunnel axis are in good agreement with the field measurements. However, the presence of a sandy soil layer above the tunnel may have contributed to the less satisfactory agreement between the predicted and observed horizontal movements above the tunnel axis.

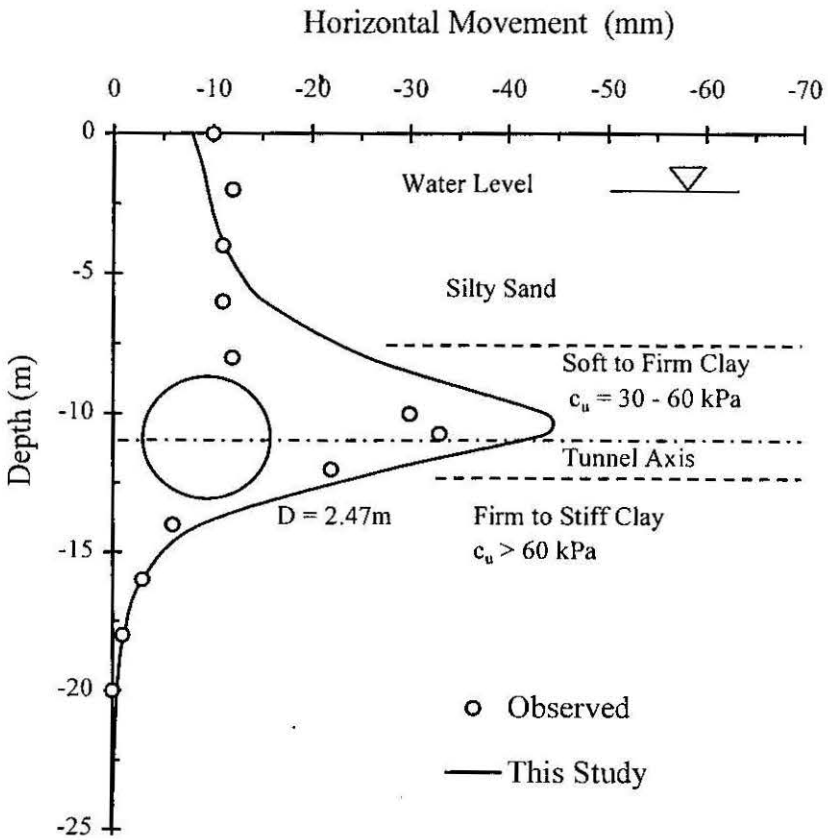

Figure 3.14:- Observed and Predicted Horizontal Displacement, 2.2m away from the Tunnel Centerline - Thunder Bay Tunnel (Field data based on Belshaw and Palmer, 1978)

3.5.4 CASE 3: Green Park Tunnel, UK

This case involved a 4.15m diameter shield driven tunnel running about 29.3m below in stiff, fissured, heavily over consolidated London clay. The tunnel was mined by hand excavation. The tunnel details, soil parameters and field measurements are based on Attewell and Farmer (1974).

The equivalent ground loss estimated using the modified method is about 1.6% which is similar to the reported empirical ground loss of 1.3%. The predicted and observed surface settlements are in good agreement as shown in Figure 3.15. Comparison of the predicted and measured maximum subsurface settlements is shown in Figure 3.16, which also shows good agreement.

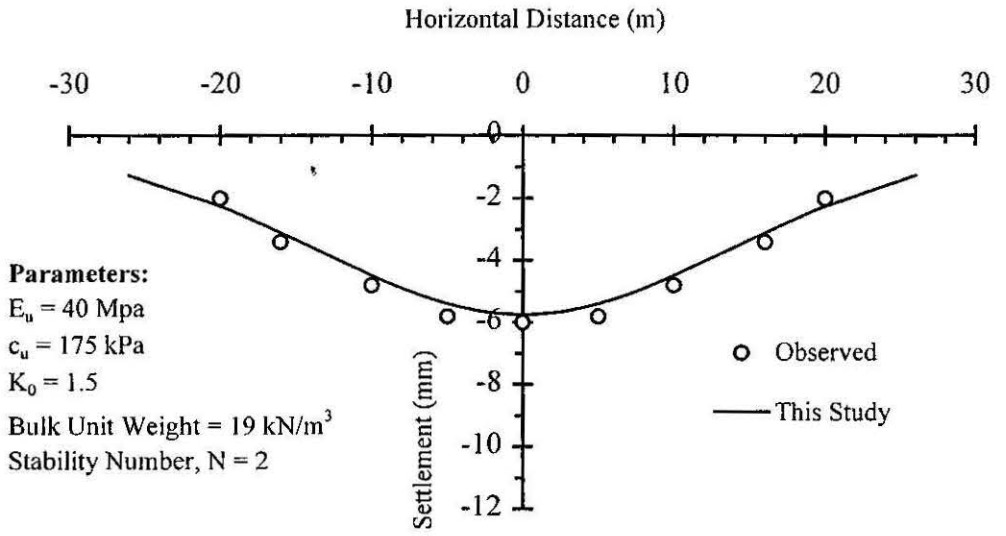

Figure 3.15: Observed and Predicted Surface Settlement - Case 3: Green Park Underground (Field data based on Attewell and Farmer, 1974).

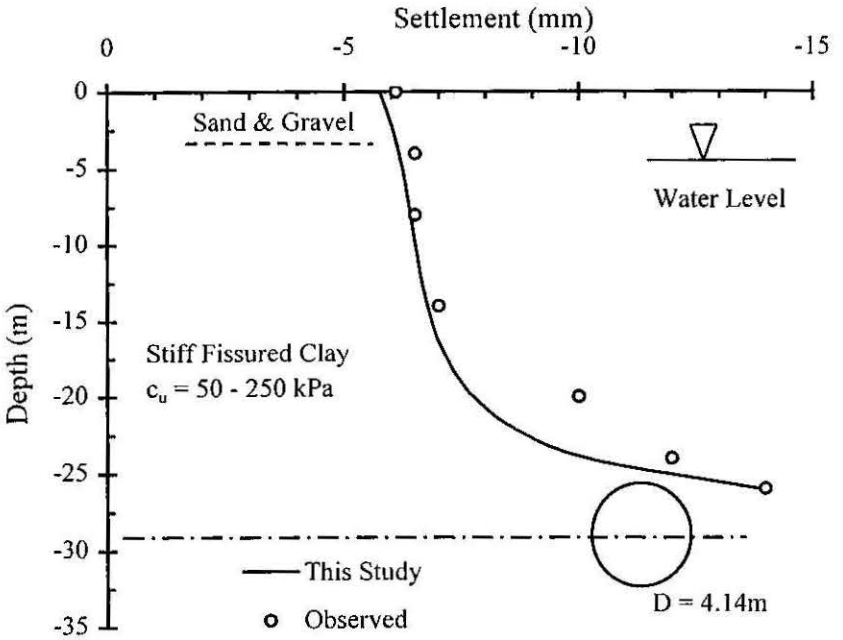

Figure 3.16: Observed and Predicted Sub-surface Settlements above Centreline - Green Park Underground (Field data based on Rowe and Lee, 1992)

3.5.5 CASE 4: Barcelona Subway Network Extension, Barcelona

An 8m diameter subway network tunnel was built in 1993 in Barcelona. The tunnelling details, soil parameters and field measurements are based on Ledesma and Romerio (1997). A few instrumented control sections were installed including surface surveying markers and inclinometers. The soil type is predominantly red clay with sand and gravel.

The equivalent ground loss parameter estimated using the proposed method (0.8%) is of the same order as the reported empirical ground loss (1.2%). Figure 3.17 shows that the predicted and observed surface settlements are in good agreement. Inclinometer measurements were not available to enable assessment of the predicted horizontal movements.

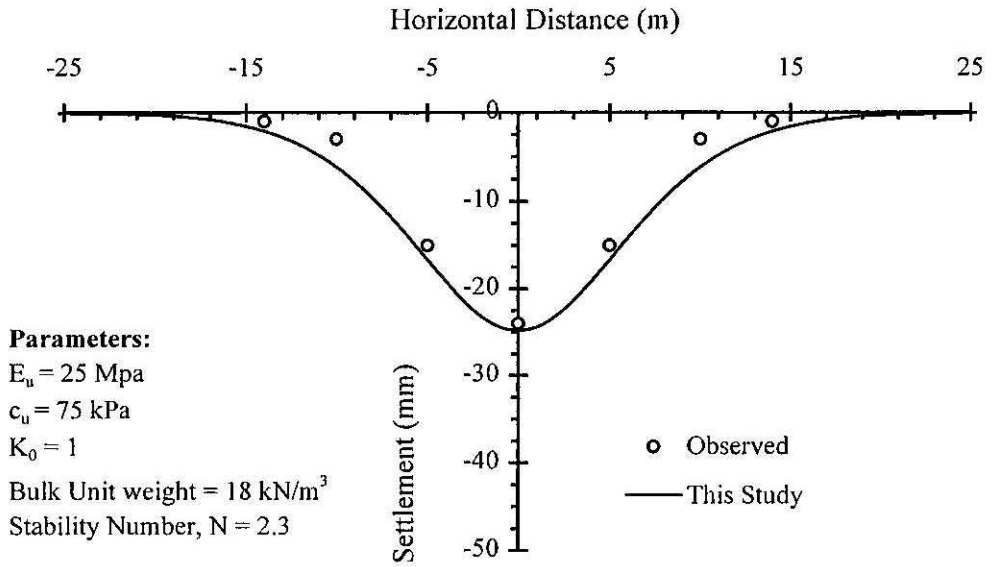

Figure 3.17: Observed and Predicted Surface Settlement - Case 4: Barcelona Subway Network (Field data based on Ledesma and Romero, 1997)

3.5.6 CASE 5: Bangkok Sewer Tunnel, Thailand

The Bangkok sewer tunnel is a part of the GT-N-6 water transmission project undertaken by Bangkok Metropolitant Water Works Authority. The length of the tunnel is about 2.2km from Ratchadaphisek drop structure to Phahonyothin riser structure. A semi-mechanical backhoe and hand mining method was used in the excavation. Primary and secondary grouting and a short stretch of chemical grouting were applied for quick setting. The soil parameters, tunnel dimensions and field measurements were published by Phienwej (1997) and Ramasamy (1992).

The equivalent ground loss estimated using the present proposed method (6.2%) is almost the same as the reported empirical ground loss (6%). Figure 3.18 shows good agreement between the predicted and observed surface settlements. The horizontal movements predicted and measured at the inclinometer location about 4m away from the tunnel axis are shown on Figure 3.19. Predicted and observed horizontal movements agree reasonably well, except at the tunnel axis, where the proposed method over-predicts the horizontal movements by about 25%.

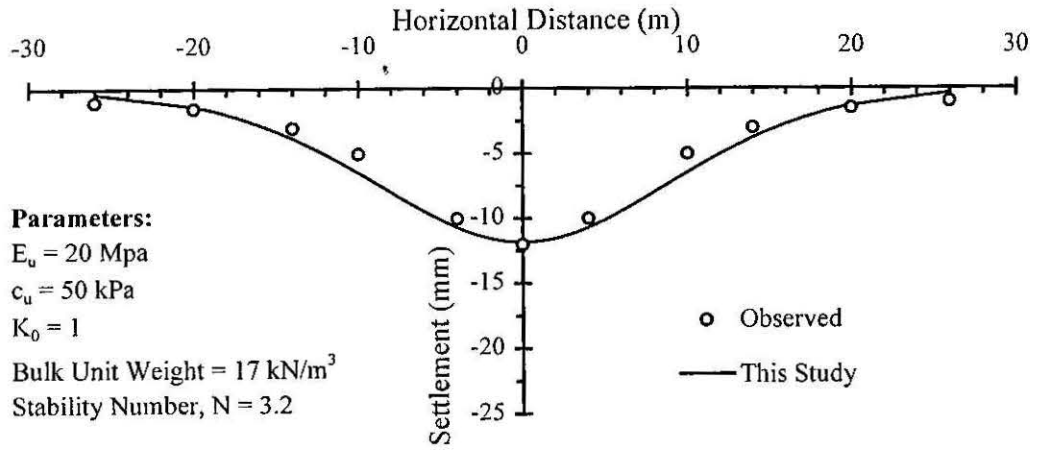

Figure 3.18: Observed and Predicted Surface Settlement - Case 5: Sewer Tunnel, Bangkok (Field data based on Ramasamy and Phienwej, 1992)

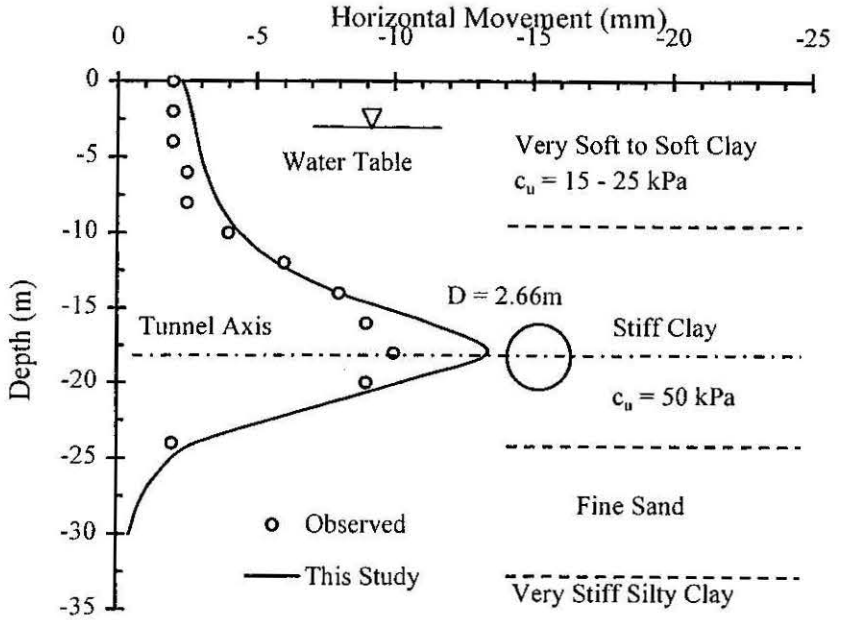

Figure 3.19: Observed and Predicted Horizontal Displacement, 4m away from the Tunnel Centreline - Case 5: Sewer Tunnel, Bangkok (Field data based on Ramasamy and Phienwej, 1992)

3.5.7 CASE 6: Taipei Transit System, Taipei

The first phase of the Taipei Rapid Transit Systems, the so-called Priority Networks, consists of six lines. Most tunnels linking the stations are constructed by shield tunnelling, with a few sections constructed by using the cut-and-cover method. Generally speaking, the Taipei Basin is underlain by thick layer of alluvium which is in turn underlain by a thick layer of the Chingmei Formation. The detailed soil profile is given in Table 3.3. The details of tunnel dimensions, ground loss values and instrumentation were obtained from Moh et al (1996).

Figure 3.20 shows the comparison of the predicted and measured surface settlement troughs for the reported average ground loss value of 1.4%, while Figure 3.21 shows the predicted and measured sub-surface settlement trough at 10m below ground level. In general, the predicted settlement troughs are in good agreement with field measurements. The maximum sub-surface settlement measured at 10m below the ground surface is slightly larger than the predicted maximum settlement at the tunnel centerline.

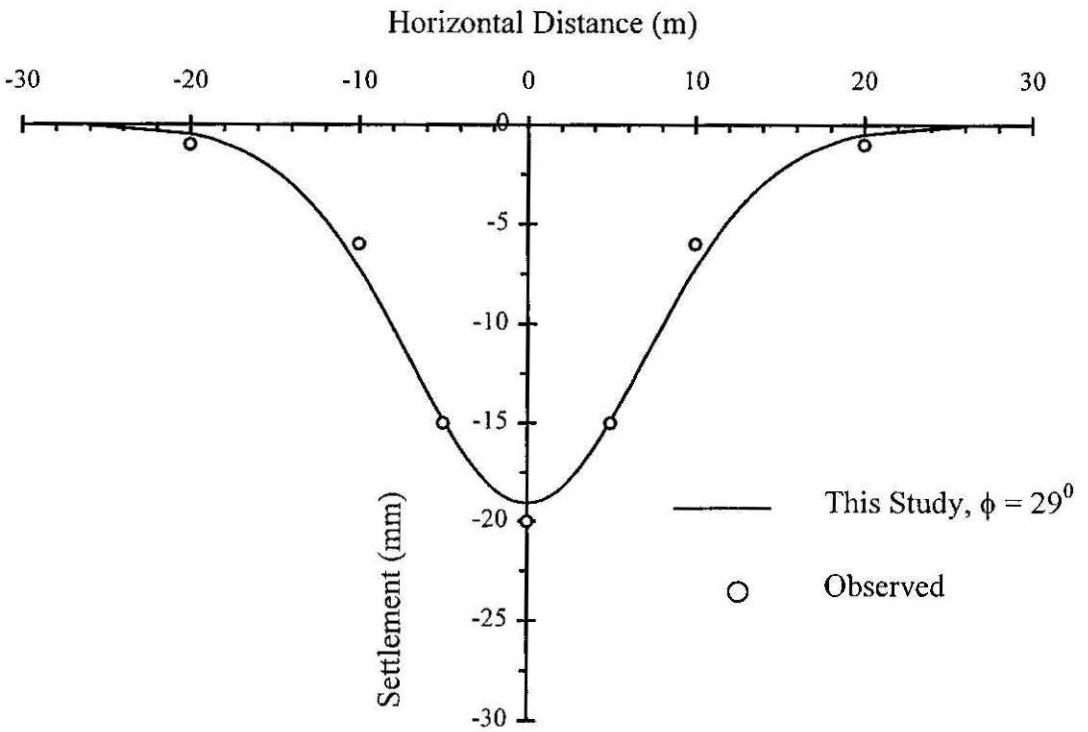

Figure 3.20: Observed and Predicted Surface Settlement - Case 6: Taipei Transit System, Taipei, GL = 1.4% (Field data based on Moh et al, 1996)

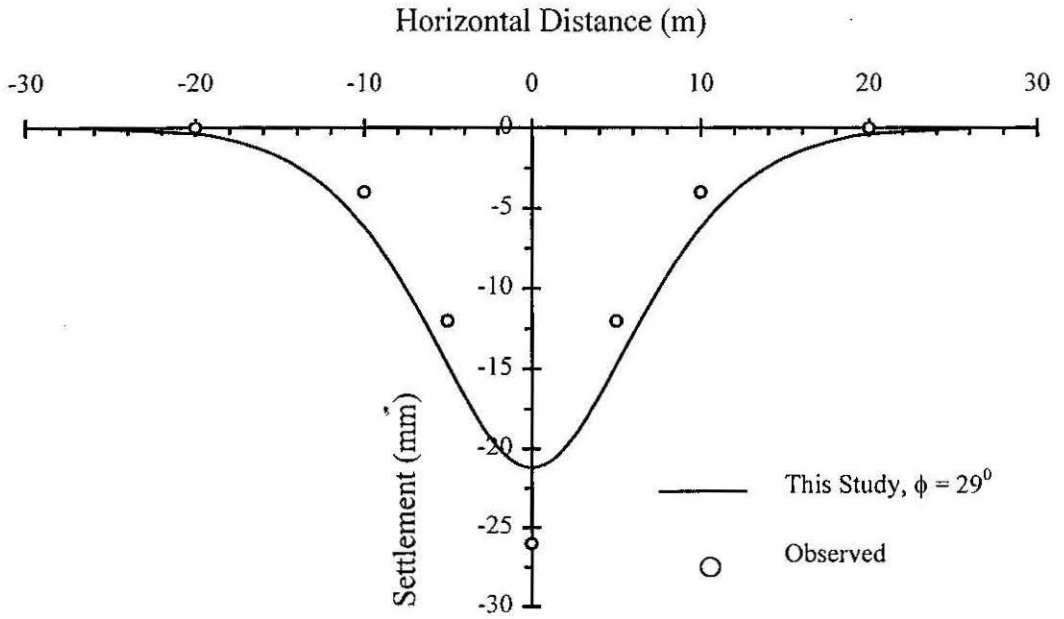

Figure 3.21: Observed and Predicted Sub-surface Settlements at z=10m, Case 6: Taipei Transit System, Taipei (Field data based on Moh et al, 1996)

3.5.8 CASE 7: Grauholz Tunnel, Switzerland

A 11.6m diameter, 5.5 km long mined section of the Grauholz tunnel has been constructed through heterogeneous glacial soils and tertiary bedrock. The detailed soil profile of the tunnel section considered is given in Table 3.3. More details may be obtained from Steiner (1997).

Figure 3.22 shows the surface settlement trough predicted for the reported average ground loss value of 1%, compared with the observed values. The predicted surface settlement trough is in good agreement with the field measurements.

3.5.9 CASE 8: Centrifuge Model Testing, City University, UK

Grant and Taylor (1996) investigated ground movements above a tunnel in layered soil by performing a centrifuge model test at City University in London. The ground loss was simulated by reducing support pressure within the model tunnel over a short period for which undrained conditions should have prevailed. The transverse surface and subsurface settlements were measured using low-voltage displacement transducers (LVDT). Figures 3.23 and 3.24 show the measured and predicted normalised transverse surface and subsurface settlement troughs.

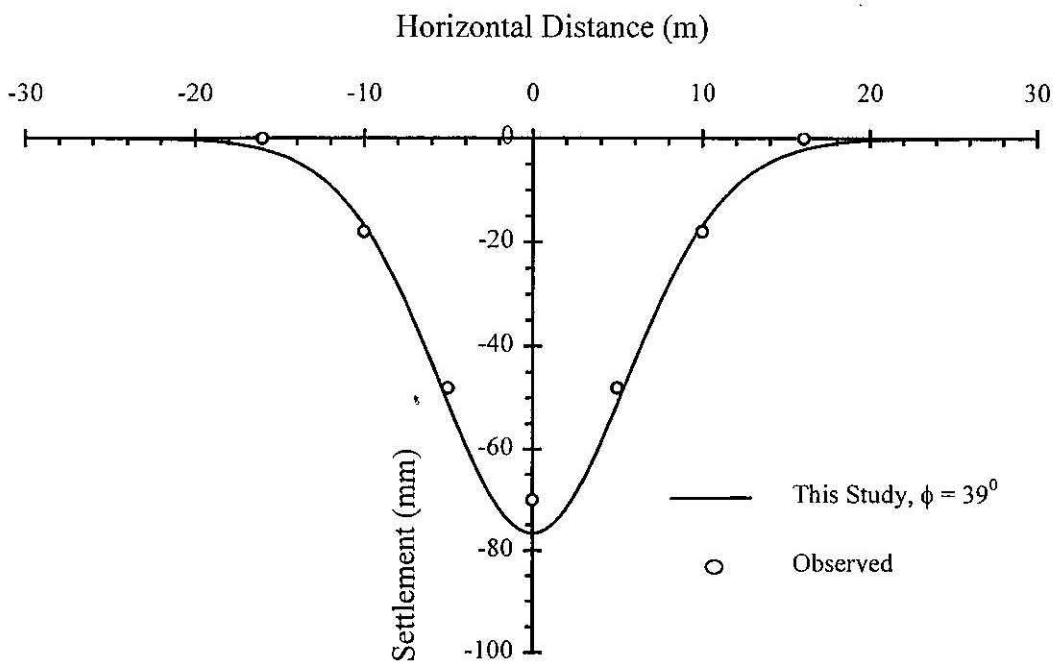

Figure 3.22: Observed and Predicted Surface Settlements, Case 7: Grauholz Tunnel, Switzerland (Field data based on Steiner, 1997)

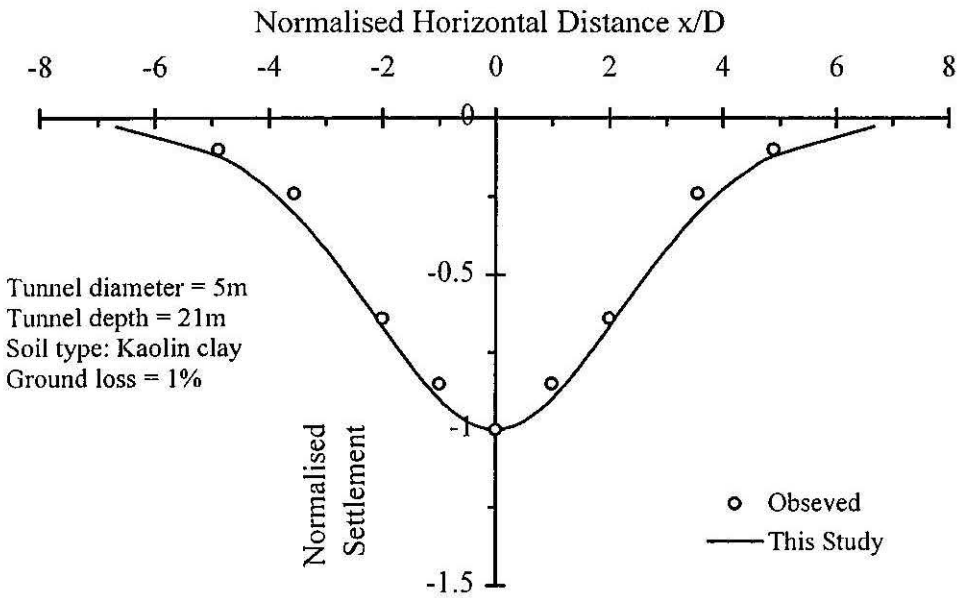

Figure 3.23: Measured and Predicted Surface Settlements, Case 8: Centrifuge Model Testing, UK (Test data based on Grant and Taylor, 1996)

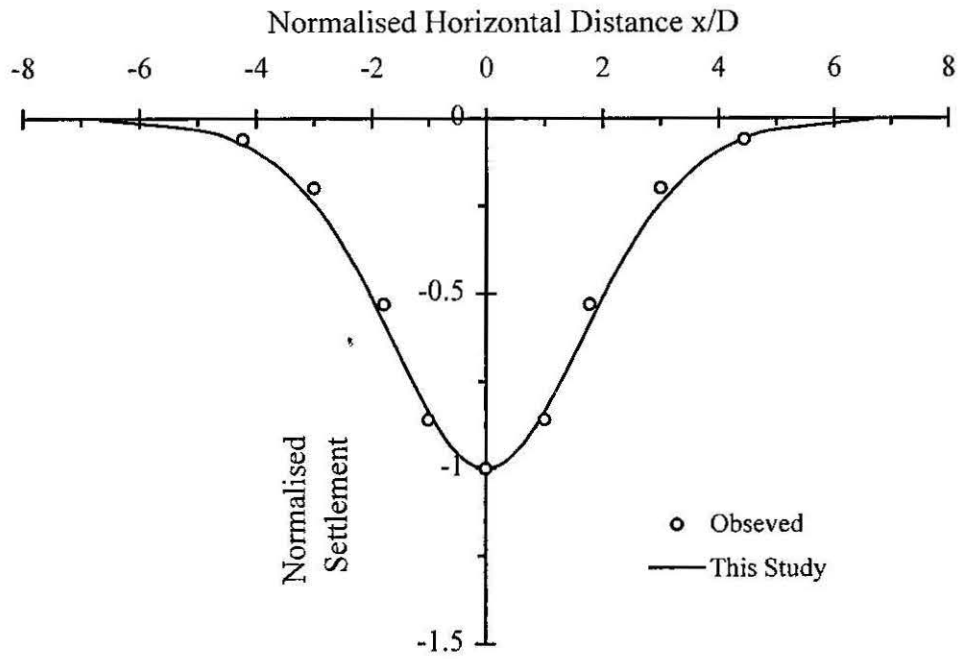

Figure 3.24: Measured and Predicted subsurface Settlements, Case 8: Centrifuge Model Testing, UK (Test data based on Grant and Taylor, 1996)

The predicted surface and subsurface settlement troughs are in good agreement with the results obtained from the centrifuge test.

3.5.10 CASE 9: Airport Link, Sydney, Australia

The New Southern Railway (NSR) in Sydney, Australia, involves the excavation of approximately 10 km of single bore tunnel from Tempe Reserve, Tempe, to Princes Alfred Park (PAP). PAP is located just south of Central Railway Station in Sydney's Central Business District (CBD). From Tempe Reserve the alignment takes the tunnel under Sydney Airport including the main north/south runway. Sydney Airport is approximately 8 km south of CDB.

Approximately 6 km of the 10 km tunnel is in soft ground (clays and sands) and it has been excavated by a 10.7 m external diameter Herrenknect slurry Tunnel Boring Machine (TBM). TBM parameters used in this study to estimate the ground loss are given in Table 3.4.

Table 3.4: TBM Parameters Used in Ground Loss Estimation

Method	Slurry tunnel boring
Length of Shield, L	10 m
Thickness of tail piece, t	50 mm
Clearence for errection of lining, Δ	35 mm
Maximum allowable excess pitch, θ	0
Bead thickness, tb	20 mm (full circle)
Skin grouting	Yes

The ground loss value for a typical section MP 7550 was estimated using the design charts presented in Section 3.2.2 and the soil parameters presented in Table 3.5.

Table 3.5: Soil Parameters, Section MP 7550

Location	B5-Runway I6, MP 7550
Depth, H	30.2 m
Diameter, D	10.7 m
Soil type	Alluvial Clay, A5
Poisons ratio, ν	0.5
Undrain Strength, c_u	120 kPa
Earth pressure coefficient, K_0	0.6
Unit weight, γ	20 kN/m^3
Depth of water table (from surface)	1 m
Slurry pressure, p_l	453 kPa

The ground loss, ε_0, estimated from the proposed design chart was 0.4%. Comparisons of predictions made using this ground loss value and the measured values are shown in Figure 3.25. The finite element (FEM) predictions presented in Report: 14.TR, by Transfield Bouygues JV are also incorporated.

It may be observed from Figure 3.25 that the measured settlement are smaller than the predictions using the method proposed in this study and FEM analysis. The maximum settlement predicted by FEM and the proposed method are almost the same. Unlike in the previous case histories, the measured surface settlement trough is flat and wide. Since the maximum measured settlement was only 4mm, there is a possibility of not insignificant measurement error associated with these field measurements.

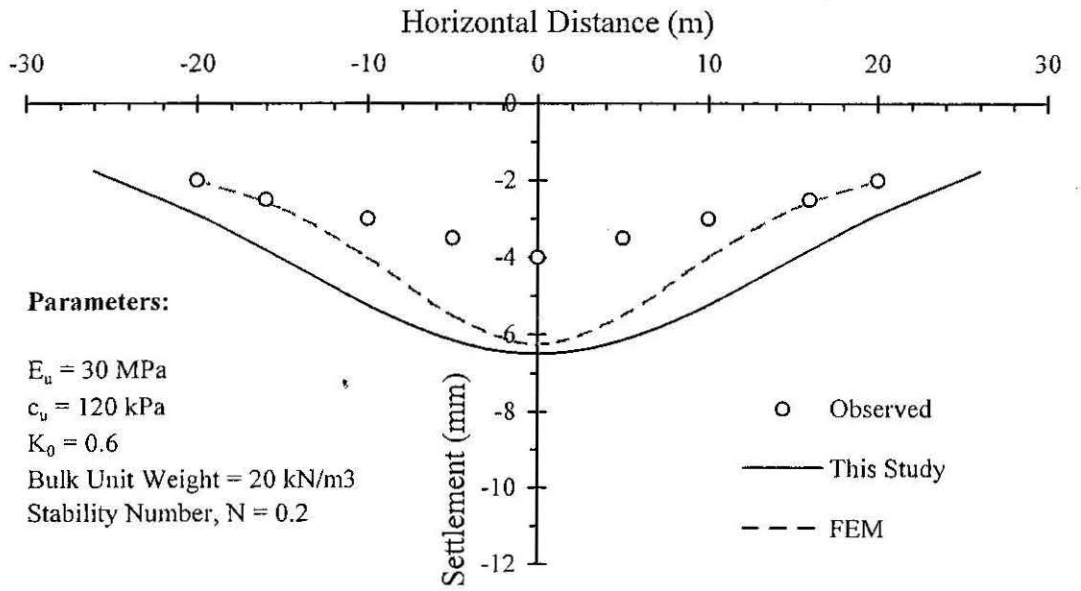

Figure 3.25: Measured and Predicted subsurface Settlements, Case 9: Airport Link, Sydney, Australia (Field measurements and FEM predictions based on Report: 14.TR.205, Transfield Bouygues JV, 1999)

Similar predictions were carried out for few other sections MP5530, MP6920, MP7750, MP8060 and MP8600. Only centerline settlements were measured for these sections and therefore it is not possible to make any comparisons with the settlement trough predicted using equation (3.13). Table 3.6 shows the estimated ground loss values using the proposed design charts, the maximum settlement predicted using equation (3.13), and the measured settlements measured at the surface above the centreline of the tunnel.

Table 3.6 shows that the maximum settlements predicted using ground loss values estimated from the proposed design charts compare reasonably well with the measured maximum surface settlements above the tunnel centreline. The differences observed in predicted and measured values may be due to the existance of a mixture of interbedded sand and clay layers.

The tunnel was partially excavated through a sandstone layer in sections MP5530, MP6925 and MP8600. The ground loss design charts over-predict the ground loss values for tunnels partially excavated through the sandstone layer and therefore the settlements predicted were slightly higher than the measured settlements.

It may be observed that ground loss values estimated for all six sections were less than 1% due to the slurry shield tunnelling method used in this project. At section MP8600, a negative ground loss, and therefore a heave in the ground surface was observed, due to excessive slurry pressure applied on the tunnel face.

Table 3.6: Estimated Ground Loss Values and Comparisons of Settlement predicted and measured.

Tunnel Section	Tunnel Depth (m)	Soil Profile	Estimated Ground Loss (%)	Measured Settlement (mm)	Predicted Settlement (mm)
MP5530	20	0 - 18m: Dune deposit 18 - 20m: Alluvial & residual clay > 20m: Sandstone	0.29	4.0	7.6
MP6925	16	0 - 14: Sandy soil 14 - 20: Alluvial clay > 20: Sandstone	0.55	16.0	17.2
MP7750	25	0 - 7: Sandy soil 7 - 30-: Alluvial clay > 30: Sandstone	0.56	5.0	9.4
MP8060	20	0 - 8: Sandy soil 8 - 32: Clay/sand mixed layer > 32: Sandstone	0.31	8.0	7.7
MP8600	20	0 - 13: Sandy soil > 13: Sandstone	-0.11	-4.0	-2.7

3.6 NUMERICAL STUDY

3.6.1 Introduction

Chapter 4 describes predictions from detailed numerical analyses and their comparisons with tunnelling-induced ground deformations and their effects on adjacent pile foundations. In order to maintain the completeness of this chapter, numerical predictions of tunnelling-induced ground deformations and their comparisons with the proposed analytical solutions are presented in this section.

3.6.2 3D Finite Element Results (PECPLAS 3D)

Reported numerical predictions using a 3D finite element computer programme, PECPLAS 3D (Mroueh, 1998) were compared with the prediction made by equation 3.13, as shown in Figure 3.26. The details of PECPLAS 3D are given in Chapter 4.

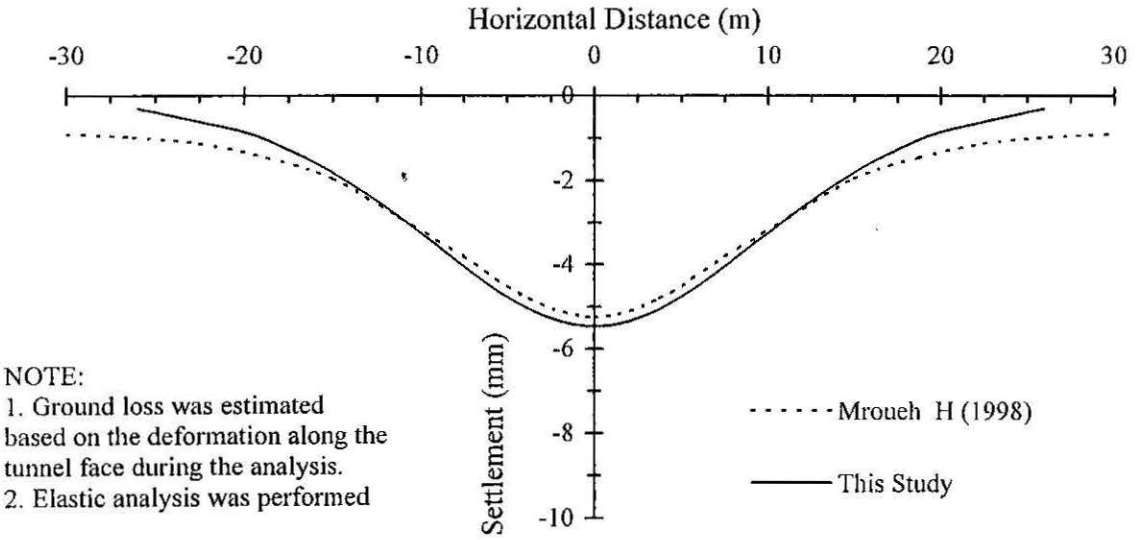

Figure 3.26: PECPLAS 3D Prediction vs. Prediction Using Equation 3.13 (Ground loss = 0.26%, Tunnel depth = 18.75m, Tunnel diameter = 7.5m)

The comparison shows that the maximum settlement predicted by both methods is almost the same. However, the settlement trough predicted by PECPLAS 3D is slightly wider than the prediction by equation 3.13.

3.6.3 3D Finite Difference Analysis (FLAC 3D)

FLAC 3D is a three-dimensional explicit finite-difference programme for engineering mechanics computation (Itasca, 1997). Details of this programme are described in Chapter 4. Three different analyses namely, elastic, Mohr-Coulomb ($K_0 = 0.5$) and Mohr-Coulomb ($K_0 = 1$) were carried out using FLAC 3D for a 6m diameter tunnel located 15m below ground. Comparisons were made for a ground loss value of 1%. Figure 3.27 shows the comparison of surface settlement troughs predicted using FLAC 3D and using equation 3.13. Material properties are given in Table 4.1.

The comparison shows that the elastic analysis slightly underestimates the maximum settlement and also results in a wider settlement trough. A similar observation was made in relation to the PECPLAS 3D prediction shown in Figure 3.26. The surface settlement

trough predicted using elastic analysis and Mohr-Coulomb analysis for $K_0 = 0.5$ were almost identical whereas the Mohr-Coulomb analysis for $K_0 = 1$ overestimats the maximum surface settlement and also results in a narrower trough width. From the above observations, it may be inferred that the differences in predictions are due to the difference in in-situ stress state. This further suggests that the tunnelling-induced ground movements for low ground loss values, typically 1%, may be predominantly elastic.

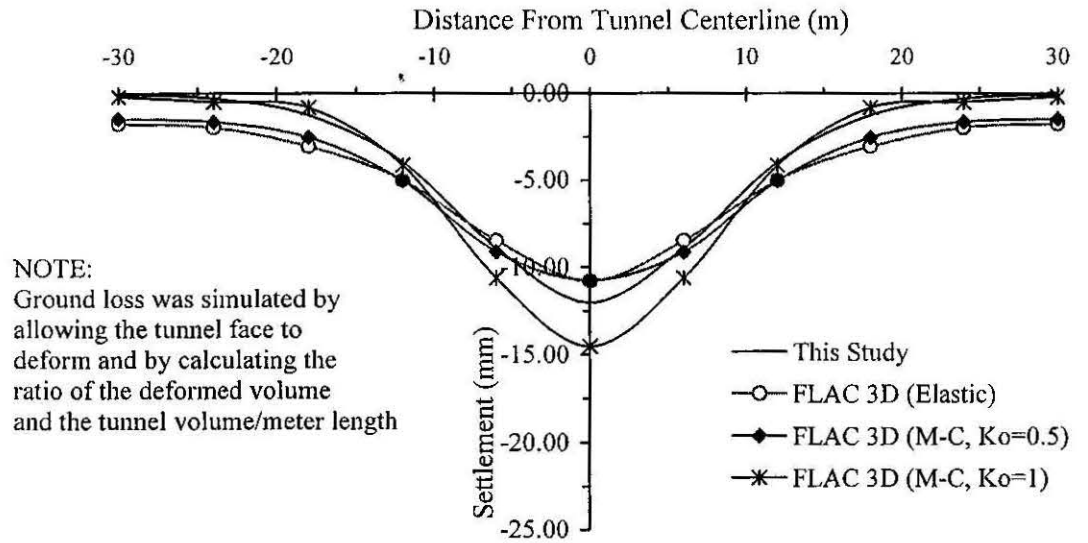

Figure 3.27: Surface Settlement Trough Predictions using FLAC 3D and Equation 3.13.

Figure 3.28 shows similar comparisons of the estimated subsurface settlement along the tunnel centreline using FLAC 3D and using equation 3.16. It may be observed that although elastic analysis slightly underestimats surface settlement, the maximum subsurface settlements predicted at the tunnel crown by elastic analysis and equation 3.16 are almost the same. Subsurface settlements predicted by Mohr-Coulomb analyses for $K_0 = 0.5$ and $K_0 = 1$ show insignificant increase with depth, except in the vicinity of the tunnel crown. Predictions using the elastic analysis give a reasonably good match with the equation 3.16.

Figure 3.29 shows the comparison of lateral deformations predicted by FLAC 3D and those using equation 3.18. It may be observed that the Mohr-Coulomb analysis results in more lateral deformation at the tunnel axis and an insignificant lateral deformation above the tunnel.

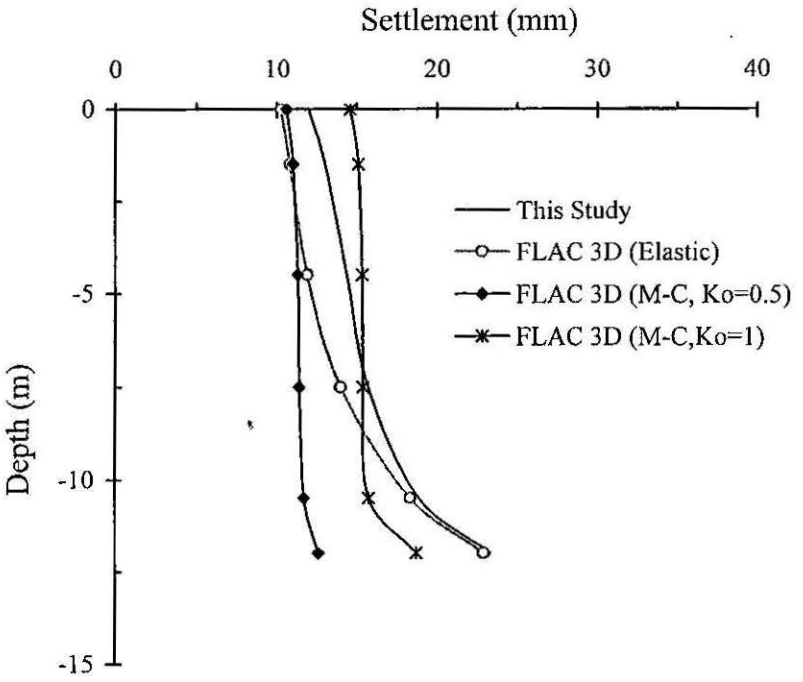

Figure 3.28: Sub-surface Settlements Predicted Along the Tunnel Centreline

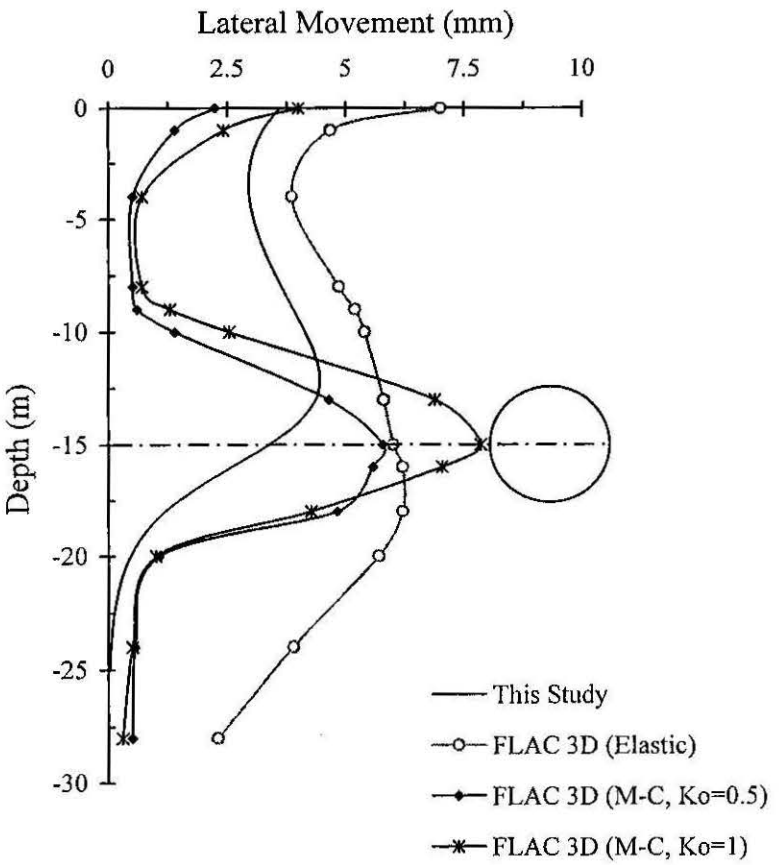

Figure 3.29: Lateral Deformation Predictions @ horizontal distance 5.0m

In contrast, the elastic analysis and equation 3.18 show considerable lateral deformation above the tunnel. Elastic predictions show large lateral deformation below the tunnel whereas equation 3.18 predicts insignificant lateral deformation below the tunnel. The maximum lateral deformation predicted at the tunnel axis using elastic analysis and Mohr-Coulomb analysis for K_0=0.5 are almost the same. In conclusion, it may also be noted that lateral deformation predictions are more inconsistent than the other predictions.

3.7 SUMMARY

In this Chapter, analytical solutions are proposed to predict tunnelling-induced ground movements around a tunnel in soft ground. In addition, a design chart to estimate the tunnelling-induced ground loss is also developed. The average equivalent undrained ground loss parameter has been defined based on the gap parameter proposed by Lee and Rowe (1992). The non-linear ground movement due to the formation of an oval-shaped gap is then modeled by adopting an exponential function to the average equivalent undrained ground loss with appropriate boundary conditions. The modified equivalent ground loss parameter has then been incorporated into the closed form elastic solutions derived by Verruijt and Booker (1996). This leads to Equations 3.13, 3.16 and 3.18 in the present study, which may be used to predict tunnelling-induced surface and subsurface settlements, and horizontal movements of the ground. The applicability of these equations has been evaluated with reference to nine (9) case studies and two (2) numerical predictions.

Table 3.1 summarizes the average equivalent ground loss values estimated for cases 1 to 5 using the revised method proposed in this paper and the gap "g" parameters estimated from the theoretical method proposed by Rowe and Lee (1992) (refer to Appendix A). It is observed that the estimated equivalent ground loss values and reported empirical ground loss values are in good agreement for tunnels in stiff clays (Cases 1, 3, 4 and 5). The reported empirical ground loss (5.5%) is very much lower than the estimated equivalent ground loss (13.7%) for the tunnel in soft clay at Thunder Bay, Canada. This suggests that the 3-D elasto-plastic face loss is more significant in soft clay tunnelling than in stiffer soils. The ground loss estimated for case 9 (Airport Link, Sydney, Australia) was about 0.4% and the settlement prediction using the predicted ground loss was in reasonably good agreement with the FEM predictions.

Horizontal movements predicted for Case 2 (Thunder Bay Tunnel) show rather poor agreement with the field measurements especially above the tunnel axis. This may be

because the soil profile above the tunnel is predominantly sandy with interbedded occasional clay seams. The horizontal movements predicted below the tunnel axis are however in good agreement with the field measurements since the soil below the tunnel axis is a uniform clay layer.

It was observed that the surface settlement troughs predicted using advanced numerical methods (PECPLAS 3D and FLAC 3D) are wider than the predictions made by equation 3.13. Subsurface settlement prediction using a FLAC 3D elastic analysis show more reliable results than the predictions for a Mohr-Coulomb model. Lateral deformation predictions using FLAC 3D were more inconsistent due to different in-situ stress states assumed. In general, elastic analyses resulted in more consistent and reliable results. Also, the trend of the maximum subsurface settlements predicted using equation 3.18 is in good agreement with observed values for all cases and the predicted horizontal movements are in good agreement with the field measurements, especially above the tunnel axis. In numerical methods, ground loss were simulated by allowing the tunnel face to deform into the void and by taking the ratio of deformed volume of the tunnel face and the tunnel cut volume per meter length.

In summary, Equations 3.13, 3.16 and 3.18 may be used to predict surface and subsurface settlements, and horizontal movements, and do not directly require the input of soil parameters other than the soil Poisson's ratio ν which may be taken to be 0.5 for saturated clays under undrained conditions. The influence of the subsurface soil type and the effect of 3-D soil flow into the tunnel face are indirectly modelled through an equivalent 2-D gap parameter. The results obtained from the case studies have revealed that the proposed method gives less satisfactory agreement with observed values for layered and sandy soils than for uniform clays. Therefore, the gap parameters for the layered soil profile should be estimated using equivalent soil parameters based on sound engineering judgement.

CHAPTER FOUR

TUNNELLING INDUCED PILE BEHAVIOUR - NUMERICAL ANALYSIS

4.1 INTRODUCTION

For an accurate estimation of tunnelling induced ground movements and their effects on adjacent structures numerical computations are preferred which provide a comprehensive picture of ground movements throughout the soil around the tunnel and the adjacent structures. Numerical analysis tools such as the finite element method, the finite difference method and the boundary element method are widely used to model the complex geometries and construction methods which are now often associated with tunnelling schemes.

The purpose of this chapter includes the following aspects:

- A numerical study on the tunnelling-induced behaviour of adjacent single pile and a pile group using a computer programme GEPAN (Xu and Poulos, 1999), which was developed at Sydney University using the boundary element method. The equations 3.13, 3.16 and 3.18 (discussed in previous chapter), to assess the tunnelling-induced ground deformations, were incorporated in GEPAN.
- A parametric study using the computer programme GEPAN to assess the influence on pile behaviour of various factors such as tunnel depth, pile length, pile diameter, ground loss value, horizontal distance between pile and the tunnel etc.
- Comparison of results obtained from the analyses using GEPAN for a typical case with a 3D finite element programme PECPLAS 3D (Mroueh, 1998) and a 3D finite difference programme FLAC 3D.

4.2 GEPAN COMPUTER PROGRAMME

At present, various numerical approaches have been employed in estimating pile group responses due to combinations of external loading. Computer programs for the analysis of pile groups vary in the type of approach used and in the sophistication of treatment of different aspects of group behaviour. Among the most widely used general programs for pile group analysis are PGROUP (Banerjee, 1976), DEFPIG (Poulos, 1979, 1990), and PIGLET (Randolph, 1980). All these programs are based on elastic continuum analysis, although DEFPIG can also be extended into the non-linear range by specifying limiting values of skin friction and lateral pressure along the pile.

Although these programs have been used widely, they all involve simplifications and idealizations, including; (1) pile to pile interactions are used instead of individual pile element to pile element interactions, (2) the actual non uniform stress distributions around the pile (especially in the lateral loading case) are modified to an equivalent uniform stress distribution over each pile elements, (3) Load-deformation behaviour is modeled individually without considering the deformation coupling effects due to three dimensional loading, and (4) off-pile loading conditions arising from adjacent constructions such as embankments, excavations, tunnelling etc. are not considered.

A computer program GEPAN, (GEneral Pile ANalysis) has been developed at Sydney University (Xu and Poulos, 1999) to overcome some of the limitations and idealizations in existing computer programs. A three dimensional boundary element analysis, together with the virtual image technique for an elastic half-space, has been used to carry out analyses of multiple single piles and pile groups which incorporate the effect of external soil movements due to embankments, tunnels and excavations. Figure 4.1 shows a typical pile element discretization used in the computer program GEPAN. Each pile is subjected to a total of six components of load.

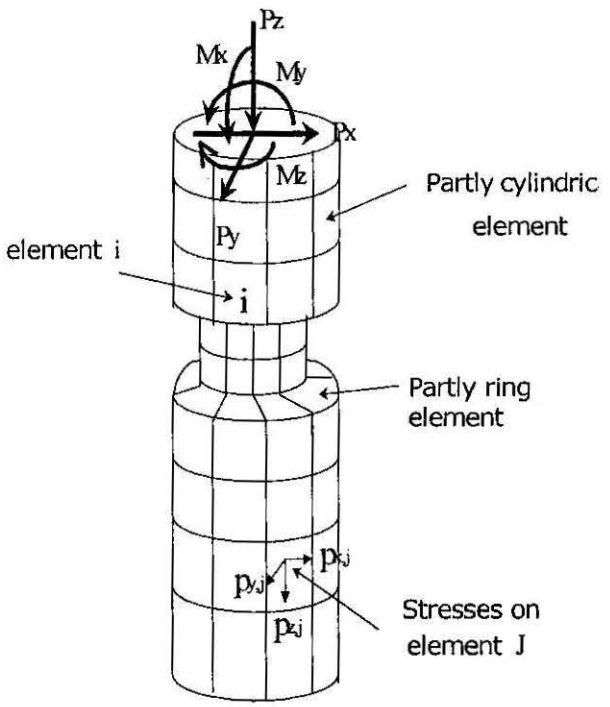

Figure 4.1: Schematic Diagram showing 3D Boundary Element Discretization, and Loads and Stresses Acting on the Pile on adjacent piles.

More accurate load-deformation pile responses are obtained by assuming load-deformation interactions occur between each element of each pile of each group. Twelve kinds of influence factors are classified and presented by corresponding influence factor matrixes (IFM) which are of a hierarchical nature. The resulting global equation for pile response is shown in equation (4.1).

$$\begin{pmatrix} A & B & \varnothing & D \\ \varnothing & \varnothing & G & H \\ O & P & Q & R \\ S & \varnothing & \varnothing & V \end{pmatrix} \begin{pmatrix} X_e \\ X_b \\ X_c \\ X_t \end{pmatrix} = \begin{pmatrix} Y_q \\ Y_c \\ \varnothing \\ Y_p \end{pmatrix} \tag{4.1}$$

where A=IFM of element displacement and stress (=*SIF*+*PIF*), *SIF*=IFM of element soil displacement and stress, *PIF*=IFM of element pile displacement and stress, B=IFM of element displacement and pile tip displacement, D=IFM of element displacement and pile head load, G=IFM of cap displacement and cap-tie-cap beam force (to allow for pile caps jointed by tie beam, H=IFM of cap load and pile head load, O=IFM of pile head displacement and element stress, P=IFM of pile head displacement and pile tip displacement, Q=IFM of pile head displacement and cap displacement, R=IFM of pile head displacement and pile head load, S=IFM of pile head load and element stress, V=IFM of pile head load and pile head load, Y_q=vector of element stress offset (=$Y_{q,t}$ + $Y_{q,e}$),$Y_{q,t}$=vector of element displacement due to pile head load, $Y_{q,e}$=vector of element displacement due to extra soil displacement/stress/force, Y_c=vector of cap load, Y_p=vector of pile head load, X_e=vector of pile-soil stress, X_b=vector of pile tip displacement, X_c=vector of cap displacement, and X_t=vector of capped pile head force.

Details of the various matrices and vectors are given by Xu and Poulos (1999). The global equation (4.1) contains the following four kinds of independent equations: compatibility equations at the pile-soil interfaces; equilibrium equations for pile heads and caps; compatibility equations for pile heads and caps; equilibrium equations for piles.

The results obtained from GEPAN for the direct loading of a group generally agree well with the other standard programs such as PIGLET and DEFPIG (Xu and Poulos, 1999). One of the most attractive advantages of the proposed 3D-boundary element modeling method is that externally imposed ground movements are very easily incorporated into the governing equations if the distributions of these ground movements are known. These ground movements are absorbed into the vector $\{Y_{q,e}\}$ in governing equation (4.1) and the soil displacement vector $\{Y_q\}$ at element 'i' is given as;

$$\{Y_q\} = \{Y_{q,t}\} + \{Y_{q,e}\} \tag{4.2}$$

where $\{Y_{q,t}\}$ = soil displacement vector on element 'i' due to pile head load on individual piles, and $\{Y_{q,e}\}$ = soil displacement vector due to external sources.

The effects of external ground movements can be considered in two ways: (1) displacements imposed directly, based on the known ground movements, and (2) induced stresses based on the known ground movements. In the first case, the free-field soil movements at the pile-soil interface are indicated by a vector $\{u_{soil}\}$ as shown in equation (4.3):

$$\{Y_{q,e}\}=\{u_{soil}\} \tag{4.3}$$

In the second case, the induced stresses are represented by a vector $\{\sigma_{soil}\}$. The corresponding soil movements due to the soil stresses are the product of the soil influence factor matrix $[SIF]$ and the soil stress vector $\{\sigma_{soil}\}$ as shown in equation (4.4):

$$\{Y_{qe}\}=[SIF]\{\sigma_{soil}\} \tag{4.4}$$

The head displacements of individual piles can be determined from the following equation (4.5).

$$\{X_i\} = -[O]\{X_e\} + [P]\{X_b\} + [R]\{Y_p\} \tag{4.5}$$

The analytical closed-form solutions presented in this study (equations 3.13, 3.16 and 3.18) to predict the tunnelling-induced ground movements have been incorporated in equation (4.3) within the computer program GEPAN.

4.3 SINGLE PILE RESPONSES

4.3.1 Introduction

The construction of a tunnel adjacent to existing piles requires a proper consideration of the pile response to the externally imposed soil movements due to tunnelling, and an assessment of the consequent axial movement, lateral deflection, bending moment and rotation of the pile head. The GEPAN computer program is used to analyse tunnelling-induced behaviour of single pile.

At first a typical tunnel-pile configuration is considered to estimate the tunnelling-induced behaviour, and then a parametric study is performed in order to assess the effects

of various parameters, such as pile length, pile diameter, horizontal distance from the tunnel, and the ground loss values.

4.3.2 Single Pile Analysis

Figure 4.2 illustrates the general problem addressed in this study, where an existing single pile is situated adjacent to a tunnel under construction. Tunnelling will generally induce both vertical and horizontal components of ground movements. The vertical ground movement above the tunnel's horizontal axis is generally downward and will impose negative skin friction on the pile, causing pile settlement and a possible reduction in the effective pile load carrying capacity. The horizontal soil movement tends to be towards the tunnel axis and will induce additional lateral deflection and bending moment in the pile.

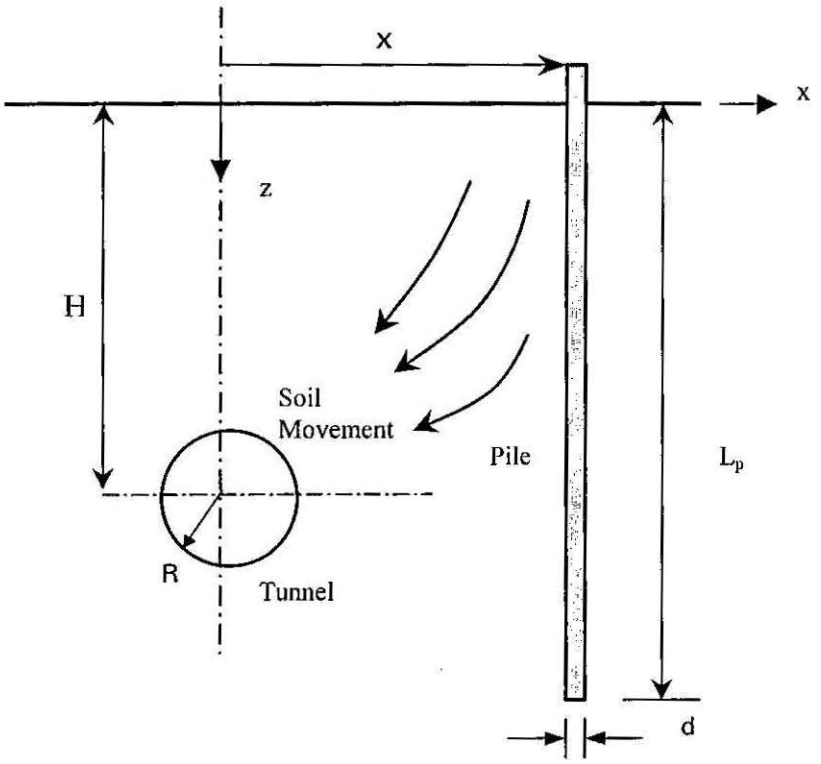

Figure 4.2: Single Pile Adjacent to Tunnelling - The Basic problem Analysed

The analyses of pile responses were carried out using computer programme GEPAN as described previously. The pile was divided into a series of elements (typically 1m long), the vertical movements of which were related to the applied load, the pile-soil interaction stress, the pile compatibility, and the pile tip movement. Elastic analysis was carried out without any limiting axial and lateral resistance. The vertical movement of each supporting

soil element depends on the pile-soil interaction stress, the modulus or stiffness of the soil, and also on any free-field movements that may be imposed on the pile.

A simple case was analysed first, involving the following assumptions for the soil, tunnel and pile geometries:

- the soil is deep homogeneous clay layer, assumed to be in an undrained condition. The undrained shear strength c_u = 60 kPa and Young's modulus E_s = 24 MPa ($400c_u$), values which are representative of a medium clay,
- the tunnel radius, R = 3m, and the depth of tunnel axis, H = 20m, and
- the pile has diameter d = 0.5m, length L_p = 25m and Young's modulus E_p=30,000MPa.

In this case, the pile tip is located below the tunnel axis ($L_p/H > 1$). The effect of a different pile tip level is also analysed and discussed later in the parametric study.

Figure 4.3 shows vertical and horizontal soil movement profiles induced by tunnelling, corresponding to three average ground loss ratios, ε_0 = 1%, 2.5% and 5%, and for a lateral distance, x = 4.5m away from the tunnel centerline.

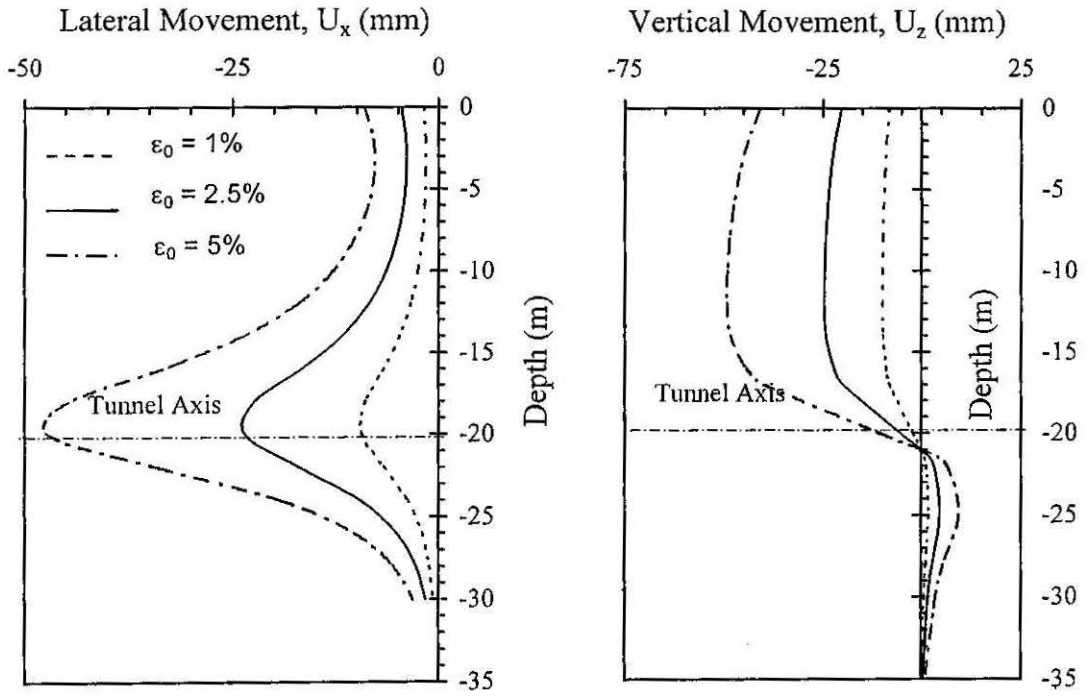

Figure 4.3: Soil Movements at x = 4.5m

The soil movements increase proportionally with increasing ground loss ratio. The maximum vertical and lateral soil movements occur slightly above the tunnel axis, reflecting the boundary conditions used in the derivation of the ground loss parameter given in equation (3.5).

Figure 4.4 shows pile response profiles for bending moment, lateral deflection, axial downdrag force and vertical movement of the pile.

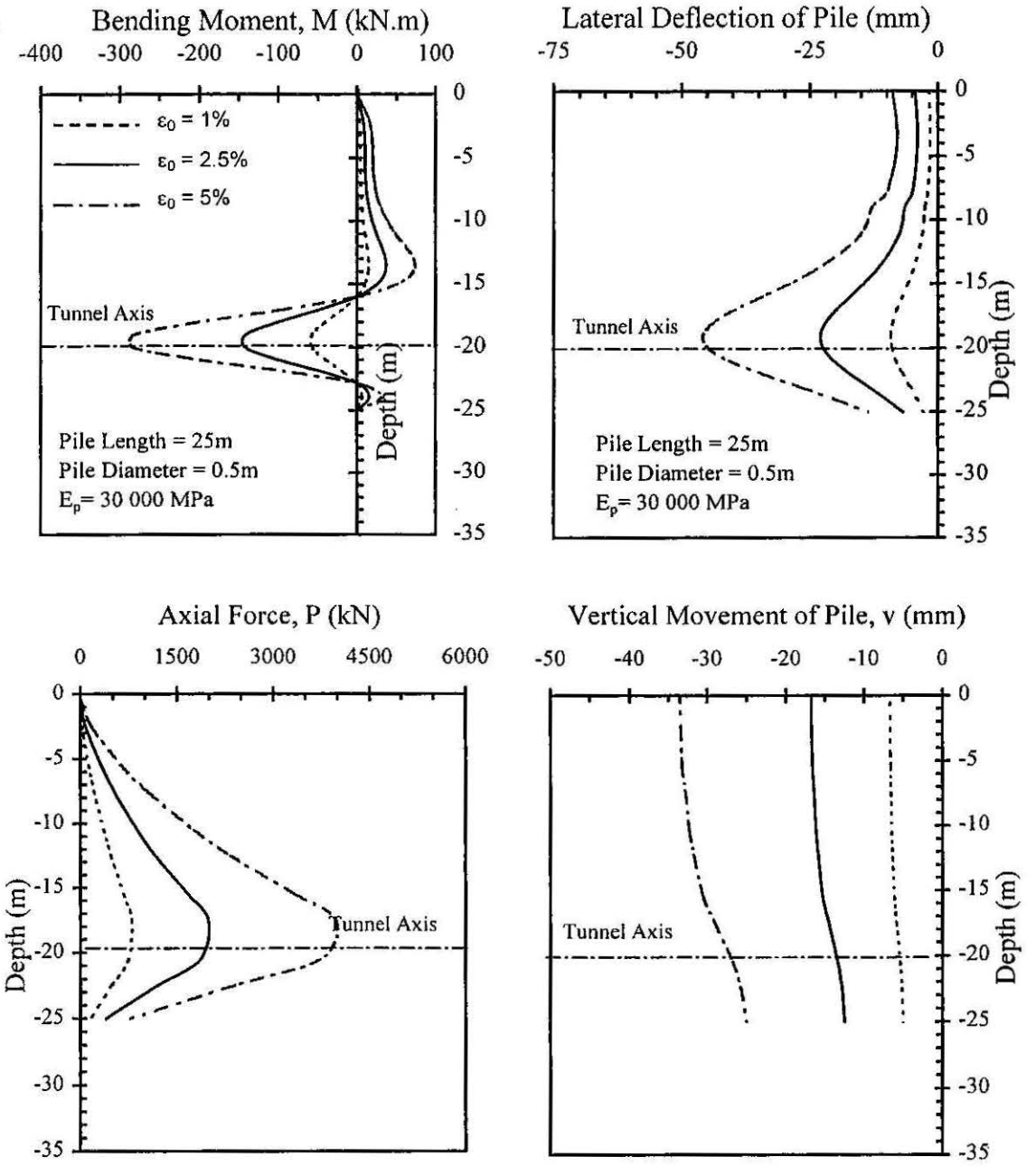

Figure 4.4: Typical Pile Response at X = 4.5m

These profiles have the following features:

- the magnitude of the pile responses are proportional to the ground loss, and thus, since the ground is assumed to exhibit elastic behaviour, the pile responses can be normalised with respect to the ground loss value,
- lateral pile deflections are very similar to lateral soil deflections, for all three ground loss ratios, reflecting the relative flexibility of the pile,
- the bending moment profile has a double curvature, with the maximum value occurring at the level of the tunnel's horizontal axis,
- the pile settlement shows that elastic compression of the pile occurs, but the pile head settlement is less than the ground settlement at the pile location, and
- a large downdrag force is developed along the pile in the elastic analysis. In actual practice, the downdrag force may be less, due to pile-soil slip and the possible formation of a gap at the pile-soil interface for higher soil displacements.

4.3.3 Parametric Study

The tunnel-pile configuration shown in Figure 4.2 has been used to investigate the significance of various factors on the axial and lateral responses of piles. The influence of the following parameters has been investigated: lateral pile location, pile length, pile diameter and ground loss values. The ranges of values used in this study are as follows:

- pile diameter, d = 0.5m, 0.8m, 1.0m and 1.2m
- pile length, L_p = 15m (pile tip above the tunnel axis), 20m (pile tip is at the tunnel axis), and 25m(pile tip below the tunnel axis),
- average ground loss value, ε_0 = 1%, 2.5%, and 5%
- normalised lateral distance, x/H = 0 to 2.

It is observed that the pile deformation patterns are identical and proportional to the magnitude of the ground loss. Therefore, all the results presented have been normalised with respect to the ground loss parameter.

Figure 4.5 shows the variation of the pile head settlement (S_p) / ground settlement (S_f) ratio with the normalised lateral distance, x/H. The following points are observed:

- the S_p/S_f ratio decreases nonlinearly with normalised lateral distance x/H for all pile lengths. Pile settlements are significant in the vicinity of the tunnel.

- For $L_p/H > 1$ (i.e. the pile tip is located below the tunnel axis), $S_p/S_f < 1$ for all pile lengths. This shows that when pile tip level is deeper than tunnel axis level, the pile head settlement trough is shallower than the soil surface settlement trough Only the pile head settlement trough should be considered in the assessment of the potential building damage due to tunnelling. It is also observed that the large diameter piles settle less than smaller diameter piles.

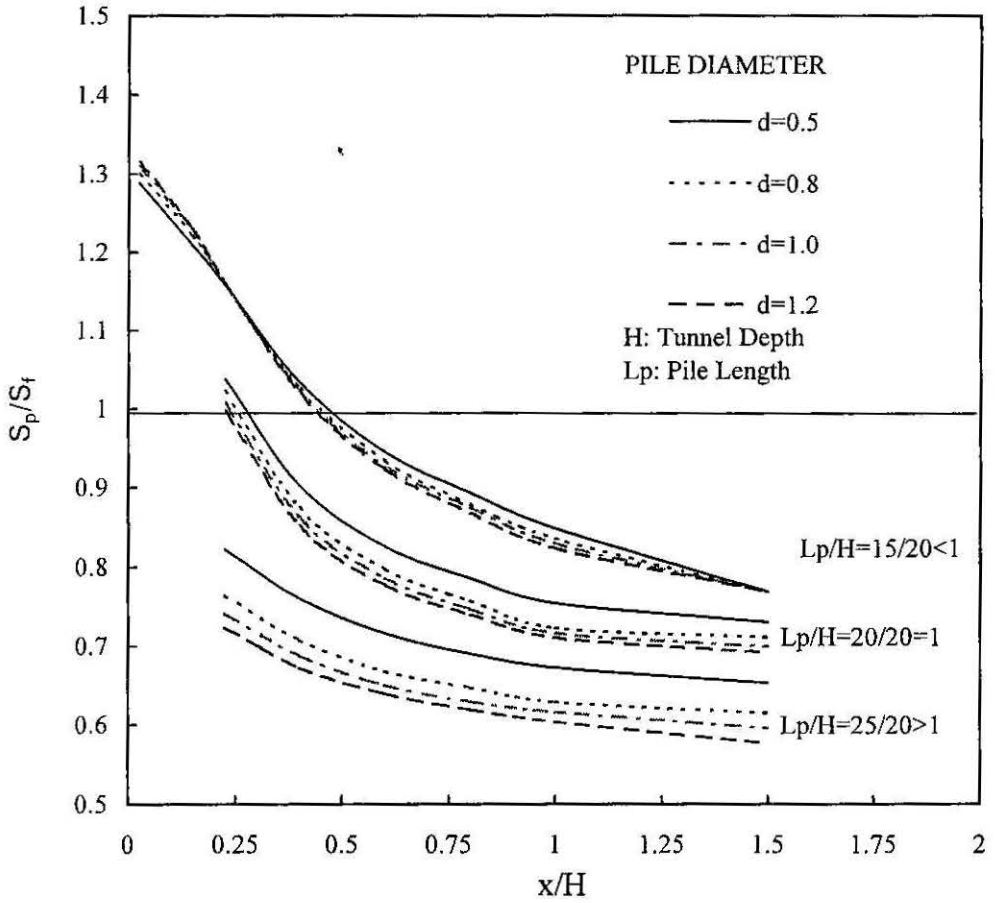

Figure 4.5: Relationship Between Pile Head Settlement/Ground Surface Settlement Ratio Vs. Lateral Distance/Tunnel Depth ratio

- For $L_p/H = 1$ (i.e. the pile tip level is at the tunnel axis level), $S_p/S_f > 1$ for a horizontal distance $x/H < 0.3$, and $S_p/S_f < 1$ beyond the distance $x/H = 0.3$. This shows that the pile head settlement trough and the soil settlement trough will interact in the vicinity of the tunnel ($x/H < 0.3$) and the resulting surface settlement trough is subjected to modification in proportion to the soil and the structure stiffness ratio. The modified surface settlement pattern should be considered in the assessment of building damage potential due to tunnelling. It is also observed that the effect of pile diameter is not significant near the tunnel but becomes more significant with increasing distance from the tunnel.

- For $L_p/H < 1$ (i.e. the pile tip level is above the tunnel axis level), $S_p/S_f > 1$ for a horizontal distance $x/H < 0.5$, and $S_p/S_f < 1$ beyond the distance $x/H = 0.5$. This shows that the ground settlement trough will be modified to some extent due to the influence of the pile foundation. It is also observed that the effect of pile diameter is not significant.

Figure 4.6 shows the variation of the maximum lateral pile deformation (max. ρ_p) / lateral pile head movement, ρ_p(PH) ratio with the normalised lateral distance, x/H.

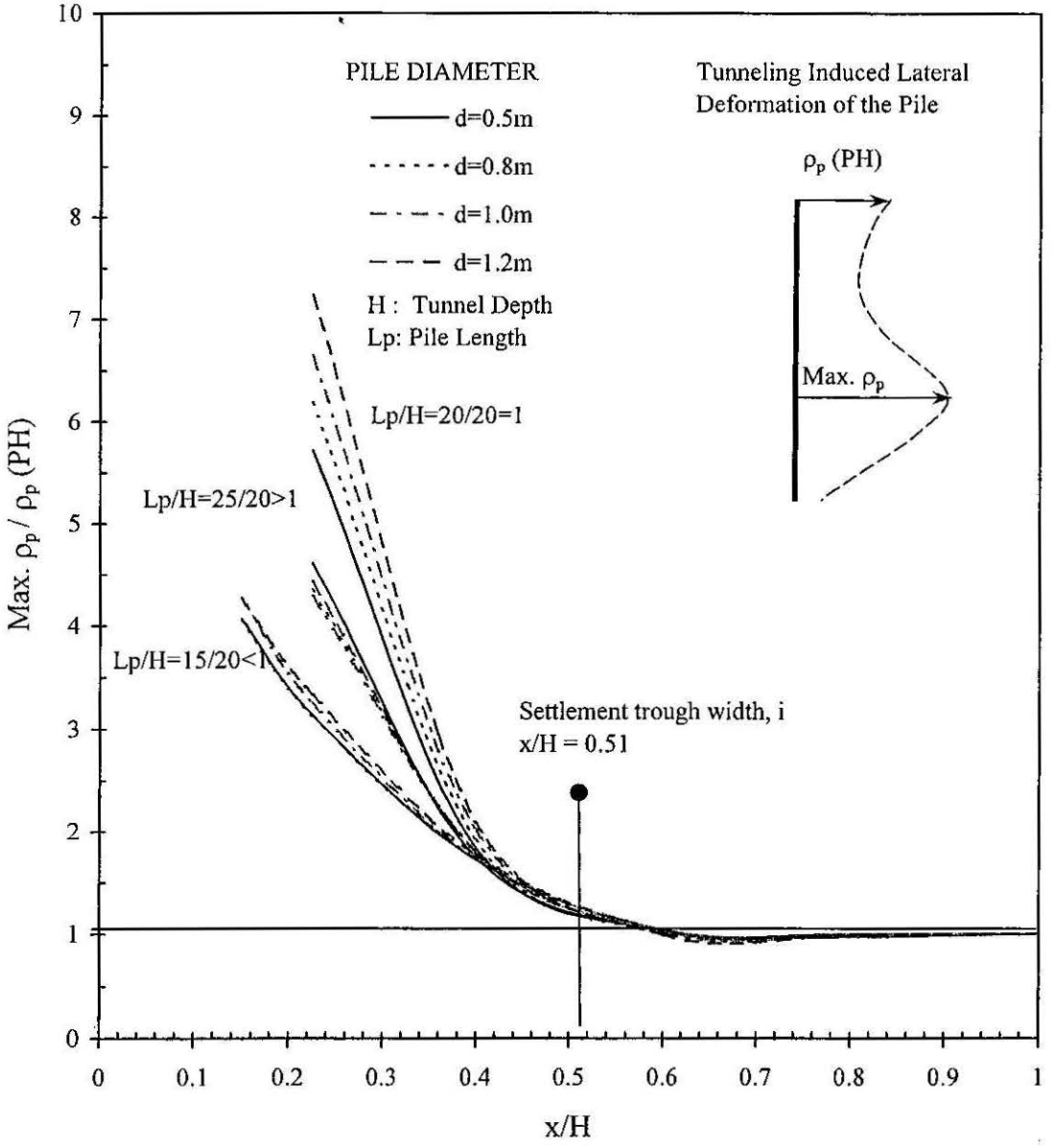

Figure 4.6: Relationship Between Maximum Lateral Movement/Lateral Pile Head Movement Ratio Vs. Lateral Distance/Tunnel Depth Ratio

The following observations are made:

- The effect of pile diameter is not significant for all three pile lengths and the maximum lateral pile deflection occurs at the pile head, beyond the settlement trough width i (x/H = 0.51)
- When the pile tip level is at the tunnel axis ($L_p/H = 1$), the difference in pile head and the pile tip lateral movement is very large since the pile tip is located at the depth where maximum lateral ground deformation occurs. The pile moves along with the soil and is subjected to free rotation
- In longer piles ($L_p/H > 1$), the pile stiffness reduces the maximum lateral deformation at the tunnel axis level.

Figure 4.7 shows the variation of normalised maximum bending moment ($M_{max}d/100\varepsilon_0EI$) with the normalised lateral distance.

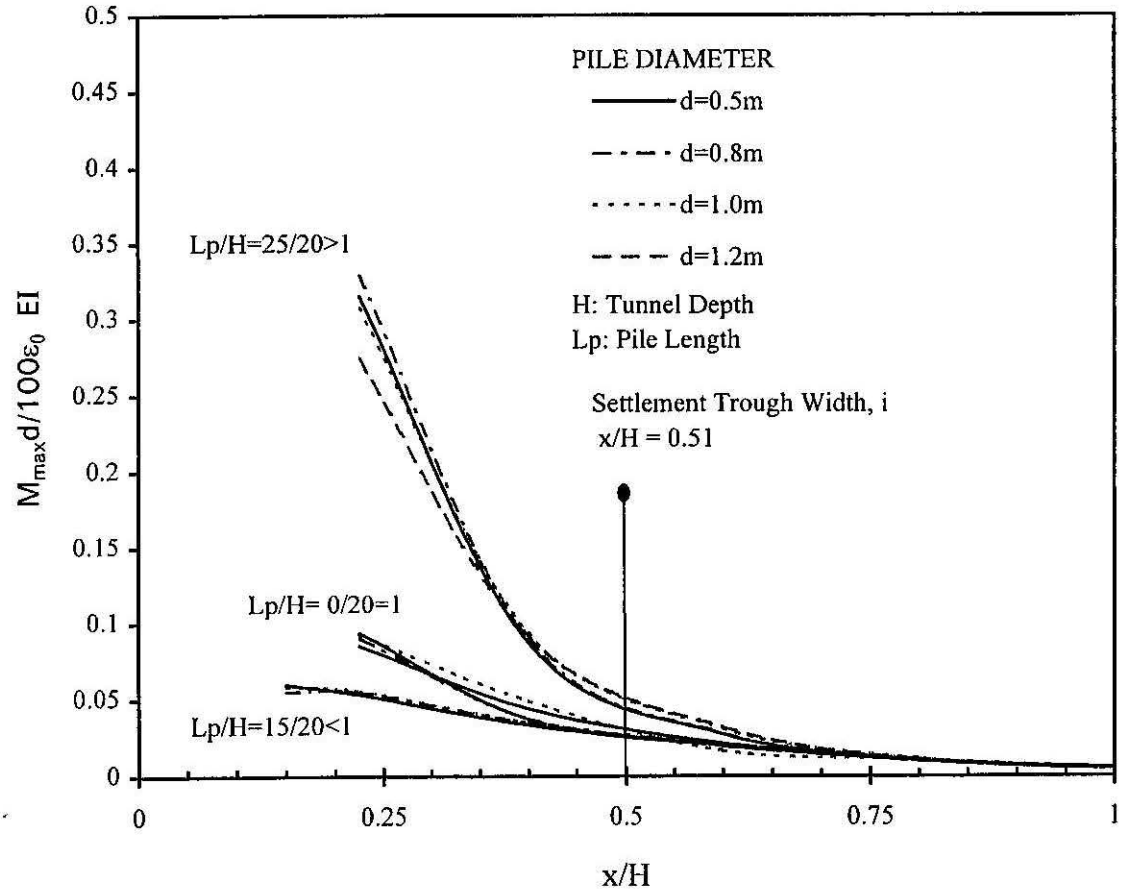

Figure 4.7: Relationship Between Normalised Bending Moment Vs. Normalised Lateral Distance

The following points are noted:

- The maximum bending moment induced in a pile is significant in the vicinity of the tunnel ($x/H < 0.5$)
- Induced bending moments are proportional to the magnitude of the curvature of the deformation pattern of the pile. Longer piles ($L_p/H > 1$) are subjected to relatively large deformations, and thus experience large induced bending moments.
- Induced bending moments are higher for large diameter piles due to their high bending stiffness.

Figure 4.8 shows the variation of the ground surface rotation (β) / pile head rotation (δ) ratio with the normalised horizontal distance.

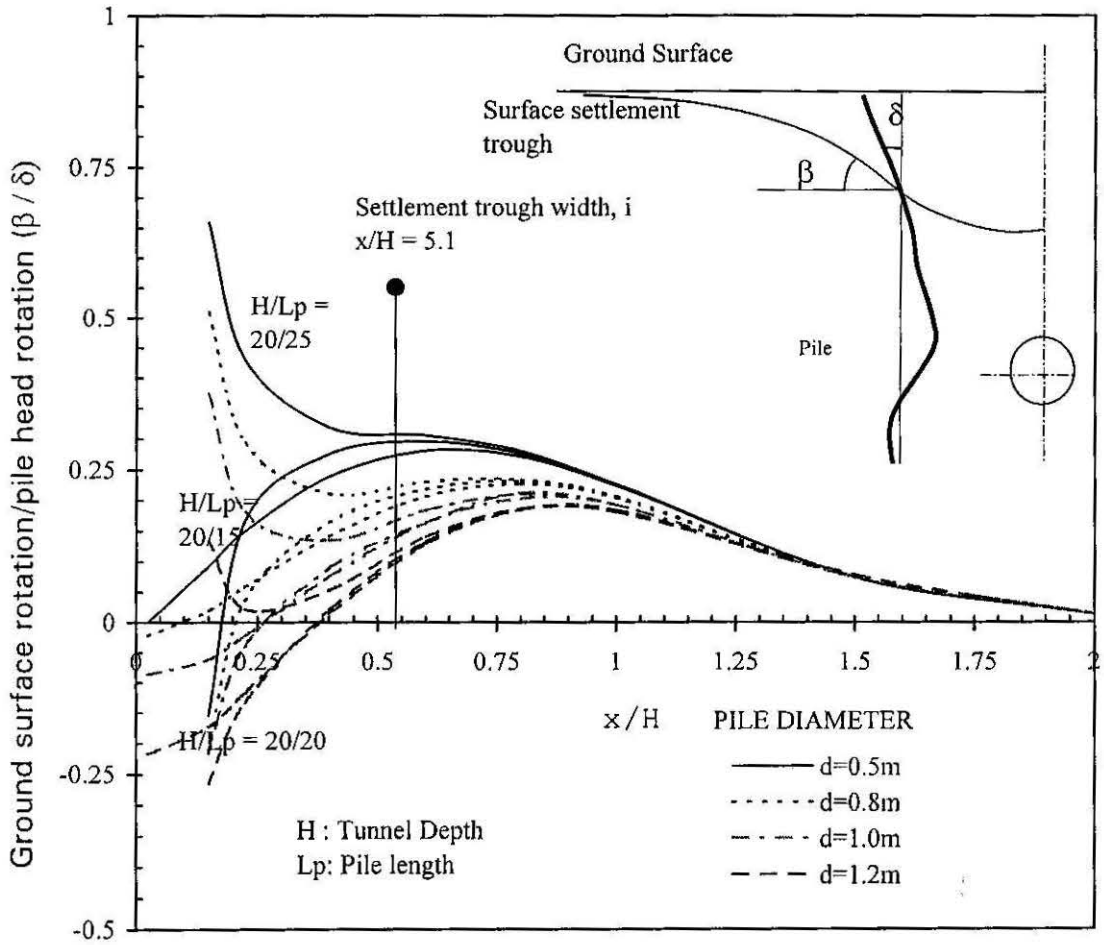

Figure 4.8: Relationship Between Ground Surface Rotation/Pile Head Rotation Ratio Vs. Normalised Lateral Distance

A free pile head condition is assumed in the analysis. Pile head rotation is an important parameter in the estimation of induced bending moment and the distortional strains in the building. The following observations are made:

- The effect of pile diameter is not significant for a horizontal distance beyond x/H=1, for all three pile lengths. When x/H<1, small diameter piles are subjected to more rotation than large diameter piles, due to their flexibility.
- For an identical pile diameter, the β/δ ratio is the same for all three pile lengths, for a horizontal distance beyond x/H = 0.51. This shows that the pile head rotation and the soil settlement trough rotation are subjected to variations with respect to the point of inflection of the surface settlement trough.

4.3.2 Concluding Remarks

The analyses show that the pile deflection generally follows the soil deflection and that the magnitudes of the pile responses are proportional to the ground loss value. Therefore, for an elastic analysis, the computed pile responses may be normalised with respect to the ground loss value. A total of three construction conditions, namely, a tunnel below the pile foundation, a tunnel at the tip of the pile foundation, and a tunnel above the tip of the pile foundation, were considered in this study. The following conclusions were reached:

- *Tunnel below the tip of the existing pile foundation ($L_p/H < 1$):* Significant pile settlements are induced, together with additional bending moments, lateral deformations and pile rotations. The pile head settlement can exceed the ground surface settlement for a distance of about half the tunnel depth from the pile axis. The modified surface settlement trough may be used in the assessment of tunnelling-induced building damage. The effect of pile diameter is not significant.
- *The tunnel is excavated at the pile tip level ($L_p/H = 1$):* The induced lateral deformations can be significant in this case. The pile head settlement exceeds the ground settlement only in the vicinity of the tunnel.
- *The tunnel is excavated above the pile tip level ($L_p/H < 1$):* The induced bending moments can be significant in this case. The pile head settlement is less than the ground settlement, and therefore the pile head settlement trough may be considered in the assessment of potential building damage due to tunnelling-induced ground movements.

The pile head rotation is not significantly affected by pile length, but the pile diameter has a significant effect on the pile head rotations. The pile head rotations are large at the point of inflection of the surface settlement trough.

4.4 PILE GROUP RESPONSES

4.4.1 Introduction

Many high-rise buildings are founded on pile groups. Due to the pile head constraints and the increase in the foundation stiffness, the tunnelling-induced pile behaviour in a group may differ from an isolated single pile. In this study, an assessment of a typical 2x2 pile group behaviour is performed and compared with the behaviour of identical isolated single piles. In addition, a parametric study is performed to assess the effect of pile length, increased number of piles in a group, and the changes in tunnelling-induced behaviour with varying lateral distance from the tunnel.

4.4.2 Pile Group Analysis

Figure 4.9 illustrates the general problem addressed in this study, where an existing 2x2 pile group is situated adjacent to a tunnel under construction. Pile group, tunnel and soil configurations and properties are as follows:

- Piles in the group are spaced at 3d, where d is pile diameter
- Pile diameter is 0.8m and pile length is 25m
- Young's modulus of pile, E_p = 30,000MPa
- Poisson's ratio of piles, ν_p = 0.25
- All four piles in the pile group are assumed to be fixed against rotation at the pile cap
- A uniform isotropic subsurface soil profile with constant soil strength, c_u = 60 kPa
- The soil modulus follows the relationship, $E_s = 400c_u$
- Poisson's ratio of soil, ν_s = 0.5 (undrained condition)
- Soil layer thickness assumed to be infinite
- The interaction between the pile cap and the ground surface is not considered
- The horizontal distance between the front row piles and the tunnel center line is 4.5m

- The depth of tunnel from the surface is 20m and the tunnel diameter is 6m
- Ground loss value used is 1%.

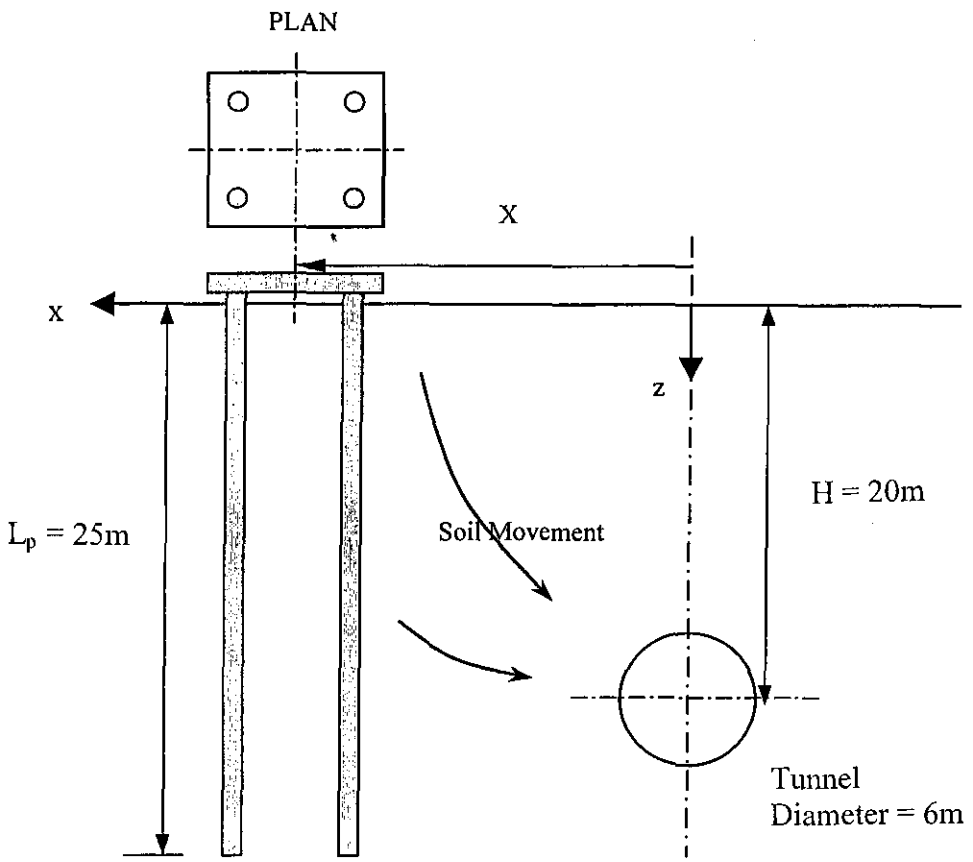

Figure 4.9: Pile Group Adjacent to Tunnelling - Typical Problem Analysed

Figure 4.10 shows a comparison of the computed settlement profile of piles in the pile group and single piles at an equal horizontal distance from the tunnel centerline.

The settlement of the "front" piles is slightly higher than the settlement of "rear" piles since the tunnelling-induced settlements decrease as the distance from the tunnel decreases. The settlement of single isolated piles at equivalent distances from the tunnel is slightly higher than the piles in the group. The settlement profiles with depth for both a single pile and a pile in the group are almost identical. Therefore, the tunnelling-induced settlement behaviour of single piles appears to be reasonably representative of the settlement behaviour of piles in a group.

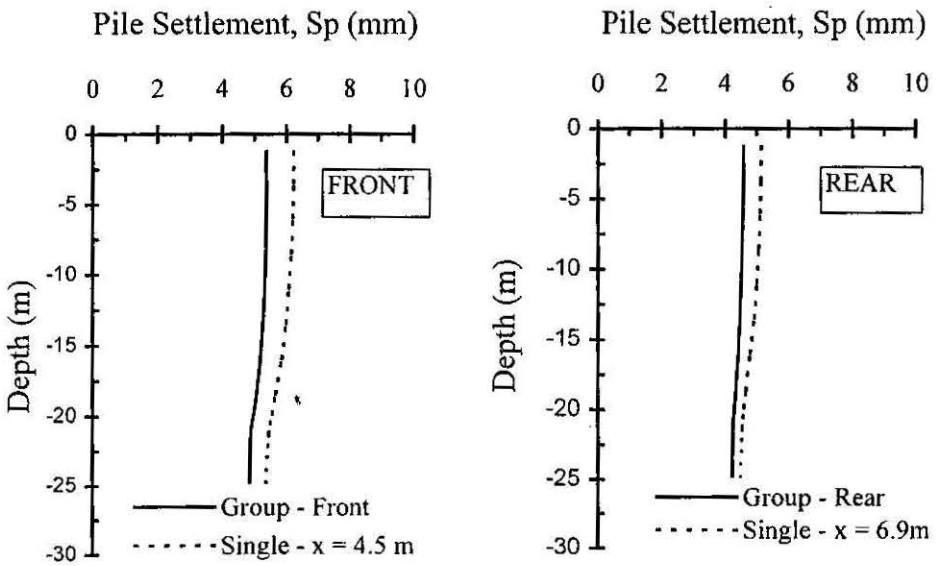

Figure 4.10: Comparison of the Settlement of a Pile in a Group and a Single Pile at Equal Distance from the Tunnel Axis

Figure 4.11 shows a comparison of the tunnelling-induced lateral deformation profile of piles in the pile group and single piles at identical horizontal distances from the tunnel. As expected, the lateral deformation of the "front" piles (closer to tunnel) in the group is higher than for the "rear" piles, and the maximum lateral deformation occurs at a depth equal to that of the tunnel center. The lateral deformation profile for single piles is almost identical to that of the piles in a group.

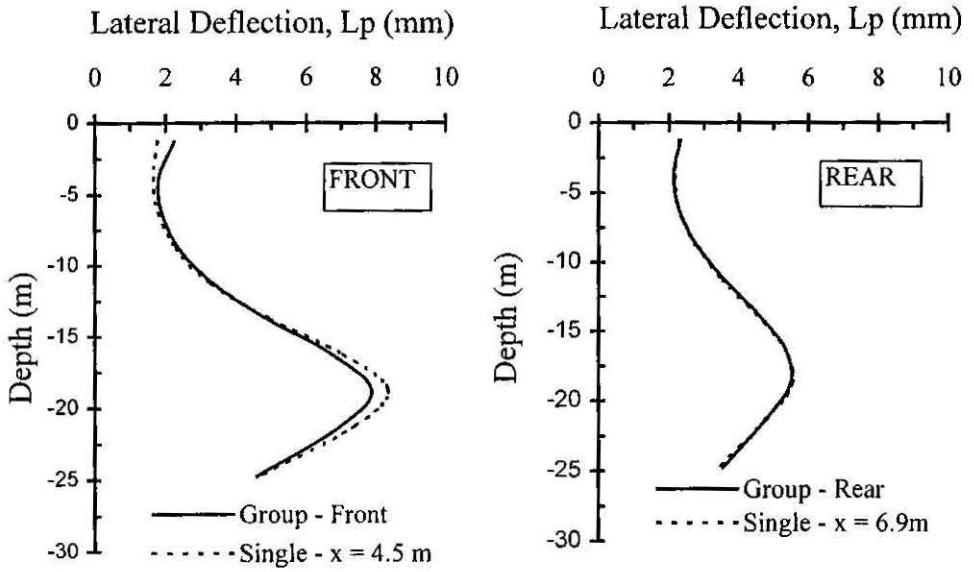

Figure 4.11: Comparison of the Lateral Deformation of a Pile in a Group and a Single Pile

Figure 4.12 shows a comparison of the tunnelling-induced bending moment profile of piles in a group and single piles at equivalent distances. The maximum bending moment occurs at about the tunnel axis depth level. The bending moment profile for piles in a group and single pile are very similar, except for a small difference at the pile cap location due to the fixity condition. Thus, the bending moment profile obtained for single piles gives a reasonable representation of the profile and of the maximum moment for a pile in a group.

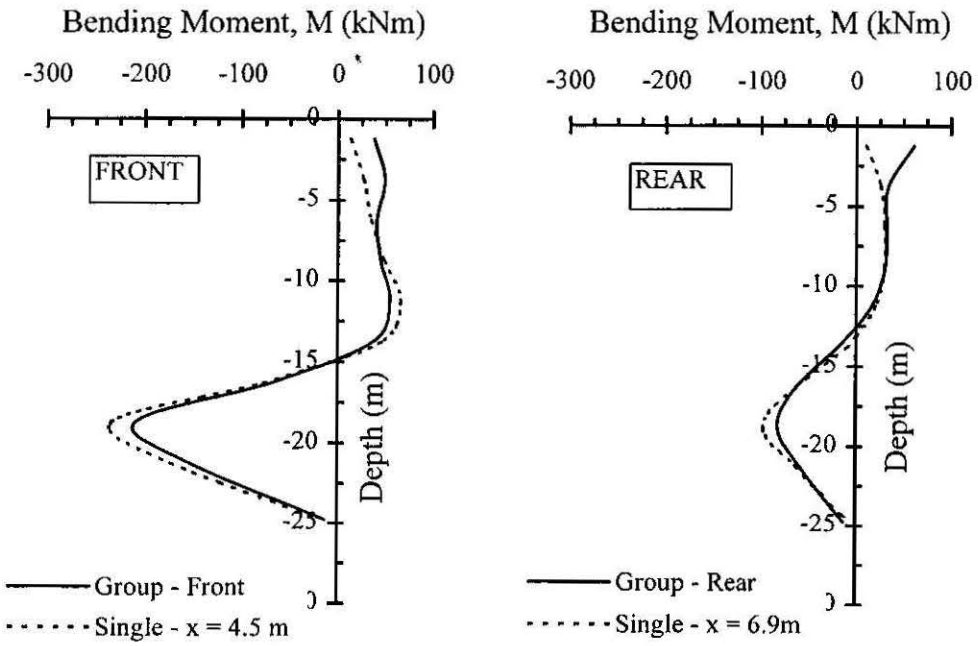

Figure 4.12: Comparison of the Induced Bending Moment on a Pile in a Group and a Single Pile

Figure 4.13 compares the induced axial force profiles for piles in a group and a single pile at an equal distance from the tunnel. The axial downdrag force estimated for a single pile is about 20% higher than the downdrag force induced in a pile within the pile group. This indicates that pile group effect reduces the induced axial downdrag forces on a pile in the group and is consistent with the findings of Kuwabara and Poulos (1989).

The above results indicate that a relatively simple single pile analysis can be used to predict the tunneling-induced bending moment, lateral deformation and settlement in a pile group at identical distances from the tunnel. However, the tunneling-induced axial down-drag force estimated for single pile may be larger than for a pile in a pile group.

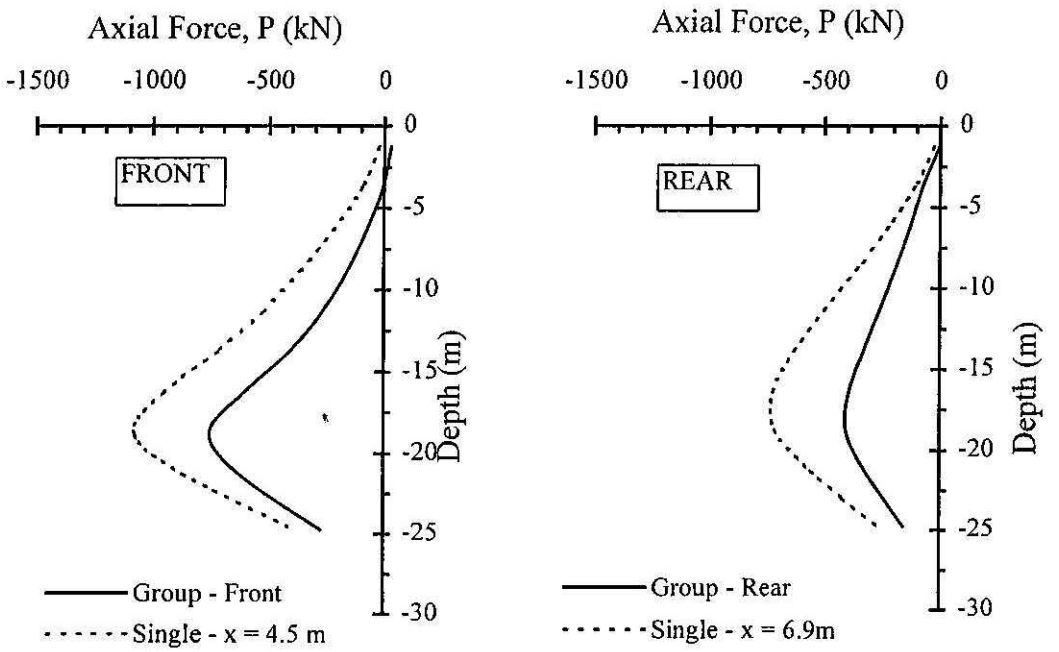

Figure 4.13: Comparison of the Induced Axial Force on a Pile in a Group and a Single Pile

4.4.3 Parametric Study

A parametric study was performed to assess the behaviour of the 2x2 pile group (considered in the previous analysis), for different horizontal distances from the tunnel centreline and varying pile lengths. Tunnelling-induced ground surface settlement, lateral deformation and the rotation are important aspects in the estimation of adjacent pile deformation.

Figure 4.14 shows a comparison of the settlement, lateral movement and rotation of a pile group (at the pile cap), a single pile (at the pile head), and the ground surface, for varying horizontal distances from the tunnel. It is observed that the settlement and the lateral deformation of the pile group and single pile are almost identical for varying horizontal distances but are less than the ground surface settlement and lateral deformation.

The maximum values of both lateral deformation and the rotation of the pile head occur at a horizontal distance equal to the ground surface settlement trough width, i. The rotation at ground level for a single pile is less than the rotation of pile cap. This is due to the difference in pile head fixity conditions of the single pile and the group pile. The ground surface rotates more than either the single pile or the pile group.

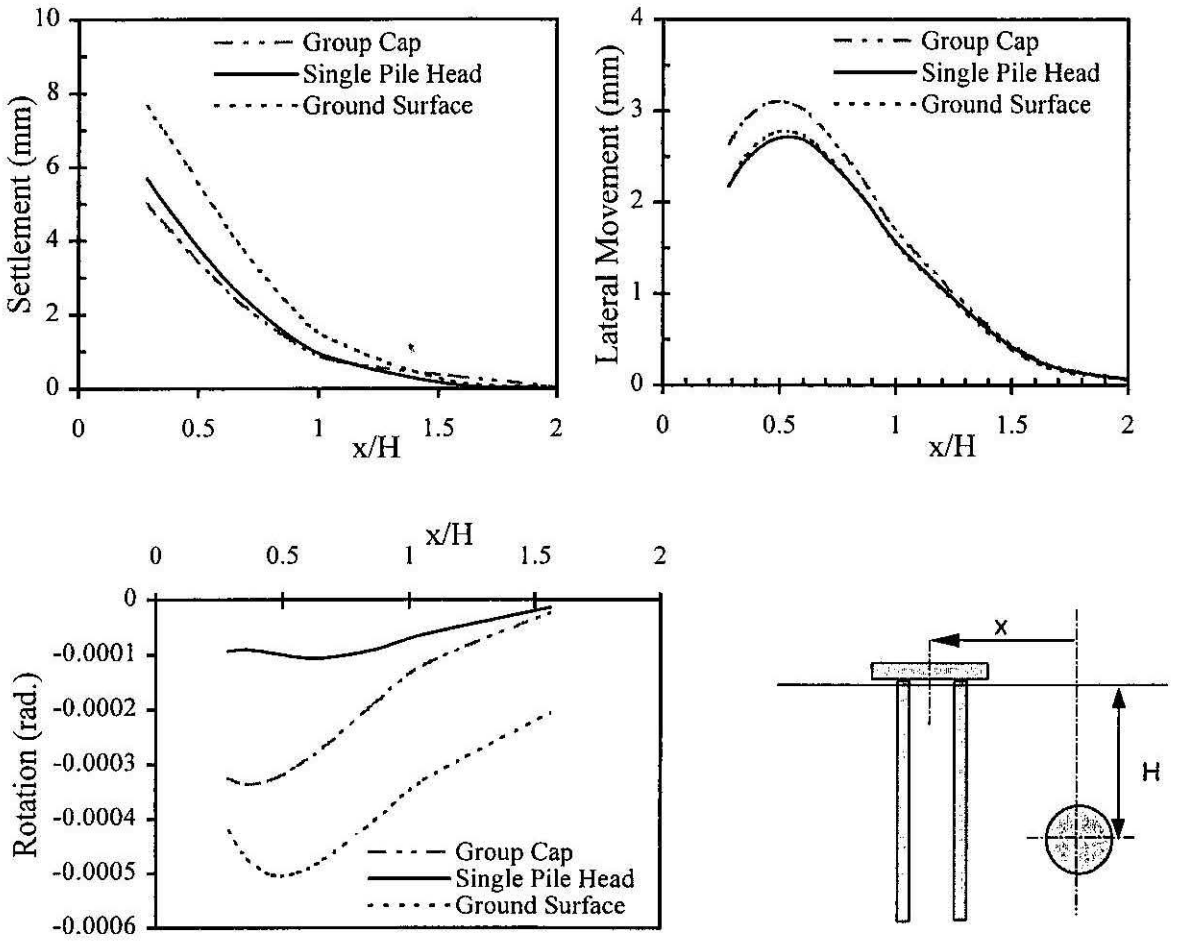

Figure 4.14: Comparison of Single Pile Head, Pile Group Cap and Ground Surface Movements

Figure 4.15 shows a comparison of "front" and "rear" pile behaviour of a 2x2 pile group, for varying pile lengths. Pile head settlement and the lateral deflection are large when the pile tip is located near the tunnel depth level, and the "front" pile laterally deflects more than the "rear" pile. When the pile tip is located below the tunnel centerline, the pile head settlement reduces. The maximum downdrag force and the maximum bending moment are high when the pile tip is located at tunnel invert level, and there is little variation in maximum downdrag force and the bending moment values when the pile tip becomes deeper and is below the tunnel invert level.

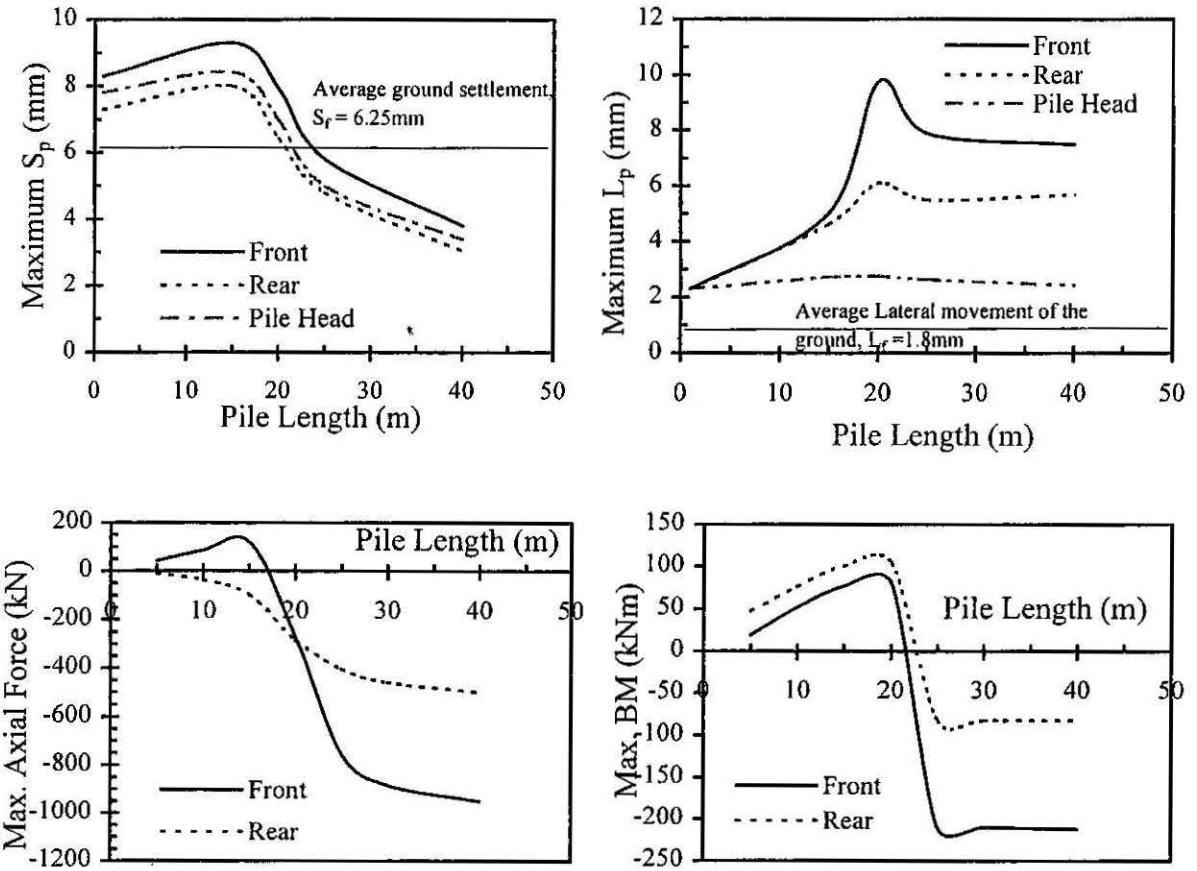

NOTE: Tunnel Depth (H) = 20m
Pile Diameter (d) = 0.8m

Figure 4.15: Comparison of Maximum Bending Moment, Axial Forces, Settlements and Lateral Deformations for Different Pile Lengths

4.4.4 Concluding Remarks

The study described in this section shows that a single pile analysis can predict adequately the tunneling-induced bending moment, lateral deformation and settlement for a pile in a pile group, at an identical distance from the tunnel. However, at least in this study, the tunneling-induced axial downdrag force estimated for a single pile is about 20% higher than for a pile in a pile group.

Significant pile settlement and lateral deformation are induced when the pile tip is located at about the tunnel depth level. Similarly the induced downdrag and bending moment are significant when the pile tip is located at the tunnel invert level.

4.5 COMPARISONS WITH 3D FEM RESULTS (PECPLAS 3D)

4.5.1 Introduction

Mroueh (1998) at the University des Sciences et Technologies de Lille, France, developed a 3D finite element computer programme to study the interaction between tunnels and nearby existing structures. In this section, comparisons are made between the results presented by Mroueh (1998) and GEPAN analyses for typical cases of a single pile and a pile group.

4.5.2 Single Pile

There are two cases presented in this study; i) a single pile located horizontally at 1D (D = tunnel diameter) and ii) a single pile located horizontally at 1.5D. Analyses of these two cases enable an assessment to be made of induced behaviour of piles located at varying horizontal distance from the tunnel. The configuration of a typical problem analysed is shown in Figure 4.16.

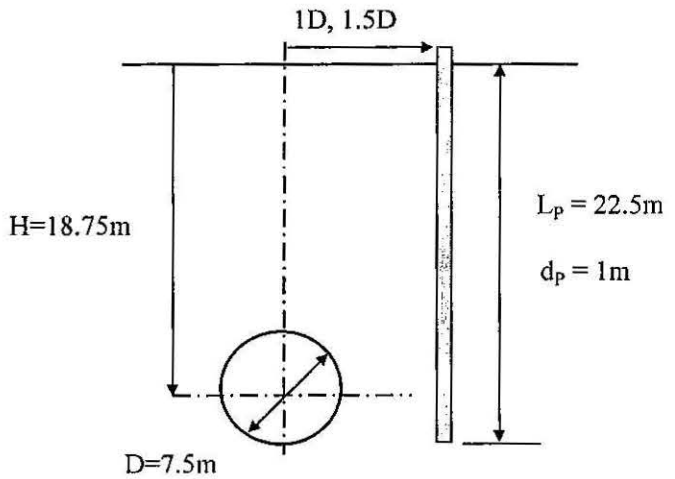

Figure 4.16: Typical Problem Configuration

The details of the tunnel-pile system used in this study are as follows:

- Tunnel depth = 18.75m and tunnel diameter = 7.5m
- Ground loss = 0.26% (obtained from tunnel face deformation).
- Pile length = 22.5m and diameter = 1m modelled as continuum elements

- Bending stiffness of pile, $(EI)_p$ = 1960 MNm^2 and Poisson's ratio of pile = 0.25
- Young's modulus of soil = 30 MPa, ν_s=0.3, c = 5 kPa, $\varphi = 27^0$ and γ = 20 kN/m^3
- A Mohr-Coulomb model with a non-associated flow rule was used for the soil.

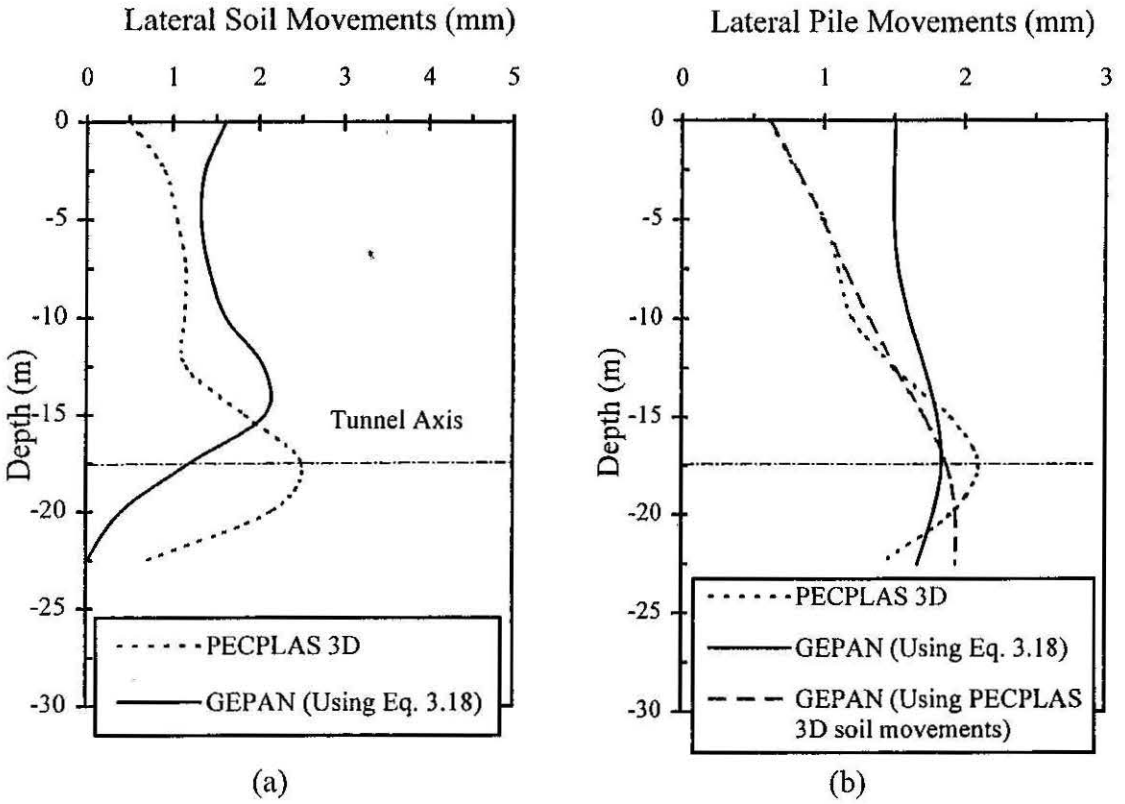

Figure 4.17: Comparisons of PECPLAS 3D and GEPAN Results for x = 1D

Figures 4.17 (a) and 4.17 (b) show comparisons of lateral soil movements of soil and pile, respectively, obtained from PECPLAS 3D and GEPAN for a single pile located horizontally at 1D distance from the tunnel. Figure 4.17 (a) shows that the prediction of lateral soil movements by both numerical tools are generally similar. In addition, it can be observed that the maximum lateral movement predicted by the equation 3.18 is slightly above the tunnel centreline, whereas that for PECPLAS 3D is at the tunnel centreline may be due to more uniform ground loss around tunnel. Yield zone around the tunnel was less than tunnel diameter.

Figure 4.17 (b) shows a comparison of computed lateral pile movements. The GEPAN prediction, using equation 3.18, shows that the pile behaves as a "stiff" pile, with nearly uniform lateral movement with depth, and a maximum value at the tunnel centreline. Predictions by PECPLAS 3D indicate a more flexible pile behaviour, where the lateral deflection of the pile increases from the ground surface to a maximum at the centreline

of the tunnel. In addition, a GEPAN analysis was performed to estimate the lateral pile deformation lateral soil movements obtained from PECPLAS 3D. Figure 4.17 (b) indicates that the GEPAN prediction shows relatively "stiff" pile behaviour with nearly uniform lateral movement with depth. Pile deflection predicted by PECPLAS 3D using identical lateral soil movements indicates slightly more flexible behaviour.

Figure 4.18 (a) and 4.18 (b) show comparisons of tunnelling-induced downdrag force and bending moment on a single pile located 1D horizontally from the tunnel axis.

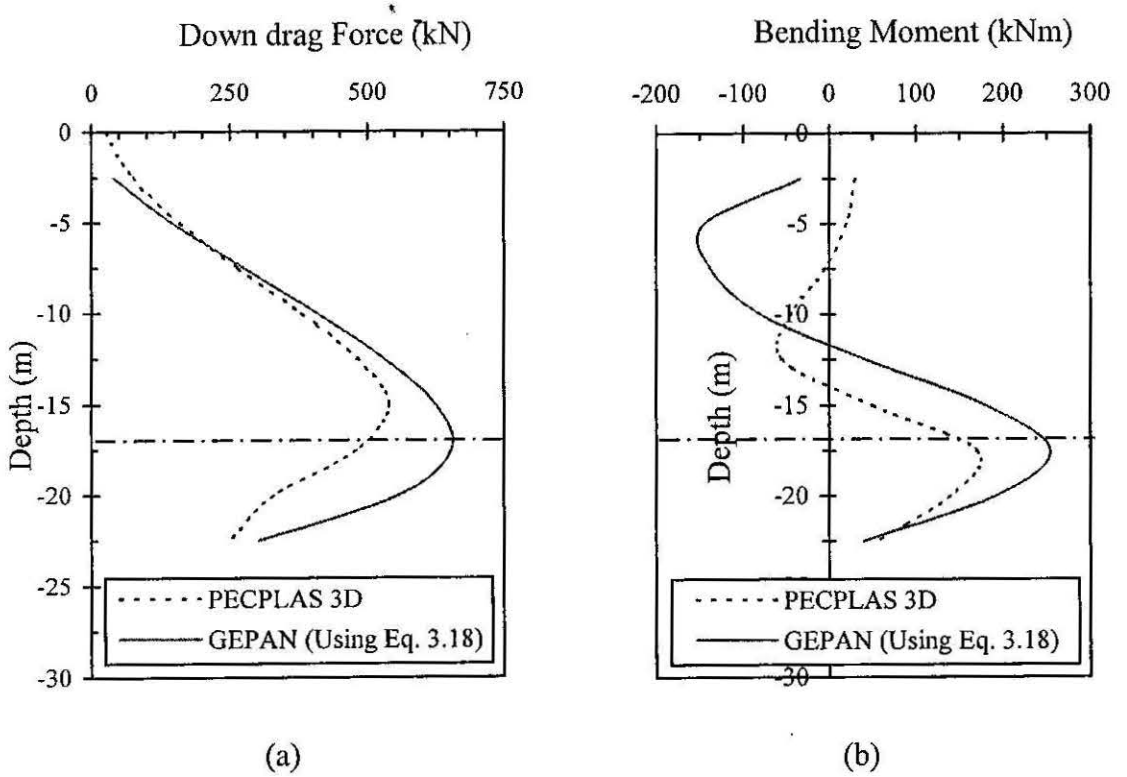

Figure 4.18: Comparisons of PECPLAS 3D and GEPAN Results for x = 1D

Figure 4.18 shows that both tunnelling-induced downdrag and bending moment predicted by PECPLAS 3D and GEPAN are almost identical shape, but that the maximum values predicted by GEPAN are slightly higher (about 15-20%) than the PECPLAS 3D predictions. It can be further observed that the maximum values of bending moment and the downdrag force occur at or near the tunnel centreline in both analyses.

In order to assess the variations in tunnelling-induced downdrag and bending moment, this analysis was repeated by locating the pile 1.5D horizontally away from the tunnel

axis. The comparisons of both downdrag and the bending moment are shown in Figure 4.19. The following are observed:

- PECPLAS 3D predicts much lower (about 50%) downdrag forces than GEPAN, although the maximum bending moment predictions are similar,
- The negative bending moment predicted by PECPLAS 3D is almost 100% less than the GEPAN predictions, and
- Both tunnelling-induced downdrag forces and bending moment are reduced by 40 - 50% when the pile is moved away from the tunnel horizontally from 1D to 1.5D.

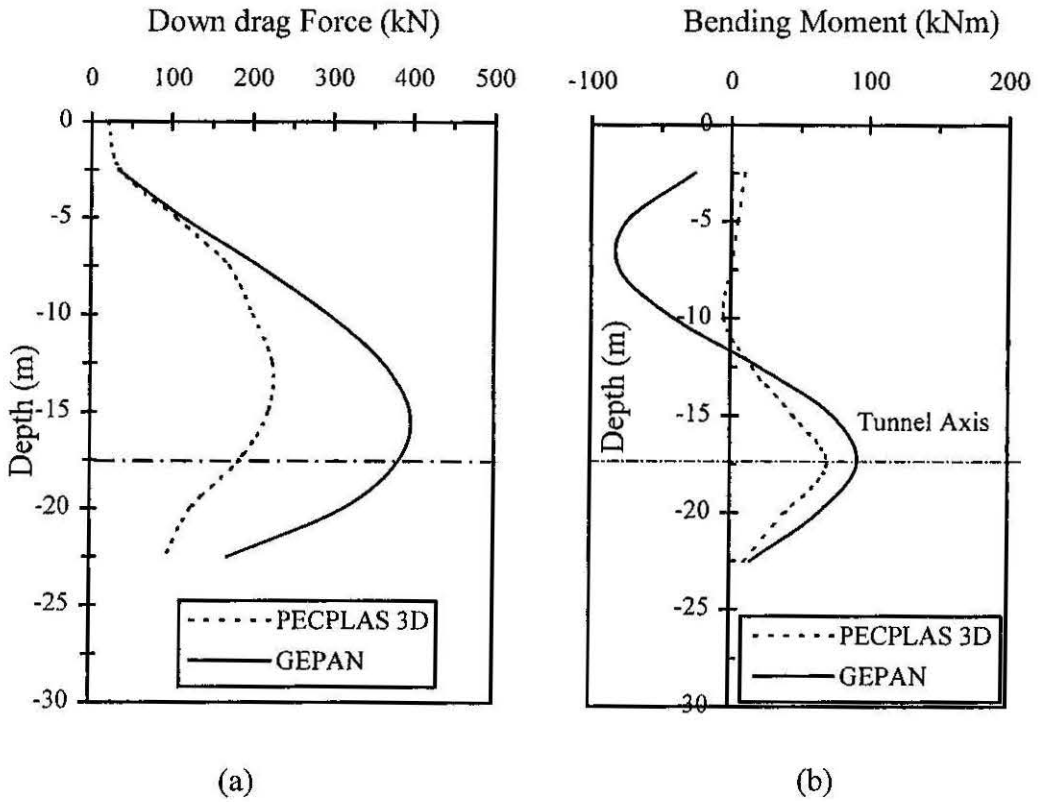

Figure 4.19: Comparisons of PECPLAS 3D and GEPAN Results for x = 1.5D

The induced downdrag force and bending moment are an indirect measure of the variation of the settlement and the lateral displacement of the soil with the pile depth. The computer program PECPLAS 3D predicted much smaller induced downdrag force and bending moment when the pile is further away from the tunnel (from 1D to 1.5D). This indicates that the tunnelling-induced ground deformation predicted by PECPLAS 3D become more uniform when moving away from the tunnel. It is shown in Section 3.5 that the settlement trough predicted by PECPLAS 3D is much wider and indicates less differential settlement than the prediction from equation 3.13.

4.5.3 Pile Group

Figure 4.20 shows the typical configuration of tunnel-pile group system used in this comparison study.

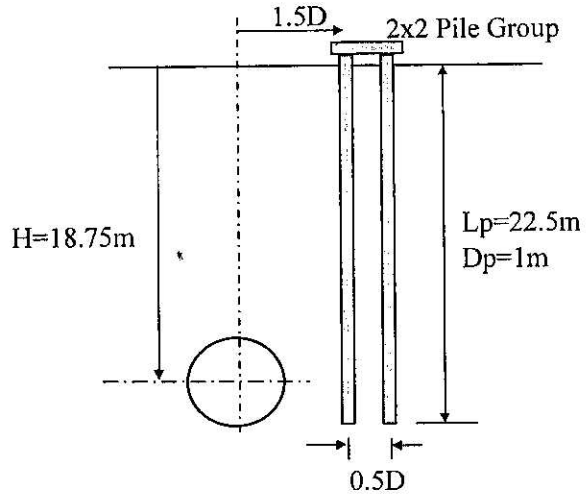

Figure 4.20: Typical Configuration of Tunnel-Pile Group Used in the Study

The soil and pile properties are the same as those used in the single pile analysis. In this study, the "front" pile refers to the pile closest to the tunnel. Figures 4.21(a) and (b) show the comparison of tunnelling-induced axial downdrag predictions made by PECPLAS 3D and GEPAN for "front" and "rear" piles respectively.

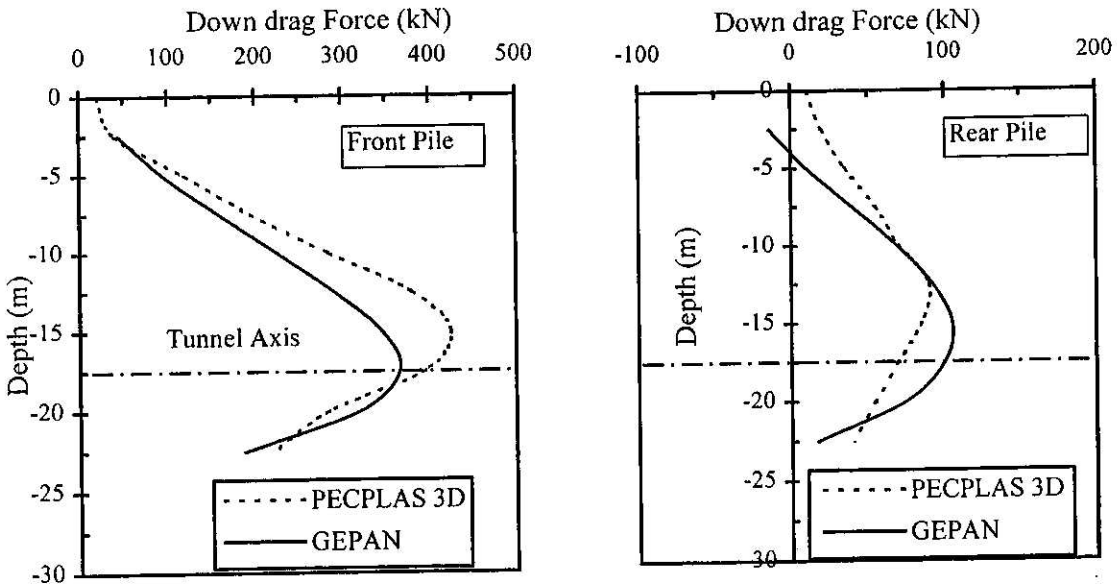

Figure 4.21: Comparisons of Tunnelling-Induced Axial Downdrag

The following are observed:

- predictions made by both PECPLAS 3D and GEPAN are similar in magnitude and distribution with depth,
- tunnelling-induced downdrag force on the "rear" pile is only about 30% of the downdrag force induced on the "front" pile, and
- the maximum downdrag force is experienced at about the depth of the tunnel centreline.

The maximum downdrag forces induced on the "front" pile of the pile group, and an isolated single pile located horizontally about 1.5D from the tunnel are about 350kN and 400kN respectively. This indicates that the reduction in downdrag force due to group effects is about 10%.

Figures 4.22(a) and (b) show the comparison of tunnelling-induced bending moment predictions made by PECPLAS 3D and GEPAN for "front" and "rear" piles respectively.

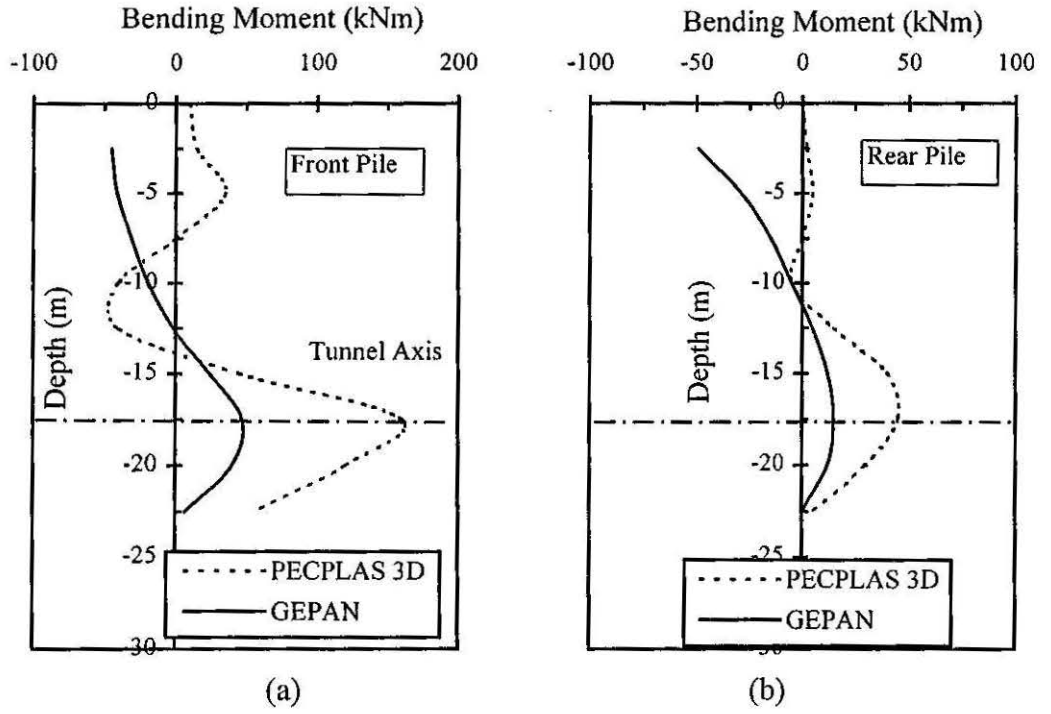

Figure 4.22: Comparisons of Tunnelling-Induced Bending Moment

The GEPAN predictions of maximum bending moment are much lower than the predictions of PECPLAS 3D. The reason for this may be because in PECPLAS 3D, the pile fixity at the pile cap was modeled inadequately or due to the difference in soil deformation field in PECPLAS 3D and GEPAN analyses. Both Figures 4.22 (a) and (b) show

that the bending moment predicted by PECPLAS 3D at the pile head is almost zero, which may not be the case in practice. Predictions by GEPAN appear to be more realistic for the group analysis.

4.6 COMPARISONS WITH 3D FDM ANALYSIS (FLAC 3D)

4.6.1 Introduction

FLAC 3D is a three-dimentional explicit finite-difference programme for engineering mechanics computation (Itasca, 1997). This programme contains an automatic 3D grid generator in which grids are created by manipulating and connecting pre-defined shapes. Structures, such as tunnel liners, piles, sheet piles, cables, rock bolts or geotextiles, that interact with the surrounding soil or rock, may be modeled with the structural element logic in FLAC 3D.

FLAC 3D has ten built-in models: the "null" model, three elastic models (isotropic, transversly isotropic and orthotropic elastic), and six plasticity models (Drucer-Prager, Mohr-Coulomb, strain-hardening/softening, ubiquitous-joint, bilinear strain-hardening/softening ubiquitous-joint, and modified Cam-clay). The material can yield and flow, and the grid can deform (in large-strain mode) and move with the material that is represented. The explicit Lagrangian calculation scheme and the mixed-discretization zoning technique used in FLAC 3D ensure that plastic collapse and flow are modelled accurately.

In this section, predictions made by FLAC 3D for a typical tunnel-pile group configuration are discussed. In addition a comparison study is performed with the predictions using GEPAN.

4.6.2 MODELLING AND ANALYSES

Figure 4.23 shows a typical tunnel-pile group configuration in this study. The configuration and the properties of the tunnel-pile group system analysed are given below;

- tunnel diameter and the depth to the centreline are 6m and 15m. A ground loss value of 1% is considered,
- a 2x2 pile group, with four identical piles of 0.8m diameter and 18m long piles, is located horizontally 5.5m ("front" pile) away from the tunnel centreline, and
- the pile cap is not in contact with the soil.

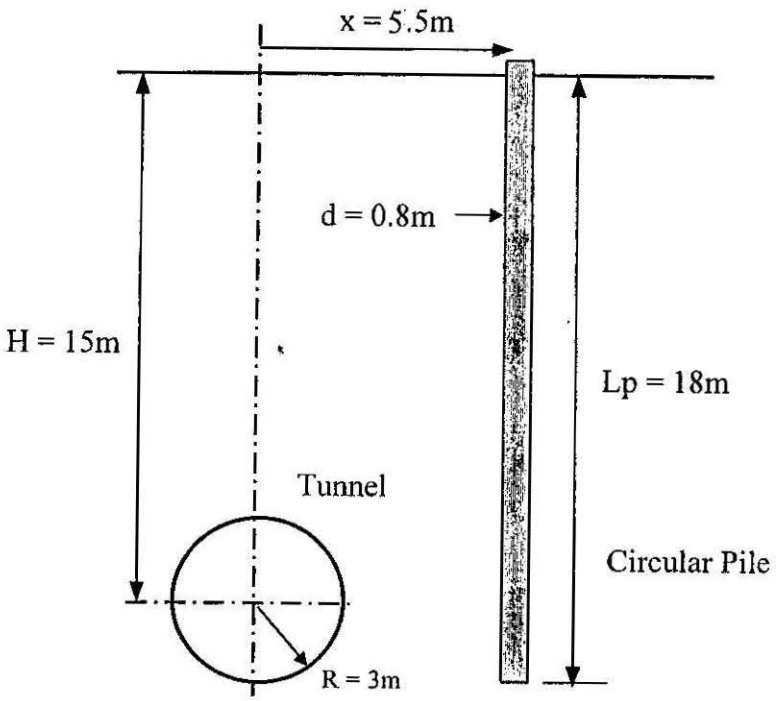

Figure 4.23: Typical Tunnel-Pile Group Configuration Analyses

Piles were modelled as structural elements and the pile-soil interaction was modelled using elastic spring constants. The stiffness of normal coupling spring, K_n, and shear coupling spring K_s were derived using the equations 4.1 and 4.2 (Randolph, 1992).

$$k_n \approx 10\left(\frac{E_p}{G}\right)^{-0.14} G \tag{4.1}$$

$$k_s \approx 1.6\ G \tag{4.2}$$

where E_p is the Young's Modulus of solid pile and G is shear modulus of pile.

Both the cohesive strength of the shear coupling and the normal coupling were assumed to be equal to the undrained shear strength of the soil. The soil strength considered in this study was 75 kPa. The friction of the normal coupling spring for the lateral load condition was assumed to be zero.

Soil, pile and pile-soil interface parameters used in this study are given in Table 4.1.

Table 4.1: Material Properties

Soil: Elastic Model	
Bulk Modulus	5×10^7 Nm^{-2}
Shear Modulus	1.07×10^7 Nm^{-2}
Density	2000 kgm^{-3}
Pile: Elastic Model	
Young's Modulus	30×10^9 Nm^{-2}
Poison's Ratio	0.25
Cross sectional Area	0.503 m^2
Exposed Perimeter	2.51 m
Second Moment of Inertia, I_y=I_z	2.0×10^{-2} m^4
Polar Moment of Inertia, J	0.643 m^4
Soil-Pile Interface: Elastic Model	
Stiffness of shear coupling, K_s	1.92×10^{10} N/m/m
Cohesive strength of shear coupling, C_s	7.5×10^4 Nm^{-2}
Friction of shear coupling, φ_s	10^0
Stiffness of normal coupling, K_n	1.6×10^{11} N/m/m
Cohesive strength of normal coupling, C_n	7.5×10^4 Nm^{-2}
Friction of normal coupling, φ_n	0^0

The in-situ stresses were assumed to be as per the K_0 condition. Once the gravitational equilibrium was reached, the tunnel excavation was carried out by applying the "null" model to the specified tunnel grid geometry. Since the analyses were only concerned with the ultimate tunnelling-induced behaviour, applying a "null" model to simulate the tunnel excavation is considered to be adequate.

The maximum deformation of the tunnel wall estimated using Equation 3.16 (for the tunnel configuration, D=6m, H=18m) is about 30mm, for a ground loss value of 1%. This indicates that the maximum tunnelling-induced strain around tunnel wall is approximately in the 10^{-3} range. Therefore, elastic analysis should predict the actual field behaviour reasonably well.

Figure 4.24 shows the three-dimensional finite difference grid discretisation of the model. The bottom face was fixed in all three directions x,y and z. Both the faces

parallel to xz-plane were fixed in the y direction and the other two faces parallel to the yz-plane were fixed in the x direction.

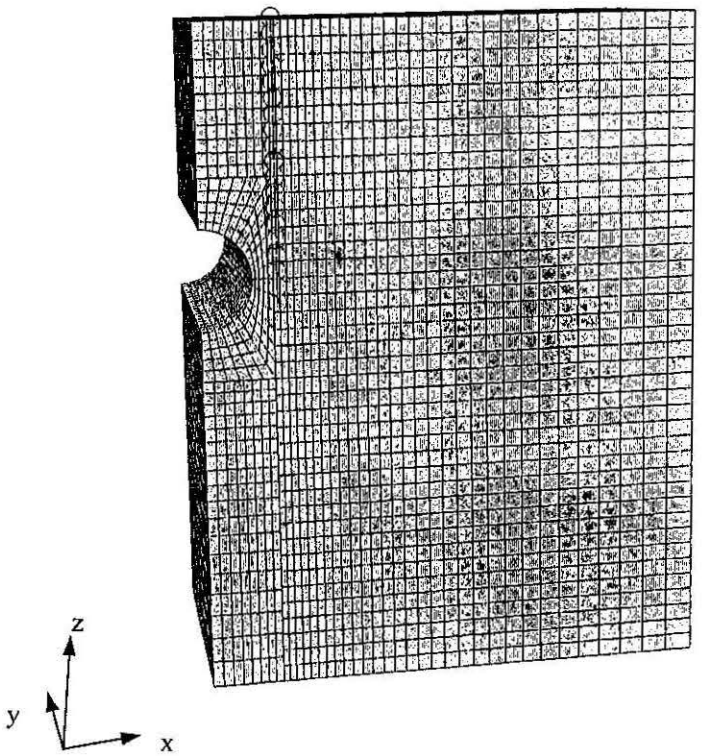

Figure 4.24: 3-D Finite Difference Grid Model

4.6.3 Comparisons

Figures 4.25 and 4.26 show the predictions of tunnelling-induced bending moment and the axial downdrag force using GEPAN and FLAC 3D. It may be observed that although the shape of the profiles are identical, the predictions made by GEPAN over estimate the bending moment and the axial down drag force. Figure 4.27 shows the comparison of the lateral deformation of the pile. The maximum lateral deformation predicted by both GEPAN and FLAC 3D are almost the same. However, the pile head deflection predicted by GEPAN is larger than the FLAC 3D prediction. The reasons for the difference in predictions may be due to the following reasons;

- Tunnelling-induced deformation pattern predicted by both programmes are different due to the difference in the displacement modelling technique, and

- The empirical formulae used in FLAC 3D to model the pile-soil interface were derived from the equivalent 2D problem, which may not model the 3D problem accurately.

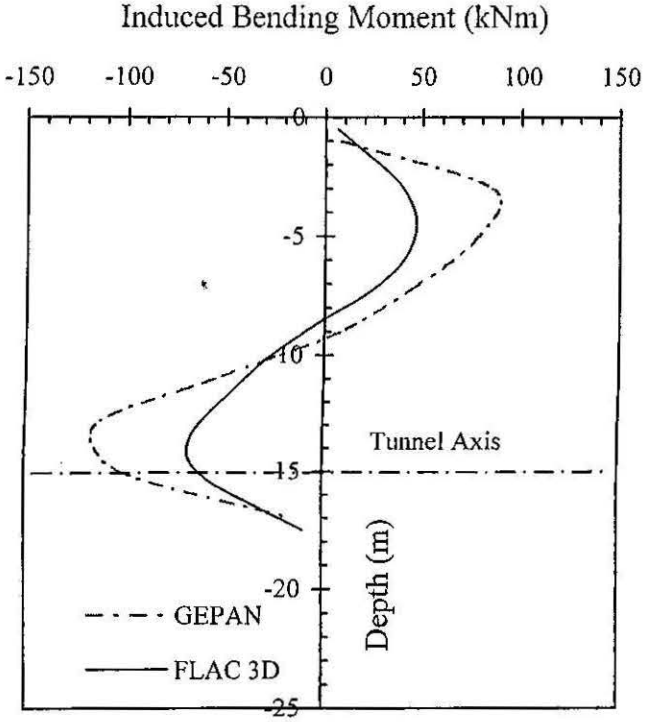

Figure 4.25: Comparison of Tunnelling-Induced Bending Moment

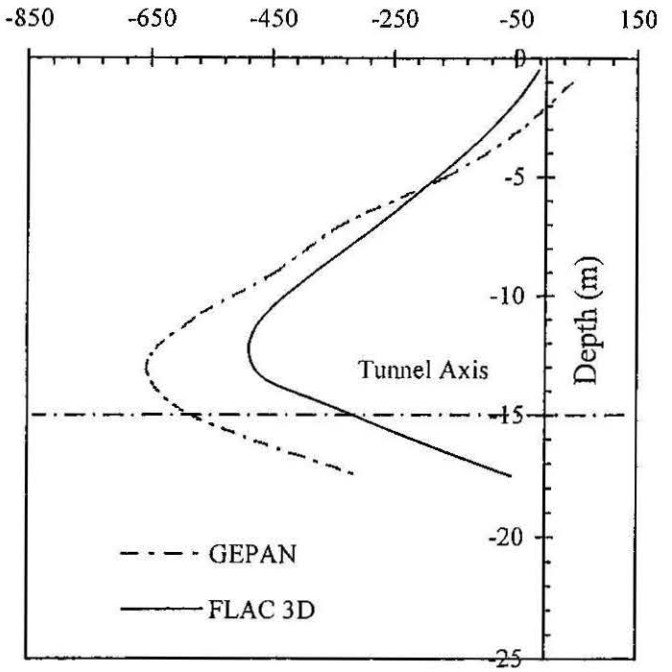

Figure 4.26: Comparison of Tunnelling-Induced Axial Down Drag Force

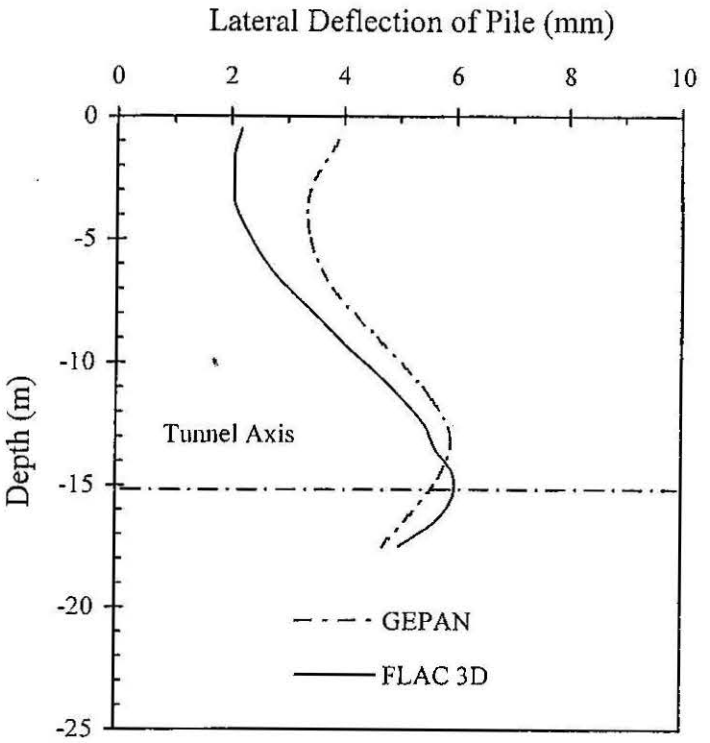

Figure 4.27: Comparison of Tunnelling-Induced Lateral Deflection of Pile

4.7 SUMMARY

An accurate assessment of the influence of tunnelling adjacent to an existing pile foundation is possible only by using 3D numerical analysis with an appropriate soil model. Three 3D numerical tools were studied in this chapter, a 3D boundary element computer programme, GEPAN (Xu and Poulos, 1998), a 3D finite element computer programme, PECPLAS 3D (Mroueh, 1998) and a 3D finite difference programme FLAC 3D (Itasca, 1997). The results of these analyses were compared by performing single pile and pile-group analyses. In general, all three programs predicted broadly similar tunnelling-induced pile behaviour.

Although the GEPAN program over-estimated the tunnelling-induced behaviour, it is very computer-cost-effective. Computer running times for an identical problem using GEPAN and FLAC 3D were about 2 minutes and about 10 hours respectively using a computer with 196MB RAM. In addition, unlike in FLAC 3D, GEPAN programme require only relatively few soil and pile parameters.

The GEPAN computer program has been used to perform a parametric study of single piles and pile groups. The findings of this study can be summarised as follows:

- Significant pile settlement and lateral deformation are induced when the pile tip is located at about the tunnel depth level. Similarly the induced downdrag force and bending moment are significant when the pile tip is located at tunnel invert level. The pile head rotation is not significantly affected by pile length, but the diameter has a significant effect on the pile head rotation.
- In an elastic analysis, the pile deflection follows the soil deflection and the magnitude of the pile responses is proportional to the ground loss value. Therefore, computed pile responses may be normalised with respect to the ground loss value.
- A single pile analysis can predict adequately the tunnelling-induced bending moment, lateral deformation and settlement for pile in a pile group, at an identical distance from the tunnel. However, the tunnelling-induced axial downdrag force estimated for a single pile is about 15-20% higher than for a pile in a pile group, reflecting the influence of pile-soil-pile interaction.

As a first approximation, the tunnelling-induced additional bending moments, lateral deflections, settlements and the rotations on piles may be added to the original design values due to structural loading, when making an assessment of the potential for pile overstressing due to tunnelling operations.

CHAPTER FIVE

CENTRIFUGE MODEL TESTING

5.1 INTRODUCTION

Centrifuge model testing is a powerful tool for investigating geotechnical problems. With this facility it is possible to simulate the full scale prototype stress field and the stress changes that take place subsequently during the construction. Soil strength and stiffness is governed by the current state of stress within the soil and the stress history to which it has been subjected and both of these can be taken into account by using careful sample preparation techniques combined with centrifuge modelling.

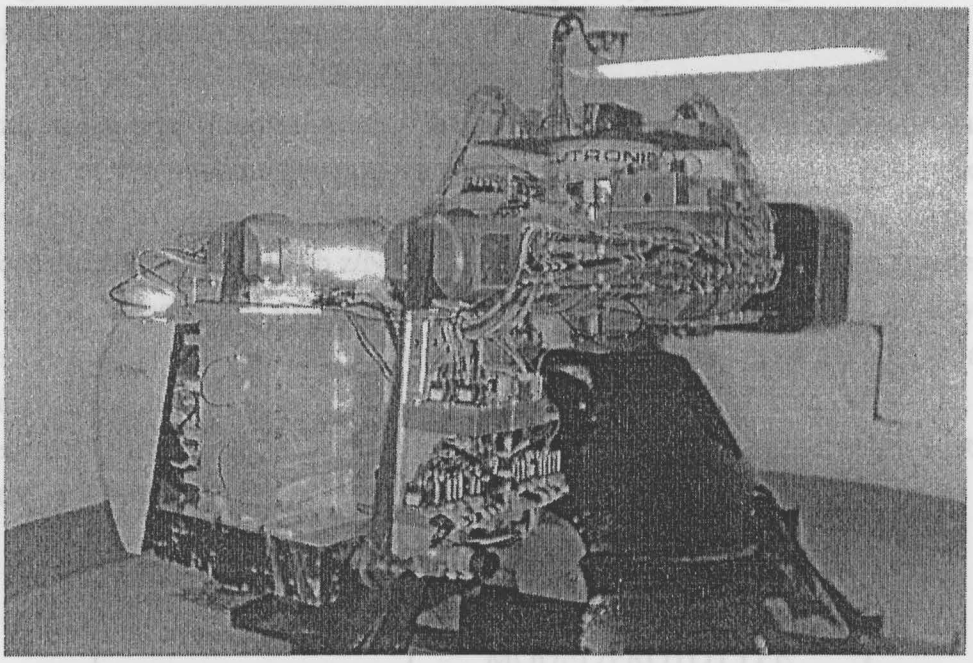

Figure 5.1: Centrifuge Test Equipment Used in the Study (Acutronic 661)

Three centrifuge model tests have been performed to assess tunnelling induced ground deformations in clays and their effects on adjacent pile foundations. All three tests were conducted in the geotechnical centrifuge at the University of Western Australia (UWA). The facility houses an Acutronic 661 centrifuge with a maximum payload of 400kg (at 100g) and a platform radius of 1.8m (Figure 5.1). The facility has been described fully by Randolph et al (1991).

The purpose of this chapter is to describe; (i) modelling techniques for single piles and a pile group, (ii) development of a model tunnel and the technique used to simulate the ground loss, (iii) soil sample preparation and instrumentation, and (iv) the testing method and data acquisition techniques.

5.2 CENTRIFUGE MODELLING PRINCIPLES

The major principle behind all forms of model testing for engineering purposes is correct scaling of the relevant parameters and equivalence of key dimensionless parameters in the model and prototype. In geotechnical modelling, one of the main dimensionless parameters of interest is usually the ratio of strength to effective stress level. The behaviour and strength of soil are critically dependent on current and past stress levels, and therefore the stress history as well as the current stress state is of major importance. Centrifuge modelling is now widely accepted as the most versatile technique for obtaining similar stress conditions in model and prototype, as the gradient of self-weight stress may be accurately reproduced.

To obtain similitude of stress between the centrifuge model and the prototype, the linear dimensions of the model are reduced by a factor N, and it is then subjected to an acceleration of N gravities, effectively increasing the self-weight by the same factor. Therefore the stresses at a depth z/N in the model will be identical to those at a depth z in the prototype. If the model soil has the same stress-strain responses as the prototype soil, strain similarity is also achieved. The principles and relevant scaling laws relating to centrifuge model testing have been discussed in detail by Schofield (1980). The scaling laws relevant to the type of centrifuge model testing conducted for this research study are presented in Table 5.1.

Table 5.1: Centrifuge Model Scaling Relationships

PARAMETER	SCALING RELATIONSHIP MODEL/PROTOTYPE
Gravity Level	N
Length	1/N
Density	1
Mass	$1/N^3$
Stress	1
Strain	1
Bending Moment	$1/N^3$
Time (diffusion)	$1/N^2$
Time (creep)	1
Force	$1/N^2$

Due to the reduced linear dimensions in the model, drainage path lengths are reduced by a factor N and consequently the consolidation time (caused by diffusion of pore water) is reduced by N^2 according to Terzaghi's consolidation theory. This presents a significant advantage over full scale experiments, as approximately 27 years of prototype behaviour may be modelled in 24 hours with a scaling ratio, N, of 100.

5.3 TESTING PROGRAMME AND MODEL LAYOUT

The programme of centrifuge tests performed for this study is listed in Table 5.2. A total of 3 centrifuge tests were conducted. The aims of these tests were to assess tunnelling-induced ground movements and their effects on adjacent piles for various tunnel depth/pile length ratios, and to compare the behaviour of a single pile with an identical pile in a group. All tests were conducted at an acceleration level of 100g.

Table 5.2: Details of Centrifuge Tests (Prototype Scale)

TEST 1	Pile Length, L_p= 18m Pile Diameter, d = 0.9m	Tunnel Depth, H= 15m
TEST 2	E_pI_p = 1400MNm2 Tunnel Diameter, d= 6m	Tunnel Depth, H= 18m
TEST 3	Stiff Kaolin Clay, ~ 75kPa	Tunnel Depth, H= 21m

The prototype consisted of a 6m diameter tunnel excavated in a stiff clay stratum. Depth to the tunnel centreline was varied (15m, 18m and 21m) between tests. The three tests were identical in all aspects except for the depth of the model tunnel. Details of these tests are given in Table 5.2. The diameter and length of the prototype foundation piles were 0.9m and 18m respectively. A single pile and a 2x2 pile group, with a centre-to-centre spacing of 2.5m, were installed on either side of the tunnel. The distance from the tunnel centerline to the front row in the group and the single pile was 5.5m. The bending stiffness EI of model pile was derived by performing back analysis of the calibration curve for load-settlement behaviour. It appears that the back calculated EI value is slightly higher than the theoretical EI value for the model pile considered in this study, may be due to the composite nature of the pile due to instrumentation and epoxy coating.

A section through the model is shown in Figure 5.2. The dimensions in this figure are expressed in model units. To approximate the dimension length in prototype terms, the values given in Figure 5.2 must be multiplied by the centrifuge model factor, N, which in this study was100.

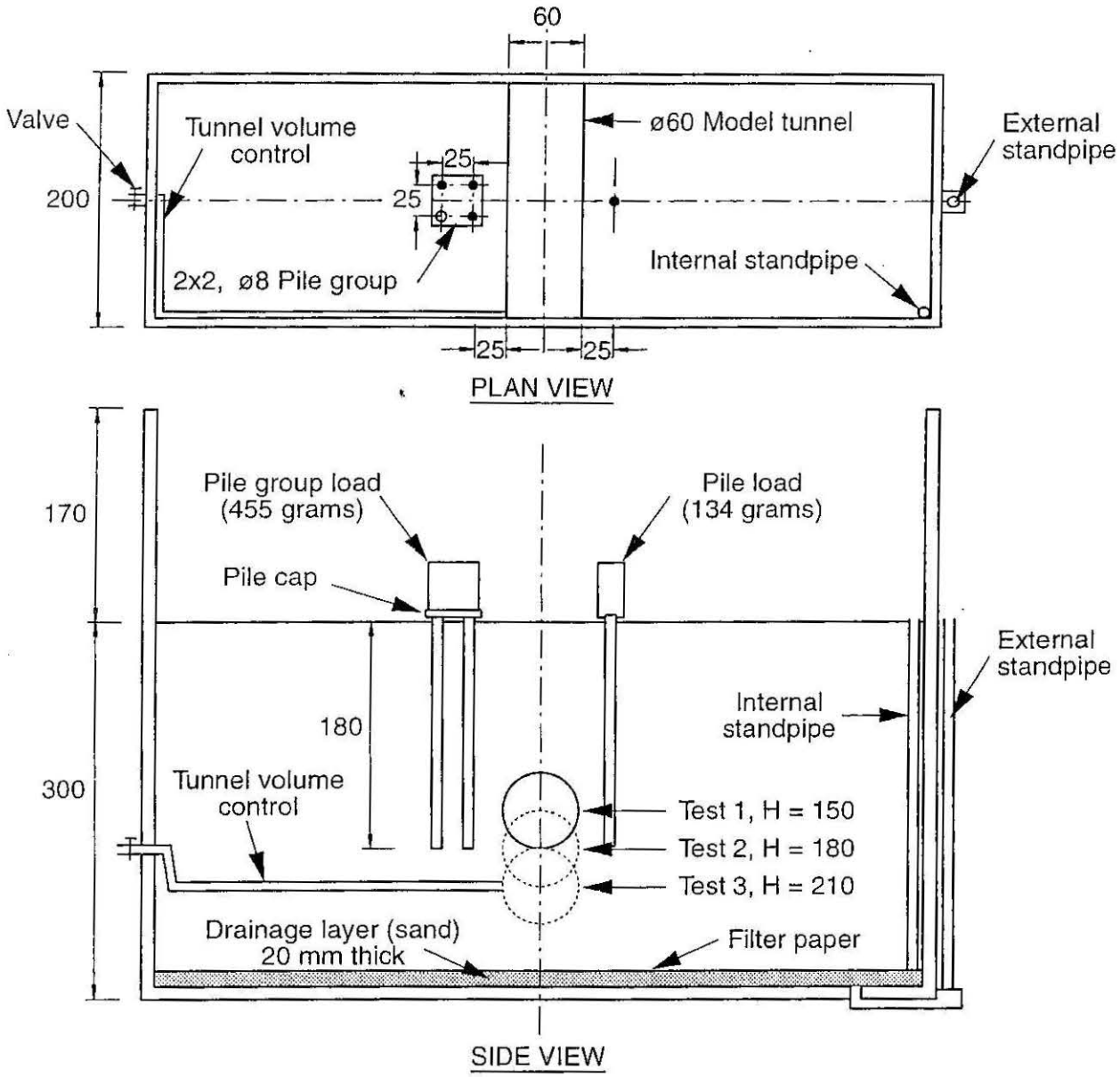

Note: i - All dimensions are in mm - model scale
ii - H = depth to tunnel centreline
iii - • - instrumented piles
o - dummy pile

Figure 5.2: Basic Configuration of Centrifuge Model

5.4 GEOTECHNICAL CENTRIFUGE

The centrifuge machine shown in Figure 5.1 features a swinging platform upon which test packages are mounted, enabling models to align normal to the resultant gravity field as machine speed increases. The swinging platform has a radius of 1.8m, with a maximum headroom of approximately 900mm during rotation. The centrifuge drive

system is microcomputer controlled, enabling continuous unbalance and safety checks to be performed.

Data acquisition is currently enabled via a stack of 23 electrical slip rings. Multiplexing and amplification of instrumentation signals is performed on the centrifuge, which currently permits monitoring of up to 106 channels. The electrical signals are then passed through the slip rings to a data-logging and actuator-controlling computer in the adjacent control room. Data are periodically saved to disk and streamed to several other computers in the control room which allow real-time graphing of the data. An auxiliary computer is also available for various control operations, such as periodic solenoid valve operation.

Vertical stress distribution with depth in the model is parabolic rather than linear, due to the variation in centrifuge acceleration with radius. The acceleration field in the centrifuge is also "curved", leading to radial inclination of body forces. The dimensions and configuration of the UWA centrifuge are such that the maximum error in stress variation with depth is less than 4.5%, and the gravity field inclination is a maximum of about 7 deg. from vertical (Stewart, 1990).

5.5 MODEL PILES

5.5.1 Single Pile and Pile-Group

Model piles were designed to replicate 0.8m diameter circular concrete piles at prototype scale. The prototype piles had a bending rigidity, E_pI_p = 1400 MNm^2. For similarity between model and prototype in bending: $E_pI_p=N^4E_mI_m$ and also $d_p=Nd_m$, where d=diameter of pile, N=centrifuge scale (in these tests N=100), E=Young's modulus, I=section moment of inertia and suffices *p* and *m* represent prototype and model respectively.

In total, four instrumented model piles and a dummy pile of the same diameter were constructed using brass tubes of 8mm outer diameter and 7.24mm internal diameter. All model piles were 180mm in length and the bottom end of each pile was sealed by a plastic end cap. Strain gauges were placed externally at 8 locations on three of the "bending" piles (single pile and two in a group, front and rear) to measure lateral response and at 6 locations on an "axial" pile (pile group-front) to measure axial response, as shown in Figure 5.3. Teflon coated electrical wires of about 0.3mm diameter were channelled through the center of the hollow model pile section. When each pile had been strain gauged and cabled, the outer surface was coated with epoxy resin for

were channelled through the center of the hollow model pile section. When each pile had been strain gauged and cabled, the outer surface was coated with epoxy resin for waterproofing. The final external diameter of each pile was 9mm. Each pile was permanently wired to a junction box containing multiplexing circuitry to enable a maximum of 10 channels to be passed down one pair of electrical slip rings.

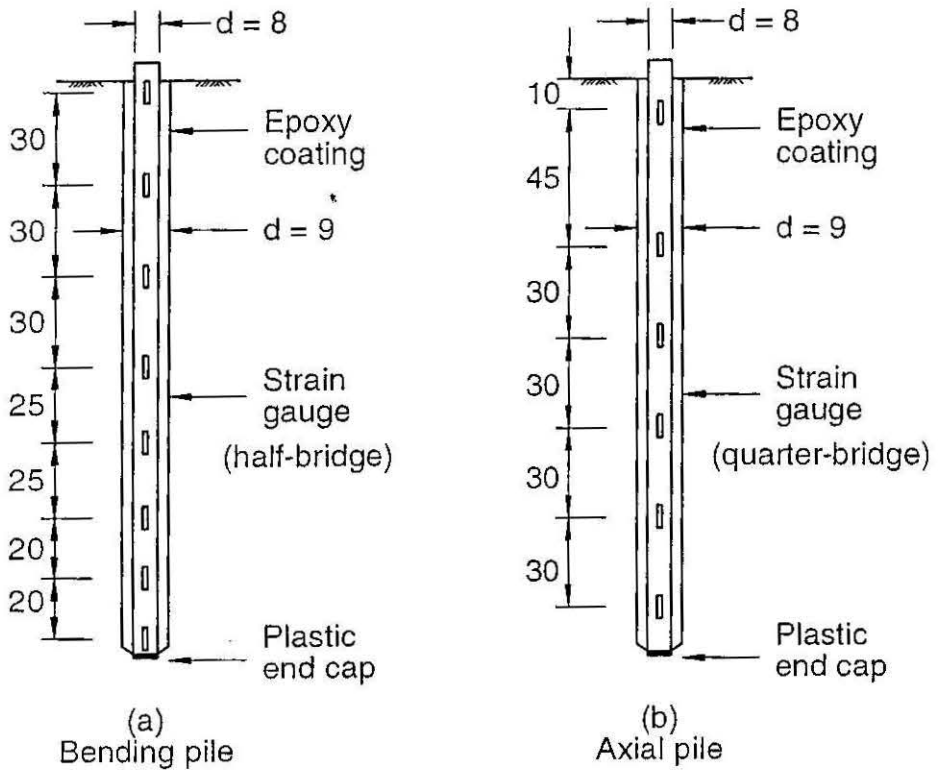

Figure 5.3: Instrumented Model Piles (dimensions in mm)

A pile cap was constructed for the 2 x 2 pile group from 10 mm thick aluminium plate. This cap held the pile vertical at a centre to centre spacing of 25mm (approximately three times the pile diameter). The ultimate axial load bearing capacity of a prototype pile was estimated to be 2.68MN for a 0.8m diameter 18m long pile installed in soil with an average undrained shear strength of 75 kPa. 50% of the ultimate load was taken as the working load, giving a global factor of safety of 2.

Applying the centrifuge scaling relationships, an equivalent mass of 130 g was applied to the top of the model single pile and 445 g was applied on top of the model 2x2 pile group to achieve the working load at 100 gravities. A group efficiency of 0.85 was used to estimate the group load carrying capacity (Poulos and Davis, 1980). The masses were fabricated using lead weights. Coupling units were fabricated to connect pile heads and pile loads to prevent any damage to the strain gauge wires. Figure 5.4 shows the

schematic details of pile loads and coupling units on both the single pile and the pile group.

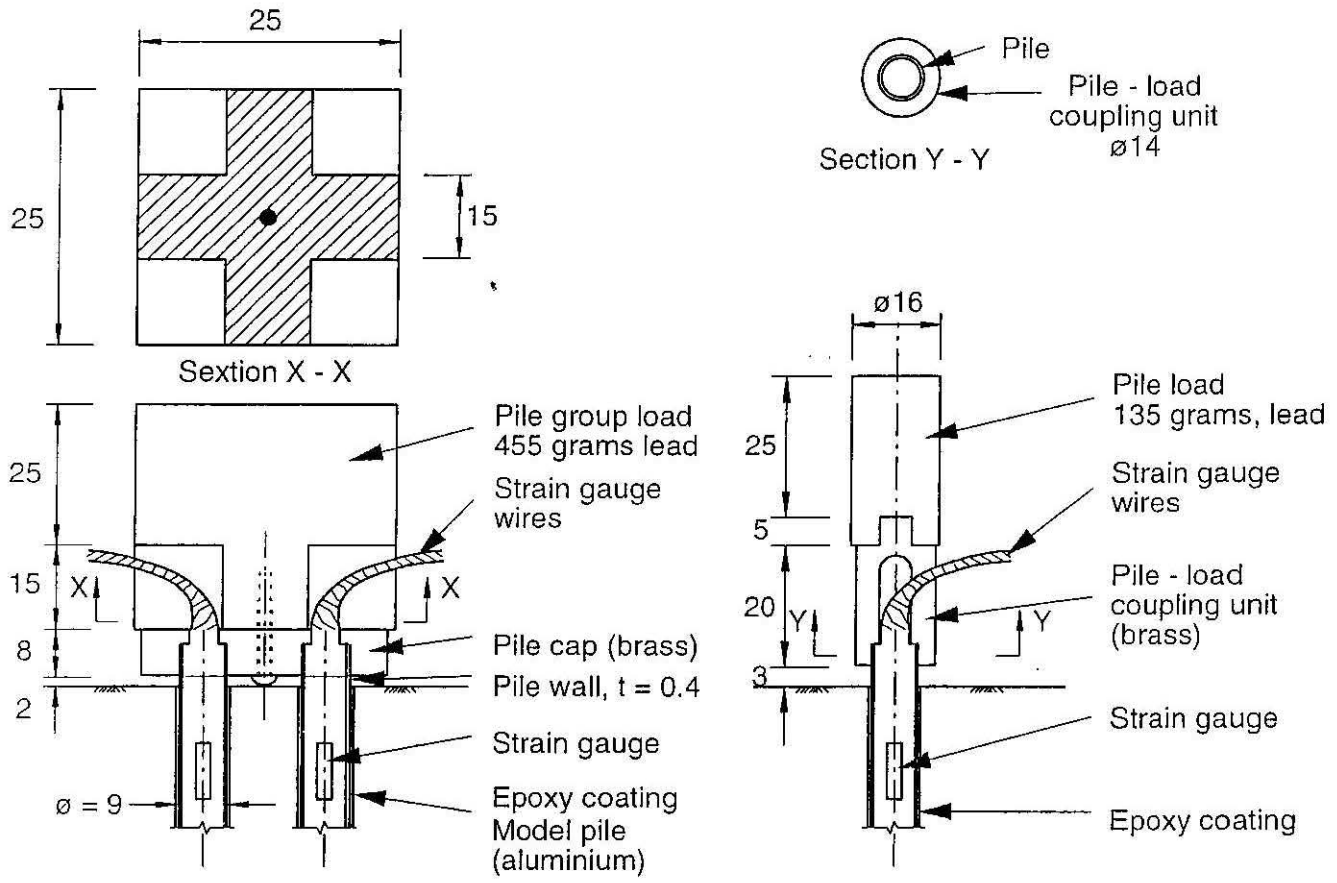

NOTE:

i - Pile - pilecap and pilecap - pile load are glued using Locktight
ii - all units are in mm - model scale

Figure 5.4: Pile Cap and Load Arrangement

A dummy pile without strain gauges or wiring was fabricated in a similar fashion to the instrumented piles described. The dummy pile was placed in the "rear" row of the pile group. Figures 5.5 (a) and (b) show model single pile and pile-group arrangements.

5.5.2 Calibration of Piles

"Bending" piles were calibrated prior to each test by suspending them between two knife edge supports and hanging a mass centrally on another knife edge. Strain gauge outputs

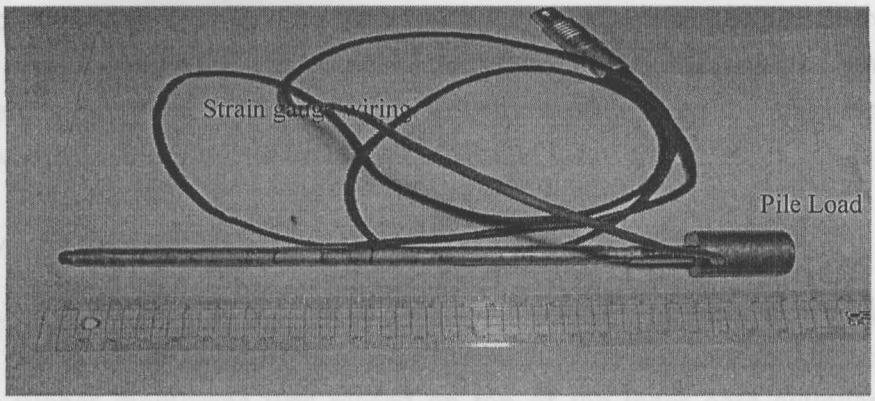

(a) Single Pile

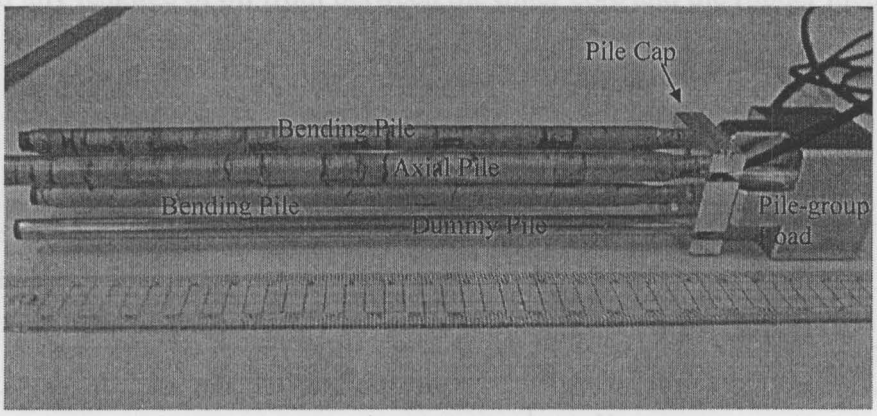

(b) Pile-group

Figure 5.5: Photographs Showing Model Single Pile and Pile Group

were then related to calculated bending moments. The process was repeated over several sections of the pile to obtain the highest possible output from each gauge. Before each calibration, all circuitry was checked and fixed resistors replaced if necessary to maintain bridge output near to zero at rest. This process may be responsible for some of the variation in calibration factors between successive tests.

The "axial" pile was calibrated by applying gradually increasing force on the top of the pile using actuators. The corresponding strain gauge outputs were then related to the axial forces.

5.6 Model Tunnel and Syringe Pump

5.6.1 Introduction

The tunnelling procedure was modelled in the laboratory centrifuge as a two-dimentional process by applying appropriate ground loss values. The technique of decreasing tunnel diameter during centrifuge flight was adopted to model the required ground loss. A syringe pump was fabricated to control the volume of oil from the tunnel that eventually controlled the tunnel diameter and thus the ground loss.

5.6.2 Model Tunnel

Figure 5.6 shows the cross section of the model tunnel. The inner core of the tunnel was made of 192 mm long, 54mm outer diameter aluminium tube, and a 0.5mm thick, 50mm diameter rubber membrane was placed on top of the inner core cylinder. The rubber membrane was attached at both ends of the inner core cylinder by end caps which prevented any leakage of oil from between the inner core and the rubber membrane.

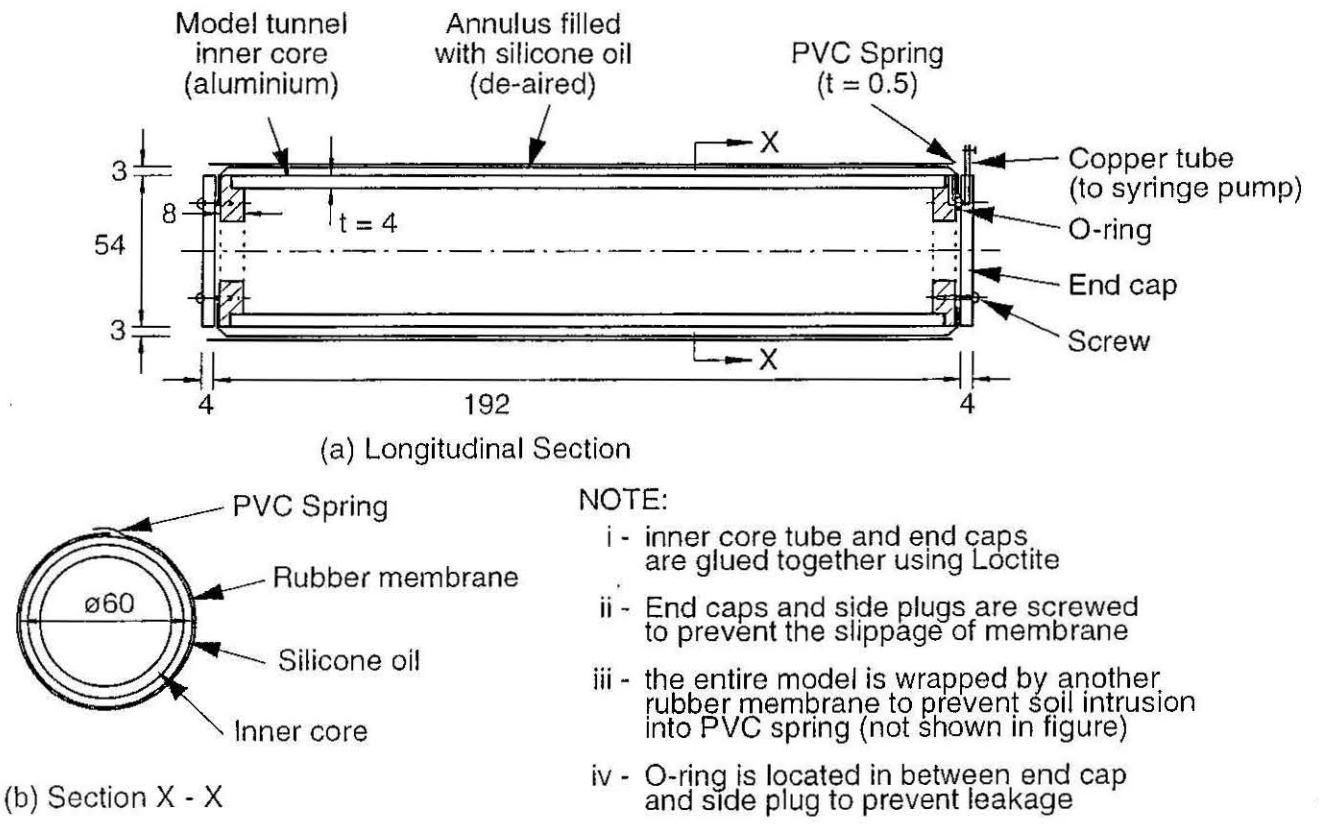

Figure 5.6: Section Details of Model Tunnel

Ground loss was controlled by varying the volume of oil in the annulus between the inner core and the membrane. A 1mm diameter hole was drilled through the end cap and inner core to allow passage of oil. The cylindrical face of the assembly was then covered by a 0.5mm thick smooth surfaced overlapping PVC spring to enhance tunnel stiffness, in an attempt to ensure uniform change in tunnel diameter during the test. The entire model tunnel was then covered by another rubber membrane to ensure watertightness and to prevent intrusion of soil particles between the leaves of the PVC spring. The total weight of the model tunnel assembly (without oil between the inner core and the rubber membrane) was about 170 g. Figure 5.7 shows different components of the model tunnel assembly.

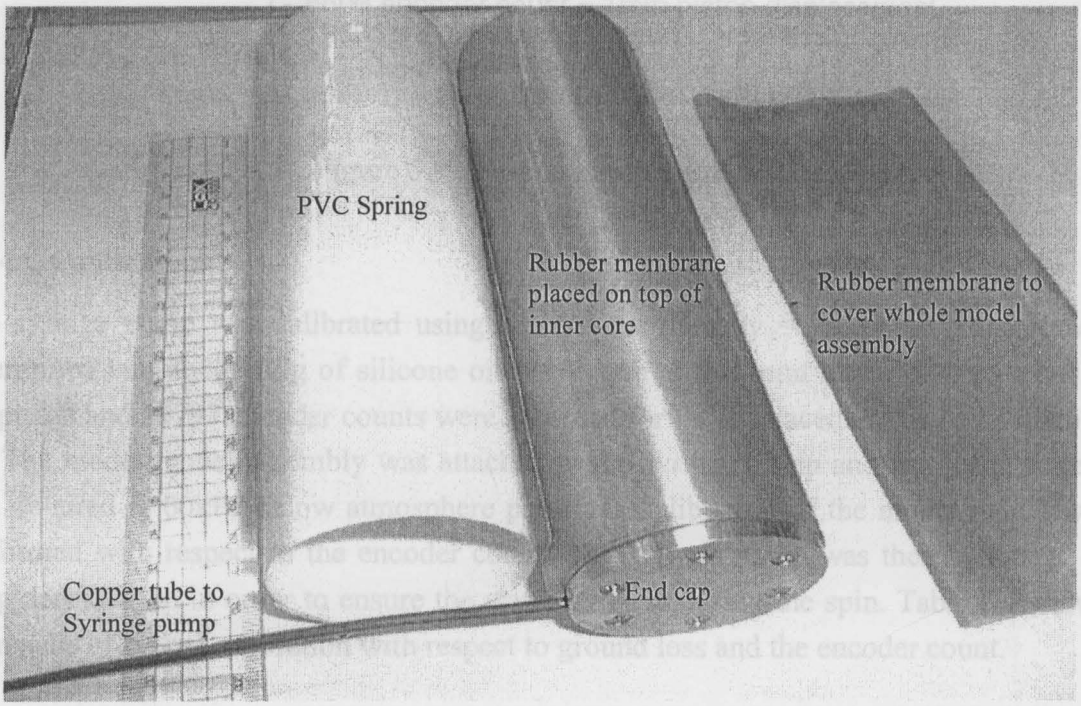

Figure 5.7: Components of Model Tunnel

5.6.3 Syringe Pump

A syringe pump was fabricated to control the volume of oil in the tunnel assembly. Figure 5.8 shows the schematic details of the syringe pump. The system consisted of a Maxon 70 Watt DC servo motor driving through a 66:1 planetary gearbox. A digital encoder with a line driver was mounted on the back of the motor. A Maxon positioning control unit (PCU 2000) was used for precise positioning by feedback from the digital encoder. A software package MPUI (Maxon PCU User Interface) was used for the configuration, programming and command interchange with the PCU2000 unit.

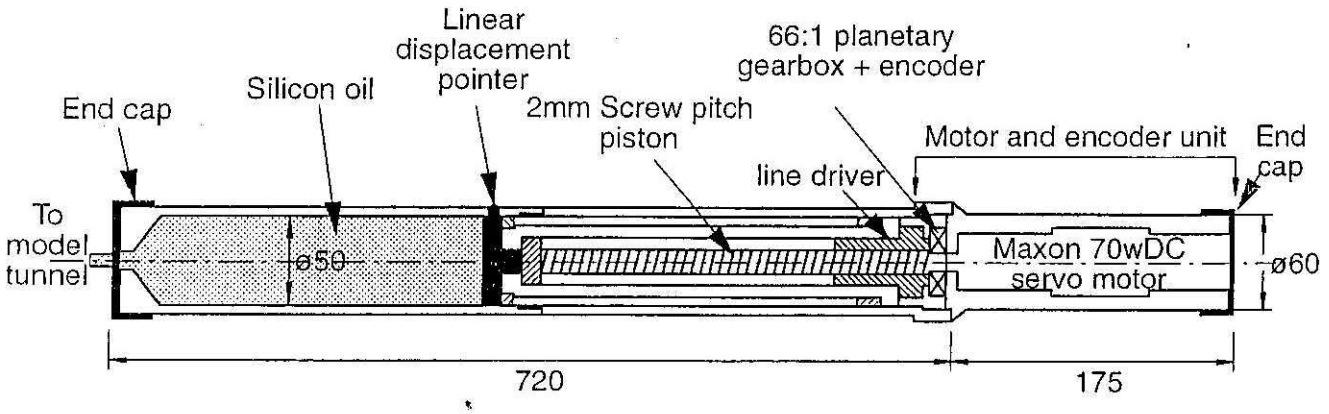

NOTE:
i - 6600 encoder count = 1mm piston displacement
ii - 1963 mm^3 oil volume = 1mm piston displacement
iii - $\rho_{silicone\ oil}$ = 966 kg/m^3
iv - 34797 encoder count = 1 gram silicon oil

Figure 5.8: Syringe Pump Section

5.6.4 Calibration

The syringe pump was calibrated using silicone oil (density = 966 kg/m^3) and it was determined that about 1.9g of silicone oil was required for 1mm linear displacement of the piston and 34797 encoder counts were recorded for the displacement of 1g of silicone oil. The model tunnel assembly was attached to the syringe pump and the entire system was de-aired at 60kPa below atmosphere pressure. Calibration of the model tunnel was performed with respect to the encoder count. The syringe pump was then calibrated at 100g accelaration in order to ensure the watertightness during the spin. Table 5.3 shows the results of tunnel calibration with respect to ground loss and the encoder count.

Table 5.3: Tunnel Calibration

Ground Loss (%)	Encoder Count
1	133878
2.5	366432
5	754022
7.5	1141612

5.7 SAMPLE PREPARATION

Models were prepared and tested in a plane strain strongbox designed for the UWA centrifuge. The strong box was made of aluminum and had an internal plan area of 200 mm by 650 mm and an internal height of 470 mm. One side wall of the box contained a window for viewing the side of the wall. A drainage hole in the base of the strongbox plumbed directly to a standpipe.

Kaolin was mixed to a slurry with a nominal water content of 120% (twice the liquid limit) using a mechanical drum mixer. Mixing was performed under vacuum for at least two hours before the slurry was carefully scooped from the mixer into a strongbox. Prior to placing the slurry a sheet of filter paper was placed over about 20mm thick drainage sand layer in the bottom of the strongbox to prevent mixing of the sand and clay. The strongbox was then placed in a consolidation frame and the sample was loaded by means of a rigid piston according to a predetermined loading pattern. The geotechnical properties of the kaolin clay used in these tests are described in detail by Stewart (1990) and are summarised in Table 5.4.

Table 5.4: Engineering Properties of Kaolin

Property	Value
Liquid limit, LL	61%
Plastic limit, PL	27%
Soil particle density, G_s	2.6 t/m^3
Angle of internal friction, ϕ'	23^0
Critical state friction constant, M	0.92
Void ratio at p'=1 kpa on critical state line, e_{cs}	2.14
Slope of normal consolidation line, λ	0.205
Slope of swelling line, κ	0.044
Parameter, $\Lambda=(\lambda-\kappa)/\lambda$	0.785
Spacing ratio, $r=p'_0/p'_{cs}$	2.14
Coefficient of consolidation (mean value), c_v	2 m^2/yr

The target average strength of the soil was about 75kPa. The required ultimate consolidation stress on the soil sample was estimated as about 600 kPa derived from the following relationship (Stewart, 1992):

$$\frac{s_u}{\sigma'_v} = 0.18 \quad OCR^{0.8} \tag{5.1}$$

where s_u = undrained shear strength, σ'_v = effective overburden pressure, and OCR = over consolidation ratio. The bulk unit weight of the kaolin was 16.5kN/m^3 and the coefficient of consolidation was about 2m^2/year. The soil sample was prepared in two layers to obtain the required sample thickness of 300mm. Figure 5.9 shows the consolidation frame used in this study.

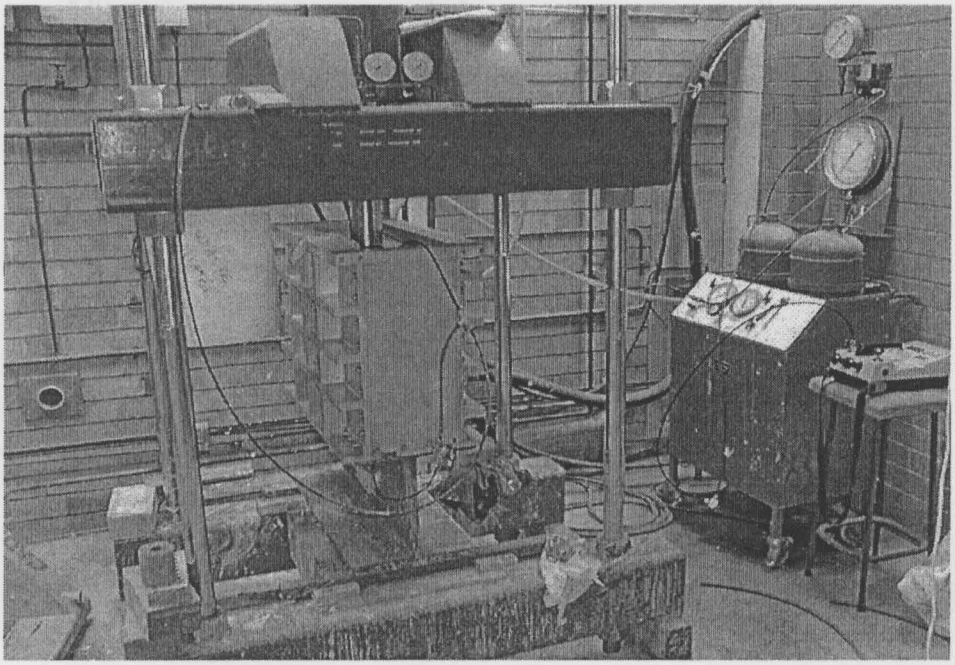

Figure 5.9: Sample Under Consolidation

5.8 INSTRUMENTATION

In total, three piles were instrumented with eight strain gauges at different locations to measure the induced bending moments and one pile was instrumented with six strain gauges to measure induced axial forces (Figures 5.3 and 5.5). Figure 5.10 shows the locations of laser displacement sensors (to measure pile head movements both vertical and lateral), potentiometers (to measure ground surface settlement), pore pressure transducers, and marker beads (to measure subsurface ground movements via video image processing).

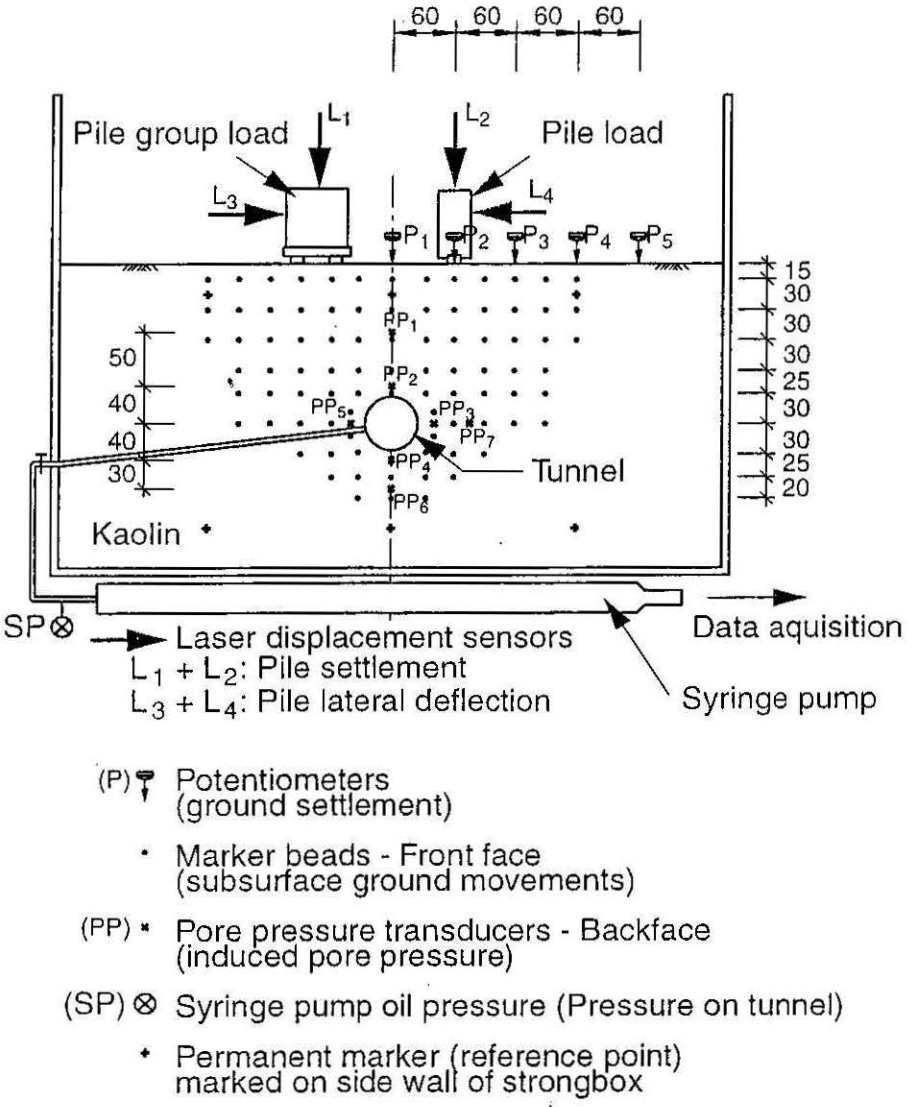

Figure 5.10: Instrumentation Configuration

A total of five potentiometers, with a 10mm stroke and a resolution of 0.005mm, were attached to an aluminium frame (instrument mounting unit) to measure the surface settlement trough. Non-contact laser displacement sensors (Keyence LB-01) were attached to the instrument mounting unit to measure the settlements and lateral deflection of both the single pile and pile group. Each laser displacement sensor had a measuring range of about 80mm, with a resolution of about 0.02mm.

Miniature pore pressure transducers (Druck PDCR 81) were used to measure pore pressures within the soil model. The transducers used were of 700kPa capacity and were de-aired by alternately applying ±100kPa pressure in a calibration chamber filled with

water. A Druck digital pressure indicator (DPI 601) was used to obtain the calibration factor and zero offset of each pore pressure transducer prior to insertion in the soil model. The resolution of pore pressure transducers was about 0.4kPa.

5.9 MODEL SETUP

When the consolidation stages were completed, the strongbox was removed from the consolidation frame and the surface free water was removed in order to prevent swelling of the clay during the model setup, which normally took 8-10 hours. The front wall of the strongbox containing the window was removed to install the model tunnel, the internal standpipe and the displacement marker beads. Tunnel excavation was performed in two stages using two different diameter thin wall tubes (50mm and then 60mm) in order to minimise the disturbance of the soil around the cylindrical cavity. The model tunnel was inserted into the cylindrical cavity and the tunnel outlet was plumbed to the syringe pump. The tunnel - syringe pump system was de-aired, and silicone oil was pumped into the model tunnel until it expanded to 60mm outer diameter. The plumb valve outside the strongbox was then closed to prevent any flow of the oil while model assembly continued.

Small black PVC marker beads (8mm long and 3mm diameter) were pushed into the vertical face of the clay (in a grid) to act as targets for the video image processing. A groove was formed in the soil sample at one corner of the strongbox and an internal standpipe was installed to maintain the surface water level during the test. The front window wall was highly greased and fixed to the strongbox. The rear wall of the strongbox was then removed and pore pressure transducers were installed at required locations (see Figure 5.10). The rear wall was highly greased and re-attached to the strongbox.

The single pile and pile group were installed at either side of the tunnel at the locations shown in Figure 5.2. Piles were pushed in at the rate of 0.5mm/s using an electric actuator (Randolph et al, 1991) clamped to the top of the strongbox. A prefabricated instrument mounting unit was fixed on top of the strongbox and the instruments were placed at the required locations. The external standpipe was plumbed into the base of the strongbox and the overflow level set. A photograph of a nearly fully assembled package is shown in Figure 5.11.

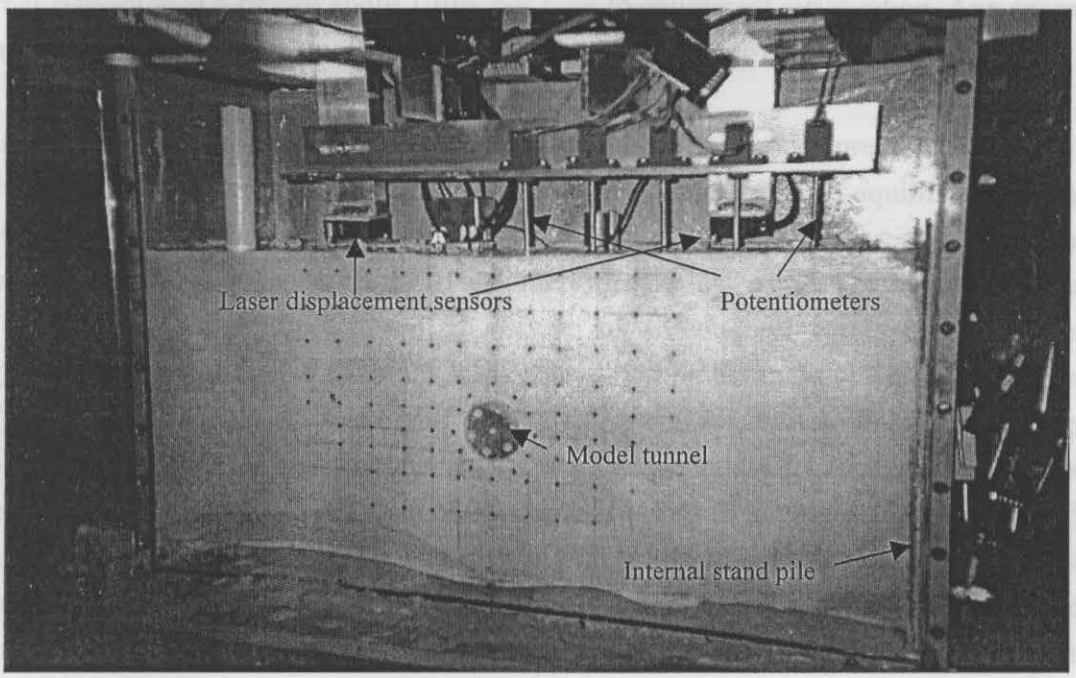

Figure 5.11: Photograph of Nearly Fully Assembled package

5.10 CENTRIFUGE FLIGHT AND TEST PROCEDURE

The model preparation for the tests was designed to be as reproducible as possible. The only difference in preparation between the three tests was the depth of the model tunnel (Table 5.2). After the assembly of the model, the package was mounted on the centrifuge arm. The water supply and drainage systems were set up so that the water table remained 5mm above the clay surface. Two miniature video cameras were attached to view the window side of the strongbox and to monitor the movement of the marker beads during the test.

The centrifuge was accelerated in 10g steps until it reached 100g. The acceleration of 100g was achieved at 1/3 depth of the strongbox, producing a vertical stress profile which was on average equivalent to the prototype. The magnitude of stress errors inherent in the centrifuge models is detailed by Stewart (1990).

Excess pore pressures were developed in the clay, corresponding to the increase in total stress due to the increased self-weight of the soil. During testing, pore pressures and surface settlements were plotted against square root of time on the screen. For the duration of the test, water was continually fed through a hydraulic slipring into the

external standpipe at a rate of about 1 litre per hour to counteract evaporation. Any excess water was allowed to overflow from the standpipe into the centrifuge enclosure.

About 30 - 45 minutes were required to allow equilibrium of pore pressure in the clay before commencing the next acceleration step. Once pore pressure equilibrium at the target acceleration (100g) was reached (approximately 8 hrs from the start of the test), the tunnel volume was reduced in-flight in specified ground loss steps. The tunnel diameter was reduced by extracting a specified volume of silicone oil corresponding to the designated ground loss value (Table 5.3). It generally took about 5s (13 hrs at prototype scale) to extract the required quantity of oil. A programme was written in MPUI language to control the volume of the silicone oil via the syringe pump to achieve the required ground losses (e.g: about 133878 encoder counts required to simulate 1% ground loss). Once the designated volume of the silicone oil was removed from the model tunnel, the pressure at the syringe pump was allowed to stabilise before commencing the next ground loss step. A typical variation of syringe pump pressure during a test (Test 3) is shown in Figure 5.12.

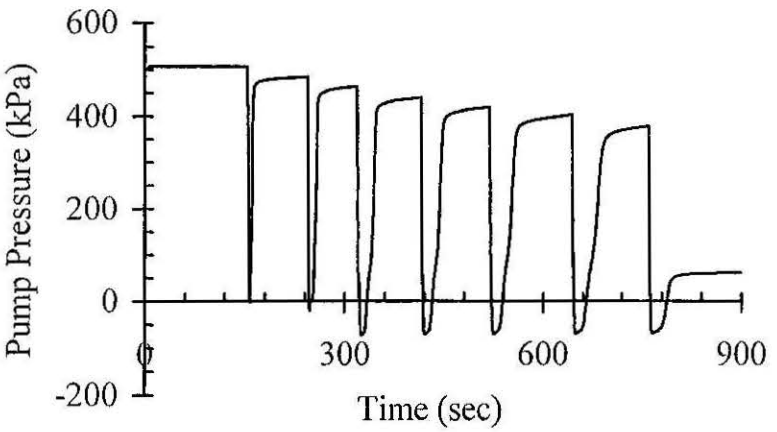

Figure 5.12: Syringe Pump Pressure Variation (Test 3)

Data were recorded at 5s intervals and the video recorder digital counts were also recorded at the beginning and the end of each ground loss step. At the end of the final ground loss step, the test was continued for 2hrs (equivalent to 2.28 years) in order to establish the ground movements and pile behaviour during long-term consolidation after excavation of the tunnel.

5.11 POST-TEST INVESTIGATIONS

Vane shear tests were performed immediately upon stopping the centrifuge, and then samples were taken for water content determination by pushing a 20mm diameter sampling tube into the clay sample. The vane (Pilcon model DR 2373) was rotated by hand at a rate of about 1 revolution per minute and the maximum value of torque read from a Pilcon laboratory vane torque meter. A dissipation time of 1 minute after insertion of the vane was used to allow partial dissipation of excess pore pressure generated during installation (Mahmoud, 1988).

The window side of the strongbox was removed and the model tunnel was removed slowly. The final diameter of the model tunnel was measured in order to confirm the tunnel calibration table prepared prior to the test. The clay sample was cut manually along the longitudinal centreline to visualise the post test deformation pattern of the soil around the tunnel and piles. Figure 5.13 shows a partial cross-section of the model after testing.

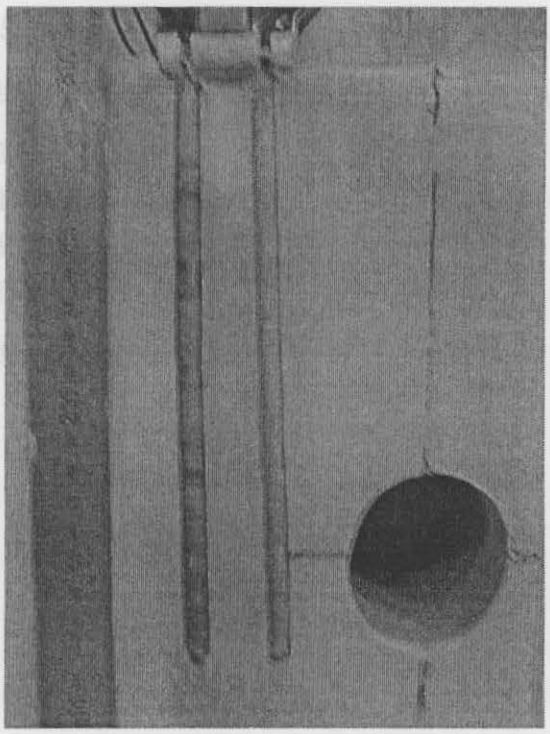

Figure 5.13: Partial Cross-Section of the Model after Test-1

CHAPTER SIX

CENTRIFUGE TEST RESULTS AND COMPARISONS

6.1 INTRODUCTION

The results obtained from three centrifuge tests, described in Chapter 5, are presented in this chapter. The responses of the tunnelling-induced ground and pile deformations are concentrated upon, although typical data associated with other aspects of the tests are also included. Brief comparisons with numerical predictions using computer programs FLAC 3D (Itasca, 1997) and GEPAN (Xu and Poulos, 1999) are also performed.

The purpose of this chapter includes the following aspects:

- comparisons of the tunnelling-induced ground deformations measured from laboratory centrifuge tests with the predictions using closed-form solutions presented in this study (Chapter 3) which are incorporated in the GEPAN computer program, and with numerical predictions using the FLAC 3D computer program,
- comparisons of tunnelling-induced pile behaviour measured from laboratory centrifuge tests with numerical predictions using computer programs FLAC 3D and GEPAN,
- comparisons of single pile behaviour with the behaviour of an identical pile in a pile group, and
- assessment of tunnelling-induced pile behaviour with increasing ground loss values.

The possible errors associated with the instruments used to measure tunnelling-induced ground and pile behaviour are also discussed. Results presented in this section are in prototype scale.

6.2 SOIL STRENGTH AND PORE PRESSURE

For the stiff kaolin clay used in these experiments, Horikoshi and Randolph (1996) reported that carrying out vane shear tests as soon as possible after stopping the centrifuge (approximately 15 to 20 minutes) gives a reasonable estimate of the shear strength during the test. Figure 6.1 shows the average shear strength profile and the moisture content values measured after stopping the centrifuge for all three tests. The soil strengths at the tunnel locations varied between 75 - 90 kPa. It is observed that the soil strength profile above the tunnel reduces more rapidly for test 1 than for tests 2 and 3. The reasons for this are believed to be (i) a relatively longer period (16 hours) of model preparation time in test 1 due to inexperience, and (ii) the free surface water was not

completely removed immediately after the removal of the strongbox from the consolidation frame in test 1.

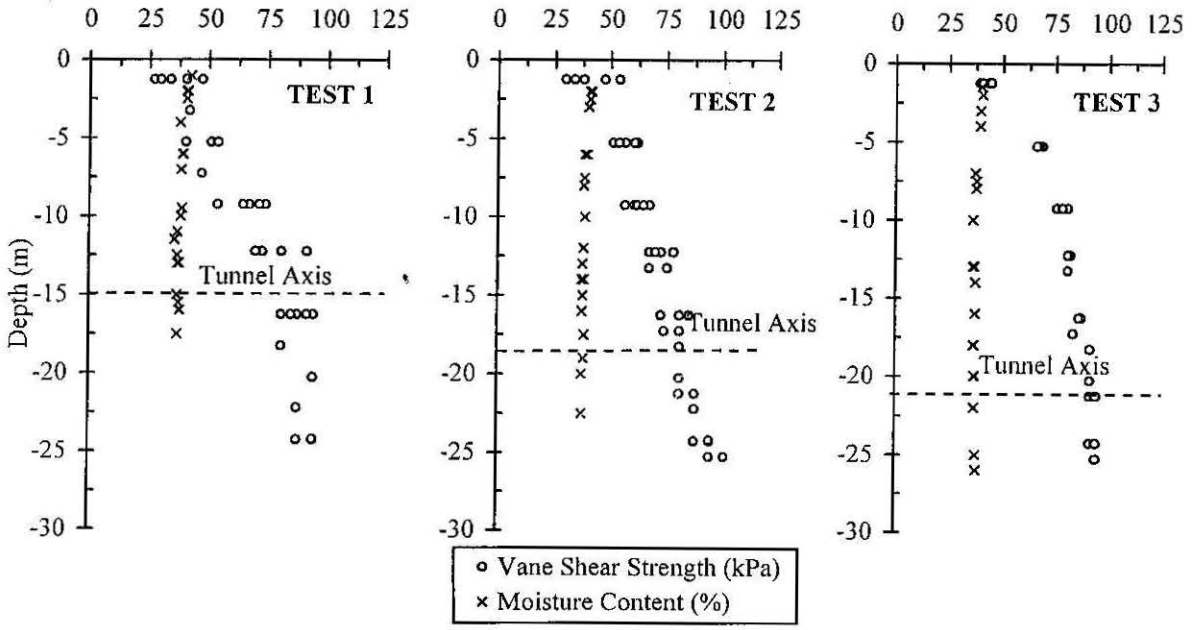

Figure 6.1: Post-test Vane Shear Strength and Moisture Content Profiles

The pore pressure changes during the test were recorded by seven pore pressure transducers located around the tunnel. Figure 6.2 and 6.3 shows a typical pore pressure changes with increasing ground loss values for centrifuge test 3.

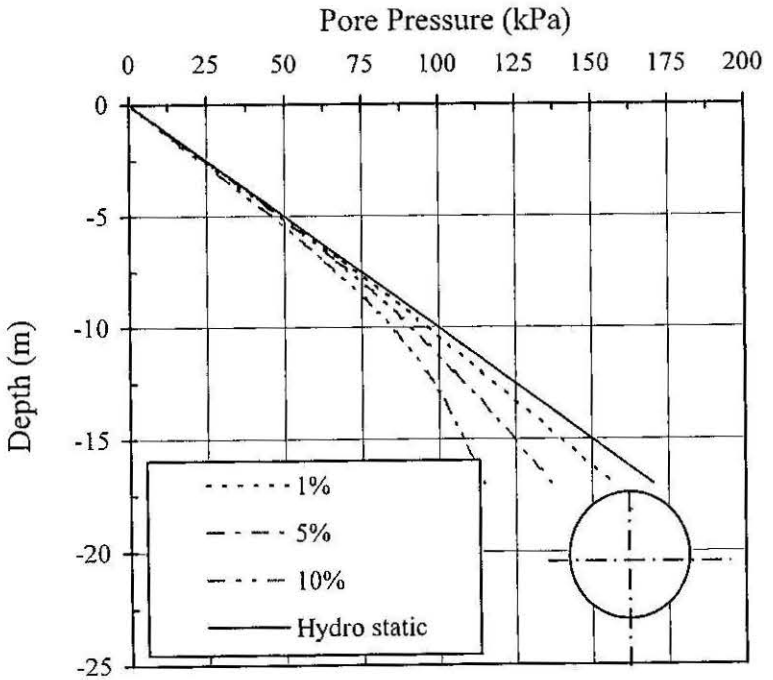

Figure 6.2: Pore Pressure Variation with the Depth

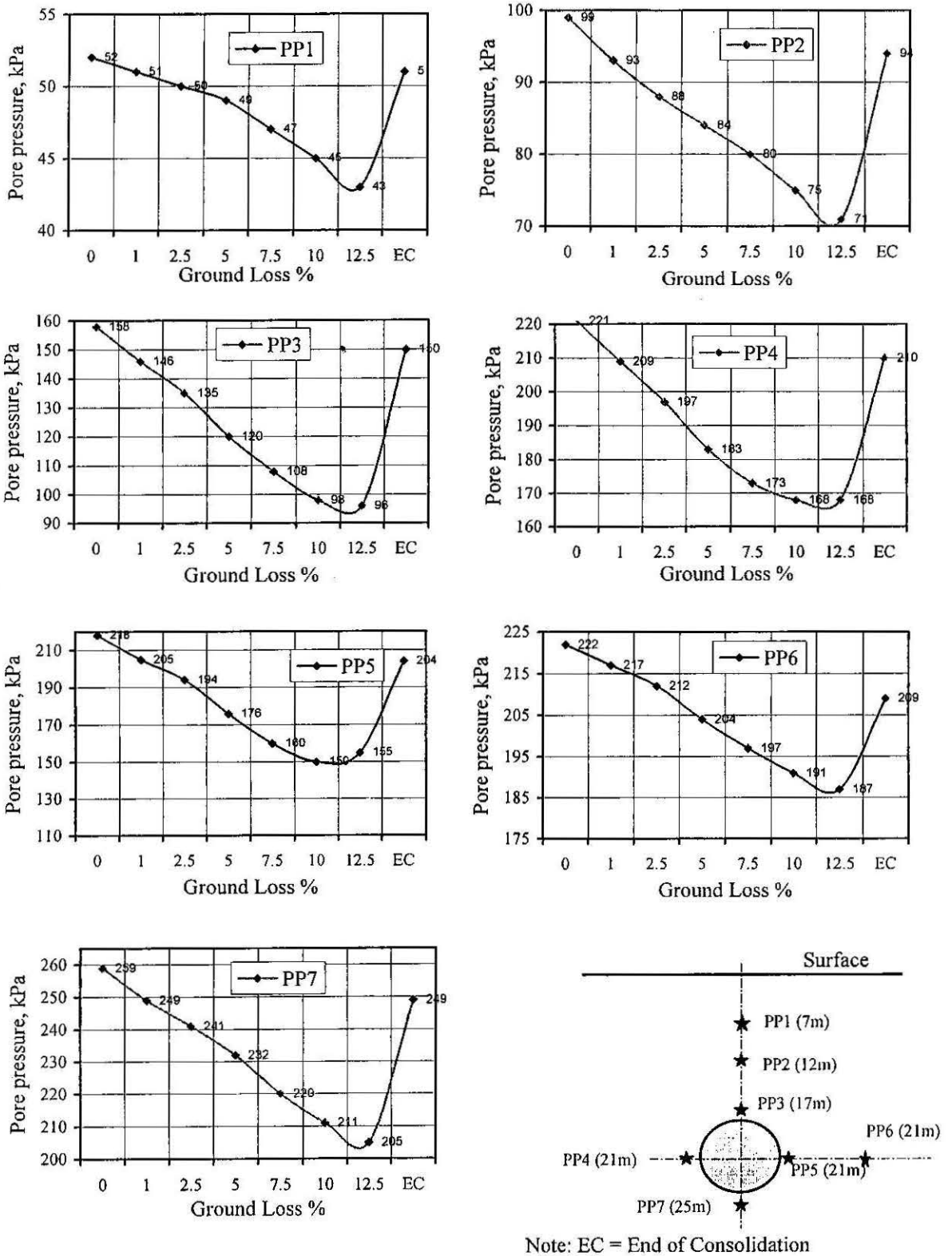

Figure 6.3: Typical Pore Pressure Changes for Different Ground Loss Values and End of Consolidation (~2years) for Test 3

Figure 6.2 shows that the undrained pore pressure changes with increasing ground loss values. During the tests, the ground loss steps (2.5% increments) were achieved at 4sec time interval in model scale (about 10hours in prototype scale), which indicate that the pore pressure changes occurred in undrained condition. In addition, it may be observed that pore pressure changes are linear until the ground loss value reached approximately 2.5% and increases non-linearly beyond 2.5%. Therefore, it may be assumed that the tunnelling-induced ground deformations follow linear elastic constitutive relationship at smaller ground loss values, typically below 2.5% ground loss for stiff clay whose soil strength exceeding 75 kPa.

Pore pressure reductions during each ground loss step were measured by transducers PP3, PP4, PP5 and PP6 that are located around the tunnel (see Figure 6.3). The overall pore pressure reductions measured by pore pressure transducers PP3, PP4, PP5, and PP7 were about 62 kPa, 53 kPa, 68 kPa and 54 kPa which indicate that the pore pressure changes around the tunnel are almost similar during tunnel excavation. This shows that uniform stress relief around the tunnel during tunnel excavation has been modelled accurately in the laboratory centrifuge testing. The pore pressure changes during tunnel excavation were stabilised (becoming hydrostatic) in the equivalent of 2 years time for the soil-tunnel configuration used in centrifuge test 3.

6.3 TUNNELLING-INDUCED GROUND DEFORMATIONS AND COMPARISONS

6.3.1 Introduction

Tunnelling-induced ground deformation measured from centrifuge tests for a ground loss value of 1% were compared with the closed-form formulae (equations 3.13, 3.16, and 3.18) proposed in this study along with numerical results derived from FLAC 3D computer program. Estimations using a few empirical correlations that are widely used in practice are also compared.

The planned ground loss steps were not achieved in test 1, due to the leakage of silicon oil from the model tunnel during the initial consolidation spin (about 12 hrs). The encoder count which models 1% ground loss in the original calibration became the representative value for 2.35% ground loss due to the reduced initial diameter of the model tunnel. Results for 1% ground loss for test-1 were obtained by linear interpolation. This enabled a comparison to be made with the results of tests 2 and 3 for a ground loss value of 1%.

6.3.2 Surface Settlements

Surface settlements were measured by potentiometers resting on the surface of the clay sample. The maximum error in potentiometer readings is ±0.5mm (at prototype scale). Figures 6.4, 6.5 and 6.6 show the surface settlement trough measurement from the centrifuge tests 1, 2 and 3, respectively, together with the surface settlement trough estimated from the closed-form solution presented in this study, empirical correlations by Mair et al (1981) and Clough and Schmidt (1981), and numerical results obtained from FLAC 3D. Comparisons were made for a ground loss value of 1%.

These figures reveal that the closed-form solution presented in this study (equation 3.13) predicts the surface settlement trough reasonably well for tests 2 and 3. In test 1, the settlement measured at the tunnel centreline is very large and is inconsistent with the subsurface settlement profile shown in Figure 6.7 and discussed in Section 6.3.3. Possible reasons for this observation may be a combination of a malfunction of the potentiometer and a soft "pocket" in the soil sample beneath the centre potentiometer.

Empirical predictions by Clough and Schmidt (1981) generally over-predict the settlements at the centre and give a narrower settlement trough width, whereas predictions by Mair et al (1983) result in better predictions, especially for test 1. Numerical results estimated from FLAC 3D elastic analysis generally under-predict the settlements at the tunnel centreline and result in wider surface settlement trough.

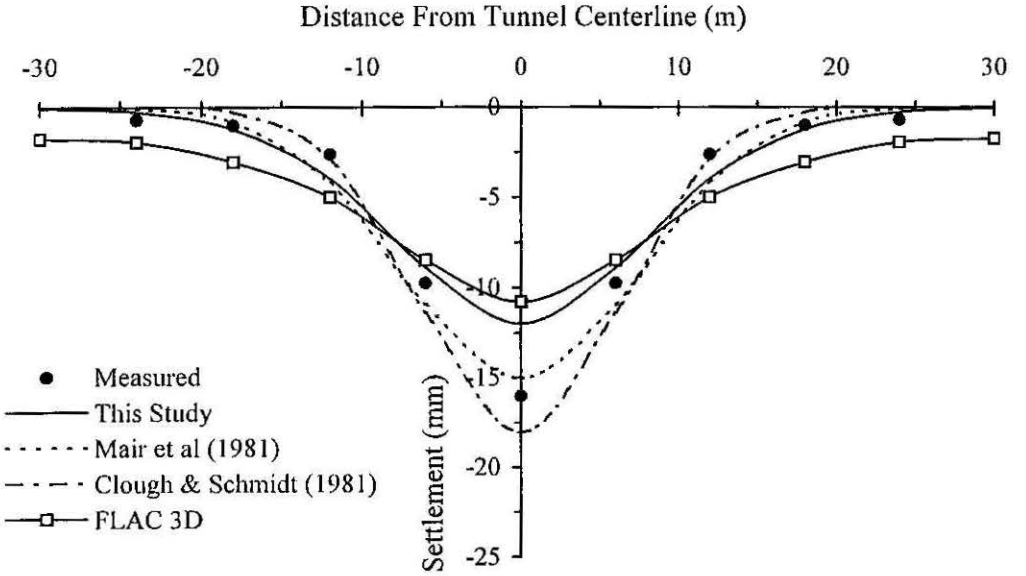

Figure 6.4: Comparison of Surface settlement Trough - Test 1 (Tunnel depth = 15m and ground loss = 1%)

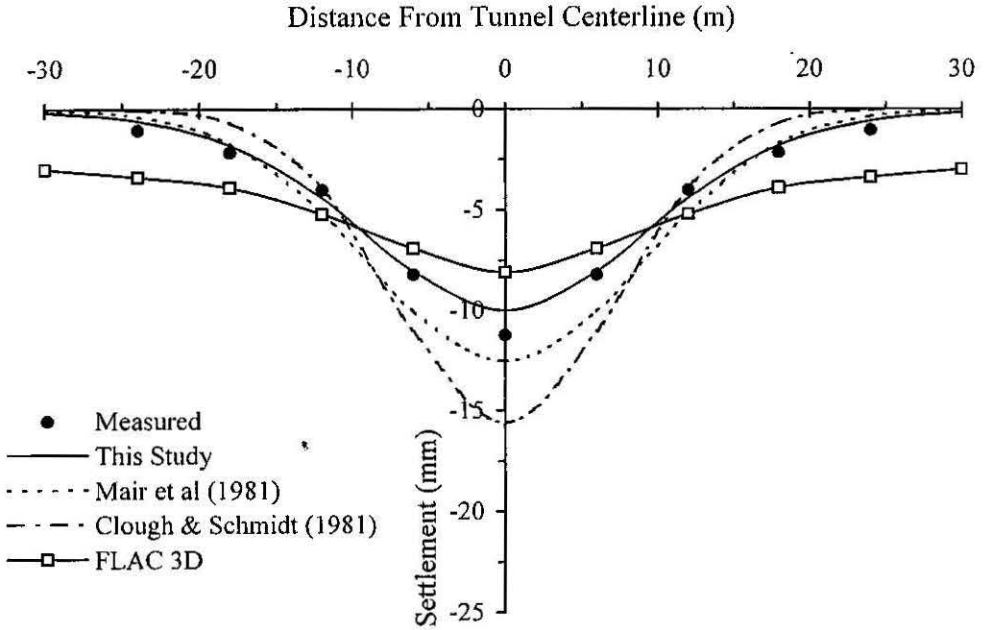

Figure 6.5: Comparison of Surface settlement Trough - Test 2 (Tunnel depth = 18m and ground loss = 1%)

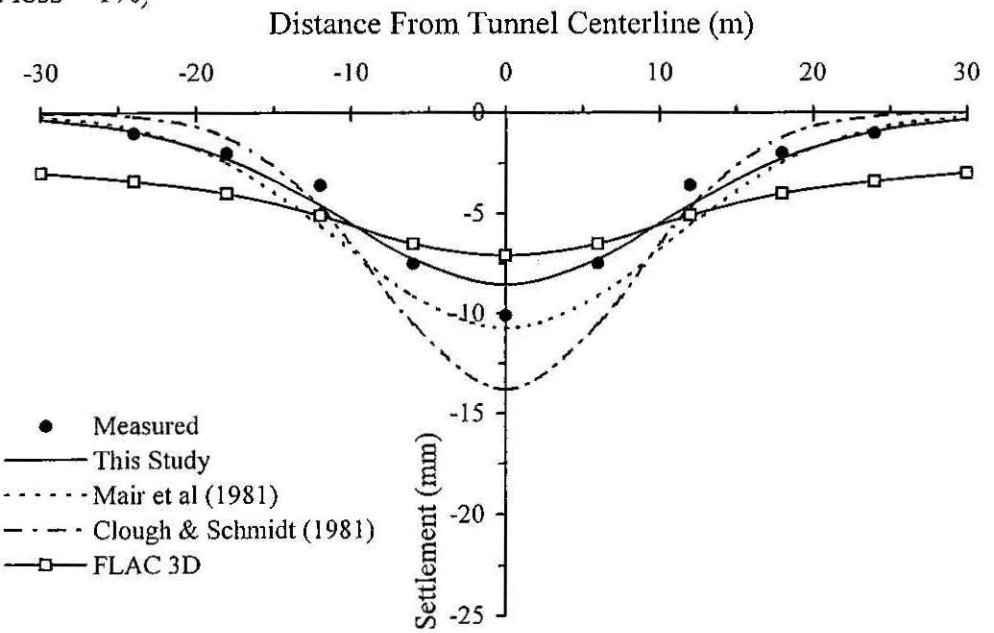

Figure 6.6: Comparison of Surface settlement Trough - Test 3 (Tunnel depth = 21m and ground loss = 1%)

6.3.3 Sub-surface Movements

Subsurface soil movements were derived by a video image processing technique. The images of marker beads pushed into a vertical side of the soil sample were videotaped by two miniature video cameras focussed on to the window of the strongbox. Video tapes

were recorded at 25 frames/sec. The video recorder digital count was used to link each video frame with its corresponding specified ground loss value. Image processing and enhancement software (ACCUWARE, ver 2.1) was used to digitise the video image in '.tif' format. Image files obtained for various stages of the test were then loaded into AutoCAD drafting software and the co-ordinates of the marker beads were recorded manually with respect to the co-ordinates of the reference point marked on the Perspex window of the strongbox. These co-ordinates were then processed for different stages of the test to establish the ground movement vectors. The accuracy of this procedure is about ±3mm(at prototype scale). The comparison study on the tunnel face deformation pattern was not possible with GEPAN and FLAC 3D study since all marker beads were placed about 10mm away from the tunnel face in the centrifuge testing.

Figure 6.7 shows comparisons of the subsurface settlement measured in the centrifuge tests along the tunnel centerline with sub-surface settlement profiles estimated from Mair et al (1993) and closed-form solution presented in this study (Equation 3.16), for a ground loss value of 1%. Estimated sub-surface settlements by FLAC 3D are also presented.

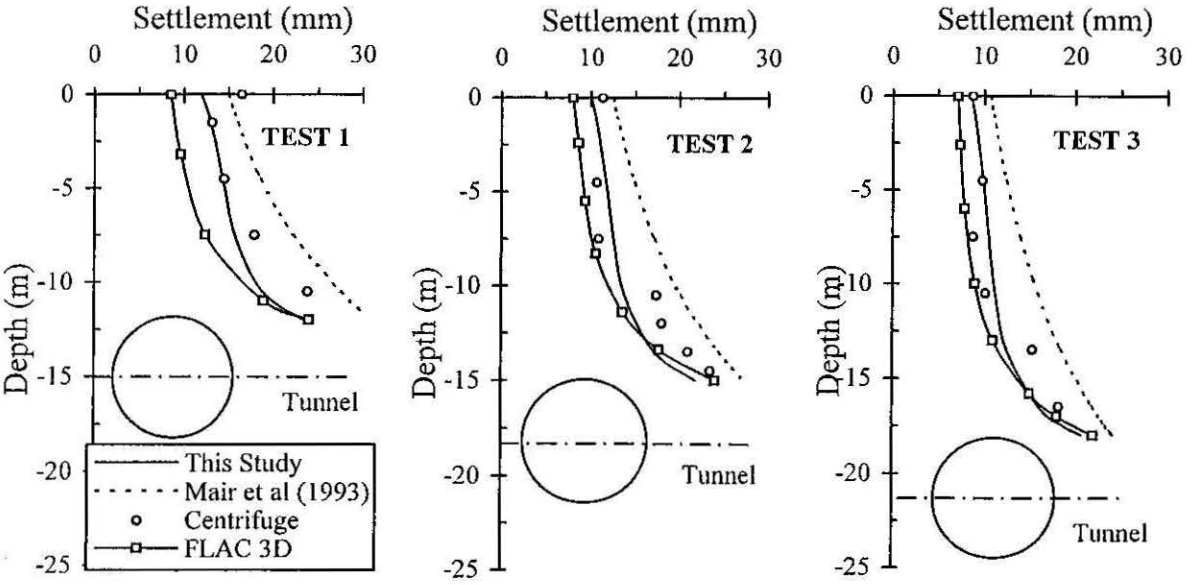

Figure 6.7: Comparison of Sub-surface Settlement Profiles (Ground loss = 1%)

The predictions using the closed-form solution presented in this study (equation 3.16) show a slightly better agreement with measured values from the centrifuge tests than the empirical approach of Mair et al (1993) and the numerical prediction from FLAC 3D. Although FLAC 3D slightly under-estimates the maximum surface settlement, the subsurface settlement estimated at the crown of the tunnel using both FLAC 3D and equation 3.16 are almost the same. It also may be observed that the subsurface settlement

profiles estimated using both FLAC 3D and equation 3.16 become almost identical for the deeper tunnel locations.

It may also be seen that in test 1, the surface settlement is larger than the subsurface settlement, possibly due to the reasons given in previous Section 6.3.2, and is therefore not believed to be representative of the real surface settlement.

Figure 6.8 compares lateral soil movements measured from centrifuge tests with those predicted from the closed-form solution presented in this study (equation 3.18) and numerical results from FLAC 3D, at a lateral distance x=5.5m, and for a ground loss value of 1%.

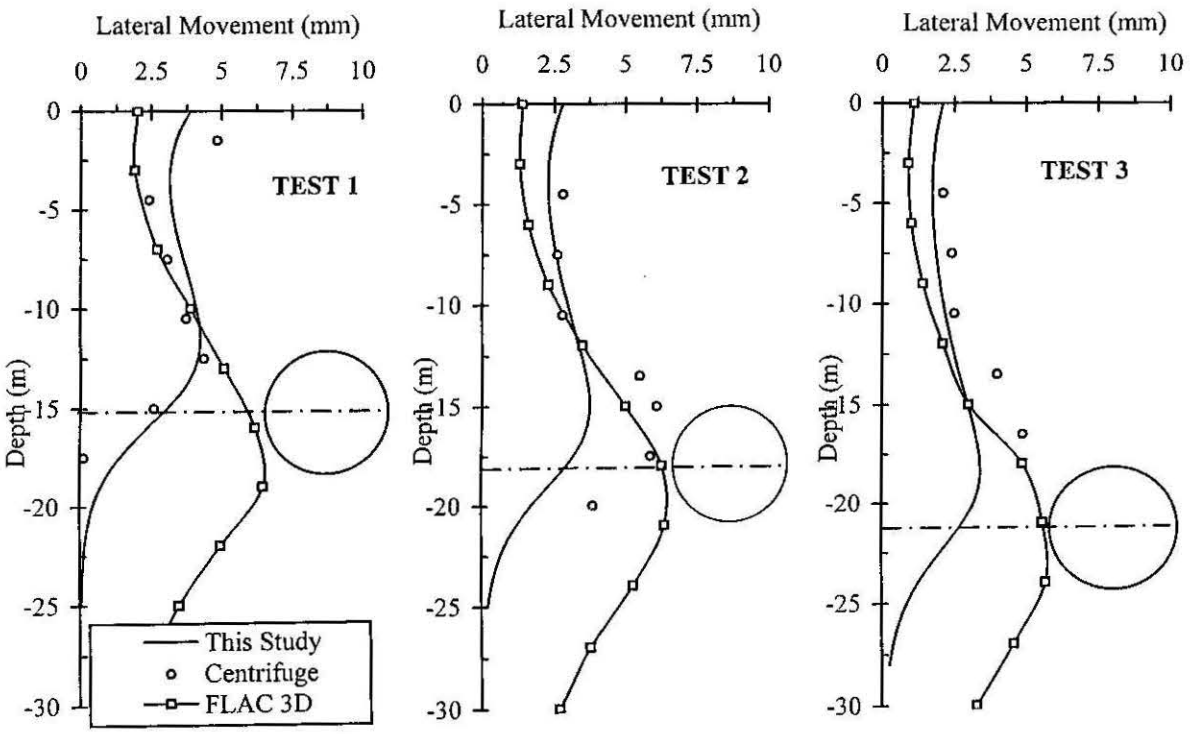

Figure 6.8: Comparison of Lateral Soil Movements at 5.5m away from Tunnel (Ground loss = 1%)

This comparison reveals that the predictions using equation (3.18) agree reasonably well with both the magnitude and distribution of the lateral movements measured in centrifuge tests. The significant scatter in the "measured" values may be due to the high error margin (±3mm) associated with the video image processing technique used. In test 3, it

was not possible to obtain data below the tunnel due to the limited vision of the model tunnel through the window of the strongbox.

Lateral deformations estimated from FLAC 3D over-predicted the lateral movements at tunnel centreline and under-predicted the lateral deformations at shallow depth. The maximum lateral deformations measured in centrifuge tests 2 and 3 are however almost the same as the FLAC 3D predictions.

6.3.4 Summary

The measured ground movements due to tunnelling compare favourably with the closed-form solutions presented in this study. It should be noted that all three centrifuge tests were performed in stiff clay samples with a soil strength in excess of 75kPa at the tunnel location.

The empirical correlation of Mair et al (1983) predict the surface settlements reasonably well whereas similar correlations by Mair et al (1993) slightly over-predict the sub-surface settlements along the centreline of the tunnel. There appear to be no empirical correlations to predict the lateral movements with reasonable accuracy.

Predictions using FLAC 3D elastic analysis slightly under-estimate the maximum surface settlement and the estimated surface settlement troughs are generally wider. Similar observations were made by Gunn (1993) from detailed finite element analyses to predict tunnelling-induced ground movements. Subsurface settlements predicted using FLAC 3D were somewhat consistent and resulted in predictions which were almost identical to the measurements for deeper tunnels. FLAC 3D over estimated lateral deformation compared to the estimations using equation (3.18). Other researchers (Gunn, 1993 and Addenbrooke et al, 1997) also reported inconsistent numerical prediction of tunnelling-induced ground deformations.

6.4 TUNNELLING-INDUCED PILE BEHAVIOUR AND COMPARISONS

6.4.1 Introduction

Tunnelling-induced bending moments, settlements, lateral deformations and axial forces in a single pile and piles in a group measured from centrifuge tests 1, 2 and 3 are presented in this section. Comparisons with numerical estimations using FLAC 3D and GEPAN are also presented.

A positive pile displacement will describe pile movement towards the tunnel. A "front row" pile in a group is the one which is nearest to the tunnel. The pile behaviour is described in prototype scale.

6.4.2 Bending Moments

Tunnelling-induced bending moment profiles along the depth of a pile were obtained for each strain gauge location along the piles. Bending moments were read directly from data acquisition software in which the calibration factors were input prior to the testing. Figure 6.9 shows the tunnelling-induced bending moments of the single pile and the front and rear row piles in the 4-pile group, for all three tests.

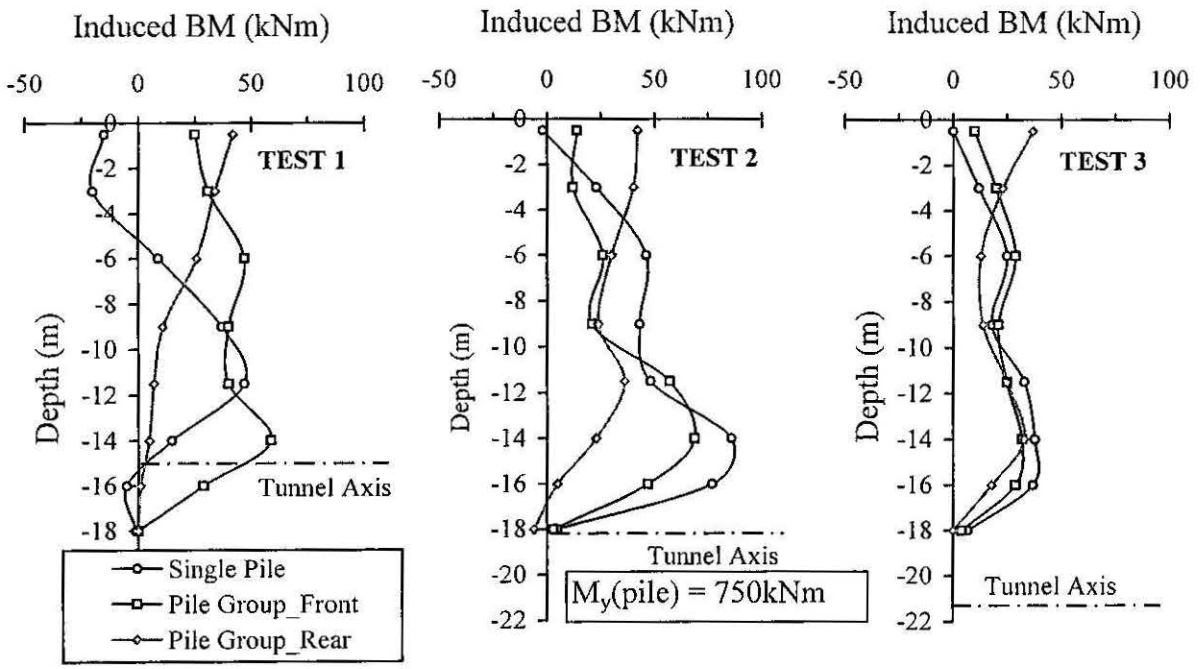

Figure 6.9: Tunnelling-Induced Bending Moments (Ground loss = 1%)

The maximum bending moment occurs almost at the bottom of the piles, for both the single pile and the front row pile on the group. The rear row pile in the group experiences the maximum bending moment at the pile head. Induced bending moment profiles in the single pile and the front row pile (both are located the same distance from the tunnel on either side) are almost the same except for a small difference near the pile cap due to the effects of fixity in the group piles. It may be observed that the induced bending moments are largest if the tunnel centre is located at the pile tip (test 2). The bending moment plot for test 3 shows that when the tunnel is located below the pile tip, the induced bending moments in all three piles are almost identical.

The yield moment of the model pile estimated during the calibration was about 0.75 Nm. Applying the centrifuge scaling, the yield moment (M_y) of the prototype pile is about 750 kNm. The maximum tunnelling-induced bending moment measured during the tests (both single and group) for the ground loss of 1% was about 90 kNm, which was about 12% of the yield moment of the pile.

Figure 6.10 shows the tunnelling-induced maximum bending moments measured for the single pile for varying ground loss ratios. It may be observed that the measured maximum bending moments vary almost linearly with ground loss values below a ground loss of about 2.5%. This suggests that tunnelling-induced behaviour of relatively large diameter piles is nearly linear in stiff clay soil. Therefore, the indications are that an elastic analysis may be performed to predict tunnelling-induced pile behaviour for ground loss values smaller than about 2.5%.

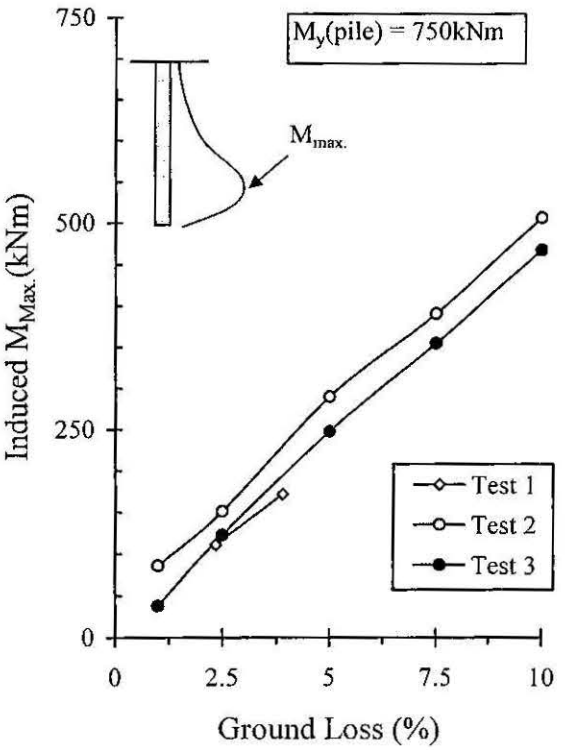

Figure 6.10: Tunnelling-Induced Bending Moments for Varying Ground Loss Values - Test 2

Figure 6.11 shows the comparison of measured tunnelling-induced bending moment on single pile with numerical predictions using FLAC 3D and GEPAN. It is assumed in the numerical analysis that the single pile head is "free" from any restraints.

Induced bending moments predicted by FLAC 3D are almost the same for all three pile-tunnel configurations since the tunnelling-induced lateral deformation predicted using FLAC 3D were also almost identical in magnitude and distribution with depth. The FLAC 3D distributions show similar characteristics to the measurements for Test 1 but rather different characteristics for the other two tests. Estimated bending moments using the GEPAN computer program are slightly higher than the centrifuge measurements, but are generally more consistent with the measurements than are the FLAC 3D results.

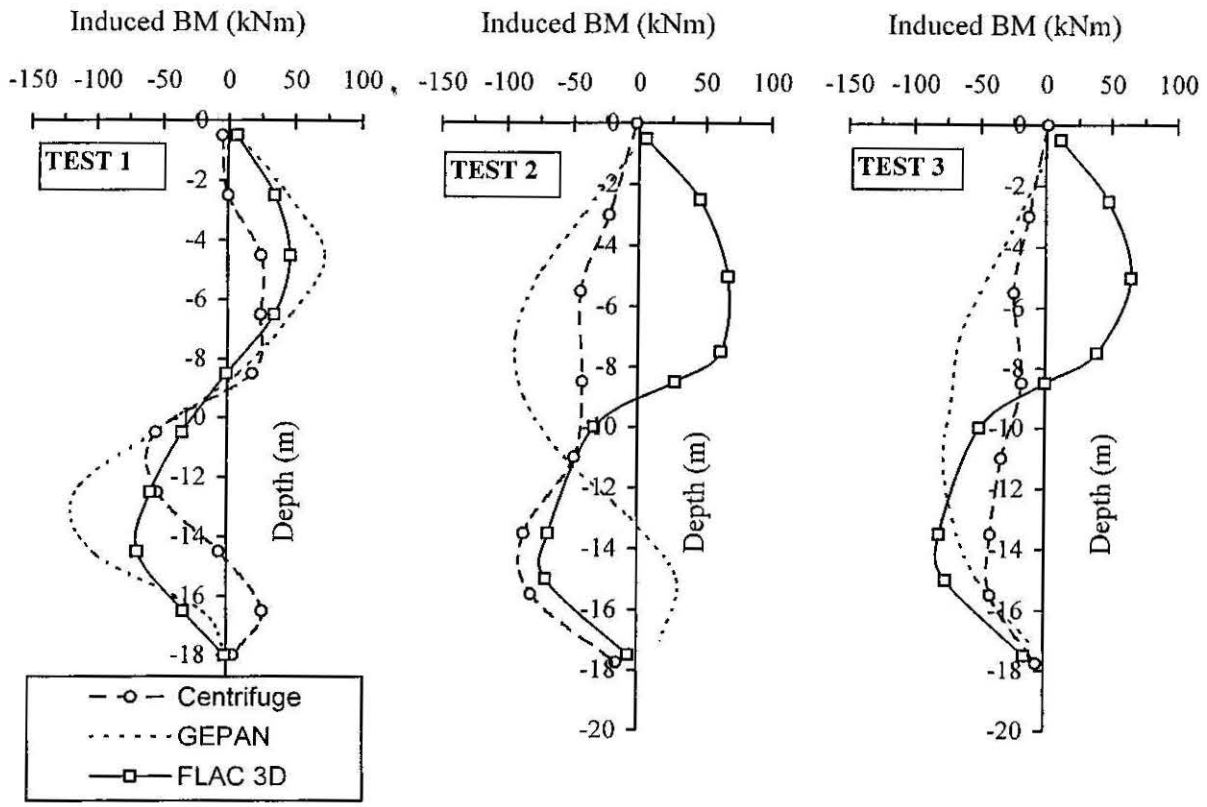

Figure 6.11: Comparison of FLAC 3D and GEPAN Predictions with Centrifuge Test results for Single Pile (Ground loss = 1%)

6.4.3 Pile Deflection

Pile deflections were derived by using an empirical curve-fitting method for the bending moment profile and double integration of the moment distribution, using the appropriate boundary conditions and the bending stiffness of the pile.

Figure 6.12 shows the tunnelling-induced lateral movements of the single pile and the front and rear row piles in the group, for all three tests. The maximum lateral deflection occurs at the pile tip for all three tests. Test 2 shows that piles experience large lateral deflection, in particular the single pile, when the tunnel centre is located at the pile tip

level. Test 3 shows that that lateral deformation profiles of all three piles are almost identical when the tunnel is located below the pile tip. The lateral movements at the pile head for both single pile and the pile group are essentially the same.

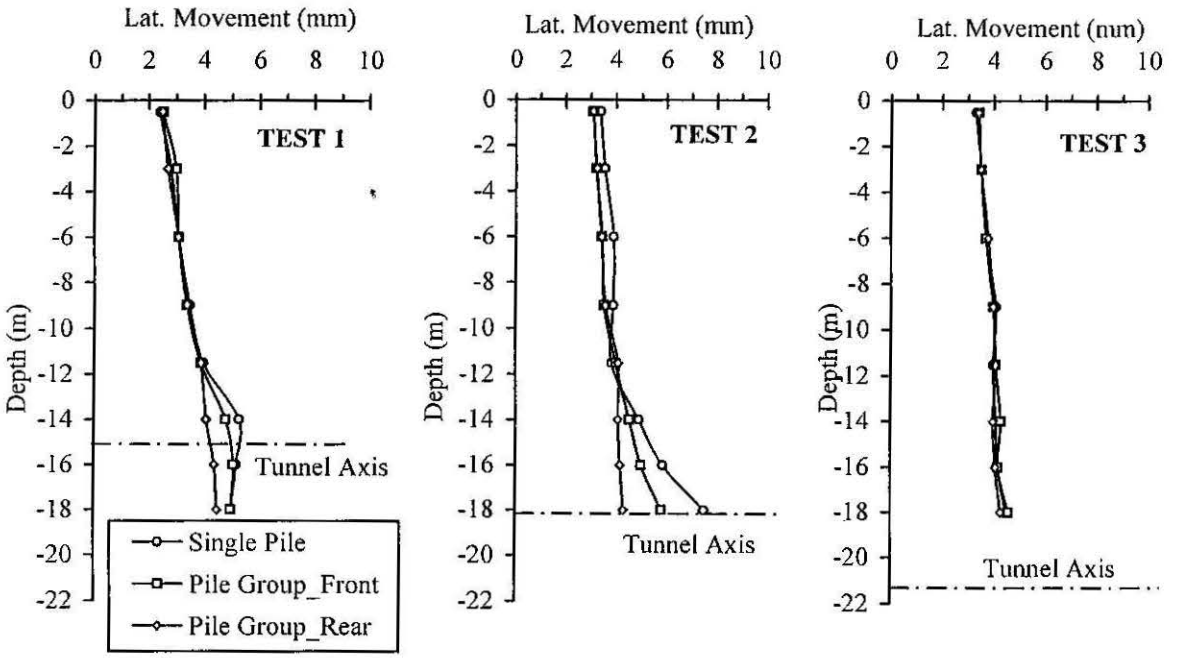

Figure 6.12: Tunnelling-Induced Lateral Movements of piles (Ground loss = 1%)

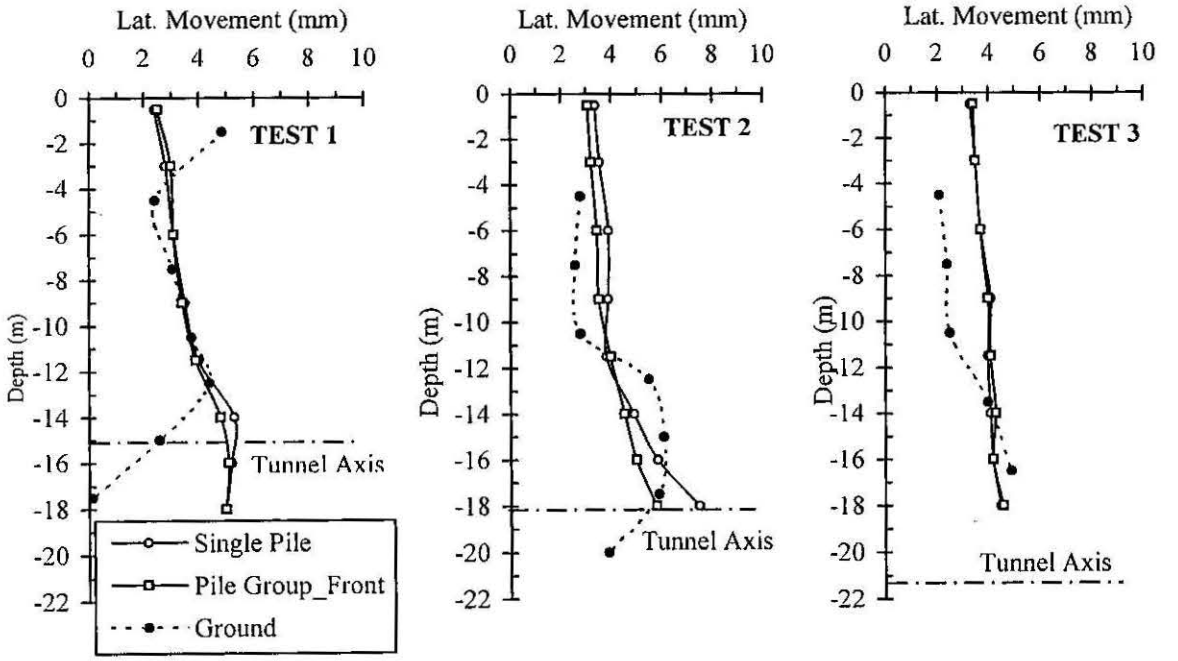

Figure 6.13: Tunnelling-Induced Lateral Movements of Ground and Pile (Ground loss = 1%)

Figure 6.13 shows the measured lateral soil movements at a lateral distance of 5.5m from the tunnel and the lateral deflections of a single pile and a front row pile in the pile group which are located at 5.5m away from the tunnel.

It may be observed that the maximum ground movement and pile movements are almost the same, but the pile movements are much "smoother" than the soil movement profile due to the effect of pile stiffness.

Table 6.1 shows the measured pile head settlements and lateral movements for both the single pile and pile group for all three tests, for a ground loss of 1%. It can be observed that the maximum pile head settlements and lateral movements occur when the tunnel is located at pile tip level (test 2). Lateral deflections measured on the pile group are almost same for all three tests.

Table 6.1: Measured Pile Head Movements

Test No.	Settlement (mm)		Lateral Deflection (mm)	
	Single Pile	Pile Group	Single Pile	Pile Group
1	5.9	6.6	5.3	4.5
2	8.7	12.2	7.5	4.4
3	7.6	7.6	4.5	4.3

Table 6.2 shows a comparison of pile head settlement and lateral deflections for single pile estimated using GEPAN and FLAC 3D. Comparisons are made for the ground loss value of 1%.

Table 6.2: Comparison of Pile Head Movements

Test No.	Settlement (mm)			Lateral Deflection (mm)		
	Centrifuge	GEPAN	FLAC 3D	Centrifuge	GEPAN	FLAC 3D
1	5.9	6.1	4.7	5.3	7.1	9.0
2	8.7	9.2	5.1	7.5	8.0	8.5
3	7.6	8.1	5.3	4.5	6.5	7.0

Elastic analysis without consideration of pile-soil slip was performed using FLAC 3D. Therefore, the FLAC 3D predictions are almost identical to the ground movement at pile head location. Pile head settlements predicted using GEPAN show reasonably good

agreement with the centrifuge measurements. Lateral deflections predicted by GEPAN were higher than the centrifuge test measurements, but are in better agreement than are the FLAC 3D predictions.

6.4.4 Down-drag Forces

Figure 6.14 compares the induced axial force profiles in the front pile in the group for all three tests (other piles were not instrumented to measure axial forces). The induced axial force profile obtained for test 3 (tunnel centreline located below pile tip level) is greater than in the other two tests. The maximum induced axial force occurs at tunnel depth level for test 1 (where the tunnel is located above the pile tip level) whereas it occurs at the pile tip when the tunnel is located below the pile tip (test 3).

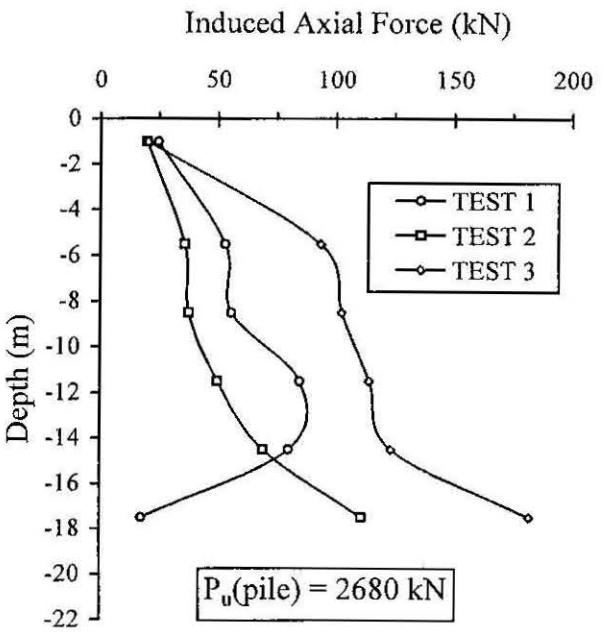

Figure 6.14: Measured Axial Downdrag Force for all Three Tests

The ultimate axial capacity of the prototype pile (18m long, 0.8m diameter pile installed in 75kPa soil) was estimated to be about 2680 kN. The maximum tunnelling-induced axial force measured was about 180 kN, in test 3, for 1% ground loss. This shows that tunnelling-induced axial force was about 7% of the ultimate load carrying capacity of the pile.

Table 6.3 shows the comparison of maximum tunnelling-induced axial forces predicted by GEPAN and FLAC 3D along with the measured values from centrifuge tests.

Table 6.3: Comparison of Maximum Downdrag Forces

Test No.	Max. Axial Downdrag Forces (kN)		
	Centrifuge	GEPAN	FLAC 3D
1	85	230	42
2	110	140	38
3	180	170	42

Table 6.3 shows that FLAC 3D predictions of tunnelling-induced axial downdrag forces are almost same for all three tests and under-predict downdrag forces in comparison to centrifuge measurements and GEPAN predictions. GEPAN over-predicts the downdrag force in tests 1 and 2 but is in good agreement with the results of test 3. FLAC 3D surprisingly under-predicts the downdrag forces in all three tests.

6.5 CONCLUDING REMARKS

In this chapter, results from three centrifuge model tests performed to assess tunnelling-induced ground deformations and their effects on adjacent pile foundations have been presented along with numerical comparisons. Measured ground movements are also compared with those predicted using existing empirical and analytical methods.

The measured ground movements due to tunnelling compare favourably with the values predicted from equations 3.13, 3.16 and 3.18. It should be noted that all three centrifuge tests were performed in stiff clay samples with soil strength in excess of 75kPa at the tunnel location.

The experimental results show that tunnelling-induced bending moments and lateral deflections of adjacent piles may be critical when the tunnel centreline is located at or near the pile tip level. In contrast, the induced axial forces are critical when the tunnel centreline is located below the pile tip. It is also observed that measured induced bending moments and lateral deformations for both a single pile and a pile in a group at an identical distance from the tunnel are almost the same. In general, lateral pile movements are similar in magnitude to the lateral soil movements but their distribution with depth is more smooth due to the effects of the pile stiffness.

A nearly linear relationship was observed between tunnelling-induced maximum bending moments and ground loss values for the tunnel-pile-soil configuration considered in this

study. Therefore, the results indicate that an elastic analysis may be performed to predict tunnelling-induced pile behaviour, with reasonable accuracy, for ground loss values less than about 2.5%, and for similar soil-pile configurations to those used in this study.

Predictions using GEPAN computer program were generally in closer agreement with the measurements than the FLAC 3D predictions.

CHAPTER SEVEN

DESIGN CHARTS TO ASSESS TUNNELLING-INDUCED PILE BEHAVIOUR

7.1 INTRODUCTION

One of the important issues of tunnelling in urban areas is the assessment of the likely impact on adjacent buildings of tunnel construction. Most of the research to date has focussed on the assessment of the ground surface settlement trough above the tunnel and its effect on settlement, in particular the differential settlement, of adjacent buildings supported on shallow foundations. For piled foundations, the subsurface soil deformations will play an important role in influencing the pile responses.

In an urban environment, many high rise buildings are supported by piled foundations and, generally, tunnelling will cause ground movements and induce bending moment, axial down-drag force and lateral deformation on adjacent piles. The purposes of this chapter include the following:

- To generate design charts for assessing maximum tunnelling-induced pile responses which may be readily used in practice for preliminary designs, and
- Examine the applicability of the design charts via the results obtained from laboratory centrifuge tests performed in this study, and also via the study of a published case history.

7.2 METHODOLOGY

The typical tunnel-pile configuration shown in Figure 4.2 was considered as the base problem for this study. Three simple cases for varying pile lengths were analyzed first, involving the following assumptions:

1. the soil is a deep homogenous clay layer, assumed to be in an undrained condition. The undrained shear strength c_u = 60kPa and Young's modulus E_s = 24MPa, values which are representative of a medium clay,
2. the tunnel radius R = 3m and the depths of tunnel axis H = 15m, 20m, and 25m for all three cases respectively, and
3. the pile diameter d = 0.5m, Young's modulus E_p = 30,000MPa.

A different pile length was chosen for each case. For the first case (a relatively short pile), the pile length L_p = 15m (pile toe level above the tunnel axis); second case L_p = 20m (pile toe at the tunnel axis), and the third case L_p = 25m (pile tip is deeper than the tunnel axis level).

The tunnelling-induced ground deformations corresponding to two different ground loss ratios, ε_0, of 1% and 5%, and for a distance x = 4.5 m are reported in Figure 4.3. The analyses of pile responses were carried out using computer programme GEPAN as described in Chapter 4. Figure 7.1 shows pile response profiles for the "short pile" case (L_p= 15 m).

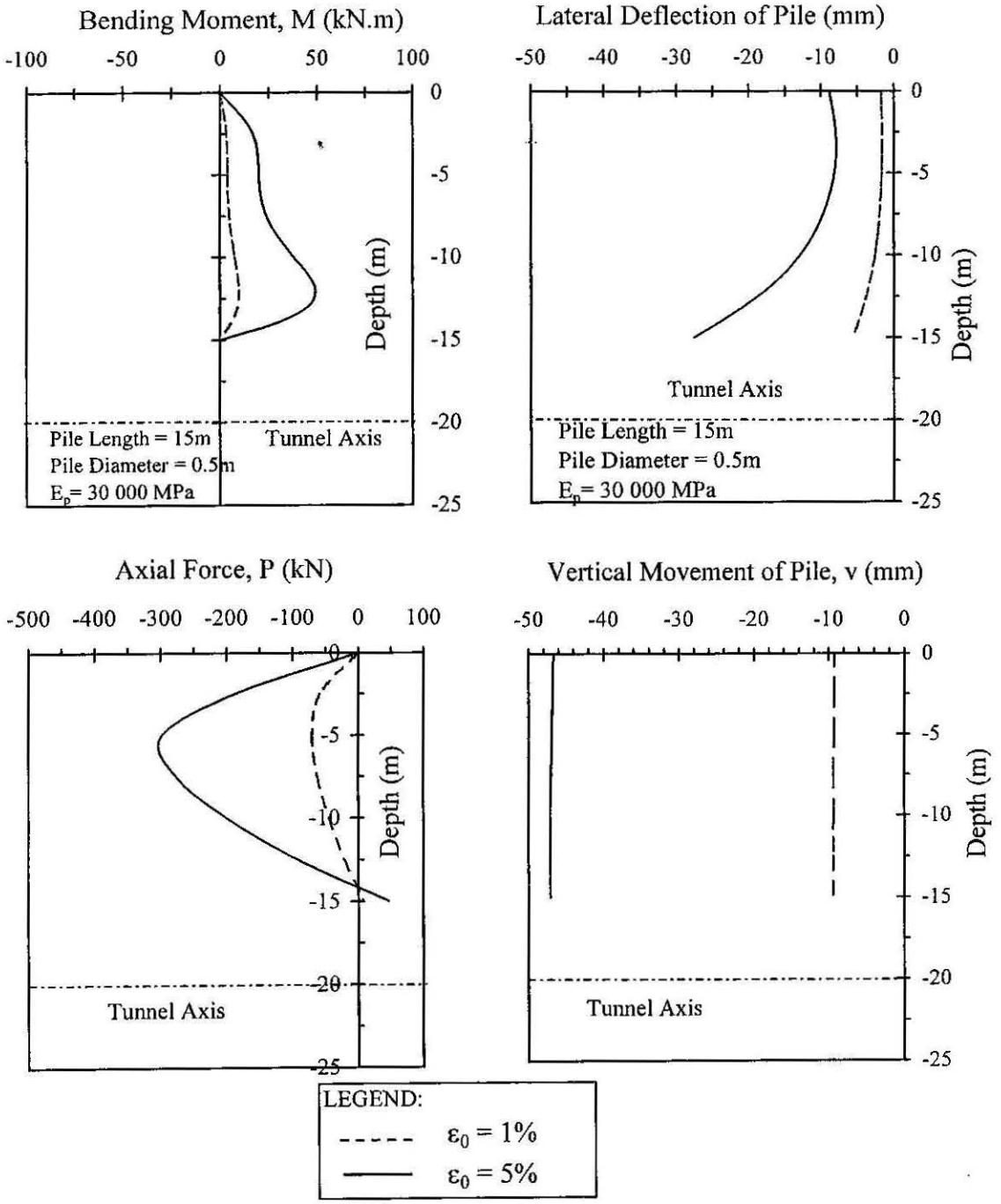

Figure 7.1: Typical "Short Pile" (L_p=15m) Response at x = 4.5m

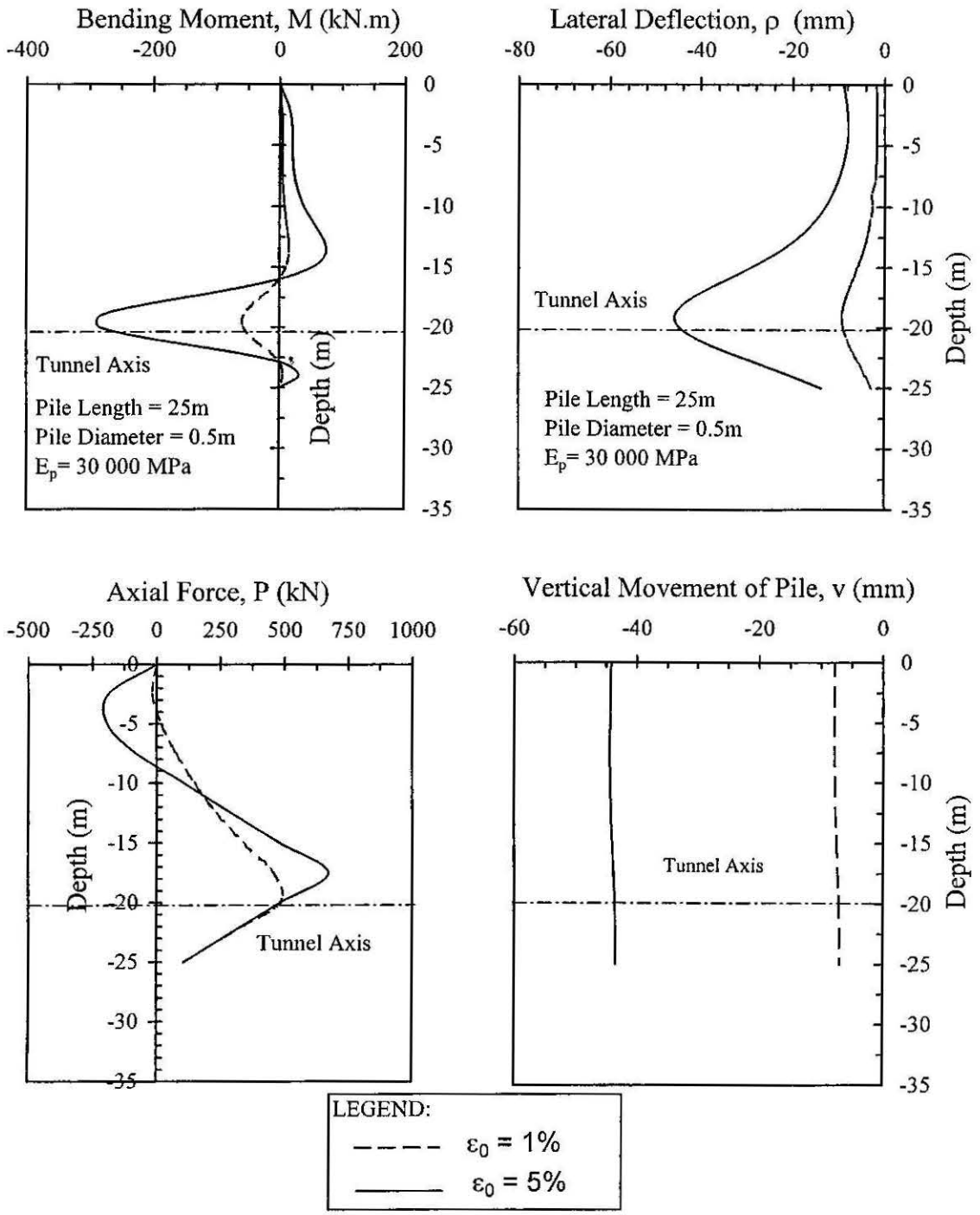

Figure 7.2: Typical "Long Pile" (L_p=25m) Response at x = 4.5m

Figure 7.2 shows the pile response profile with the depth for "long Pile" case for ground losses 1% and 5%. Figure 7.3 shows the maximum pile responses for three different pile length cases (L_p=15 m, L_p=20 m and L_p=25 m) for the ground loss of 1%.

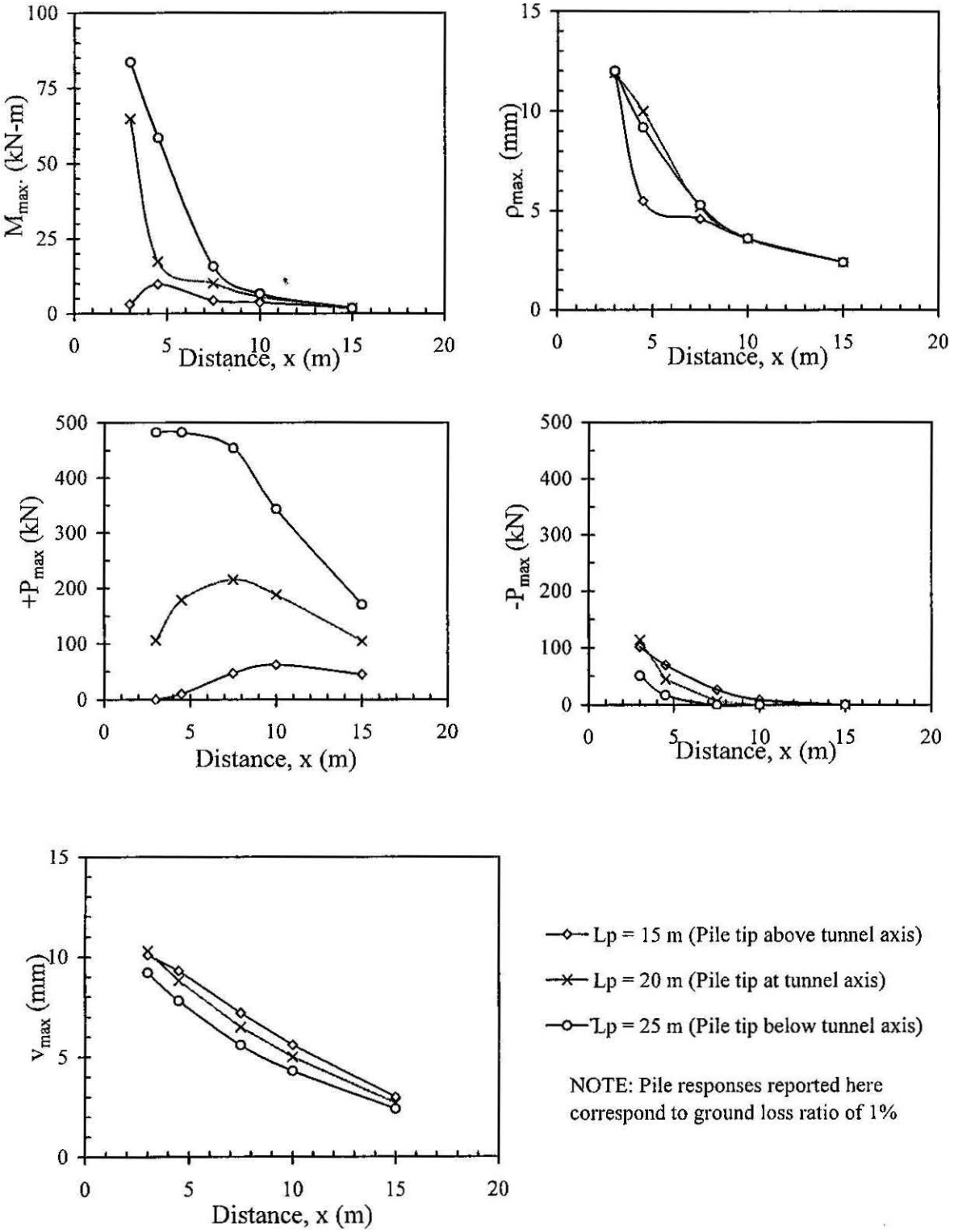

Figure 7.3: Maximum Pile Responses for Three Different Pile Lengths

The following features were observed:

- in short piles (L_p=15 m) the bending moment in the pile is much smaller than in longer piles, apparently because the pile did not experience the largest lateral soil movement, which is located below the pile tip,
- the maximum bending moment and the axial forces are high in the longest pile (L_p=25 m),
- lateral deformations are almost the same for piles founded at or below the tunnel axis level, and
- differences in vertical settlements at the pile head are not significant for all three cases.

The comparisons of the above three cases seem to indicate that the behaviour of a pile is influenced significantly by whether the pile tip is above or below the axis level of a tunnel. The reason is because the soil movements reach a maximum value at about the axis level of a tunnel and decrease rather rapidly (especially for the lateral soil movement) above and below the axis level.

The maximum pile responses for the "short pile" case (L_p=15m) are plotted against the distance away from the vertical axis of the tunnel, x, in Figure 7.4 for ground loss ratios of 1% and 5% (the latter is a rather extreme value in practice). For the "short pile" case, it is found that maximum tunnelling-induced bending moment M_{max} increases with increasing x to about x = 5 m, where it reachs a peak. Thereafter, it decreases markedly with increasing x. The maximum pile head settlement v_{max} also decreases markedly with increasing x and becomes negligible at a distance of about 20 m. For a distance of less than about 8 m, only tensile axial forces, decreasing with increasing x, are developed in the pile. Beyond x = 8 m, only compressive axial forces are developed, and these reach a peak at a distance of between 10 and 15 m from the tunnel axis.

The maximum pile responses for the "long pile" case (L_p=25m) are plotted against the distance away from the vertical axis of the tunnel, x, in Figure 7.5, for ground loss ratios of 1% and 5%. Any required pile responses for different ground loss values may be obtained adequately by linear interpolation or extrapolation of the values for these two ground loss values. However, it was found in Chapter 4 that in an elastic analysis, computed pile responses may be normalised with respect to ground loss values. It may be observed from Figure 7.5 that the maximum induced-bending moment M_{max}, lateral deflection ρ_{max}, pile head settlement v_{max} and tensile axial force $-P_{max}$ all decrease with increasing x value, while the compressive axial force $+P_{max}$ reaches a maximum at an x

value ranging between about 10m and 15m. It is worth noting that the tensile axial force occurs mainly for x less than about 9m (i.e. about 3 times the tunnel radius) and thereafter it becomes almost negligible.

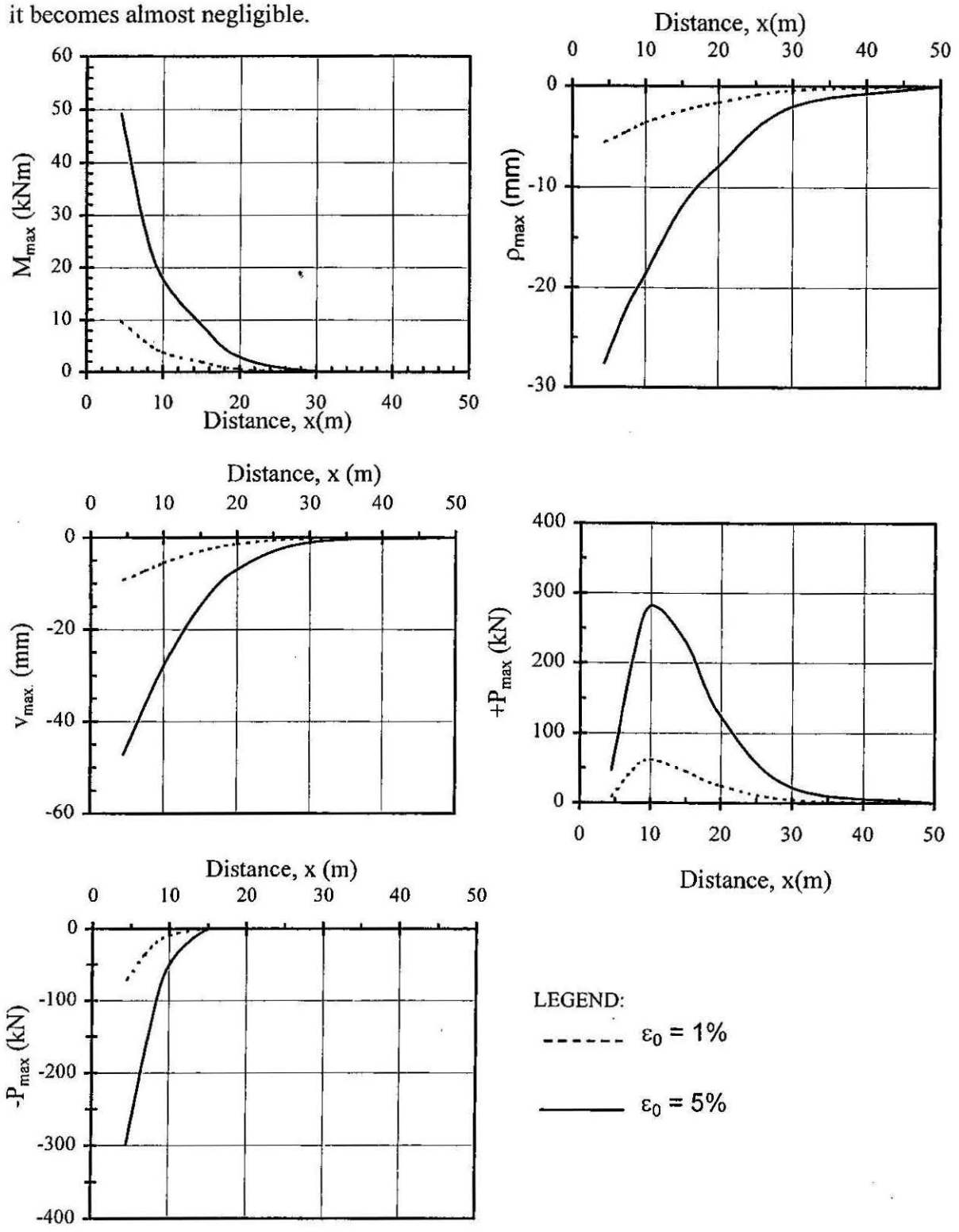

Figure 7.4: Maximum Pile Responses vs. Distance, x, for the "Short Pile" Case

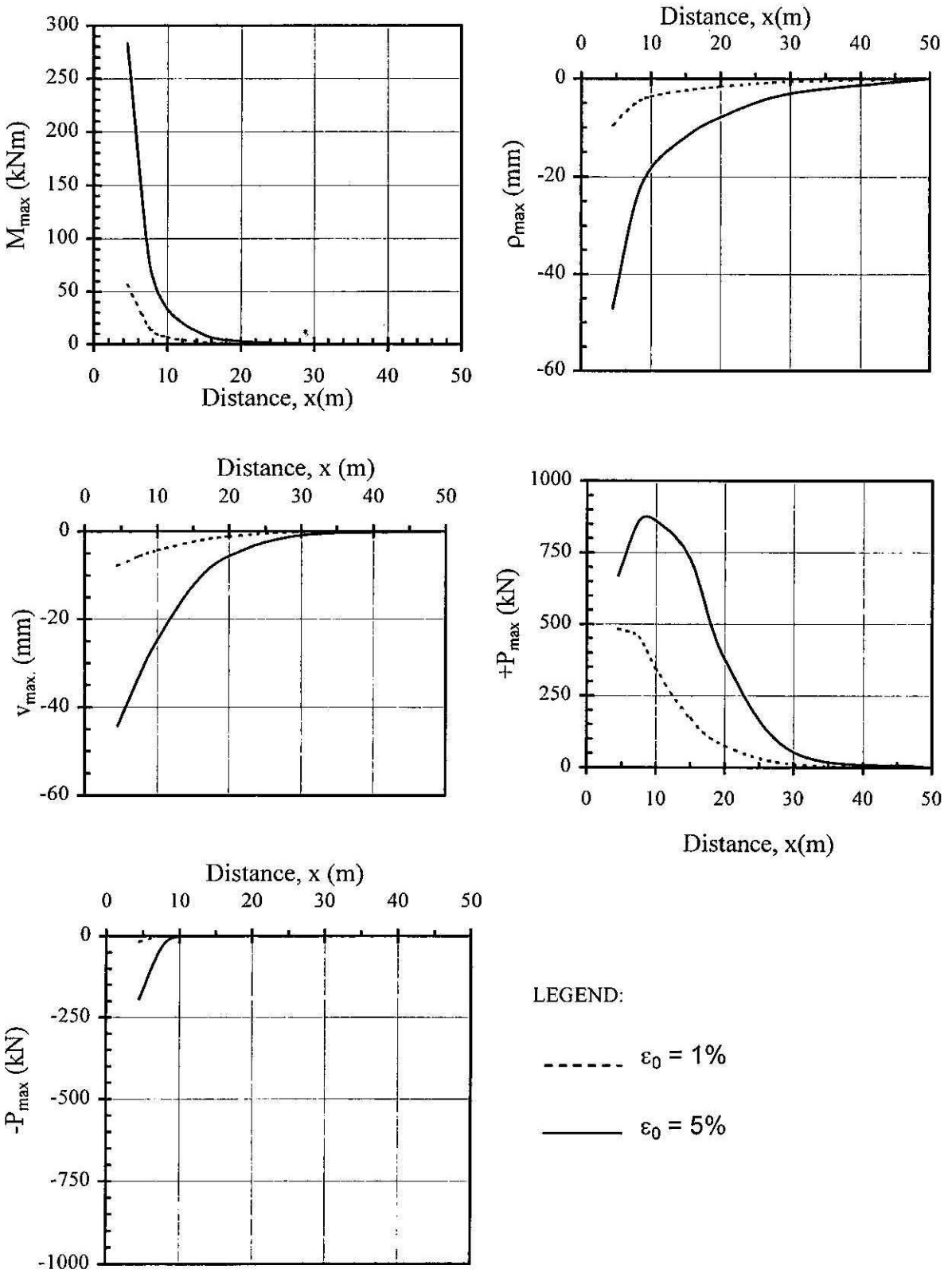

Figure 7.5: Maximum Pile Responses vs. Distance, x, for the "Long Pile" Case

It is obvious that the variation of pile behaviour with distance from the tunnel is different for the "long pile" and "short pile" cases.

In order to investigate the influences of various parameters on the pile responses, some parametric studies were carried out in which the following parameters were varied: the tunnel radius R, the ground loss ratio ε_0, the undrained soil shear strength c_u, the depth of tunnel axis level H, the pile diameter d and length L_p. Young's modulus E_s was also varied at the same time as c_u, assuming the relationship $E_s = 400c_u$. The following observations are made from the parametric studies:

1. maximum bending moment M_{max}, lateral pile deflection ρ_{max}, compressive axial force $+P_{max}$, tensile axial force $-P_{max}$ and settlement v_{max} all increase with increasing tunnel radius R and ground loss ratio ε_0, and may be related conveniently to the product of $R^2\varepsilon_0$,
2. M_{max}, ρ_{max}, $+P_{max}$, and $-P_{max}$ increase with increasing c_u because of an increase of the lateral soil pressure and skin friction. v_{max} also increases with increasing c_u,
3. increasing the pile diameter tends to increase M_{max} but decrease ρ_{max}, due to an increase of pile lateral rigidity; $+P_{max}$, and $-P_{max}$ increase, while v_{max} decreases, with increasing pile diameter, and
4. The effects of the depth of tunnel axis level H and the pile length L_p depend on the ratio L_p/H; the maximum pile responses may either increase or decrease with changing L_p/H, depending on the other parameters.

Based on the above parametric studies, it was found that, within the range of parameters examined, the various maximum pile responses may be approximated as follows:

Lateral response

$$M_{\max} = M_b . k_{cu}^{M} \; . k_d^{M} . k_{L_p/H}^{M} \tag{7.1}$$

$$\rho_{\max} = \rho_b . k_{cu}^{\rho} \; . k_d^{\rho} . k_{L_p/H}^{\rho} \tag{7.2}$$

Axial response

$$+P_{\max} = +P_b . k_{cu}^{+P} \; . k_d^{+P} . k_{L_p/H}^{+P} \tag{7.3}$$

$$-P_{\max} = -P_b . k_{cu}^{-P} \; . k_d^{-P} . k_{L_p/H}^{-P} \tag{7.4}$$

$$v_{max} = v_b . k^{v}_{cu} . k^{v}_{d} . k^{v}_{L_p / H} \quad (7.5)$$

where M_{max} = maximum bending moment, kNm, ρ_{max} = maximum lateral deflection, mm, $+P_{max}$ = maximum compressive axial force, kN, $-P_{max}$ = maximum tensile axial force, kN, v_{max} = maximum pile head settlement, mm, M_b, ρ_b, $+P_b$, $-P_b$, v_b = basic bending moment, lateral deflection, compressive axial force, tensile axial force and pile head settlement, respectively, k^{M}_{cu}, k^{ρ}_{cu}, k^{+P}_{cu}, k^{-P}_{cu}, k^{v}_{cu} = correction factors for undrained shear strength, k^{M}_{d}, k^{ρ}_{d}, $.k^{+P}_{d}$, k^{-P}_{d}, k^{v}_{d} = correction factors for pile diameter, and $k^{M}_{Lp/H}$, $k^{\rho}_{Lp/H}$, $k^{+P}_{Lp/H}$, $k^{-P}_{Lp/H}$, $k^{v}_{Lp/H}$ = correction factors for the ratio of pile length to tunnel axis level.

7.3 DESIGN CHARTS FOR SHORT PILES

In order to construct design charts, the maximum pile responses for the "Short Pile" case (Figure 7.4) were considered as the "base" tunnelling-induced behaviour of a pile. Based on the observations made from the parametric study, it is convenient to produce charts using the ground loss factor $\varepsilon_F = R^2\varepsilon_0$. Figure 7.6 shows the base values of tunnelling-induced pile behaviour for $\varepsilon_{FB} = R^2\varepsilon_0 = 3^2 \times 1\% = 0.09$, where . ε_{FB} is the base ground loss factor.

Figure 7.7 shows the variation of correction factor for undrained shear strength of the soil and it shows that the effect of soil strength on the tunnelling-induced behaviour for varying lateral distance 'x' is negligible. Figure 7.8 shows the variation of correction factor for pile diameter and it shows that pile diameter effect is considerable in the estimation of tunnelling-induced lateral deformation and downdrag force. Figure 7.9 shows the variation of correction factor for pile length/tunnel depth ratio. This ratio has most influence on the response of the pile

The steps involved in using the design chatrs are given below:

STEP 1: Estimate the ground loss ratio, ε_F for given problem using $\varepsilon_F = R^2\varepsilon_0$. Estimate the factor, $L_R = \varepsilon_F/\varepsilon_{FB}$, where $\varepsilon_{FB} = 0.09$

STEP 2: Estimate the tunnelling-induced base behaviour from Figure 7.6 for the given horizontal distance, x, and multiply these values by the factor L_R.

STEP 3: Estimate undrained soil shear strength, pile diameter, and pile length/tunnel depth ratio correction factors from Figures 7.7, 7.8 and 7.9 and multiply the values estimated in Step 2 by these correction factors (via Equations 7.1 to 7.5).

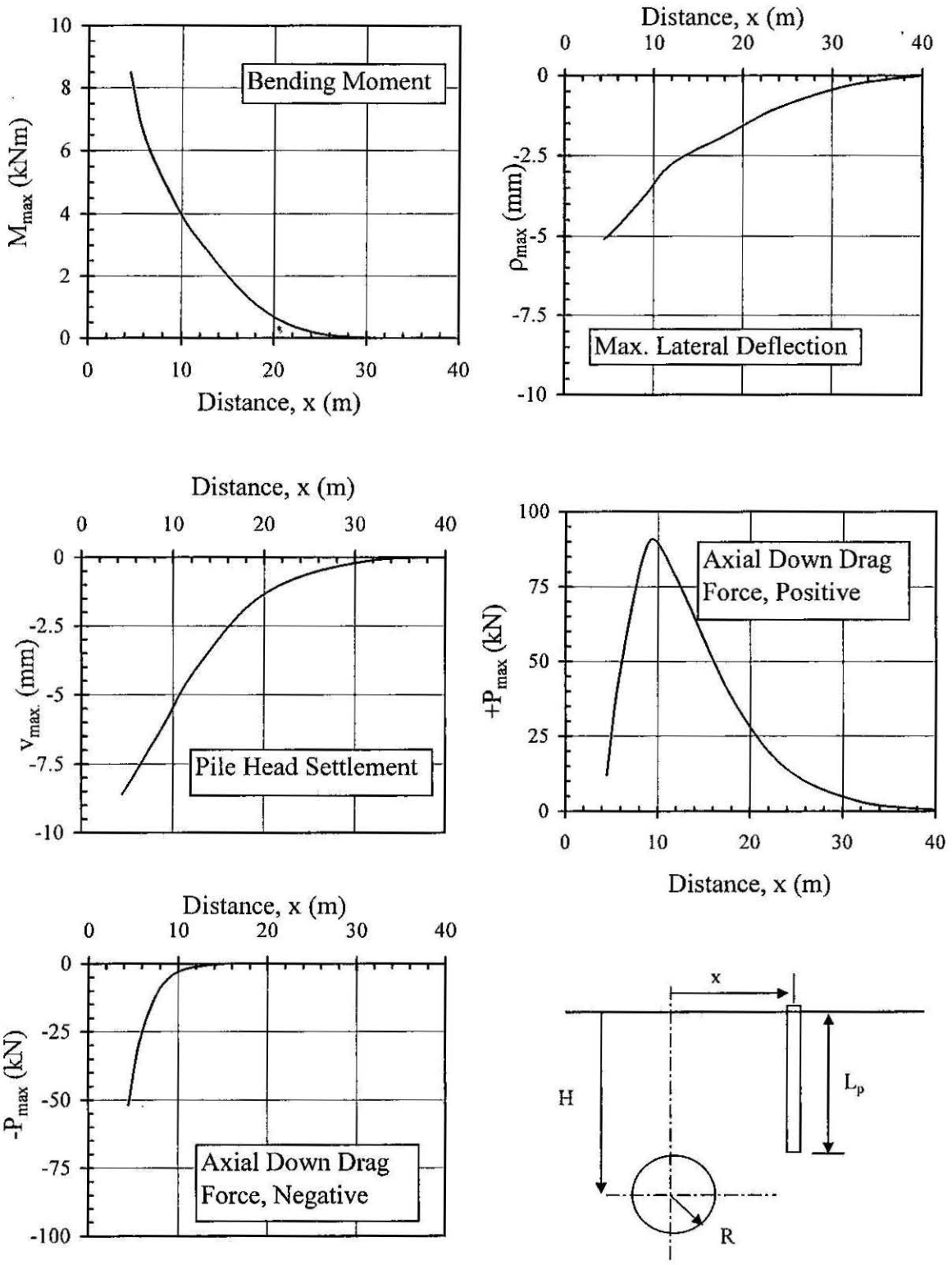

Charts for Base Ground Loss Ratio, $\varepsilon_{FB} = 0.09$

Figure 7.6: Maximum Pile Response vs. Distance

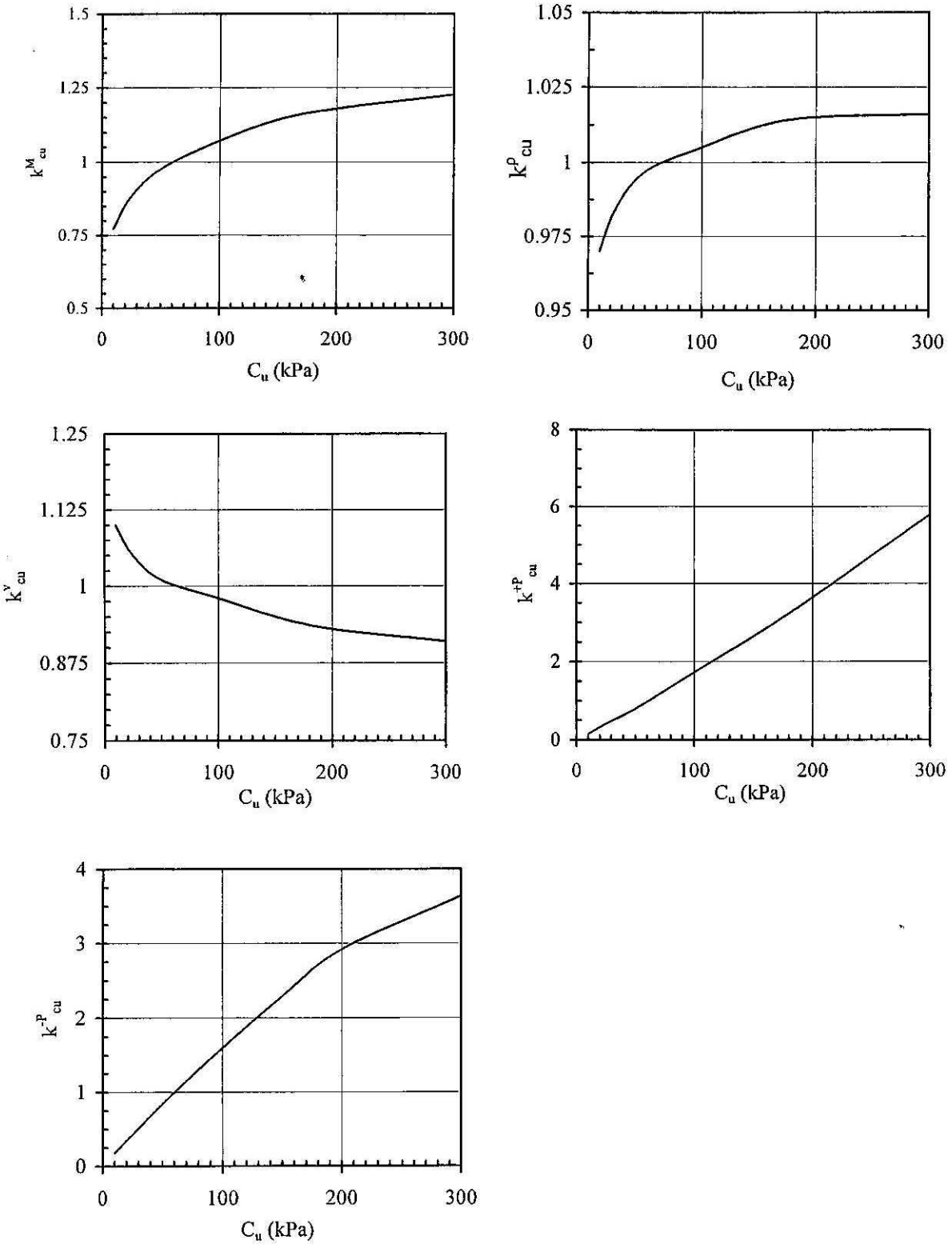

Figure 7.7: Correction Factor for Soil Strength

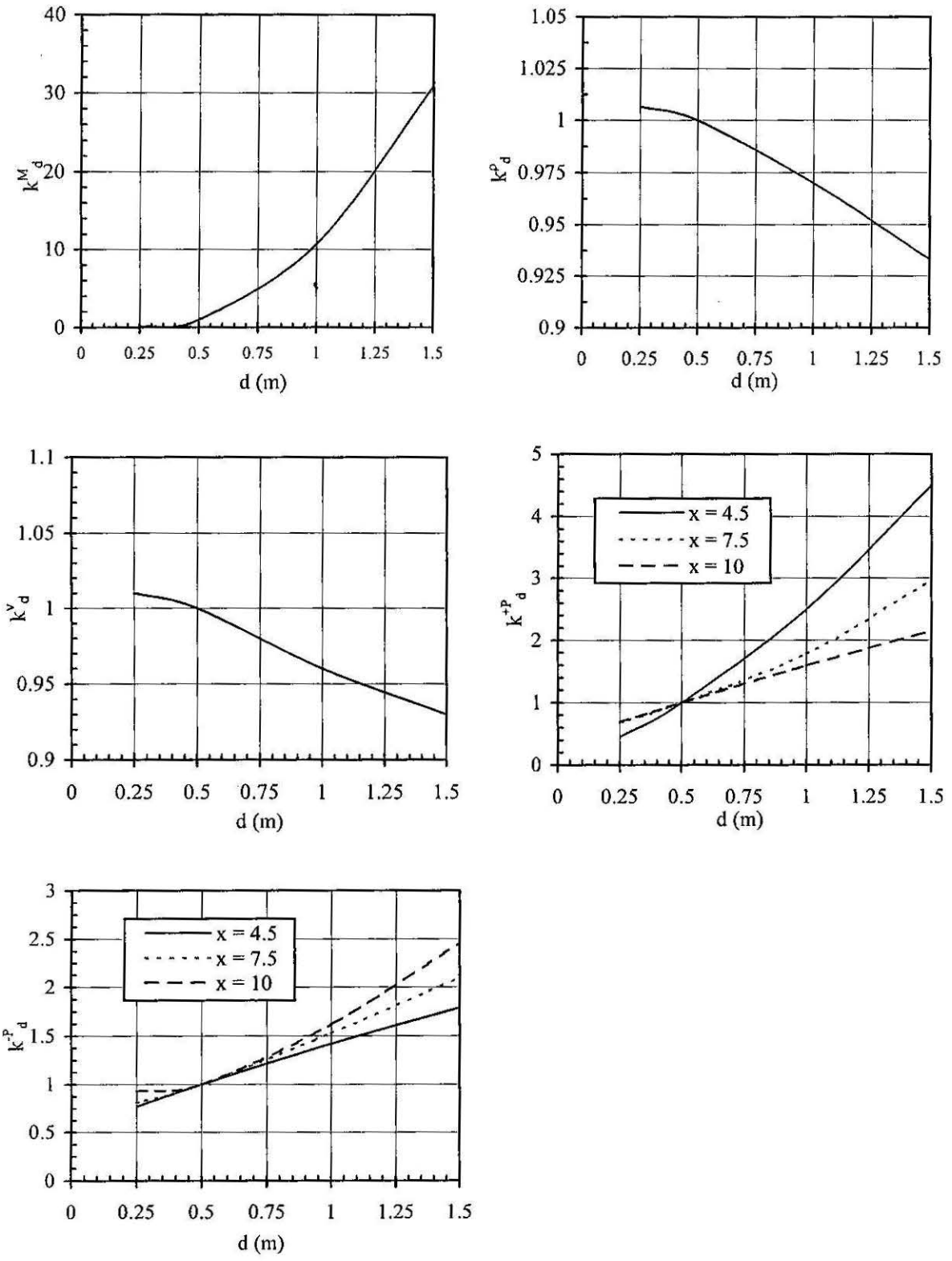

Figure 7.8: Correction Factor for Pile Diameter

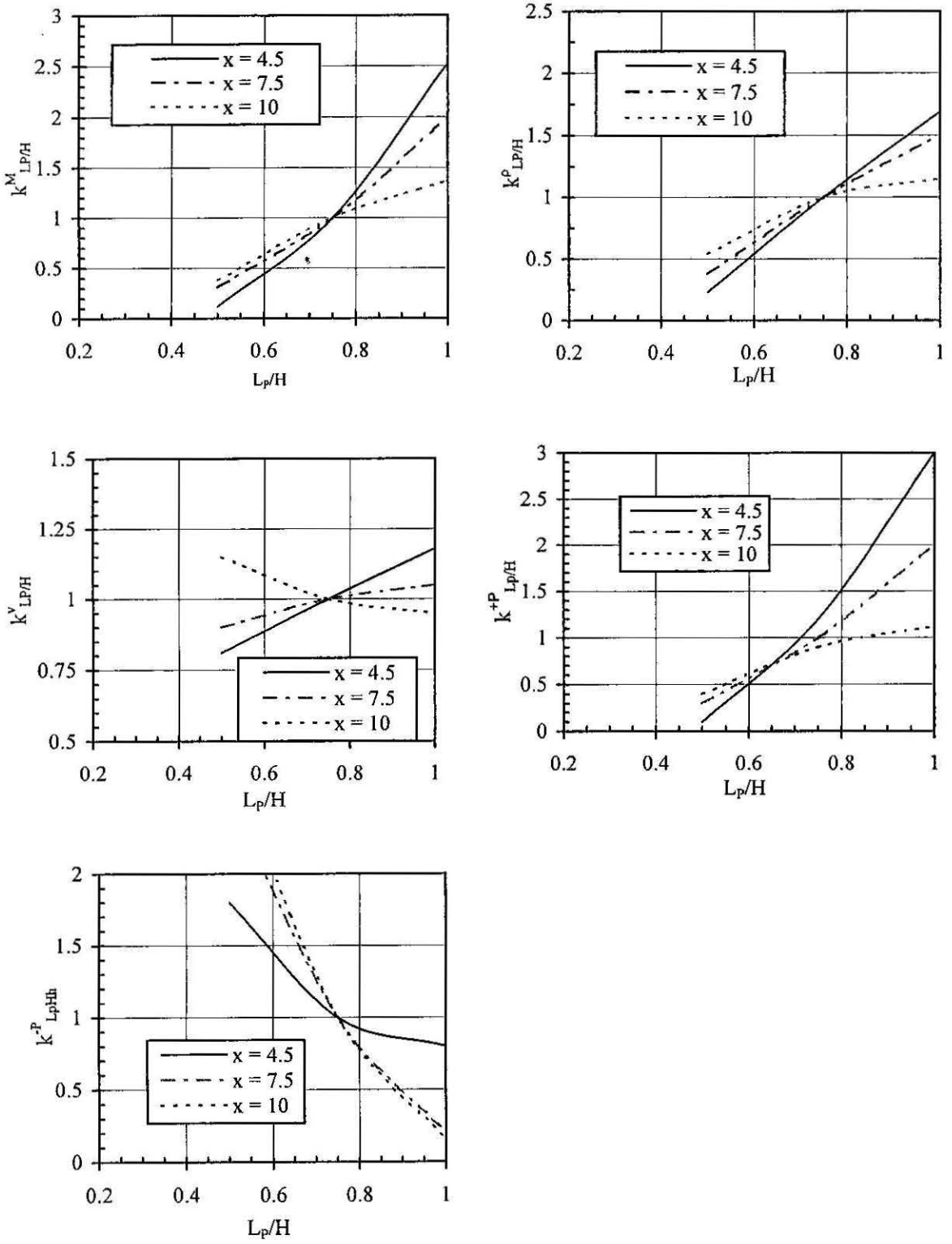

Figure 7.9: Correction Factor for Pile Length/Tunnel Depth Ratio

7.4 DESIGN CHARTS FOR LONG PILES

Design Charts for "Long Piles" were constructed as described for "Short Pile" case. The maximum pile responses for "long pile" case, shown in Figure 7.5, was considered as the base tunnelling-induced behaviour of a pile. Figure 7.10 shows the base values of the tunnelling-induced pile behaviour for a base value of ground loss factor $\varepsilon_{FB} = 0.09$.

Figure 7.11 shows the correction factors for undrained shear strength of the soil. It can be seen that all the tunnelling-induced behaviours are increasing with the increasing soil strength. Bending moment and axial down drag force vary considerably with the undrained shear strength of the soil.

Figure 7.12 shows the correction factors for varying pile diameter. It can be observed that induced bending moments and axial down drag force are increasing with increasing pile diameter but the lateral deflection and the settlement of the pile decrease with increasing pile diameter.

Figure 7.13 shows the correction factors for the pile length/tunnel depth ratio. It can be observed that induced bending moments and pile head settlements decrease with increasing pile length/tunnel depth ratio but the lateral deformation and the axial down drag forces increase.

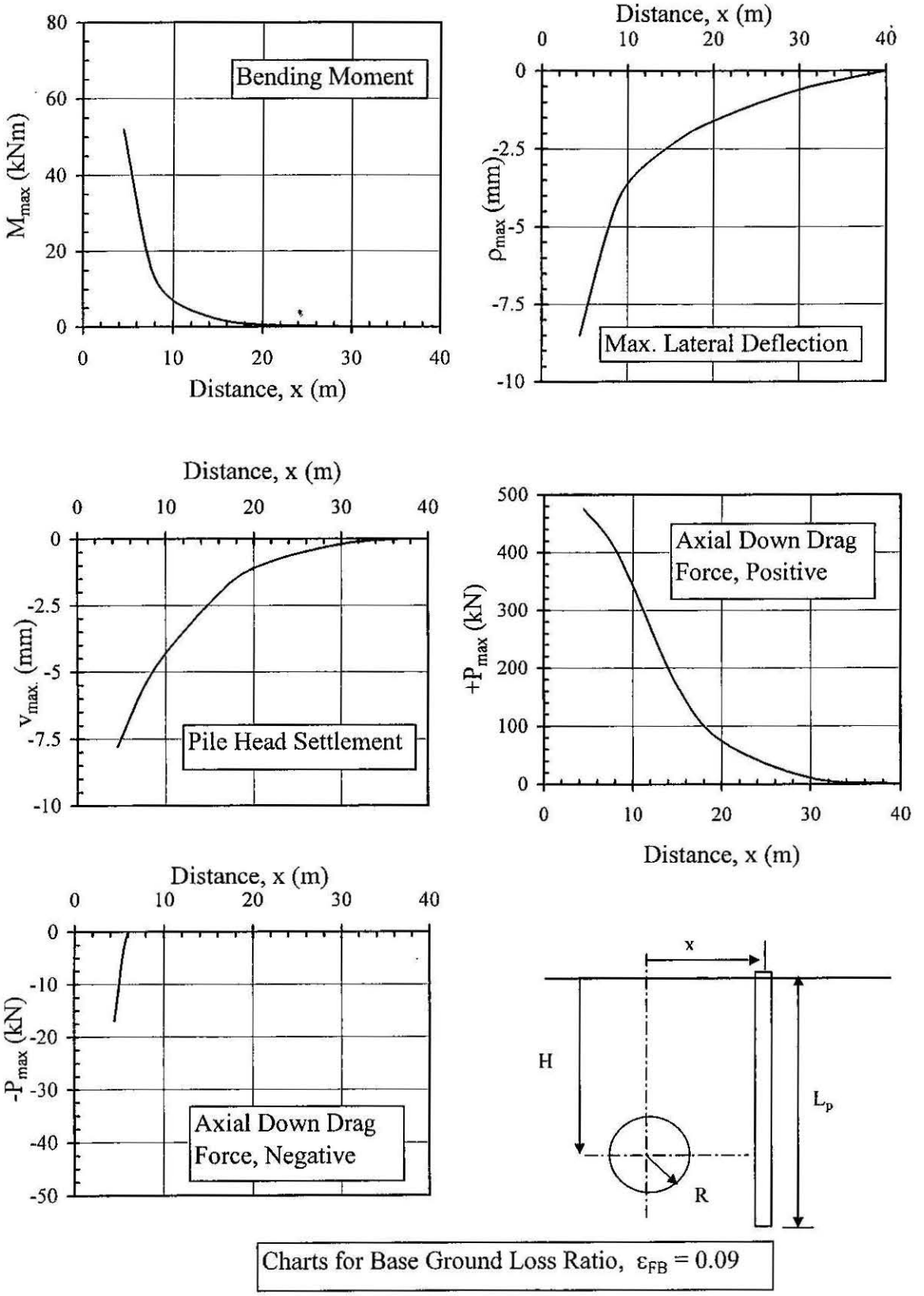

Figure 7.10: Maximum Pile Response vs. Distance

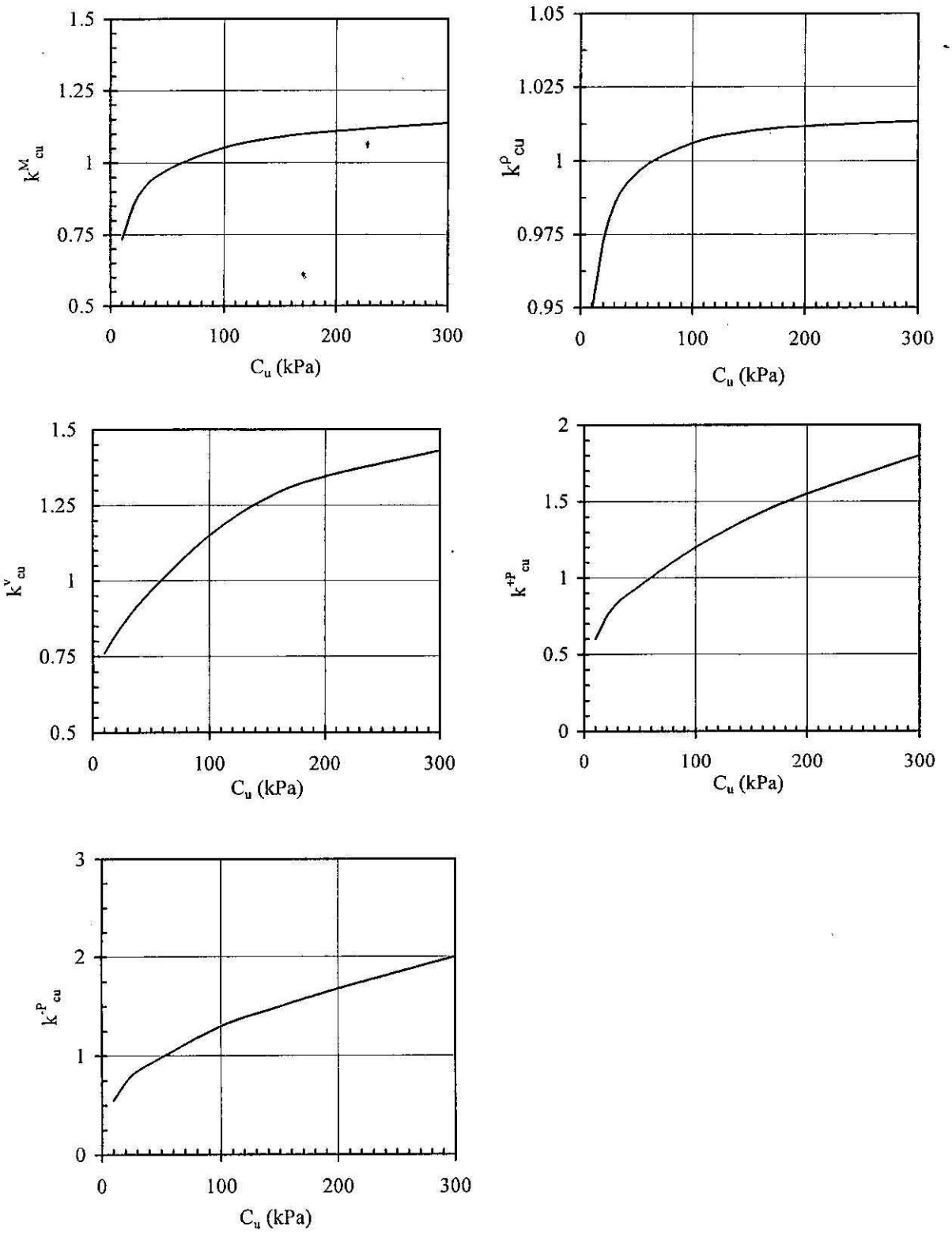

Figure 7.11: Correction factor for Soil Strength

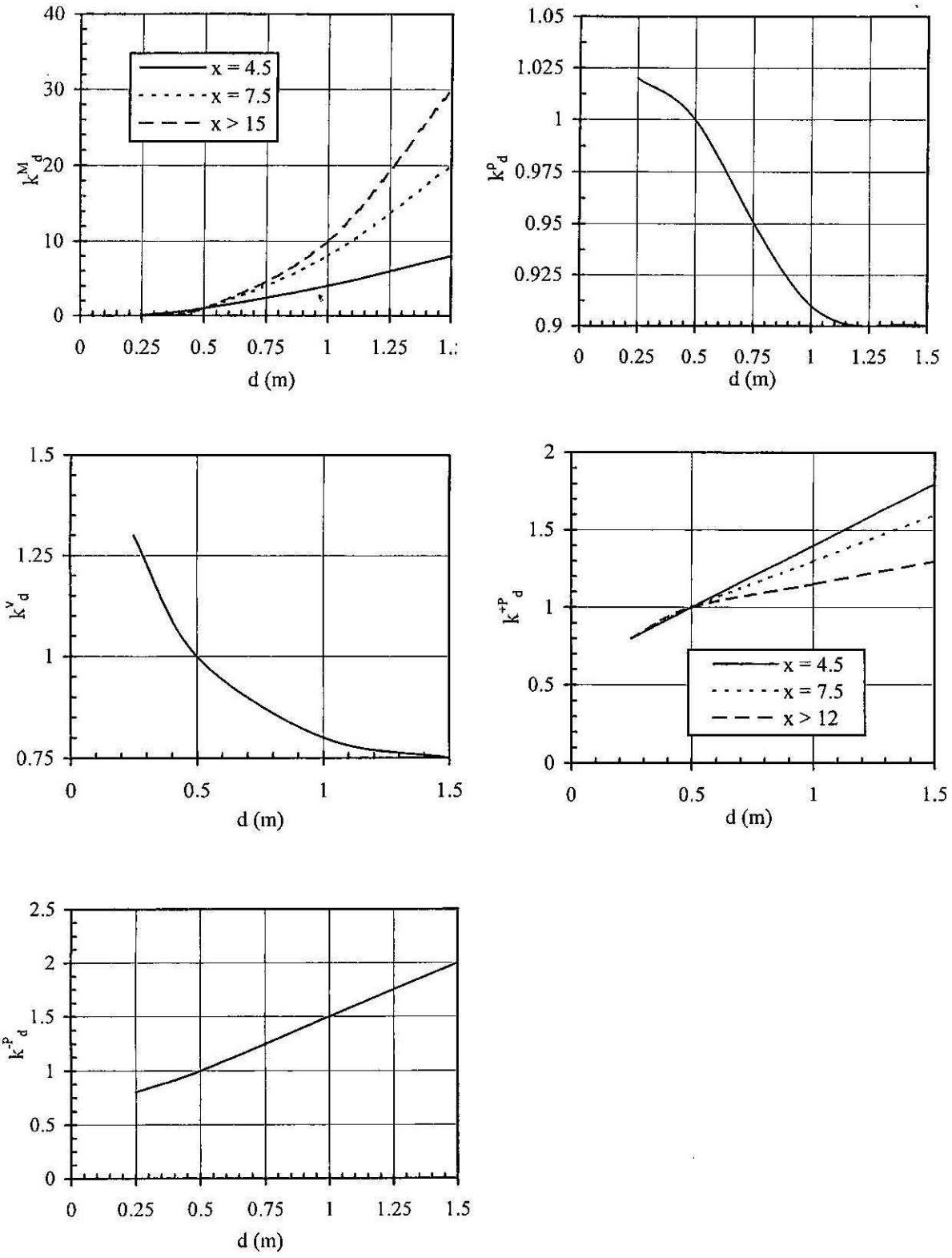

Figure 7.12: Correction Factors for Pile Diameter

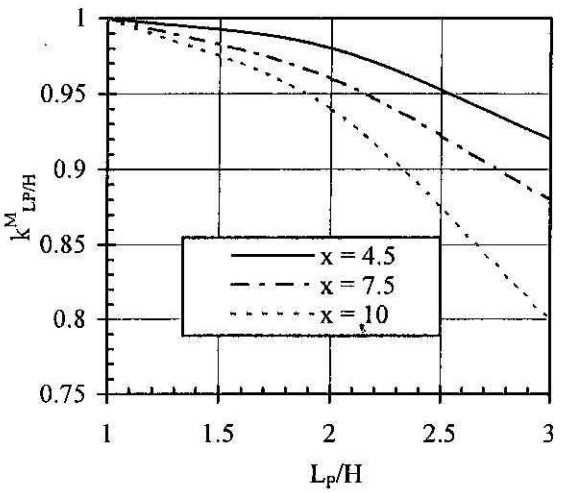

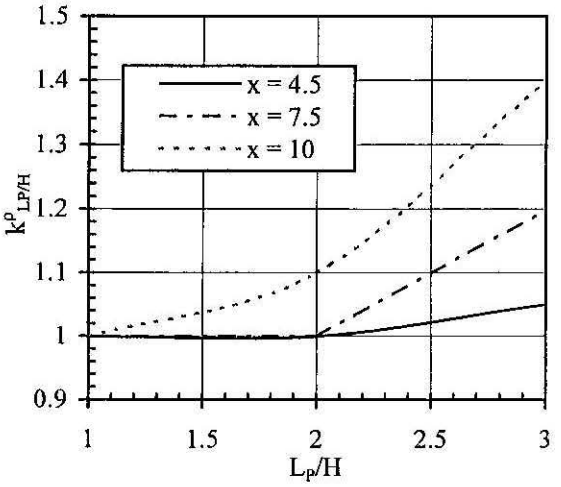

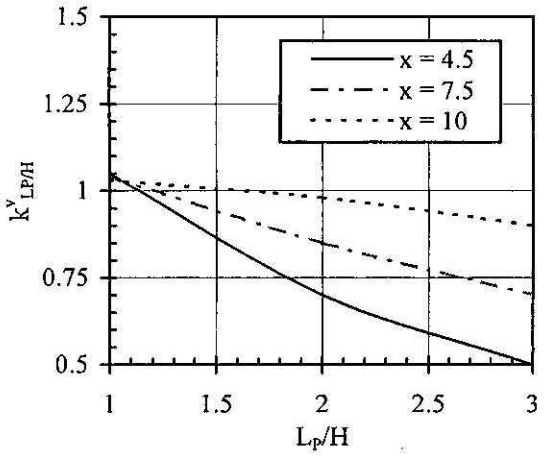

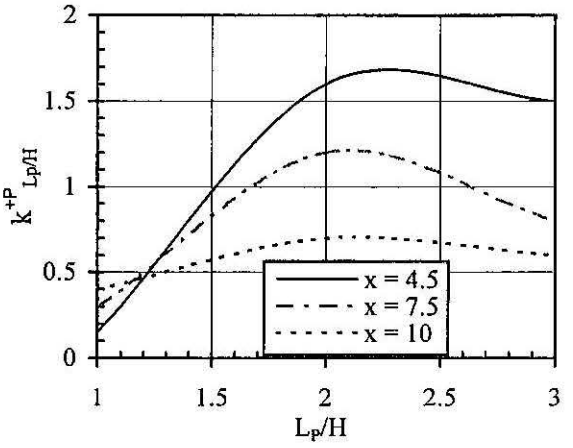

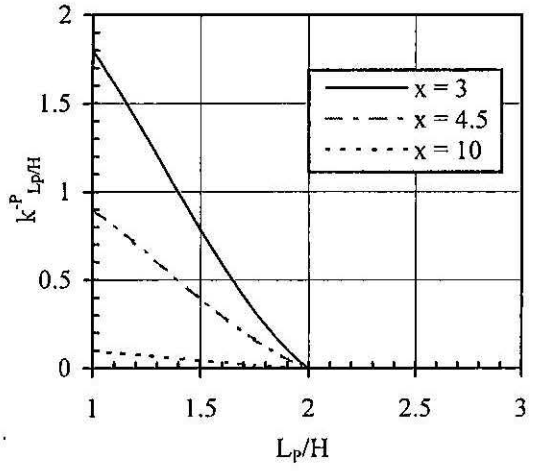

Figure 7.13: Correction Factors For Pile Length/Tunnel Depth Ration

7.5 APPLICATIONS

7.5.1 Centrifuge Tests

Three centrifuge tests were performed in this research study, as described in Chapter 5, and the comparisons of the results obtained from the centrifuge tests and the values estimated from the design charts are presented in this section. Table 7.1 gives the required design chart parameters for all three centrifuge test configurations.

Table 7.1: Design Chart Parameters

	ε_F $(=\varepsilon_0 R^2)$	$L_R=\varepsilon_F/\varepsilon_{FB}$	Aveg. c_u (kPa)	d (m)	L_p/H
Test - 1	0.09	1	60	0.8	1.2
Test - 2	0.09	1	60	0.8	1.0
Test - 3	0.09	1	65	0.8	0.83

Design charts for the "Long Pile" case were used to estimate the tunnelling-induced behaviour for piles in Tests 1 and 2, and similarly the "Short Pile" design charts were used for Test 3. The comparisons of results measured during the tests, and those estimated using design charts for a single pile located 5.5 m away from tunnel, are shown in Table 7.2.

Table 7.2: Comparison of Centrifuge Test Results vs. Design Chart Estimation, x=5.5 m)

Tunnelling-Induced Behaviour of a Pile @ x = 5.5 m	Test - 1		Test - 2		Test - 3	
	Test Result	Design Chart	Test Result	Design Chart	Test Result	Design Chart
Max. Bending Moment (kNm)	47	105	87	97	43	59
Pile Head Settlement (mm)	5.9	6.2	8.7	9.2	8.9	8.4
Max. down Drag Force (kN)	85	230	110	135	180	160
Max. Lateral Deflection (mm)	5.3	7.0	7.5	8.1	4.5	6.4

Similarly Table 7.3 shows the comparisons of tunnelling-induced behaviour estimated from the design charts and those measured from centrifuge tests for pile located horizontally at 8m from tunnel centreline. This pile is a "rear" pile of a 2x2 pile group used in the laboratory centrifuge testing. Axial downdrag force measurements are not available for this pile since it was instrumented to measure only tunnelling-induced bending moments. In addition, measured pile head settlements were not compared with the design chart estimation since the pile group settlement measured was not representative of single pile settlements.

Table 7.3: Comparison of Centrifuge Test Results vs. Design Chart Estimation (x = 8m)

Tunnelling-Induced Behaviour of a Pile @ x = 8 m	Test - 1		Test - 2		Test - 3	
	Test Result	Design Chart	Test Result	Design Chart	Test Result	Design Chart
Max. Bending Moment (kNm)	42	47	47	48	32	35
Pile Head Settlement (mm)	6.1	4.3	6.8	4.5	7.2	5.7
Max. down Drag Force (kN)	-	225	-	125	-	105
Max. Lateral Deflection (mm)	4.5	4.3	4.4	4.3	4.3	4.1

It may be observed from Table 7.2 that the estimated tunnelling-induced pile behaviour from the design charts matches reasonably well the measured values from centrifuge tests, especially for tests 2 and 3. It should be noted that there were a few problems during the execution of test 1 as reported in Chapter 6. In addition, the measured down drag forces are much lower than the design chart estimations for all three tests. This may be due to the fact that the design charts assume elastic behaviour at the pile-soil interface whereas some slip may well have developed.

Table 7.3 shows that design chart estimations of tunnelling-induced bending moments and lateral deflection of piles match well with the results obtained from laboratory centrifuge tests for x = 8m.

7.5.2 Case Study: Angel Underground Station, UK

Case histories regarding pile responses due to tunnelling are very scarce in the literature, but one useful case history is that reported by Lee et al (1994) in which measurements of lateral pile deflections induced by a nearby tunnel construction were recorded. The case history has been analysed to investigate the validity of the design charts presented in Chapter. Equation (3.18) presented in Chapter 3 was also used to predict the lateral movements due to tunnelling.

The case involves the construction of a tunnel for the Angel Underground Station in London, as shown in Figure 7.14 (a). The tunnel was driven between pile foundations supporting a seven storey building with a two storey basement, the tunnel axis line being about 5.7m from the centreline of the nearest piles. The tunnel was excavated using hand tools in two stages, the first a pilot tunnel of 4.5m diameter and the second an enlargement of 8.25m diameter. Measured ground loss ratios were approximately 1.5% for the pilot tunnel and 0.5% for the tunnel enlargement (Mair, 1993).

The piles were driven through 28m of London Clay to the underlying Woolwich and Reading Beds. Ground investigation data showed that the average undrained shear strength of London Clay increased linearly from about 50 kPa at the top to about 220 kPa at the bottom (see Figure 7.14 (b)). Inclinometers were installed at various locations of the ground and within some of the piles to measure the lateral soil movements and lateral pile deflections. Measured results were presented for a pile which had a diameter of 1.2m and was located 5.7m away from the tunnel horizontal axis line. At the pile location the depth, h, of the tunnel axis level was about 15m.

Based on available data, the following assumptions were made in the analyses:

- due to limited data available, the pile was treated as a single pile in the analyses
- average undrained shear strength c_u = 135 kPa and soil Young's modulus E_s = 54 MPa (E_s = 400 c_u).

The computed lateral pile deflection profiles corresponding to each tunneling stage and the total deflection are shown in Figure 7.15, together with that measured and that predicted by Lee et al., (1994). The agreement between the computed final profile and the measured is good, although the predicted maximum lateral deflection occurred slightly above the measured maximum deflection, which occurred at tunnel centreline.

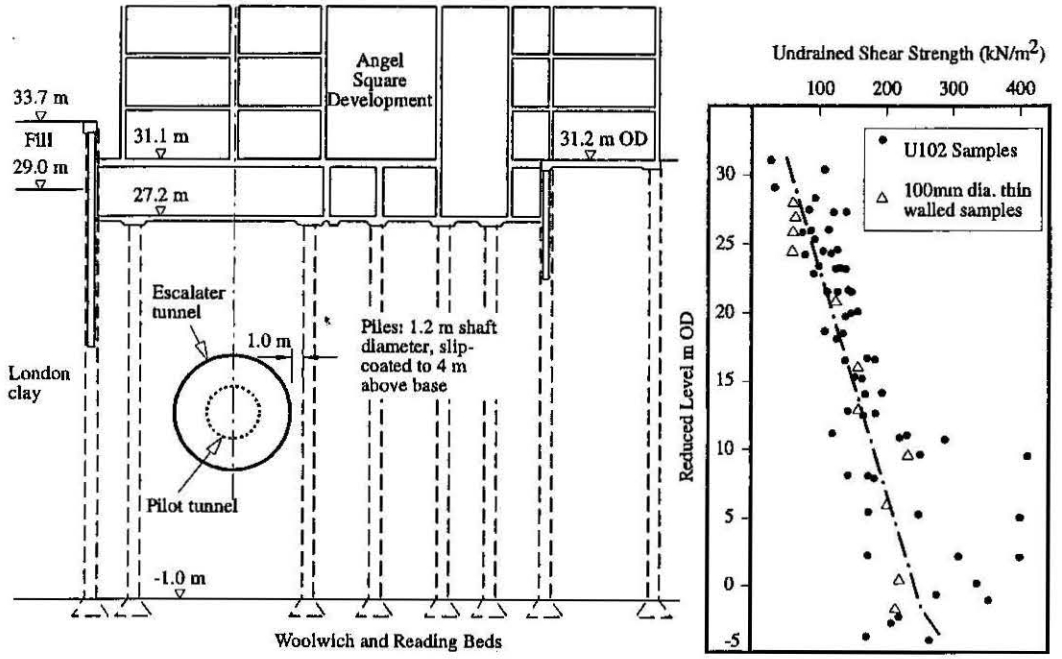

(a) Section through Angel escalator tunnel and building foundations

(b) Undrained shear strength

Figure 7.14: Case History Studied: Tunnelling for Angel Underground Station (Mair, 1993 and Lee et al., 1994)

An estimate of the maximum lateral deflection was also made using "Long Pile" design charts presented in Section 7.4. The estimation procedure and the results are as follows:

1. **Pilot Tunnelling Stage:**

   Ground loss factor, $\varepsilon_F = 1.5\% \times 2.25^2 = 0.076\ m^2$

   Ground loss factor ratio, $L_R = \varepsilon_F/\varepsilon_{FB} = 0.076/0.09 = 0.84$

   From Figure 7.10, base maximum lateral deflection $\rho_b = 7.25$ mm for x = 5.7m

   From Figures 7.11, 7.12 and 7.13 the soil strength, pile diameter and pile length/Tunnel depth ration correction factors are 1.01, 0.9 and 1.0 respectively.

   Therefore, from equation (7.2),

   $$\rho_{max.} = (7.25 \times 1.01 \times 0.9 \times 1.0) \times 0.84 = 5.5 \text{ mm}$$

2. **Enlargement Stage:**

   Ground loss factor, $\varepsilon_F = 0.5\% \times 4.13^2 = 0.085\ m^2$

   Ground loss factor ratio, $L_R = \varepsilon_F/\varepsilon_{FB} = 0.085/0.09 = 0.95$

From Figure 7.10, base maximum lateral deflection ρ_b = 7.25 mm for x = 5.7m
From Figures 7.11, 7.12 and 7.13 the soil strength, pile diameter and pile length/Tunnel depth ratio correction factors are 1.01, 0.9 and 1.0 respectively.

Therefore, from equation (7.2),

$$\rho_{max.} = (7.25 \times 1.01 \times 0.9 \times 1.0) \times 0.95 = 6.2 \text{ mm}$$

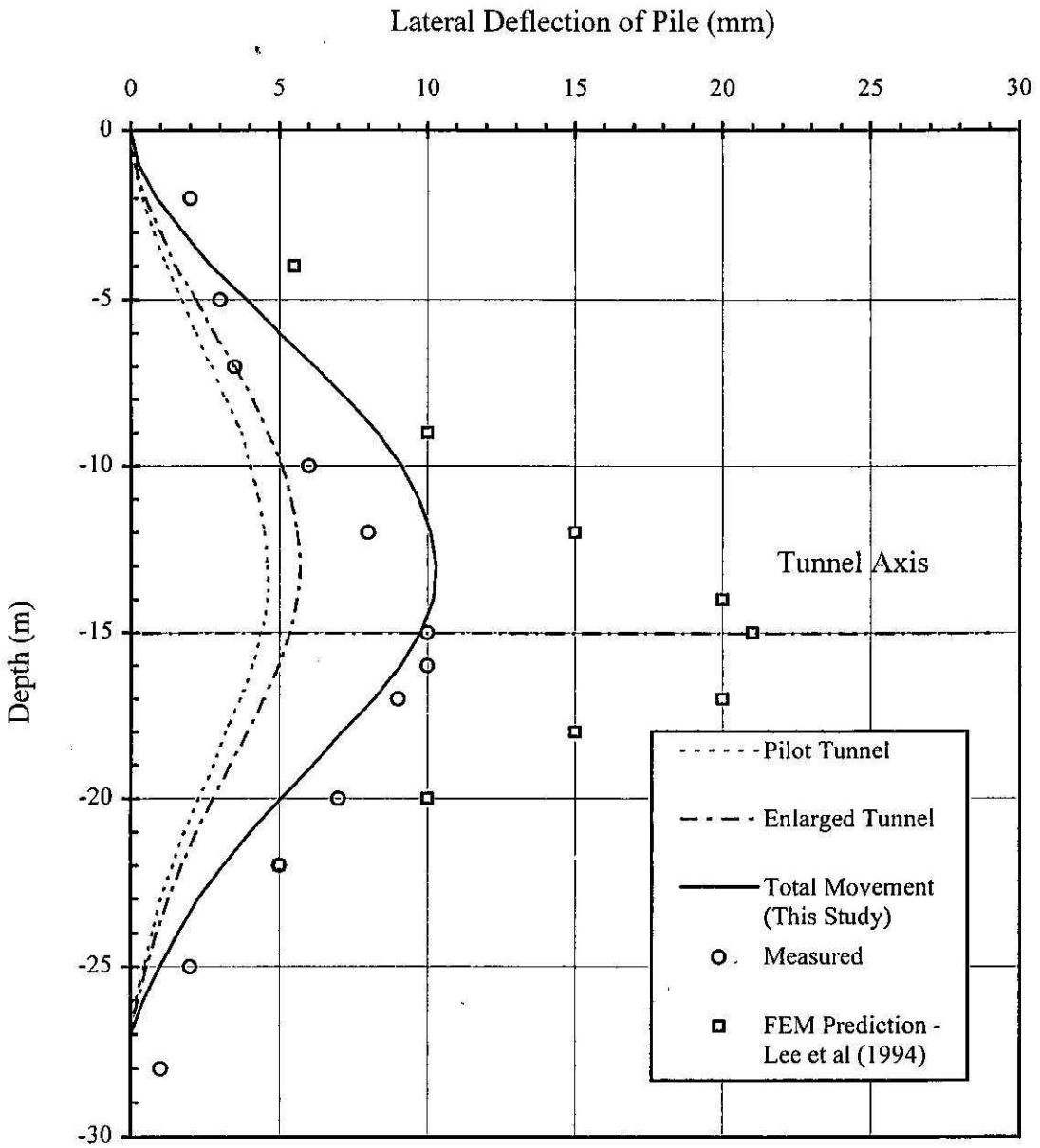

Figure 7.15; Predicted and Measured Lateral Deflection of Piles Adjacent to Angel Underground Station, London (Field data and FEM predictions based on Lee et al, 1994)

Therefore, from above, the total maximum lateral pile deflection due to total ground loss = 5.7 + 6.2 = 11.9 mm. The estimated lateral pile deflection is comparable to the maximum value of about 10mm shown in Figure 7.15.

7.6 SUMMARY

Pile behaviour, especially the lateral behaviour, is rather different for "long piles" (piles whose tip is below tunnel axis level) and "short piles" (piles whose tip is above tunnel axis level) because the maximum soil movements occur at or about the tunnel axis level. Simple design charts have been presented to estimate the tunnelling-induced pile behaviour. It should be noted that the design charts are for computing only the additional responses of the pile, assuming that the pile is initially stress free (both laterally and axially) before tunneling. Also, these design charts have been derived for single isolated piles and are likely to provide an upper-bound estimate of response for piles in a group.

The estimations of tunnelling-induced pile behaviour using design charts compare reasonably well with the centrifuge test results obtained for three different tunnel-pile configurations. A published case history has also been studied in which the measured lateral pile deflections are compared with those computed using the present method and reasonably good agreement is found.

CHAPTER EIGHT

CONCLUSIONS

8.1 OUTLINE

Tunnelling-induced ground deformations and their effects of adjacent pile foundations were investigated in this research study. The output of the study includes an analytical procedure to estimate tunnelling -induced ground loss and ground deformations, and design charts to estimate tunnelling-induced pile behaviour. Detailed conclusions arising from the work have been presented in each of the previous chapters, and the main findings are summarised below.

8.2 TUNNELLING-INDUCED GROUND DEFORMATIONS

Excavation of a tunnel provides an opening into which the soil deforms, and gives rise to "ground loss". In practice, the ground loss values are estimated from empirical correlations based on past experiences. In this study, theoretically based design charts were established in order to predict the ground loss values prior to the tunnel construction. The ground loss ε_0 may be expressed as shown below:

$$\varepsilon_0 = \varepsilon_{NP} f_{cu} f_{PG} \tag{8.1}$$

where ε_{NP} = base ground loss component attribute to the stability factor, f_{cu} = undrained soil strength correction factor, and f_{PG} = physical gap parameter correction factor. These correction factors are shown in Figures 3.3, 3.4 and 3.5.

The ground loss values estimated using these design charts for some case histories are in good agreement with reported empirical ground loss values for tunnels in stiff clay but are overestimated for tunnels in soft clay.

The ground loss which occurs during tunnel excavation causes the ground movements around the tunnel. At present, these tunnelling-induced ground movements are predicted using empirical methods, but these have a number of limitations in their application. In this study, closed-form solutions are presented to estimate the tunnelling-induced surface settlements, subsurface settlements and lateral deformations, and are summarised below:

$$U_{z=0} = \varepsilon_0 R^2 . \frac{4H(1-\nu)}{H^2 + x^2} . \exp\left\{ - \frac{1.38x^2}{(H \cot\beta + R)^2} \right\} \tag{8.2}$$

$$U_z = \varepsilon_0 R^2 \left(-\frac{z-H}{x^2+(z-H)^2} + (3-4\nu)\frac{z+H}{x^2+(z+H)^2} - \frac{2z[x^2-(z+H)^2]}{[x^2+(z+H)^2]^2} \right) \cdot \exp\left\{ -\left[\frac{1.38x^2}{(H\cot\beta+R)^2} + \frac{0.69z^2}{H^2} \right] \right\} \tag{8.3}$$

$$U_x = -\varepsilon_0 R^2 x \left[\frac{1}{x^2+(H-z)^2} + \frac{3-4\nu}{x^2+(H+z)^2} - \frac{4z(z+H)}{(x^2+(H+z)^2)^2} \right] \cdot \exp\left\{ -\left[\frac{1.38x^2}{(H\cot\beta+R)^2} + \frac{0.69z^2}{H^2} \right] \right\} \tag{8.4}$$

where R = tunnel radius, H = depth of tunnel, ε_0 = ground loss estimated from equation (8.1), $\beta = 45^0+\varphi/2$ (soil movement wedge angle), ν = Poisson's ratio of soil, z = the depth measured from the ground surface, and x = the lateral distance from the tunnel axis.

These equations allow rapid estimation of the ground deformations and require only an estimate of the Poisson's ratio, ν, of the soil. The influence of the subsurface soil type and the effect of 3D soil flow into the tunnel face are indirectly modelled through and equivalent 2D gap parameter which was used in the derivation of the ground loss design charts shown in figures 3.3, 3.4 and 3.5.

In general, the tunnelling-induced surface settlement trough for cohesive soils is wider than the granular soils. The study on case histories revealed less satisfactory predictions of tunnelling-induced deformations for layered soils.

The surface settlement trough width "i" introduced by Peck (1969) may be estimated using the equation given below:

$$\frac{i}{R} = \frac{1.15}{(\tan\beta)^{0.35}} \left(\frac{H}{2R} \right)^{\frac{0.9}{(\tan\beta)^{0.23}}} \tag{8.5}$$

The applicability of these proposed analytical solutions were checked with eleven case records and with the results obtained from laboratory centrifuge tests performed in this study and found to be in generally good agreement.

8.2 CENTRIFUGE TESTING

In total, three well controlled and high quality centrifuge model tests were performed to examine the tunnelling-induced ground deformations and their effects on adjacent foundations. The tunnelling procedure was modelled by imposing equivalent two-dimensional ground loss values. The technique of decreasing tunnel diameter during the flight was adapted to model the required ground loss. The technique used in this study to control the tunnel volume during flight was successful and it has the potential to be used for further similar experiments.

The tunnelling-induced ground deformations measured from the centrifuge tests match reasonably well with the similar predictions using equations (8.2), (8.3) and (8.4). The measurement of subsurface settlements and the lateral deformations are subjected to an error margin of ± 3mm in prototype scale.

An equivalent mass on top of the model pile may be used to represent pile loads on existing pile foundation if the centrifuge speed is increased in small acceleration steps while maintaining pore pressure equilibrium.

The experimental results show that tunnelling-induced bending moments and lateral deflections of adjacent piles may be critical when the tunnel centreline is located at or near the pile tip level. In contrast, the induced axial forces are critical when the tunnel centreline is located below the pile tip. It is also observed that measured induced bending moments and lateral deformations for both a single pile and a pile in a group at an identical distance from the tunnel are almost the same. In general, lateral pile movements are similar in magnitude to the lateral soil movements but their distribution with depth is more smooth due to the effects of the pile stiffness.

Therefore, centrifuge testing is considered to be a useful tool for assessing tunnelling-induced ground deformations and their effects on adjacent foundations.

8.4 TUNNELLING-INDUCED PILE BEHAVIOUR

Design charts to estimate the tunnelling-induced pile behaviour are presented in Chapter 7. These design charts were checked with centrifuge test results and with numerical analyses. As a first approximation, the tunnelling-induced additional bending moments, lateral deflections, settlements and the rotations on piles, estimated using these design

charts, may be added to the original design values due to structural loading, when making an assessment of the potential for pile overstressing due to tunnelling operations.

Some of the findings of this study can be summarised as follows:

- An elastic analysis may be performed to predict tunnelling-induced pile behaviour in stiff clay, with reasonable accuracy, for ground loss values less than about 2.5%. In an elastic analysis, the pile deflection follows the soil deflection and the magnitude of the pile responses is proportional to the ground loss value. Therefore, computed pile responses may be normalised with respect to the ground loss value.
- Significant pile settlement and lateral deformation are induced when the pile tip is located at about the tunnel depth level. Similarly, the induced axial downdrag forces and bending moments are significant when the pile tip is located below the tunnel depth level. The pile head rotation is not significantly affected by pile length, but the diameter has a significant effect on the pile head rotation.
- The bending moment profile for piles in a group and single pile are almost the same, except for a small difference at the pile cap location due to the fixity condition. The maximum tunnelling-induced bending moment occurs at about the tunnel axis depth level. Therefore, pile head fixity condition may not be significant in the assessment of tunnelling-induced maximum bending moment of a pile.
- A single pile analysis can predict adequately the tunnelling-induced bending moment, lateral deformation and settlement for a pile in a pile group, at an identical distance from the tunnel. However, the tunnelling-induced axial downdrag force estimated for a single pile is about 15-20% higher than for pile in a pile group, reflecting the influence of pile-soil-pile interaction.
- The settlement and the lateral deformation of a pile group and a single pile are identical for varying horizontal distances but are less than the ground surface settlement and lateral deformation. The maximum values of both lateral deformation and the rotation of the pile head occur at a horizontal distance approximately equal to the ground surface settlement trough width, i.
- The tunnelling-induced bending moment and lateral deflection of a pile become insignificant if pile is located horizontally at equivalent distance of the tunnel depth ($x/H > 1$) from the tunnel centreline. Similarly, pile settlement and the pile head rotation become negligible if the pile is located horizontally at twice the

equivalent distance of the tunnel depth (x/H > 2). Therefore, it may be assumed that tunnelling-induced effect on an adjacent pile is negligible if the pile is horizontally located beyond twice the tunnel depth.

8.5 SUGGESIONS FOR FUTURE RESEARCH WORK

Suggestions for future research work on tunnelling-induced ground deformations and their effects on adjacent pile foundations are described below.

The analytical solutions presented in this study may be further modified by incorporating soil strength parameters. This may be carried out by performing well-controlled laboratory tests and performing back analysis to fit the analytical predictions. An attempt was made in this study by performing back analysis to the available case histories and the preliminary results showed that the analytical solutions presented in this study are more suitable to tunnels excavated in a subsoil for which the soil strength exceeds about 65 kPa. The trial formula to perform the back analysis is given below.

$$U_{z=0} = \varepsilon_0 R^2 . \frac{4H(1-\nu)}{H^2 + x^2} . \exp\left\{ - \frac{A\, x^2}{(H \cot\beta + R)^2} \right\} \tag{8.6}$$

The factor 'A' was adjusted by fitting surface settlement troughs for varying soil strengths. Only 10 case histories were used in this study, as there were only a few cases involving a soil strength less than 65 kPa. Figure 8.1 shows the variation of factor 'A' with soil strength.

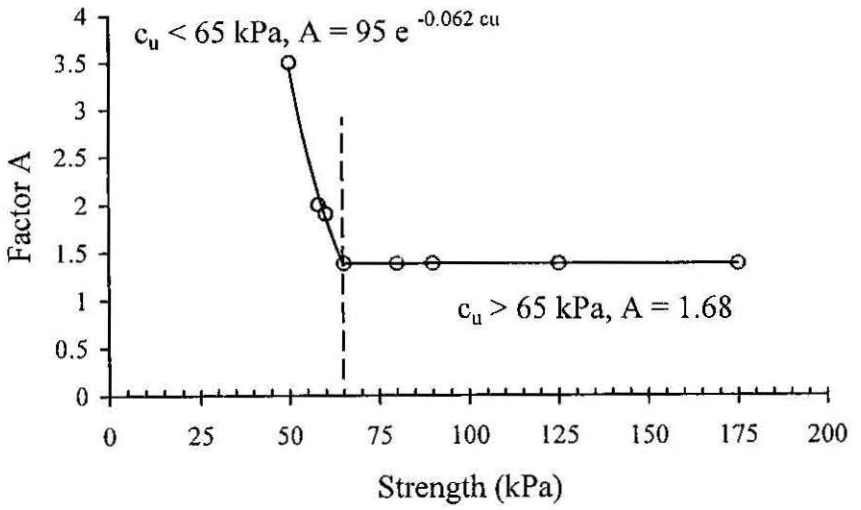

Figure 8.1: Factor A vs. Soil Strength

The preliminary assessment indicated that the soil strength is related to factor 'A' as shown below for soils with strength less than 65 kPa:

$$A = 95 \exp(-0.062\ c_u)$$

where c_u = undrained soil strength.

This relationship may be further refined by performing more laboratory and centrifuge tests.

The analysis assumes that the soil is unloaded and shear-free. In many cases, basement slabs forming part of a building will be present and these will have some influence on the free field soil movements due to tunnelling. It would be useful to develop a design procedure for assessing the effect of surface or near-surface constraints on the ground movements arising from tunnelling.

Only three centrifuge tests for varying pile length/tunnel depth ratio were performed in this study. Further centrifuge tests may be performed to investigate the tunnelling-induced effect of pile diameter.

REFERENCES

REFERENCES

Adachi T, Mochida Y and Tamura T (1979), Tunnelling in fully saturated soft sedimentory rocks, *3rd Int. Conf. On Numerical Methods in Geomechanics*, Aachen, pp 599-610.

Addenbrooke, T. (1995), Meeting report, Ground Engineering, September, pp. 40-43.

Addenbrooke, T, Potts, D M, and Puzrin A M (1997), The influence of pre-failure soil stiffness on the numerical analysis of tunnel construction, *Geotechnique 47*, No. 3, pp 693-712.

Akagi H (1994), Computational simulation of shield tunnelling in soft ground, From memoirs of School of Science and Engineering, Waseda University, No. 58, pp 85-119.

Atkinson J H, Potts D M and Schofield A N (1977), Centrifuge model tests on shallow tunnels in sand, *Tunnels & Tunnelling*, January 1977, pp:59-64

Atkinson J H and Potts D M (1979), Subsidence above shallow tunnels in soft ground, *Journal of Geotechnical Engineering*, ASCE, GT4, pp: 307-325.

Attewell P B (1977), Ground movements caused by tunnelling in soil, *Proc. of the Large Ground Movements and Structures Conference*, Cardiff, Edited by Geddes, Pentech Press, London, pp: 812-948.

Attewell P B and Farmer I W (1974), Ground deformations resulting from shield tunnelling in London Clay, *Canadian Geotechnical Journal 11*, 380-395.

Attewell P B and Woodman J P (1982), Predicting the dynamics of ground settlement and its derivatives by tunnelling in soil, *Ground Engineering 15*, 13-22.

Attewell, P.B., Yeates, J. and Selby, A.R. (1986), Soil movements induced by tunnelling and their effects on pipelines and structures, Blackie and Son Ltd, London.

Atzl G V and Mayr J K (1994), FEM-Analysis of Heathrow NATM Trial tunnel, *Proc. of Numerical Methods in Geotechnical Engineering*, Smith (ed.), balkema, Rotterdam, pp 195-201.

Banerjee P K and Driscoll R M C (1976), Three-dimensional analysis of raked group, Proc., *Inst. Civ. Engng, 61*, pp: 653-671.

Bezuijen A and Schrier J S van der (1994), The influence of a board tunnel on pile foundations, *Centrifuge 1994*, pp 681-686.

Burland J B (1997), Assessment of risk of damage to buildings due to tunnelling and excavation, *Earthquake Geotechnical engineering*, Ishihara (ed), Balkema, Rotterdam, pp 1189-1201.

Cairncross, A M (1973), Deformation around model tunnel in stiff clay, *Phd Thesis*, cambridge university, London.

Clough G W and Schmidt B (1977), Design and performance of excavations and tunnels in soft clays, State-of-the-art report, *Int. Symp. On Soft Clays*, Bangkok.

Clough G W and Schmidt B (1981), Excavations and Tunnelling, Chapt. 8 in Soft Clay Engineering, Edited by E W Brand and R P Brenner, Elsevier.

Cording E J and Hansmire W H (1975), Displacement around soft ground tunnels, deneral report: Session IV, Tunnels in Soil, *5th Panamerican Congress on Soil Mechanics and Foundation Engineering*, Bueno Aires, Argentina, Nov. 1975.

De Moor, E K (1987), Geotechnical aspects of tunnel construction in deep clay formations for radioactice waste disposal, *Ground Engineering, Vol. 20, No. 6*, pp 8, 10, 12.

Deane A P and Bassett R H (1995), The Heathrow Express Trial Tunnel, Proc. Institution of Civil Engineers, *Geotechnical Engineering, 1995, 113*, July, 144-156.

Eisenstein Z, El-Nahhas, F and Thomson S (1981), Strain field around a tunnel in stiff soil, *Proc. of 10th Int. Conference on Soil Mechanics and Foundation Engineering*, Stockholom, 1:283-288, Rotterdam:A.A.Balkema.

Grant, R.J. and Taylor, R.N. (1996), Centrifuge modelling of ground movements due to tunnelling in layered ground, *Proc. Int. Symp. On Geotechnical Aspects of Underground Construction in Soft Ground,* City University, London.

Gunn M J (1993), The prediction of surface settlement profiles due to tunnelling, predictive soil mechanics, *Proc. of the Wroth Memorial Symposium*, Edited by G T Houlsby and A N Schofield, Oxford, pp: 304-316.

Guo C, Nguyen-minh D, and Braham S (1994), Steady finite element method for analysis of advancing tunnels under non-uniform loading, *Proc. of Numerical Methods in Geotechnical Engineering*, Smith (ed.), Balkema, Rotterdam, pp 209-213.

Heath G R and West K J F (1996), Ground movement at depth in London clay, *Proc. Instn Civ. Engrs. Geotech. Engng., 1996, 119*, April 65-74.

Hergarden H J A M, Van der Poel J T and Van der Schrier J S (1996), Ground movements due to tunnelling: Influence on pile foundations, *Geotechnical*

Aspects of Underground Construction in Soft Ground, Mair & Taylor (eds.), Balkema, Rotterdam, pp 519-524.

Horikoshi, K. and Randolph, M.F. (1996), Centrifuge modelling of piled raft foundations on clays, *Geotechnique 46(4)*, 741-752.

Ingles O G (1972), Soil Stabilisation, Butterworths, Sydney.

Itasca (1997), FLAC 3D Users Manual, Itasca Consulting Group, USA.

Kishida H (1964), Ultimate bearing capacity of piles driven into loose sand, *Soils and Foundations, Vol. 7, No. 3*, pp:20-29.

Kuwabara, F. and Poulos, H.G. (1989), Downdrag forces in group of piles, *Journal of Geotechnical Engineering, ASCE, Vol. 115, No. 6*, pp.806-818.

Leca, E and Clough, G W (1992), Preliminary design for NATM tunnel support in soil, *Journal of Geotechnical Engineering, ASCE, Vol. 118, No. 4*, pp 558-575.

Ledesma A and Romero E (1997), Systematic backanalysis in tunnel excavation problems as a monitoring technique, *Proc. of 14th Int. Conference on Soil Mechanics and Foundation Engineering, Vol. 3*, Hamburg, Germany, pp: 1425-1428.

Lee K M and Rowe R K (1989), Deformations caused by surface loading and tunnelling: the role of elastic anisotrophy, *Geotechnique, Vol. 39:1*, pp 125-140.

Lee K M, Rowe R K and Lo K Y (1992), Subsidence owing to tunnelling. I. Estimating the gap parameter, *Canadian Geotechnical Journal 29*, 929-940.

Lee R G, Turner A J and Whitworth L J (1994), Deformations caused by tunnelling beneath a piled structure, *Proc. XIII Int. Conf. Soil Mechanics and Foundation Engineering*, New Delhi, India, pp: 873-878.

Lo K Y, Ng R M C and Rowe R K (1984), Predicting settlement due to tunnelling in clays, Tunnelling in Soil and Rock, *American Society of Civil Engineers, Geotech III Conference*, Atlanta, Ga., pp:48-76.

Mahmoud, M (1988), Vane testing in soft clays, *Ground Engineering*, October, 36-40.

Mair R J (1979), Centrifuge modelling of tunnel construction in soft clay, *Ph. D Thesis*, University of Cambridge.

Mair R J, Gunn M J and O'Reilly M P (1981), Ground movements around shallow tunnels in soft clay, *10th Int. Conference on Soil Mechanics and Foundation Engineering*, Stolkhom, pp:323-328.

Mair, R.J. (1993), Developments in geotechnical engineering research: application to tunnels and deep excavations Unwin Memorial Lecture 1992, *Proc. Instn. Civ. Engrs. Civ. Engng, Vol. 93*, pp.27-41.

Mair, R.J., Taylor, R.N. and Bracegirdle, A. (1993), Subsurface settlement profiles above tunnels in clays, *Geotechnique, Vol. 43, No.2*, pp.315-320.

Moffatt J D J (1977), The effect of shield tunnelling beneath pile foundations in non-cohesive soils-model tests, *B.A.Sc Thesis*, University of Toronto.

Moh Z C, Ju D H and Hwang R N (1996), Ground movements around tunnels in soft ground, *Proc, of Int. Symposium on Geotechnical Aspects of Underground Construction in Soft Ground*, London, April 1996.

Morton, J.D. and King, K.H. (1979), Effects of tunnelling on the bearing capacity and settlement of piled foundations,, *Proc. Tunnelling '79*, Ed. M.J. Jones, IMM, London, pp. 57-68.

Mroueh H (1998), Interaction between tunnels and nearby existing structures encountered in urban areas, *PhD Thesis*, Universite des Sciences et Technologies de Lille, France, May 1998.

New B M and O'Reilly M P (1991), Tunnelling-induced ground movements, predicting their magnitude and effects, *Proce. of 4th Int. Conference on Ground Movements and Structures*.

Norgrove W B, Cooper I and Attewell P B (1979), Site investigation procedures adopted for the Northumbrian water authority's Tyneside sewerage scheme, with special reference to settlement prediction when tunnelling through urban area, *Tunnelling'79*, pp: 79-104.

Orr T L L (1976), The behaviour of lined and undrained model tunnels in stiff clays, *PHD Thesis*, University of Cambridge, England.

O'Reilly M P and New B M (1982), Settlements above tunnels in the U.K.- their magnitude and prediction, *Tunnelling '82*. pp: 173-181.

Ortigao J A R, Kochen M M, and Assis A P (1996), Tunnelling in Brasilia porous clay, *Can. Geotech. Jour. 33*, pp 565-573.

Palmer J H and Belshaw D J (1978), Deformations and pore pressures in the vicinity of a precast, Segmented Concrete-Lined Tunnel in Clay, *Canadian Geotechnical Journal 17*, 174-184.

Peck R B (1969), Deep excavations and tunnelling in soft ground, *Proc. of 7th Int. Conference on Soil Mechanics and Foundation Engineering*, Mexico City, State of the art volume, pp: 225-290.

Phienwej N (1997), Ground movements in shield tunnelling in Bangkok soils, *Proc. of 14th Int. Conference on Soil Mechanics and Foundation Engineering, Vol. 3*, Hamburg, Germany, pp: 1469-1472.

Potts D M and Addenbrooke T I (1996), The influence of an existing surface structure on the ground movements due to tunnelling, *Int. Symp. On Geotechnical Aspects of Underground Construction in Soft Ground*, City University, London, R Mair & R Taylor (eds.), Rotterdam, pp 573-578.

Poulos H G (1979), An approach for the analysis of offshore pile group, *Proc. Confe. On Numerical Methods in Offshore Piling*, Inst. of Civ. Engrs, London, pp:119-126.

Poulos H G (1990), DEFPIG Users Guide, Center for Geotechnical Research, University of Sydney, Australia.

Poulos, H.G. and Davis, E.H. (1980), Pile Foundation Analysis and Design, New York, John Wiley and Sons

Ramasamy N (1992), Soft ground tunnelling in Bangkok subsoils, *M. Eng Thesis*, Asian Institute of Technology, Bangkok, Thailand.

Randolph M F (1980), PIGLET:A Computer program for the analysis and design of pile groups under general loading conditions, *Soil Report TR91*, CUED/D, Cambridge University, Cambridge, England.

Randolph, M.F (1992), Short Course Notes on "Engineering of Piled Foundations", Kuala Lumpur.

Randolph, M.F., Jewell, R.J., Stone, K.J.L. & Brown, T.A. (1991), Establishing a new centrifuge facility, *Proc. Centrifuge 1991,* Uni. of Colorado, (Ed: Hon Yim Ko), Balkema, 3-9.

Rowe R K and Lee K M (1989), Parameters for predicting deformations due to tunnelling. Proceedings, *12th Int. Conf. On Soil Mech. and Found. Engrng.*, Rio de Janeiro, pp: 793-796.

Rowe R K and Kack G J (1983), A theoretical examination of the settlements induced by tunnelling: Four Case Histories, *Canadian Geotechnical Journal, Vol. 20*, pp:299-314.

Rowe R K and Lee K M (1992), An evaluation of simplified techniques for estimating three-dimensional undrained ground movements due to tunnelling in soft soils, *Canadian Geotechnical Journal, 29*: 39-52.

Sagaseta C (1987), Analysis of undrained soil deformation due to ground loss, *Geotechnique 37*, 301-320.

Schofield A N (1980), Cambridge Geotechnical Centrifuge, The 20th Rankine Lecture, *Geotechnique 30*, N0. 3, pp 227-268.

Simpson B, Atkinson J H and Jovicis V (1996), The influence of anisotropy on calculations of ground settlements above tunnels, *Proceedings of Int. Symp. On Geotechnical aspects of the Underground Construction in Soft Ground*, London preprint vol., pp 511-514.

Stallebrass S E, Grant R J and Taylor R N (1996), A finite element study of ground movements measured in centrifuge model tests of tunnels, *Proc. of the Int. Symposium on Geotechnical Aspects of Underground Construction in Soft Ground, London*, UK, April 1996, Ed: Mair R J and Taylor R N: Balkema

Steensen-Bach, J O and Steenfelt J S (1991), Subsidence due to shield tunnelling in sand, *Proc. of European Conf. On Soil Mech. and Found. Engrng,* 10, Florence, May 1991, pp: 863-868.

Steiner W (1997), Slurry penetration into coarse grained soils and settlements from large slurry sheild tunnel, *Proc. of 14th Int. Conference on Soil Mechanics and Foundation Engineering, Vol. 3*, Hamburg, Germany, pp: 329-333.

Stewart, D.P. (1992), Lateral Loading of piled bridge abutments due to embankment construction, *PhD Thesis*, The University of Western Australia, Australia.

Stewart, D.P. (1990), The response of piles in soft clay to nearby embankment construction, Research Report GEO:90086, Department of Civil and Environmental Engineering, The University of Western Australia.

Szoke I S (1977), Tunnelling beneath piled ground - aspects of pile and pile group capacity and soil collapse mechanisms in granular soils as determined by model tests, *B.A.Sc Thesis*, University of Toronto.

Taylor R N (1998), Modelling of Tunnel Behaviour, *Proc. Instn. Civ. Engrs*, Geotech. Engng, UK, July 1998, 131, pp:127-132.

Vermeer P A and Bonnier P G (1991), Pile settlements due to tunnelling, *Proc. of European Conf. On Soil Mech. and Found. Engrng,* 10, Florence, May 1991, pp: 869-872.

Verruijt, A. and Booker, J.R. (1996), Surface settlements due to deformation of a tunnel in an elastic half plane, *Geotechnique, Vol. 46, No. 4*, pp: 753-756.

Wong R C K and Kaiser P K (1987), Prediction of ground movements above shallow tunnels, *Prediction and Performance in Geotechnical Engineering*, Calgary, June 1987, pp 329-343.

Xu K J and Poulos H G (1999), Principles of Program GEPAN for General Pile Elastic Analysis, University of Sydney, Dept. of Civil Engineering, Research Report No: R782.

APPENDIX A

GAP Parameters

Theoretical Background of GAP Parameters

The gap parameter (g) is defined (Rowe and Lee, 1992) as:

$$g = G_p + U^*_{3D} + \omega \qquad (A.1)$$

where G_p = physical gap (usually the difference between the maximum outside diameter of the tunnelling machine and the outside diameter of the lining for a circular tunnel), U^*_{3D} = three dimensional (3-D) elasto-plastic deformation into the tunnel face, and ω = workmanship factor.

Figure A.1 shows the tunnel head and the 2-D plane strain representation of tunnel heading.

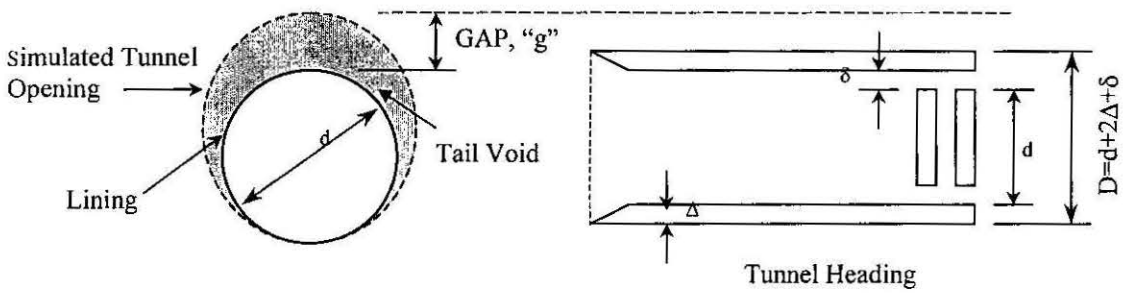

Figure A.I: Definition of GAP

Determination of G_p

The physical gap is given by $G_p = 2\Delta + \delta$, where, Δ = the thickness of tailpiece, and δ = the clearance for erection of lining.

In modern tunnelling practice the physical gap and the void created by the over-cutting are generally filled by grout mix which theoretically results in a negligible physical gap ($G_p \sim 0$). However, in practice there will be a time-dependent shrinkage in the grout-soil mix. Laboratory tests carried out on cement-soil mix by Ingles (1972) showed that about 7-10% of the time-dependent length reduction was observed in the cement-soil mix samples. Therefore, if grouting is employed to fill the physical gap, the value of physical gap is assumed to be; $G_p = 7-10\%\ (2\Delta + \delta)$. Since the shrinkage occurs within a short time

period, the gap created by the shrinkage of the grout-soil mix is considered as an undrained gap.

Determination of U^*_{3D}

The free field stress state at a given section is modified as the excavation of the tunnel approaches it. If the net pressure on the tunnel face (resultant of the slurry plus cutter head pressure) is lower than the free field stress, then the soil mass will move towards the tunnel face. The volume of soil that intrudes into the tunnel face owing to pressure release at the face will eventually be excavated. The U^*_{3D} component is defined as:

$$U^*_{3D} = (k/2)\ \delta_x \tag{A.2}$$

where k = soil-cutter resistance factor, and δ_x = face intrusion.

Lee et al (1992) established experimental and elasto-plastic analytical relationships for k and δ_x. They suggested that the value of k = 0.7 – 0.9 for stiff to soft clays and k=1 if plastic flow occurs (very soft clays). Face intrusion was defined as:

$$\delta_x = \frac{\Omega R P_0}{E} \tag{A.3}$$

where Ω = a dimensionless displacement factor (refer to Lee et al, 1992), R= tunnel radius, E= Young's Modulus (typically the undrained modulus in extension), and P_0 is given as:

$$P_0 = K'_0 P'_v + P_w - P_t \tag{A.4}$$

where K'_0 = effective coefficient of earth pressure at rest, P'_v = vertical effective stress at springline of the tunnel, P_w = pore water pressure at springline of the tunnel, and P_t = tunnel support pressure.

Determination of ω

Lo et al (1984) have derived an expression for the elasto-plastic plane strain displacement (U_t) at the tunnel crown as:

$$\frac{U_i}{R} = 1 - \left(\frac{1}{1 + \frac{2(1+\nu_u)c_u}{E_u}\left[\exp\left(\frac{N-1}{2}\right)\right]^2} \right)^{1/2} \qquad \text{(A.5)}$$

where R = tunnel radius, E_u = undrained Young's Modulus, c_u = undrained strength of the soil, ν_u = undrained Poisson's ratio and N = stability number.

The smallest of $0.6G_p$ and $(1/3)U_i$ is chosen and designated as ω^*.

The component (ω) also includes the radial ground loss due to the over-cutting bead. Three cases are considered as given below:

1. No bead, then $\omega = \omega^*$
2. The bead spans the upper 180^0 of hood, then $\omega = \omega^* + 1$ x bead thickness
3. The bead covers full circumference, then $\omega = \omega^* + 2$ x bead thickness

One the gap parameter 'g' is determined, the ground loss value may be estimated using the equation (3.1).

A typical EXCEL worksheet to estimate the gap parameter is shown in the following page.

Typical Worksheet to Estimate Ground Loss Value

CASE 1: Heathrow Express Trial Tunnel

General Project Information

Location:	Heathrow Express Trail Tunnel	
Depth:	19	m
Diameter :	8.5	m
Soil Type:	Stiff London Clay	
Poison ration:	0.3	
Stability Number:	2.5	
Undrained Modulus:	40000	kPa
Undrained Strength:	150	kPa
Earth Pressure Coef:	1.5	
Dry unit weight:	8	kN/m3
Depth of WT:	9	m
Internal air Pressire:	0	kPa

Tunneling Method Information

Method:	
Length of the Shield:	5
Thickness of Tail Piece:	15
Clearence for errection of Lining:	12
Max. allowable excess Pitch:	
Bead Thickness:	12

If bead spans the upper 180 deg. of the hood,
If the bead covers full circumference, Type "2"
No bead, Type "0"

Grouting

No- Type "1" and "0"	0
Yes- Type"0" and "1"	1

Note: It is assumed that grout shrinks with time in the range 7 - 10%
Ref: Ingles O G (1972), "Soil Stabilisation", Butterworths, Sydney

Radial Displacement at Crown:	89.9 mm	(1/3)Ui =	30.0 mm
Physical gap, Gp =	**4.2** mm	0.6 Gp =	2.52 mm

Gap due to workmanship = **14.52** mm

If N < 2.5	Gap due to Face loss =	39.0 mm
if 2.5 <N<5	Gap due to Face loss =	39.2 mm
if N >5	Gap due to Face loss =	69.7 mm

GAP = **57.8** mm

Ground Loss = 1.36 %

This thesis has been accepted for the award of the degree in the Faculty of Engineering

UNIVERSITY OF SYDNEY LIBRARY
0000000604792090

ALLBOOK BINDERY
91 RYEDALE ROAD
WEST RYDE 2114
PHONE: 9807 6026